Development of Photosensitiser Functionalised Electrospun Nanofibre for Water Sterilisation

Kaniz Fatema Chowdhury

Submitted in accordance with the requirements for the degree of
Doctor of Philosophy

The University of Leeds

School of Biomedical Sciences

Faculty of Biological Sciences

September, 2018

The candidate confirms that the work submitted is her own and that appropriate credit has been given where reference has been made to the work of others.

Assertion of moral right:

Acknowledgements

Firstly, I would like to express my sincere gratitude to my supervisor Professor Paul Millner for the continuous support of my PhD study research through his patience, motivation, and immense knowledge and humour. His intellectual guidance helped me during the research and writing of this thesis. I am grateful not only for his insightful comments and encouragement but also for the critical interrogation, which encouraged me to widen my knowledge from various perspectives. I could not have imagined having a better advisor and mentor for my PhD journey. He was always there for any types of problems to listen and to give scientific advice. I learnt what could be the best supervisor-student relationship. He will remain as a role model for the rest of my life.

Besides my supervisor, I appreciate the efforts of my co-supervisor Dr Natalia Sergeeva. She was always there for me in chemistry. I obtained several skills and gained experience under her supervision. She has made me better scientist for which I will be grateful forever. Her supportive and positive attitude made me stronger in those stressful days when nothing seemed to work. I am also thankful to two of my lab mates Simran Channa and David Martin in Dr Sergeeva's lab. Without their support, it would not be possible to progress on my research. I am also thankful to another co-supervisor Dr Robin Bon. Without his support and advice, it would not be possible to overcome the problems related to chemistry. Special thanks to him also for introducing and include Dr Sergeeva in my PhD supervisory team.

My sincere thanks also go to Professor Stephen Russell for his kind support of giving me access to the electrospinning facility in the School of Design and arranging electrospinning training for me. I would like to thank Dr Muhammad Tausif and Dr Robabeh Gharaei, who provided me with training and valuable advice during electrospinning of nanofibres.

I thank my fellow lab mates for the stimulating discussions. I am especially thankful to my friend, more than lab-mate, Dr Thanison Mahatnirkul for being always there and for all the fun we had in the last four years. I am thankful to my present and previous colleagues, Dr Arindam Pramanik, Dr Tim Gibson, Dr Alex Vakurov, Dr Jack Goode, Dr Asif Ahmed for their happy and supportive attitude and suggestions all through my PhD. All of them made my PhD journey easier and convenient.

I am grateful to BBSRC iCASE funding body for sponsoring my research. I am also thankful to School of Biomedical Science, University of Leeds for providing me all the necessary supports to pursue my PhD degree.

Finally, I will forever be grateful to my family members, my mother and my beloved husband Khaled Abdullah for supporting me mentally, for encouraging me throughout the PhD in general. Without his selfless, sincere support and sacrifices, it would not be possible to produce my PhD. I am thankful to the sunshine of my life, my son Kaysan and daughter Kenitra. Their smiling faces made my every stressful day easier with their love and presence.

Abstract

Waste water treatment is highly energy consuming in both developed and developing countries energy efficient water treatment techniques are continuously being sought. Ensuring microbiological safety of water is one of the utmost importance. However conventional disinfection processes produce toxic by-products which are difficult and costly to remove and photodynamic inactivation may provide a cheap and eco-friendly alternative. Photosensitisers kill microorganisms by a process known as photodynamic inactivation (PDI). In PDI, photosensitisers transfer energy to O_2 to yield highly reactive singlet oxygen and its products. These reactive oxygen species cause PDI of bacteria with no toxic by-products and without chemical alteration of the photosensitiser which allows its re-use. In the work presented covalent immobilisation of photosensitiser onto electrospun nanofibre mats prevented photosensitiser release into the water during PDI and allowed continued use of the photosensitiser loaded mats. The synthesis and characterisation of antibacterial tetra cationic photosensitisers; tetra allyl pyridyl porphyrin (TAllylPyP) and tetra amine pyridyl porphyrin (TAminePyP) is reported and also the preparation and characterisation of water resistant polyacrylic acid cross-linked with polyvinyl alcohol (PAA-PVA) and ethylene glycol (PAA-EG) electro spun nanofibre (ENF) mats. Protocols for covalent immobilisation of photosensitises TAllylPyP and TAminePyP onto the mats and their characterisation is described. Successful PDI of *E.coli* by these nanofibres were carried out using 32 mW/cm^2 white light which is around 3% of bright mid-day time sunlight under clear sky conditions in sub-Saharan Africa to study a graded PDI response. The PDI data imply that this system could be operated by using direct natural sunlight, to rapidly kill water borne bacteria. Both Gram-positive and Gram-negative bacteria were killed and this sunlight driven water disinfection system could be an economical and efficient solution to provide clean water to some of the world's poorest people.

Table of Contents

Acknowledgements ..... **iii**
Abstract ..... **v**
Table of Contents ..... **vi**
List of Tables ..... **xii**
List of Figures ..... **xiii**
Chapter 1 Introduction **1**
1.1 Overview 1
1.2 Types, sources and consequences of contaminants 4
1.3 Microbial contaminants 4
1.4 Chemical contaminants 6
1.4.1 Organic water pollutant 6
1.4.2 Inorganic pollutants 7
1.5 Common disinfectants for drinking water 9
1.5.1 Disinfection methods 10
1.6 Photodynamic Inactivation (PDI) of microorganisms 14
1.7 Antimicrobial activity of reactive oxygen 16
1.8 Why photosensitiser needs to be immobilised 19
1.9 Nanofibre mats supported photosensitisers 21
1.10 Nanofibre mats materials 23
1.11 Advantages of electrospun nanofibre mats and challenges 25
1.11.1 Photosensitised inactivation of microbial cells: general aspects bacterial cell wall 26
1.12 Synthesis of photosensitisers 29
1.13 Experimental setup for PDI of water pollutants 31
1.13.1 Light source 32
1.13.2 Model pollutants 32
1.14 Research aims 32
Chapter 2 Materials and Methods **34**
2.1 Materials 34
2.1.1 Light source and conditions for PDI 34
2.2 Electrospinning 38
2.2.1 PAA-PVA nanofibres: preparation of polyacrylic acid nanofibre crosslinked with polyvinyl alcohol 39
2.2.1.1 Post electrospinning crosslinking of PAA-PVA nanofibre 39

2.2.2 PAA-EG nanofibre: preparation of ethylene glycol crosslinked polyacrylic acid 40

2.2.3 PAA-EG-PEI: Covalent modification of PAA-EG nanofibre by Poly (ethyleneimine) 40

2.2.4 PAA-EG-TPP: 10% (w/w) PAA-EG nanofibre doped with TPP 41

2.2.4.1 PAA-EG / PVA-PEI bilayer nanofibres 41

2.2.5 Polyacrylonitrile nanofibre blended with Jeffamine (PAN-JEF) 41

2.2.5.1 Flow channel made of PAN-JEF nanofibres mat: 42

2.3 Water stability of nanofibre mats 44

2.3.1 Mass spectroscopic analysis 44

2.4 Detection of PAA leaching from heat treated PAA-PVA electrospun nanofibre 45

2.5 Synthesis of photosensitisers 45

2.5.1 Synthesis and structure of TAllylPyP 46

2.5.2 Synthesis and structure of TAminePyP 47

2.6 Determination of *E. coli* NCTC 10418 growth curve 49

2.6.1 Determination of E. coli BL21 (DE3) growth curve 49

2.7 Determination of dark toxicity of photosensitisers in solution 50

2.8 Photodynamic inactivation (PDI) of bacteria by photosensitisers in solution 50

2.8.1 PDI of bacteria in solution 51

2.9 Functionalisation of nanofibres with photosensitisers 52

2.9.1 Adsorption 52

2.9.1.1 TMPyP immobilisation onto PAA-PVA nanofibre mats by adsorption 53

2.9.1.2 TAllylPyP immobilisation onto PAA-EG by adsorption 53

2.9.2 Covalent immobilisation of photosensitisers 53

2.9.3 Immobilisation of PPIX onto (PAN-JEF) electrospun nanofibre mats 54

2.9.3.1 Amidation of carboxylic groups 55

2.9.4 Determination of amine availability and confirmation of PPIX conjugation onto (PAN-Jeff) 55

2.9.5 Hydoxylation of PAN to polyacrilic acid (PAA) and conjugation of PPIX with PAA 57

2.9.6 Covalent immobilisation of TAllylPyP onto PAA-EG nanofibre mats 58
2.9.7 Covalent immobilisation of TAminePyP onto PAA-EG nanofibre mats 59
2.10 Characterisation of functionalised nanofibre 61
2.10.1 Scanning electron microscopy (SEM) 61
2.10.2 FTIR 61
2.10.3 Estimation of TMPyP bound to PAA-PVA nanofibre mats 61
2.10.4 Estimation of functional groups 61
2.11 Assay of singlet oxygen generation by photosensitiser functionalised nanofibre mats 62
Chapter 3 PDI of bacteria in water by photosensitiser in solution 63
3.1 Overview 63
3.2 Determination of growth kinetics of model bacteria 64
3.2.1 Growth kinetics of *E. coli* NCTC 10418 64
3.2.2 Growth kinetics of *E. coli* BL21 (DE3) 65
3.3 Measurement of light intensity on the sample surface 66
3.4 Selection of photosensitisers 68
3.4.1 PDI of Gram-negative bacteria with PPIX in solution 68
3.4.2 PDI of Gram-positive bacteria with PPIX in solution 70
3.5 PDI with TMPyP in solution 71
3.5.1 Study of dark toxicity of TMPyP 71
3.6 Photodynamic inactivation by cationic photosensitiser 72
3.6.1 PDI of *E. coli* NCTC 10418 TMPyP in solution 72
3.6.2 The effect of light intensities and duration of light illumination 73
3.7 PDI effects of TAllylPyP in solution 74
3.7.1 Concentration optimisation of TAllylPyP for PDI 75
3.7.2 Optimisation of light intensity 76
3.8 PDI with tetra amine pyridyl porphyrin (TAminePyP) 77
3.9 PDI of antibiotic resistant bacteria 79
3.9.1 PDI of carbenicillin resistant bacteria BL21 (DE3) with TMPyP in solution 79
3.9.2 PDI of carbenicillin resistant bacteria BL21 (DE3) by TAllylPyP in solution 80
3.10 Conclusion 82

Chapter 4 Characterisation of photosensitiser and photosensitiser functionalised electrospun nanofibre 83

4.1 Overview 83

4.2 Characterisation of photosensitisers 87

4.2.1 Tetra allyl pyridyl porphyrin (TAllylPyP) 87

4.2.2 FTIR 87

4.2.3 Tetra amine pyridyl porphyrin (TAminePyP) 89

4.2.4 FTIR of TAminePyP 89

4.3 Characterisation of electrospun nanofibres 91

4.3.1 PAA-PVA 91

4.3.2 FTIR: PAA-PVA nanofibre mat before and after thermal crosslinking. 93

4.3.3 Crosslinking of PAA-PVA and PVA-GA 95

4.3.3.1 Water resistance of PAA in PAA-PVA crosslinked nanofibres 96

4.3.4 Water resistance of nanofibre: mass spectrometry 97

4.3.5 Ethylene glycol crosslinked polyacrylicacid (PAA-EG) nanofibre mats 100

4.3.6 FTIR: PAA-EG crosslinked nanofibre mats 101

4.3.7 TAllylPyP$_{ads}$-(PAA-EG) 101

4.4 Characterisation of covalently functionalised electrospun nanofibres (ENF) with photosensitisers 102

4.4.1 Morphology of PAN-Jeff nanofibres mats 103

4.4.2 Immobilisation of PPIX onto PAN-Jeff nanofibres 103

4.4.3 Determination of amine availability on functionalised ENF 106

4.4.4 TAllylPyP$_{cov}$-(PAA-EG) 110

4.4.5 Functionalisation of PAA-EG with TAllylPyP 110

4.4.6 FTIR TAllylPyP$_{cov}$-(PAA-EG) 111

4.4.7 SEM of TAllylPyP$_{cov}$-(PAA-EG) 112

4.4.8 TAminelPyP$_{cov}$-(PAA-EG) 113

4.4.9 Functionalisation of PAA-EG with TAminePyP 113

4.4.10 SEM of TAminePyP$_{cov}$-(PAA-EG). 116

4.5 Confirmation of covalent immobilisation of TAllylPyP and TaminePyP onto PAA-EG nanofibre 117

4.6 Confirmation of singlet oxygen generation by photosensitiser immobilised nanofibre mat. 119

Chapter 5 Photodynamic inactivation by functionalised electrospun nanofibres 120

5.1 Overview 120

5.1.1 Adsorption of photosensitiser to nanofibre mats 121

5.1.2 Covalent modification of nanofibre mats with photosensitisers 121

5.2 PDI by Jeffamine doped polyacrilonitrile (PAN-Jeff) nanofibre mats 122

5.2.1 PDI of *E.coli* by PPIX-(PAN-Jeff) nanofibre mats 122

5.2.2 PDI of *E.coli* by PPIX-(PAN-Jeff) nanofibre mats 124

5.3 PDI of carbenicillin resistant *E. coli* BL21 (DE3) by TMPyP immobilised (adsorbed) onto PAA-PVA nanofibre mats 126

5.4 PDI of *E. coli* NCTC 10418 by TMPyP immobilised (adsorbed) onto PAA-EG nanofibre mats 129

5.5 PDI of *E. coli* NCTC 10418 by TAllylPyP immobilised (adsorbed) onto PAA-EG nanofibre mat 130

5.6 PDI of *E. coli* NCTC 10418 by TAllylPyP covalently immobilised onto PAA-EG nanofibre mats 132

5.7 PDI of *E. coli* NCTC 10418 by TAminePyP covalently immobilised onto PAA-EG nanofibre mats 134

5.8 Conclusions 136

Chapter 6 General Discussion 137

6.1 Introduction 137

6.2 Specific outcomes: covalent immobilisation of tetra cationic photosensitisers with ENF 137

6.2.1 Porphyrin conjugation with polymer for water sterilisation 140

6.3 Nanofibre electrospinning 141

6.4 Photosensitiser synthesis 142

6.5 Covalent immobilisation of photosensitisers onto electrospun nanofibres 143

6.6 Solar energy and water disinfection capacity by photosensitiser functionalised nanofibre mats 143

6.7 Unique contribution and scopes of future research 144

List of Abbreviations 146

List of References 148

Appendix A. Proton NMR of TAllylPyP

Appendix B. Mass Spectra of TAllylPyP

Appendix C. Proton NMR of TAminePyP

Appendix D. Mass Spectra of TAminePyP

Appendix E. List of Publications

List of Tables

Table 1.1 Sources and health risk of common microorganisms responsible for water borne diseases. 5

Table 1.2 Sources of most common organic pollutants in water and the potential health risks due to the presence of these pollutants in water. 7

Table 1.3 Sources and potential health risk results from common hazardous inorganic contaminants in water accumulated from different anthropogenic activities. 8

Table 1.4 Suggested periods of vulnerability for different outcomes associated with disinfection-by-product exposure. 10

Table 1.5 Types of membranes for wastewater treatment. 11

Table 1.6 Sources and potential health risk results from common hazardous disinfectants and their by-products in water. 12

Table 1.7 Overview of different kinds of disinfection processes against several parameters. 13

Table 1.8 Photosensitisers loaded or immobilised on nanomaterials or polymers for water disinfection by PDI. 20

Table 1.9 Some recently electrospun synthetic and natural polymers and the main function in the water treatment sector, adopted from Feng (2009) 24

Table 2.1 Polymers, cross-linkers and solvents used for electrospinning of nanofibres. 36

Table 2.2 Electrospinning condition and parameters for nanofibre production 44

Table 2.3 Description of photosensitisers used for PDI of contaminants in water 46

Table 2.4 Antibacterial activity of photosensitiser in solutions. 50

Table 4.1 Percentage of amount of PPIX uptake by PAN-Jeff with varying concentration of PPIX. 105

Table 4.2 Determination of amount of PPIX (100µm) immobilised onto PAN-Jeff with varying incubation time. 105

List of Figures

Figure 1.1 Schematic illustration of photodynamic action mechanism of photosensitiser. 15

Figure 1.2 Mechanism of antibacterial activity exerted by ROS. 17

Figure 1.3 Schematic diagram showing photo-remediation of contaminated water by photosensitiser (PS) loaded electrospun nanofibre mats. 19

Figure 1.4 Five commercial applications for electrospun nanofibre mats, a function of overall patent filing percentage, during 1994–2012. 22

Figure 1.5 Structural difference between Gram-positive and Gram-negative bacterial cell wall. 27

Figure 1.6 Structure of Tetra cationic photosensitisers used in this research. 30

Figure 2.1 Light source of PDI experiments. 35

Figure 2.2 Experimental setup for PDI in solution. 35

Figure 2.3 Schematic diagram of key steps of this project. 37

Figure 2.4 Electrospinning of nanofibre mats: apparatus and process. 38

Figure 2.5 Sandwiched electrospun nanofibre (ENF) in between two polypropylene sheets. 42

Figure 2.6 Structural design of flow cell for water treatment. 43

Figure 2.7 Structure of TAllylPyP - (5,10,15,20-Tetrakis(4-N-allylpyridyl)- porphyrin (Tall4PyP). 46

Figure 2.8 Synthesis of TAllylPyP - (5,10,15,20-Tetrakis(4-N-allylpyridyl)- porphyrin (Tall4PyP). 47

Figure 2.9 Structure of TAminePyP (5,10,15,20-Tetrakis(1-ethylamine-4-pyridyl)-21H,23H-porphyrin). 48

Figure 2.10 Synthesis of TAminePyP (5,10,15,20-Tetrakis(1-ethylamine-4-pyridyl)-21H,23H-porphyrin). 48

Figure 2.11 Schematic of experimental set up of PDI by photosensitiser in solution and photosensitiser functionalised electrospun nanofibre mats. 52

Figure 2.12 Reaction scheme of photosensitiser immobilisation onto the electrospun nanofibre surface. 54

Figure 2.13 Amidation to block the free carboxylic group of PPIX by Propylamine was coupled to free –COOH using EDC. 55

Figure 2.14 Amine determination onto nanofibre surface (midland blotting). 56

Figure 2.15 Schematic of palladium catalysed allylic acyloxylation to immobilise TAllylPyP onto PAA-EG nanofbre. ( ), nanofibre mats. 58

Figure 2.16 Schematic of TAminePyP immobilisation on to PAA-EG nanofibre mats. 60

Figure 3.1 Growth curves of *E. coli* NCTC 10418..... 65

Figure 3.2 Growth curve of *E.coli* BL21 (DE3). 66

Figure 3.3 Calibration of light intensity at sample surface. 67

Figure 3.4 PDI of Gram-negative bacteria *E. coli* NCTC 10418 by PPIX in solution. 69

Figure 3.5 PDI of Gram-positive bacteria *Staphylococcus epidermidis* with PPIX in solution. 70

Figure 3.6 Dark toxicity of TMPyP in solution with Gram-negative bacteria *E. coli* NCTC 10418. 72

Figure 3.7 PDI of Gram-negative bacteria *E. coli* NCTC 10418 with TMPyP in solution. 73

Figure 3.8 PDI of Gram-negative *E. coli* NCTC 10418 at higher intensity light with TMPyP in solution. 74

Figure 3.9 PDI of bacteria *E. coli* NCTC 10418 by different concentration of TAllylPyP solution at low intensity of light. 75

Figure 3.10 PDI of bacteria *E. coli* NCTC 10418 by low intensities of cold light with 50 µM TAllylPyP in solution. 76

Figure 3.11 PDI of bacteria *E. coli* NCTC 10418 by high intensities of cold light with 50 µM TAminPyP solution. 77

Figure 3.12 PDI of bacteria *E. coli* NCTC 10418 at high intensity of cold light with 30 µM TAminePyP in solution. 78

Figure 3.13 PDI of carbenicillin resistant bacteria BL21 (DE3) by TMPyP in solution at low intensity of light. 79

Figure 3.14 PDI of carbenicillin resistant bacteria BL21 (DE3) by TAllylPyP in solution at 70 mW/cm^2. 81

Figure 4.1 Structure of 5, 10, 15, 20- tetrakis (1- methylpyridinium-4-yl) porphyrin (TMPyP). 84

Figure 4.2 Structure of Tetra allyl pyridyl porphyrin (TAllylPyP). 85

Figure 4.3 Structure of Tetra amine pyridyl porphyrin (TAminelPyP). 85

Figure 4.4 FTIR spectra of tetra allyl pyridyl porphyrin (TAllylPyP). Nicolet 5700 FTIR spectrometer (Thermo Nicolet Corporation) 88

Figure 4.5 FTIR spectra of tetra amine pyridyl porphyrin (TAminePyP). Nicolet 5700 FTIR spectrometer (Thermo Nicolet Corporation) 90

Figure 4.6 SEM images of different stages of functionalisation of PAA-PVA nanofibre mats. 92

Figure 4.7 SEM images of $TMPyP_{ads}$-(PAA-PVA) after reuse several times of nanofibres. 93

Figure 4.8 FTIR spectra of PAA-PVA electrospun nanofibre mat before and after thermal crosslinking. 94

Figure 4.9 Expected crosslinking between PAA and PVA because of heat treatment. 95

Figure 4.10 Schematic illustration of expected intramolecular and intermolecular crosslinking between PVA and GA. 96

Figure 4.11 Absorbance (405 nm) of polyacrylic acid during incubation of PAA/PVA nanofibre into water over 60 days. 97

Figure 4.12 Ionisation Mass spectra of pure PAA-PVA washing. 99

Figure 4.13 SEM images of PAA-EG before and after heat treatment of nanofibre. 100

Figure 4.14 FTIR spectrum of PAA-EG before and after thermal crosslinking. 101

Figure 4.15 FTIR spectrum of PAA-EG before and after TAllyl adsorbed nanofibres. 102

Figure 4.16 Microscopic pictures of nanofibres with three different thickness of same mother ENF sheet. 103

Figure 4.17 Calibration of PPIX immobilisation onto ENF with OD_{410}..... 105

Figure 4.18 Percentage of PPIX immobilisation with time. 106

Figure 4.19 Characterization of photosensitiser functionalized electrospun nanofibre surface by midland blotting. 107

Figure 4.20 Acetic anhydride reacts with amines to form amide bond derivatives. 108

Figure 4.21 Characterization of photosensitiser functionalized electrospun nanofibre surface by Midland blotting. 109

Figure 4.22 Reaction scheme of TAllylPyP immobilisation onto PAA-EG electrospun nanofibres mate surface. 111

Figure 4.23 Tetra allyl pyridyl porphyrin functionalised PAA-EG: TAllylPyPcov-(PAA-EG). 111

Figure 4.24 FTIR spectra of tetra allyl pyridyl porphyrin (TAllylPyP) immobilised onto PAA-EG nanofibre mat $TAllylPyP_{cov}$-(PAA-EG). 112

Figure 4.25 SEM of tetra allyl pyridyl porphyrin (TAllylPyP) immobilised onto PAA-EG nanofibre mat $TAllylPyP_{cov}$-(PAA-EG). 113

Figure 4.26 Reaction scheme of TAminePyP immobilisation onto PAA-EG electrospun nanofibres mate surface. 114

Figure 4.27 Tetra amine pyridyl porphyrin functionalised PAA-EG: $TAminePyP_{cov}$-(PAA-EG) 115

Figure 4.28 FTIR spectra of tetra amine pyridyl porphyrin (TAminePyP) immobilised onto PAA-EG nanofibre mat TAminePyP$_{cov}$-(PAA-EG). 116

Figure 4.29 SEM image of PAA-EG nanofibre before and after covalent modification with TAminePyP photosensitiser. 117

Figure 4.30 Confirmation of strong binding of TAllyLPyP and TAminePyP onto PAA-EG nanofibres instead of adsorption. 118

Figure 4.31 TMPyP release in water due to weak electrostatic bonding with PAA-EG nanofibre mat in NaOH. 118

Figure 4.32 Singlet oxygen production by TMPyP and TAllylPyP immobilised nanofibre mats. 119

Figure 5.1 PDI with PPIX-(PAN-Jeff) (with and without blocking the remaining carboxylic group of PPIX). 123

Figure 5.2 PPIX immobilised onto PAN-Jeff (before and after). 124

Figure 5.3 Flow system to convert of PAN to PAA and PPIX immobilisation onto PAA. 125

Figure 5.4 Photo treatment of *E. coli* NCTC 10418 in flow cell made of PPIX conjugated PAA nanofibre. 126

Figure 5.5 Effect of PDI of BL21 (DE3) by TMPyP$_{ads}$-(PAA-PVA) in bacteria agar plates. 127

Figure 5.6 PDI of carbenicillin resistant *E. coli* strain BL21 (DE3) with TMPyP$_{ads}$-(PAA-PVA) nanofibre. 128

Figure 5.7 PDI of *E. coli* NCTC 10418 with TMPyP$_{ads}$-(PAA-EG) nanofibre mat. 129

Figure 5.8 PDI Study of *E. coli* NCTC 10418 with TAllylPyP$_{ads}$-(PAA-EG) nanofibre mat. 131

Figure 5.9 Effect of PDI of *E. coli* NCTC 10418 by TAllylPyP$_{cov}$-(PAA-EG) in bacteria agar plates. 132

Figure 5.10 PDI study of *E. coli* NCTC 10418 with covalently immobilised TAllylPyP with PAA-EG nanofibre mat. 133

Figure 5.11 Effect of PDI of *E. coli* NCTC 10418 by TAminePyP$_{cov}$-(PAA-EG) in bacteria agar plates. 134

Figure 5.12 PDI Study of *E. coli* NCTC 10418 with covalently functionalised TAminePyP with PAA-EG nanofibre mats. 135

Chapter 1

Introduction

1.1 Overview

Water is the most essential need in human life. Assuring access of safe drinking water is one of the best ways to improve health sector. The rapid growth of undesirable microbes spread widely in the environment, is a threat to human and wildlife. Only waterborne diseases can cause for millions of deaths annually worldwide (Malato *et al.*, 2009). Waterborne microorganisms have caused the outbreak of almost two hundred human diseases in just 7 years (2004–2010) (Baldursson and Karanis, 2011). According to the WHO/UNICEF joint monitoring programme, nearly nine million children under five years of age die each year (WHO and UNISEF, 2008). Another report recently published that 29% of the global population (2.1 billion people) lacked safely managed drinking water services in 2015 (WHO and UNICEF, 2017). Two hundred and sixty-three million people need to spend over 30 min per round trip to collect water from an improved source (constituting a limited drinking water service) and 10,159 million people still collected drinking water directly from surface water sources. Of them 58% lived in sub-Saharan Africa (WHO and UNICEF, 2017). Diarrhoea and pneumonia are a major cause of deaths in population. WHO/UNICEF also reported that nearly 10% of the global disease burden could be reduced through supply of safe water. On the other hand, developed countries are more concerned to reduce energy consumption in wastewater treatment sector. Global water demand continues to escalate, driven by an increasing population and resulting in increasing energy consumption. Water professionals are emphasising the need for low cost, minimal energy techniques for water treatment to meet the emergence global need.

Conventional disinfection mainly involves chlorination or ozonisation. Another cheap alternative for disinfection is using direct sunlight solar disinfection (SODIS) (Pooi and Ng, 2018; Shannon *et al.*, 2008; Somani and

Ingole, 2011). However these methods face limitations such as production of harmful by-products, involving high cost, limited water volume, and time consuming. In order to overcome these inadequacies, remarkable efforts have been carried out to develop more effective water disinfection methods than the conventional systems that are environmentally friendly, cost effective, and highly efficient (Farhaoui and Derraz, 2016; Pooi and Ng, 2018; Somani and Ingole, 2011).

This study is aimed at developing a cost effective low energy approach by combining photodynamic inactivation (PDI) using sunlight activated photosensitisers attached to a solid surface. The surface is a nanofibre mats mat produced by electrospinning, which is a versatile and low-cost technique to fabricate very high surface area nanofibre fabric. PDI of micro-organisms by photosensitisers is a well-established approach which relies on light driven production of reactive oxygen species (ROS). This study describes photodynamic inactivation by photosensitisers immobilised onto electrospun nanofibre mats for water sterilization. To keep the treated water free of chemicals or disinfectants, the photosensitiser is immobilised onto the electrospun nanofibre (ENF) mats covalently, and the ENF composite is developed to be water stable.

The water stable nanofibre mats spun using a range of polymers, using industrial scale electrospinning nanospider technology. To avoid the use of hazardous solvents, water-soluble polymers were used to make the nanofibre mats, and pre and post crosslinking were carried out to make the electrospun nanofibre mats stable in water. After initial studies the most durable combination of polymers were chosen. In addition, the electrospinning voltage was optimising to allow to get the continuous production of nanofibre mats. Different tip to collector distances were also studied to optimise the electrospinning process.

For this study photosensitisers were initially selected from commercial sources and subsequently, analogues were synthesised to facilitate covalent attachment. Microorganisms such as bacteria and viruses are typically

anionic (Spagnul *et al.*, 2015) so ideally cationic photosensitisers are needed to avoid electrostatic repulsion. At present there are few commercially available photosensitisers that are cationic, and these do not have functional groups for covalent attachment. Accordingly, it was necessary to synthesise novel photosensitisers. The synthesised photosensitisers were characterised using UV-Visible spectroscopy, nuclear magnetic resonance (NMR), infra-red (IR) spectroscopy and mass spectroscopy (MS) techniques.

Functionalisation of the nanofibre mats was the most critical part of this study. The nanofibre mats were developed with pendant carboxylic groups so the overall charge of the nanofibre mats became negative. Although this would on its own be repulsive to anionic microorganisms, it permits construction of easy linkage and straight forward bonding to amine group on photosensitisers, or simple electrostatic bonding with polycationic photosensitisers.

PDI was carried out both with photosensitiser in solution and with photosensitiser functionalised nanofibre mats. Optimisation of photosensitiser loading, intensity of light and duration of illumination were also studied. Since they are the most problematic of water pollutants, Gram-negative bacteria were used as model microorganisms. For example, the Gram-negative *E. coli* was routinely checked as a surrogate for more pathogenic water-borne bacteria, as is an abundant indicator of faecal contamination. However, Gram-positive bacteria were also studied to find out the efficiency of photosensitiser mediated cell killing. In addition to the commonly used *E. coli* strains, antibiotic resistant strains were studied. Finally, the potential of PDI to degrade organic pollutants were investigated.

1.2 Types, sources and consequences of contaminants

There are two basic types of water contaminants; microbial and chemical pollutants. Chemical pollutants can be further classified into organic and inorganic pollutants. Generally, all surface water contains pollutants such as inorganic chemical contaminants from the geological strata through which the water flows. There are natural contaminants i.e. minerals, turbidity and dead plants, whereas microorganisms and industrial chemicals are known as anthropogenic pollutants. The aim of this study is photo-remediation of microbial contaminants.

1.3 Microbial contaminants

The primary microbial pathogens of concern that are transmitted by water are divided into three groups, bacteria, viruses, and protozoans. The most common pathogens that are responsible for water borne diseases are listed in Table 1.1.

Microbial contaminants	**Sources**	**Health Effects**
Bacteria		
Escheria coli	Domestic and animal faecal	Gastroenteritis, diarrhoea, vomiting
Salmonella typhi	Domestic and animal faecal	Typhoid fever
Legionella	water; multiplies in heating systems	Legionnaire's Disease, a type of pneumonia
Vibrio cholera	Sediments, shellfish asymptomatic	Severe diarrhoea
Protozoan		
Cryptosporidium	Human and animal faecal waste	Severe diarrhoea, nausea, abdominal cramps, and fever
Giardia lamblia	Human and animal faecal waste	Gastrointestinal illness (such as diarrhoea, vomiting, and cramps)
Viruses		
Adenovirus serotypes; 40 and 41 are primary concern	Human and animal faecal waste	Acute respiratory disease, pneumonia-Gastrointestinal illness : diarrhoea, vomiting, conjunctivitis and cramps
Astroviruses, Calcivirus, Sapporovirus, Reovirus, Rotavirus, Enterovirus	Human	Gastroenteritis, diarrhoea, vomiting, Heart anomalies

Table 1.1 Sources and health risk of common microorganisms responsible for water borne diseases.

1.4 Chemical contaminants

1.4.1 Organic water pollutant

Organic pollution in water originates from domestic sewage, urban run-off, industrial effluents and agriculture wastewater, sewage treatment plants and industry including food processing, pulp and paper making, agriculture and aquaculture. During the decomposition process of organic pollutants, the dissolved oxygen in the receiving water may be consumed at a greater rate than it can be replenished, causing oxygen depletion and having severe consequences for the watercourse biota. Wastewater with organic pollutants contains large quantities of suspended solids which reduce the light available to photosynthetic organisms and, on settling out, alter the characteristics of the river bed, rendering it an unsuitable habitat for many invertebrates. The most common organic pollutants are termed persistent organic pollutants (POPs). A few of common organic water contaminants are listed in Table 1.2.

Several methods such as coagulation, filtration with coagulation, precipitation, ozonation, adsorption, ion exchange, reverse osmosis and advanced oxidation processes have been used for the removal of organic pollutants from polluted water and wastewater. These methods have been found to be limited in effectiveness, since they often involve high capital and operational costs. Ion exchange and reverse osmosis are more attractive processes because the pollutant can be recovered (Kumar, 2006; Rashed, 2013; Turneaure and Russell, 1916) along with their removal from the effluents. However, in general reverse osmosis, ion exchange and advanced oxidation processes are not economically feasible because of their relatively high investment and operational cost. Researchers continuously search for efficient, low cost techniques for the removal of highly toxic organic compounds from water.

Contaminants	Potential Health Effects	Sources of Contaminants
Acrylamide	Nervous system or blood problems; increased risk of cancer	Added to water during sewage/wastewater treatment
Benzo(a)pyrene (PAHs)	Reproductive difficulties; increased risk of cancer	Leaching from linings of water storage tanks and distribution lines
Chlorobenzene	Liver or kidney problems	Discharge from chemical and agricultural chemical factories
o-Dichlorobenzene	Liver, kidney, or circulatory system problems	Discharge from industrial chemical factories
Ethylene dibromide	Problems with liver, stomach, reproductive system, or kidneys; increased risk of cancer	Discharge from petroleum refineries
Hexachlorobenzene	Liver or kidney problems; reproductive difficulties; increased risk of cancer	Discharge from metal refineries and agricultural chemical factories
Polychlorinated biphenyls (PCBs)	Skin changes; thymus gland problems; immune deficiencies; reproductive or nervous system difficulties; increased risk of cancer	Run off from landfills; discharge of waste chemicals
Toluene	Nervous system, kidney, or liver problems	Discharge from petroleum factories
Vinyl chloride	Increased risk of cancer	Leaching from PVC pipes; discharge from plastic factories

Table 1.2 Sources of most common organic pollutants in water and the potential health risks due to the presence of these pollutants in water. (Avetta *et al.*, 2013; Cabral, 2010; John and Mark, 2003).

1.4.2 Inorganic pollutants

Generally industrial, agricultural, and domestic waste results in the pollution of water, and water pollutants can cause severe damage to human and animal health. One of the most important categories of water pollutants is inorganic chemicals. The sources of few common hazardous inorganic contaminants in water and potential health risk are listed in Table 1.3.

Inorganic Contaminants	Sources of Contaminant in Drinking Water	Health Effects
Arsenic	Mining, pesticides, and natural leaching /erosion, heavy pumping of groundwater	Toxic, carcinogenic, Skin damage or problems with circulatory systems,
Chromium	Steel and pulp mills Discharge; erosion of natural deposits	Skin irritation, damage kidney, liver, and nerve tissues.
Lead	Corrosion of pipes, plumbing, or faucets	Adversely affect the nervous system, and damage red blood cells, kidney function, decreased intelligence development,
Nitrates	Fertilizers and human or animal waste,	Blue baby syndrome, shortness of breath, nausea, vomiting, diarrhoea, lethargy, loss of consciousness and possible death.
Perchlorate	Rocket fuel, spills or leaks at military facilities	Thyroid harms, carcinogenic, delayed development
Antimony	Petroleum refineries discharge; fire retardants, ceramics; electronics;	Increased in blood cholesterol; decrease in blood sugar
Barium	Drilling wastes; metal refineries; erosion of natural deposits	Increased blood pressure
Cadmium	Corrosion of galvanized pipes; erosion of natural deposits; metal refineries; waste batteries and paints industries runoff	Kidney damage
Copper	Corrosion of household plumbing systems; erosion of natural deposits	Short term exposure: G gastrointestinal distress, Long term exposure: Liver or kidney damage, Wilson's Disease patients are affected
Fluoride	Water additive promotes strong teeth; erosion; fertilizer and aluminium factories discharge	Bone disease (pain and tenderness of the bones); Children may get mottled teeth
Mercury (inorganic)	Erosion; discharge refineries; landfills croplands runoff	Kidney damage

Table 1.3 Sources and potential health risk results from common hazardous inorganic contaminants in water accumulated from different anthropogenic activities.

1.5 Common disinfectants for drinking water

Europe and USA have taken a similar course for drinking water disinfection. Most European countries started to apply drinking water disinfection from the end of the nineteenth century to the beginning of the twentieth century. The oldest and best-known drinking water disinfectant in Europe is chlorinated bleach. After researching the disinfection mechanism of chlorine for water purification, in 1905 the London Metropolitan Water Board started disinfecting drinking water (Corfield, 1897). In Europe, most drinking water production companies use chlorine as a disinfectant. It is added to water as chlorine gas, calcium hypochlorite or sodium hypochlorite. For odour control, ozone is added (Neumann, 1981). Generally, for surface water disinfection, chlorine is used as a primary disinfectant. European countries use ozone often as an alternative disinfectant for drinking water. Many countries in 1906 started applying ozone disinfect drinking water and now, as a primary oxidant and disinfectant, ozone or chlorine dioxide is used in Italy and Germany. Great Britain, like several other EU countries, uses chloramines for residual disinfection in the distribution network and for the removal of disinfection by-products. After the discovery of chlorinated by-products (Baker *et al.*, 2002), the search for alternative disinfectants intensified. Disinfection by-products are chemical, organic and inorganic substances that form during a reaction of the disinfectant like chlorine with naturally present organic matter in the water such as humid acid and fluvic acid. These materials end up in water during the decomposition of plant matter (Barrett *et al.*, 2000). During the seventies, after developing analytical methods such as gas chromatography scientists discovered the formation of disinfection by-products (Weinberg, 2009). These by-products can be harmful to human health.

Researchers particularly became alarmed by evidence that long-term ingestion of small amounts of these chemicals (Table 1.4) could be hazardous to health. Thus, the scientists are actively seeking to change the disinfection processes involved in water treatment process.

Reproductive outcomes	Vulnerable period	References/comments
Intrauterine growth-related	2nd/3rd trimesters of gestation	(Lewis *et al.*, 2006) (Wright *et al.*, 2003)
Congenital anomalies	1st trimester of gestation	Organogenesis period
Sperm quality	3 months	Spermatogenesis period
Cancer (bladder)	Decades (>25 years)	(Villanueva *et al.*, 2004)
Respiratory outcomes (swimming pools)	<2 years of age? Childhood?	Not established (Villanueva *et al.*, 2015)

Table 1.4 Suggested periods of vulnerability for different outcomes associated with disinfection-by-product exposure.
(Villanueva *et al.*, 2015)

1.5.1 Disinfection methods

Worldwide, many commonly used disinfection agents have been proved to be toxic. So, there is an urgent need to find alternative methods of disinfection. The methods of disinfection are classified into three categories, i.e., physical methods; (ii), chemical methods; and (iii), membrane processes (Baker *et al.*, 2002). The physical methods of disinfection mainly include - boiling/heating; direct solar exposure; TiO_2 films and sunlight; U-V radiation; other electromagnetic radiation; ultra-sonic sound and activated carbon as an absorbent (Baker *et al.*, 2002). Chemical methods used for disinfection of water are ozone, hydrogen peroxide, acid and alkali, other halogens, lime, chlorite and chlorine dioxide, anodic oxidation and potassium permanganate. Membrane processes include microfiltration and ultrafiltration; reverse osmosis and photosensitisers immobilised on membrane. Membrane filtration is powerful system for various applications including wastewater treatment and filtration of particulate contaminants. Although, this system is not efficient enough to remove soluble contaminants (Muruganandham *et al.*, 2014; Amin *et al.*, 2013; Jackson *et al.*, 1999a)

There are different kinds of membranes available for wastewater treatment (Table 1.5). Regarding lifetime and cost effectiveness membrane filtration systems are more expensive than other conventional methods of wastewater disinfection (Jackson *et al.*, 1999b). An overview of different kinds of disinfection processes against several parameters shows that the combined effect of two or more disinfection processes and pre-treatment gave better and efficient water purification (Table 1.5).

	Microfiltration (MF)	**Ultrafiltration (UF)**	**Reverse osmosis (RO)**	**Nano-filtration (NF)**
membrane cut-off	0.05-2 µm.	~ 100 Da	> 50 Da.	>200 Da
Reject	Particles	organic materials, viruses and large pathogens	Na and organic molecules, desalination	multivalent ions, dissolved organic matter

Table 1.5 Types of membranes for wastewater treatment.

This project focuses on the antimicrobial mechanism of photosensitisers immobilised on electrospun nanofibre mats that can be used for disinfection of water. The antimicrobial activity of photosensitiser related with Gram-negative and Gram-positive bacteria also discussed. Photo-remediation activity of photosensitisers on organic pollutants is also highlighted.

Disinfectant to control microbes	**Health Effects from Long-Term Exposure**	**Organo-halogenic disinfection by-products**	**Inorganic disinfection by-products**	**Non-halogenic disinfection by-products**
chlorine (as Cl_2)/ hypochloric acid (HOCl)	Eye/nose irritation; stomach discomfort	trihalomethanes, halogenic acetic acids, haloacetonnitrils, chlorine hydrates, chloropicrin, chlorophenols, N-chloramines, halofuranones, bromohydrins	chlorate (particularly the application of hypochlorite)	aldehydes, alkanic acids, benzene, carboxylic acids
Chlorine dioxide (ClO_2)	Anemia; infants and young children: nervous system effects	-	chlorite, chlorate	unknown
Chloramines (NH_3Cl etc.)	Eye/nose irritation; stomach discomfort, anemia	haloacetonnitrils, cyano chlorine, organic chloramines, chloramino acids, chlorohydrates, haloketons,	nitrite, nitrate, chlorate, hydrazine	aldehydes, ketons
ozone (O_3)	Toxic but limited Residual disinfection power, need Cl for long term disinfecting effect	bromoform, monobromine acetic acid, dibromine acetic acid, dibromine acetone, cyano bromine	chlorate, iodate, bromate, hydrogen peroxide, hypo bromic acid, epoxy, ozonates	aldehydes, ketons, ketoacids, carboxylic acids

Table 1.6 Sources and potential health risk results from common hazardous disinfectants and their by-products in water. (Baker *et al.*, 2002; John and Mark, 2003; Weinberg, 2009).

		Microbiological safety	Chemical safety	Customer aesthetic	Ease of monitoring	Ability to treat difficult water	Operating cost	Capital cost	Commercial development	Scale up	Waste and easy use	Reliability
Ground water	Chlorine	-	-	-	+	+	+	+	+	+	+	+
	UF only	-	+	+	-	+		■	-	-	■	-
	UV only	+	+	+	■	+	+	■	+	+	■	■
Surface water and sewage	Chlorine only	-	-	-	+	-	+	+	+	+	+	-
	Pre-treat+ Chlorine	+	-	-	+	-	■	■	+	+	■	-
	UF only	-	-		-	-	■	■	-	-	■	-
	Pre-treat+ UF	■	+	+	-	+	-	-	-	-	-	-
	Pre-treat+ Ozone+ UF	-		-	-	+	-	-	-	-	-	-
	MF+ UV	■	+	-	■	-	+	■	-	-	■	+
	Pre-treat+ UV	■	+	+	■	-	+	■	+	+	■	■
	Pre-treat+ ozone+ UV	+		+	+	+	-	-	+	+	■	+

Table 1.7 Overview of different kinds of disinfection processes against several parameters.

(UF), ultrafiltration; (MF), microfiltration; (UV), ultraviolet; Pre-treatment e.g. coagulation/ sedimentation; +, better than average; - , worse than average; ■, average (Jackson *et al.*, 1999b).

1.6 Photodynamic Inactivation (PDI) of microorganisms

Visible light of the appropriate wavelength typically 400-600 nm is able to excite photosensitisers, resulting in photodynamic inactivation. In the molecular ground-state or triplet state of oxygen ($^3O_2$), the excited-state photosensitiser transfers energy to produce reactive oxygen species (ROS) that are able to kill cells (Liu *et al.*, 2012). Nowadays, photodynamic therapy (PDT) has become popular for cancer therapy (Liu *et al.*, 2012). Recently PDI has been used as an antimicrobial treatment (Liu *et al.*, 2012) as it has many favourable features for the inactivation of microbial pathogens. This has a broad spectrum of action, efficient inactivation of antibiotic-resistant strains, low mutagenic potential for resistance developments and lack of selection of photo-resistant microbial cells (Liu *et al.*, 2012).

After absorption of a photon of light at specific wavelength, an electron in the highest occupied molecular orbital (HOMO is excited to the lowest unoccupied molecular orbital (LUMO) and causes the photosensitiser to reach the unstable and short-lived excited singlet state (Figure 1.1), although at this stage, several processes may occur rapidly such as fluorescence and internal conversion to heat. However, for PDI the reversal of the spin of the excited electron to the triplet state (Figure 1.1) of the photosensitiser is the most important. This excited triplet state is less energetic than the excited singlet state and has a considerably longer lifetime, 4.3 times higher than lifetime of single state. Because of this longer lifetime (many microseconds as compared to a few nanoseconds) (Liu *et al.*, 2012) the triplet photosensitiser can survive long enough to carry out diffusion mediated interaction, which is much less likely for the excited singlet photosensitiser. There are two different pathways of photochemical reactions of the triplet state. The Type I mechanism comprises transfer of electron or hydrogen atom from one molecule to another whereas the Type II mechanisms involves energy transfer to molecular oxygen. The type I pathway can involve an electron transfer reaction from the photosensitiser to O_2 in the triplet state, which results in the formation of toxic oxygen species such as

$O_2^{\bullet-}$ that are able to further transfer and form ROS, such as H_2O_2 and $^{\bullet}OH$, which are formed by the Fenton reaction in the presence of divalent metal ions as Fe^{2+}.

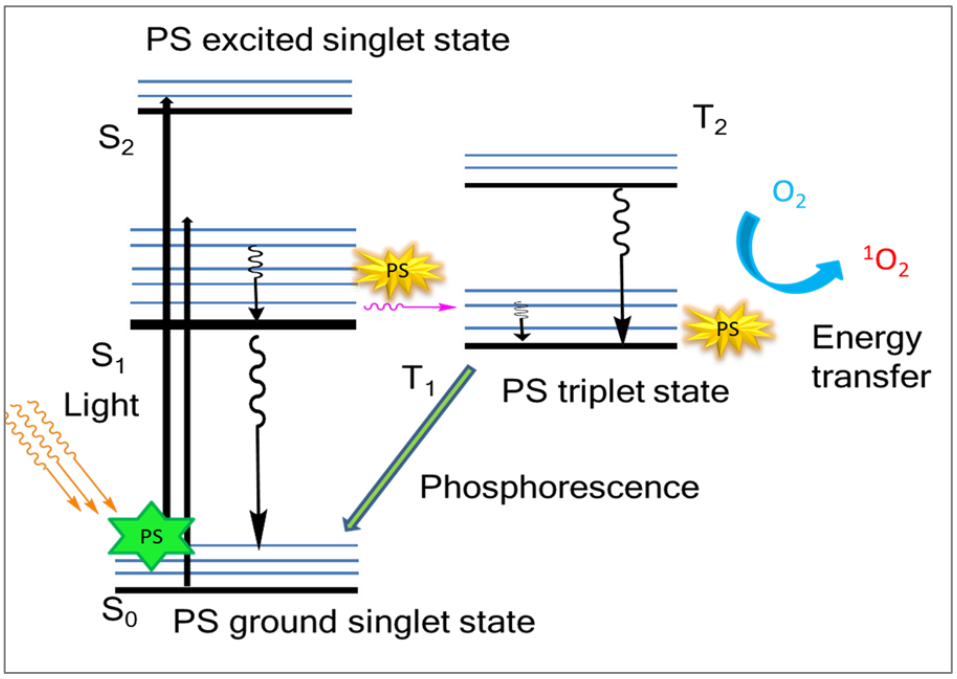

Figure 1.1 Schematic illustration of photodynamic action mechanism of photosensitiser.

The photosensitiser initially absorbs a photon that excites it to the first excited singlet state ($^1O^*_2$) and this can relax to the more long lived ground triplet state ($^3O_2$). This triplet photosensitiser ($^3O_2$) can interact with molecular oxygen in two pathways. Type I (T_1) and Type II (T_2) leading to the formation of reactive oxygen species (ROS) and singlet, respectively.

Interestingly both mechanisms can occur at the same time, but the relative proportion depends on the photosensitiser structure and also on the microenvironment the photosensitiser is in.

Another possible mechanism has been proposed that may operate in cases where the triplet-state photosensitiser is a good e^- donor. Here, H_2O_2 (formed from ($O_2^{\bullet-}$) can undergo a one electron reduction to form $^{\bullet}OH$ $^+$ ^-OH. The two most prevalent damaging ROS ($^{\bullet}OH$ and $^1O_2$) can react with many biomolecules in microbial cells. The exact targets and reaction mechanisms depend on the localisation of the photosensitiser generation. This is critical because most of the ROS are highly reactive and not able to travel far

(~100-200 nm) (Skovsen *et al.*, 2005; Frederiksen *et al.*, 2005; Triantaphylidès *et al.*, 2008) from their site of production because of their short lifetime (3-10 µs) (Maisch *et al.*, 2007). The relative abundance of the target biomolecules also plays a key role.

1.7 Antimicrobial activity of reactive oxygen

The history of evolution reveals the introduction of O_2 in the atmosphere as the first major pollutant. The abundant reaction between ferrous iron and oxygen results in the formation of harmful superoxide and hydroxyl radicals, which mainly affected macromolecules such as DNA, lipids and proteins (Cabiscol *et al.*, 2000). This section will briefly highlight how antimicrobial strategies are centred on reactive oxygen species. The reason for using photosensitisers to create excess oxidative stress to kill bacteria and the action of mechanism of photosensitiser will also be discussed (Farr and Kogoma, 1991).

Major classes of bactericidal activity, regardless of target, cause oxidative damage resulting in cellular death. Generally, major classes of antimicrobial agents follow a common mechanism (Figure 1.2) to cause cellular death in Gram-negative and Gram-positive bacteria. Harmful ROS are formed as a function of drug-induced disruptions to cellular metabolism and respiration.

Extremely toxic ROS can readily damage membrane lipids, proteins, and DNA. Being capable of attacking a diverse range of targets to exert antimicrobial activity, ROS are very versatile agents against a broad range of pathogens. Normally, partial reduction of molecular oxygen generates the most ROS.

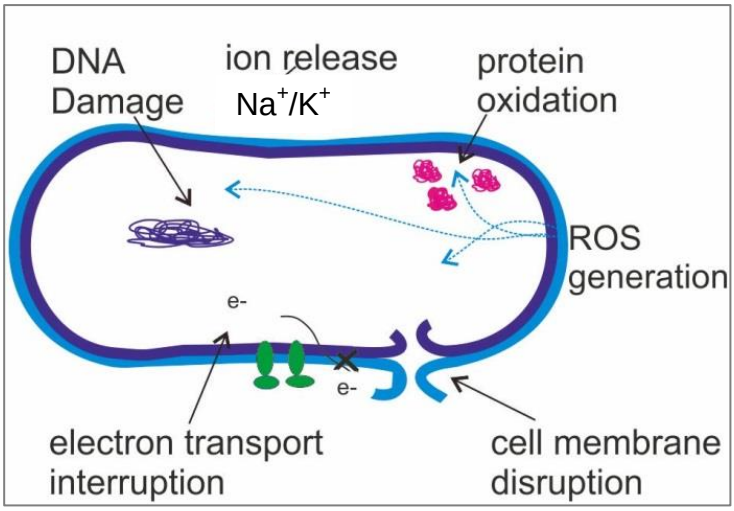

Figure 1.2 Mechanism of antibacterial activity exerted by ROS.

Common oxidative damage resulting in cellular death in bacteria by ROS is caused by disruptions in cellular metabolism, respiration and electron transportation through membrane. Extremely toxic ROS can readily damage membrane lipids, proteins, and DNA.

There are four major ROS species consisting of superoxide ($O^{\bullet -}_2$), hydrogen peroxide (H_2O_2), hydroxyl radical (•OH), and singlet oxygen ($^1O_2$) (Vatansever, 2013). The intensity and reactivity of $O^{\bullet -}_2$ and H_2O_2 are much less than those of $^{\bullet}OH$ and $^1O_2$, and can be detoxified by endogenous antioxidants, both enzymatic and non-enzymatics, that are induced by oxidative stress. On the contrary, $^{\bullet}OH$ or $^1O_2$, are extremely toxic and acutely lethal as there are no enzyme to detoxify them (Vatansever, 2013). Here in this research mainly advantage of antibacterial activity of singlet oxygen is acknowledged.

Almost all reactions involving singlet oxygen with biomolecules are additions of the $^1O_2$ to conjugated bonds. Typically, peroxides are the initial products. $^1O_2$ can add to olefins to produce allylic hydroperoxides and a shift in the double bond, or it can add to diene systems to produce endo-peroxides (Farr and Kogoma, 1991). Reactions of $^1O_2$ with unsaturated fatty acids or histidine are good examples of these types of reactions. $^1O_2$ can also undergo (2 + 2) cycloadditions to dienes to produce dioxetanes, which decompose to yield carbonyl compounds (Farr and Kogoma, 1991; Kwon and Foote, 1988). Finally, $^1O_2$ will react with a-tocopherol to produce a stable tocopherol radical called chromoxal. Many of the sensitizers which produce

$^1O_2$ are embedded within the membrane, and it is possible that $^1O_2$ is capable of initiating lipid peroxidation (Farr and Kogoma, 1991; Dargel, 1992).

It is likely that a lipid peroxidation chain reaction begins after hydrogen abstraction from an unsaturated fatty acid to form a lipid radical. The lipid radical (L) thus formed reacts with molecular oxygen to form a lipid peroxy radical ($ROO^{\cdot}$). The reaction is continues when the lipid peroxy radical attacks another unsaturated fatty acid and abstracts a hydrogen atom to form a fatty acid hydroperoxide (ROOH) and continues the initial reaction. The hydroperoxides thus formed will break down thermally or in the presence of O_2 or reduced transition metals to form lipid peroxy radicals (LOO') or lipid alkoxy radicals ($LO^{\cdot}$), both of which can initiate new rounds of peroxidation. It is also possible that NADH will donate an electron to the hydroperoxide to generate another lipid radical and water (Dargel, 1992). Lipid alkoxy radicals can undergo cleavage of C-C bonds to form unsaturated fatty acid aldehydes and alkyl radicals. The peroxidation of lipids thus generates products which are shorter than the initial fatty acid. In addition to producing fatty acyl chains that are shorter than the parent chain, the end products of lipid peroxidation include alkanes, ketones, epoxides, and aldehydes (Farr and Kogoma, 1991; Dargel, 1992; Niki *et al.*, 2005). When fatty acid chains become shortened or gain charges, their mobility within the membrane is altered and the membrane becomes more fluid (McCord *et al.*, 1971; Benga, 1985; Farr and Kogoma, 1991). An increase in membrane fluidity results directly in a loss of structural integrity. Structural integrity is required for transport of most nutrients, ATPase activity, motility, and prevention of osmotic imbalance (Kashket, 1985; Larsen, 1974). Because membrane permeabilisation will destroy the proton gradient across the cell membrane, the internal pH will drop, which in turn is likely to result in further oxidative damage (Farr *et al.*, 1988).

1.8 Why photosensitiser needs to be immobilised

Recently, immobilised photosensitisers for singlet oxygen generation have raised interest. There are several advantages to the use of immobilised photosensitisers in practical applications. In the case of water purification, for example, the potential to reuse photosensitisers without their ion into water makes environmental and economic sense. In the case of photochemical synthesis, immobilisation of the photosensitisers offers easy isolation of the reaction products from the photosensitiser.

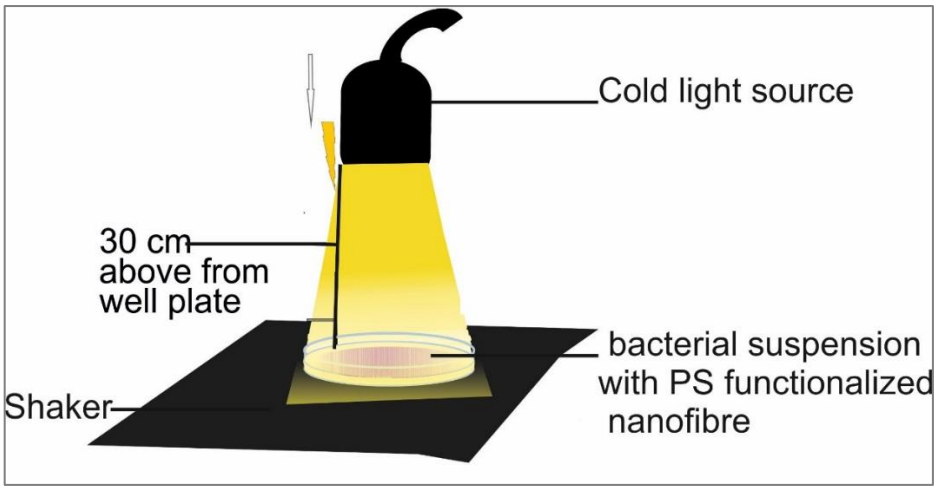

Figure 1.3 Schematic diagram showing photo-remediation of contaminated water by photosensitiser (PS) loaded electrospun nanofibre mats.

Contaminated water treated with photosensitiser immobilised electrospun nanofibre mats, visible light source activated photosensitiser produce singlet oxygens that cause the photo-inactivation of microorganism in water.

Recently studied photosensitisers immobilised or loaded on nanomaterials or as polymers for photodynamic inactivation of water are listed in Table 1.8. In addition, immobilised photosensitisers can be employed in a number of solvents, allowing flexibility in fine chemical synthesis

Photosensitiser	Immobilised on	Light Source	Microorganism	Ref
a) 9,10-anthraquinone-4-carboxylic acid b) cyanoaromatic, 9,14-dicyanobenzo [b]triphenylene-3-carboxylic acid (DBTP-COOH)	commercial silica	400-420nm UVA and visible light	*E. coli*	(Benabbou *et al.*, 2011)
Methylene blue (MB) Rose Bengal	Polystyrene	white luminescent lamp 400-700 nm	*S.aureus (ATCC 25923),* *E. coli (ATCC 10798)*	(Nakonechny *et al.*, 2013)
(a) tetra tertiary butyl zinc phthalocyanines(TBZnPc) (b) zincphthalocyanine tetrasulfonic acid (ZnPcTS)	siloxane polymers	Bonnett-Pell lamp 430 nm	*E. coli*	(Artarsky *et al.*, 2006)
a) [[tris(4,7-diphenyl-1,10-phenanthroline)ruthenium(II)]dichloride b) [tris(4,4′-diphenyl-2,2 bipyridine)ruthenium (II)] dihexafluorophosphate	porous silicone	360–700 nm range	*E. coli negative, Enterococcus faecal is positive*	(Najm and Trussel, 1999; Villén *et al.*, 2006)
cationic 5,10,15,20-tetrakis(1-methylpyridinium-4-yl)porphyrin (TMPyP)[i]	Immobilised on polystyrene nanofibre mats fixed on quartz surface	xenon lamp (300 or 500 W, Newport).	*DH5α E. coli strain with the pGEM11Z plasmid.*	(Zhu and Sun, 2012)
Protoporphyrin IX (PPIX),	poly(ethylene-co-methacrylic acid) (PE-co-MAA)	150 W halogen bulb for 60 min	*E. coli*	(Mosinger *et al.*, 2007)
5,10,15,20-tetraphenylporphyrin (TPP)	polyurethane nanofibre mats	White light source	*E. coli, DH5a with plasmid pGEM11Z t*	(Bonnett *et al.*, 1997)
5,10,15,20-tetrakis(N- methylpyridinium)porphyrin tetra-p-tosylate	Impregnation (dyeing), co dissolution, casting, copolymerization. Cellulose	White light source	*S. aureus, E. coli,* *P. vulgaris, B. subtilis.*	(Bonnett *et al.*, 2006)
a) 5,10,15,20-Tetrakis(p-hydroxyphenyl)porphyrin (1, p-THPP) b) 5,10,15,20-tetrakis(p-aminophenyl)porphyrin (2, p-TAPP) c) Zn(II)Phthalocyanines tetra sulphonic acid Zap	chitosan reinforced with nylon	halogen lamp, type- CY-118A, 500W, 230 v, 50 Hz, SLAG, Water IR filters	*E. coli* [1752 NBIMCC (ATCC 9637)]	(Aussawasathien *et al.*, 2008)

Table 1.8 Photosensitisers loaded or immobilised on nanomaterials or polymers for water disinfection by PDI.

Generally, immobilised photosensitisers have reduced quantum yields as compared to their unbound state (De Rosa and Crutchley, 2002), due in part to the need for oxygen to diffuse into and out of the polymer matrix in order to be sensitized and detected. Nevertheless, the simple reuse ability of these systems tends to outweigh this shortcoming. The efficiency of singlet oxygen production of free Rose Bengal was compared to Rose Bengal immobilised on Merrifield polymer (De Rosa and Crutchley, 2002). Results found that the free photosensitiser had a 100-fold higher production rate of singlet oxygen, due most likely to the diffusion problem.

1.9 Nanofibre mats supported photosensitisers

Photosensitiser immobilised onto electro spun nanofibre mats for removal of contaminants in water is an alternative nano-technological disinfection method. The overall aim is to develop nanofibre mats-based devices for water purification; Nanofibre mats are fabricated by low cost electro spinning.

Photosensitiser functionalised nanofibre mat potentially offers:

i. the oxidative degradation of surrounding species- microbes and chemicals, by reactions with photo produced $^1O_2$; and
ii. Physical filtration of metals and residual nano-sized pollutants in water.

The development of nanofibre mats materials immobilised with photosensitiser is a key aim that generates high yields of reactive oxygen species (ROS); upon visible light irradiation. Photochemically generated $^1O_2$ (Section 1.6) efficiently kills bacteria (Henke *et al.*, 2013; Mosinger *et al.*, 2007; Somani and Ingole, 2011) and viruses (Somani and Ingole, 2011).

Currently elecrospun nanofibrous membranes (ENMs) are a very attractive solution in filtration technology due to their unique properties such as high porosity, micro to nano scaled pore sizes, interconnected open pore

structure, and a large surface area per unit volume. Report shows that (Han *et al.*, 2009; Razavi, 2011) 4% of overall, ENMs are commercially using for water filtration (Figure 1.4). Due to the flexibility of the electrospinning process, it is anticipated that membranes can be produced with various novel functionalities which could effectively remove salts and various toxic compounds to produce clean water for human consumption and various other day-to-day uses. Low-cost electrospun materials that are composed of fibres with diameters ranging from ten nanometres to a few micrometres are advantageous for this application (Doyle *et al.*, 2013; Greiner and Wendorff, 2007; Reneker and Chun, 1996).

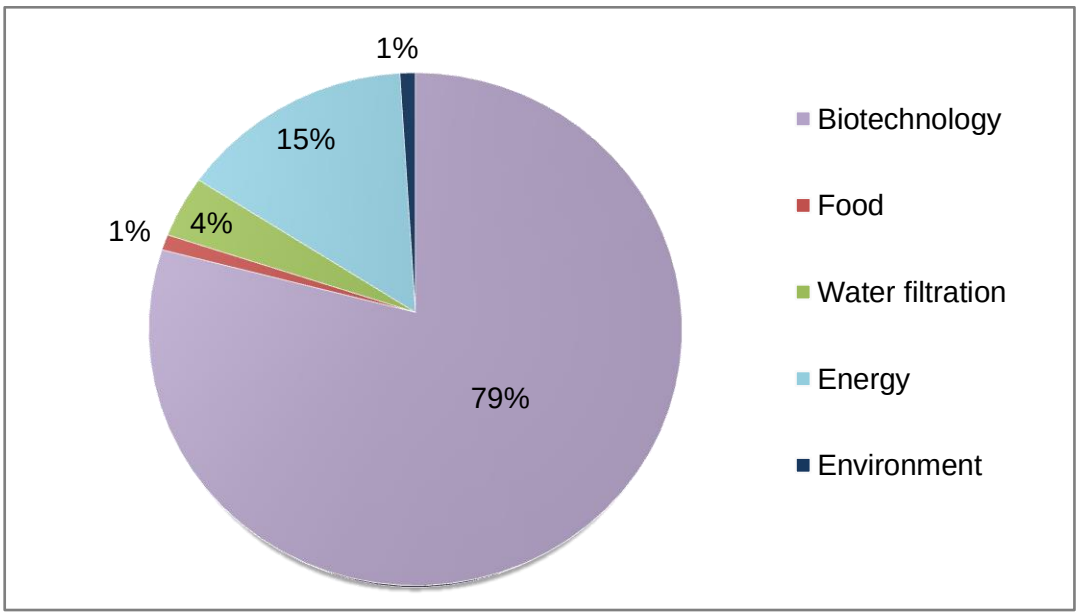

Figure 1.4 Five commercial applications for electrospun nanofibre mats, a function of overall patent filing percentage, during 1994–2012.
(Kohn and Nelson, 2007; Kohn *et al.*, 2007; Romero *et al.*, 2011)

The small diameters of the photosensitiser loaded nanofibre mats allow the diffusion of singlet oxygen outside of the fibres, where it photo-oxidizes biological targets. It is also well established that photo chemically generated $^1O_2$ acts as a primary oxidant in the photosensitised transformation of organic substances (Escalada *et al.*, 2011; Gryglik *et al.*, 2007; Kim *et al.*, 2012; Kong and Ferry, 2004; Costa *et al.*, 2012) and antimicrobial, antifungal activity (Foote and Peters, 1971; Jensen and Daniels, 2003; Vatansever *et al.*, 2013) in waters. The polycyclic aromatic hydrocarbons, chlorophenols

and pesticides are organic pollutants found to be vulnerable to oxidative stress (Bonnett *et al.*, 2006; Raetz and Whitfield, 2002; Strassert *et al.*, 2009), that occurs due to the energy transfer from the photochemically excited natural organic material (NOM) to oxygen. It was demonstrated that in natural waters under sunlight illumination MS-2 coliphage was inactivated by the production of $^1O_2$ upon irradiation of NOMs (Xing *et al.*, 2009b). This occurs due to the high reactivity of $^1O_2$ and its widespread occurrence in the naturally-occurring photo-oxidation reactions. Researchers are keen to photochemical remediation approaches and to exploit the oxidizing capacity for water treatment and disinfection processes. As electrophilic $^1O_2$ are able to oxidize electron-rich olefins, dienes, sulfides, and aromatic hydrocarbons (Zhu *et al.*, 2011; Gad *et al.*, 2004), the capability of photosensitiser $^1O_2$ production enables oxidation of photochemical organic pollutant such as macro cyclic dyes, aromatic hydrocarbons, and transition metal complexes as well as caring microbial disinfection (Xing *et al.*, 2009b).

1.10 Nanofibre mats materials

Polymers are also an important class of nanomaterial; those have attracted increasing interests in the last decade. Some natural and synthetic polymers that commonly used to fabricate nanofibre mats are listed in Table 1.9.

Although there are numbers of polymers are used for nanofibre mats production which are water insoluble. But as this research devoted to water treatment so use of hazardous solvents were avoided consciously. So that use of large amount of solvents like DMF for polymer solution can cause secondary contamination. Usually water-soluble polymers were chosen for nanofibre mats on the other hand simple but effective crosslinking technique was used to make the nanofibre mats water insoluble. Although initially polyacrilonitrile nanofibre mats was studied, which was kindly provided by Professor Bob Stevens (Nottingham Trent University).

Polymer	Process	Application	Year
Poly(vinyl alcohol) (PVA) cross-linked with glutaraldehyde	Filtration	Oil/water emulsion filtration	2005
Polyvinylidene (PVDF)	Filtration	Pre-treatment of water, Prior to RO or UF	2006
Nylon 6	Filtration (to remove micron/micron particles)	Water treatment	2006
PAN/chitosan	Ultrafiltration nanofiltration	Water filtration	2006
PVA/PVA hydrogel	Ultrafiltration	Oil/water emulsion	2006
Polysulfone	Filtration	Pre-filters for particulate removal	2007
UV cured PVA	Ultrafiltration	Oil/water emulsion	2009
Polyamide/PAN	Nanofiltration	Water treatment	2009
Polyether sulfone	Filtration	Water treatment	2009
Polystyrene/beta-cyclodextrin	Nanofiltration	Removal of organic compounds from water	2009
Polyvinylenedifluoride	Air gap membrane distillation	Desalination	2009
Polyvinylenedifluoride	Gas stripping membrane distillation	Removal of VOCs from water	2009
Polyether sulfone	Pre-filtration	Water and other liquid separation	2010
Fluorinated co-polyimide	Filtration	Water treatment	2010
PVA/PAN	Ultrafiltration	Oil/water emulsion	2010
Interfacial polymerization using piperazine (PIP)	Ultrafiltration	Water treatment	2010
CA (molecularly imprinted with glutamic acid)	Adsorption	Chiral separation	2010
Carbonized nanofibrous (precursor PAN) membrane	Filtration	Removal of disinfection by-products from water	2010
Cellulose/polyacrilonitrile (PAN)	Filtration	Bacteria and virus removal	2011
Polysaccharide (cellulose and chitin)	Ultrafiltration	Water purification	2011
PAN	Nanofiltration	Salt removable	2011
Cellulose acetate	Heavy metal ion adsorption	Water treatment	2011

Table 1.9 Some recently electrospun synthetic and natural polymers and the main function in the water treatment sector, adopted from Feng (2009).

1.11 Advantages of electrospun nanofibre mats and challenges

Nanofibre mats can be effectively produced by electrospinning, which is a simple and low-cost technique. In addition, electrospinning allows the production of nanofibre mats from various materials e.g. inorganic and organic compounds and with different functionalities. This is highly beneficial in filtration membranes for environmental remediation, can minimizes the pressure drop and provide better efficiency than conventional fibre mats. Although the process is predominantly used to make polymeric nanofibres, ceramic and metal nanofibres have also been constructed indirectly through electrospinning of their precursor material

The nano-dimension of nanofibres naturally gives them a high surface area (1 - 100 m^2/g) to volume ratio. This characteristic makes them very attractive in applications where a large surface area is desirable such as in sensors and affinity membranes. The large surface area-to-volume ratio of nanofibre mats allows greater surface adsorption of contaminants from water and increases the life-time of the filtration media. In addition, high porosity (ca. 90%), small fibre-to-fibre distance, high surface area, small diameters (10 nm - 10 µm) are advantageous. The nanofibre mats are breathable fabric, its small size prevents bacteria from entering. These properties make nanofibres a potential candidate in this research as a vehicle to deliver the photosensitisers for water treatment.

This benefit relates to the variety of polymer that can possibly be used to electrospun nanofibres. Functionalization of electrospun nanofibres can be achieved through simple blending of polymer solution prior to spinning, post-spinning surface functionalization or using core-shell electrospinning setup (Maisch *et al.*, 2007).

For the determination of immobilised photosensitiser on ENF surface need proper and robust method. To do that it is important to characterise the ENF. But inconsistent morphology is the main challenge to do these tasks.

1.11.1 Photosensitised inactivation of microbial cells: general aspects bacterial cell wall

The microbial cells contain large variety of size, sub-cellular architecture and biochemical composition; thus, the susceptibility to photosensitiser significantly differs for the different microorganisms.

Thus, Gram-positive bacteria are surrounded by an outer wall, which is separated from the plasma membrane by a periplasmic space. The 20–80 nm thick wall represents a protective mesh mainly constituted by peptidoglycan layers, which contains negatively charged lipoteichoic and teichuronic acids, anchored in the membrane. This kind of spatial arrangement does not act as a strict permeability barrier and Gram-positive species are more susceptible towards photodynamic inactivation. Their outer wall, located outside the cytoplasmic membrane, is a relatively porous structure that is permeable to nutrients, glycopeptides and polysaccharides with a molecular weight in the 30 KDa–60 KDa range and in the same way it allows photosensitisers to cross (Spagnul *et al.*, 2015; Jori *et al.*, 2011). Therefore, the most common photosensitising agents, whose molecular weight is generally less than 1500 Da, can cross the outer wall and localize in the immediate surroundings of the photosensitive endocellular sites.

On the other hand, Gram-negative bacteria are characterized by the presence of an additional 10-15 nm thick structural element, external to the peptidoglycan network, whose constituents (e.g. lipoproteins, lipopolysaccharides, teichoic and lipoteichoic acids) provide the outer surface with a quasi-continuum of densely packed negative charges. his highly organized system inhibits the penetration of compounds with molecular weight larger than 600–700 Da (Nikaido, 1994; Leive, 1974). Since the Gram-negative outer membrane is more negatively charged (Malik *et al.*, 1992; Spagnul *et al.*, 2015), cationic hydrophilic photosensitisers are attracted to it, while anionic photosensitisers are repelled, and thus are generally only active against Gram-positive bacteria. The structures of

Gram-positive and Gram-negative cell walls are showing below in Figure 1.5.

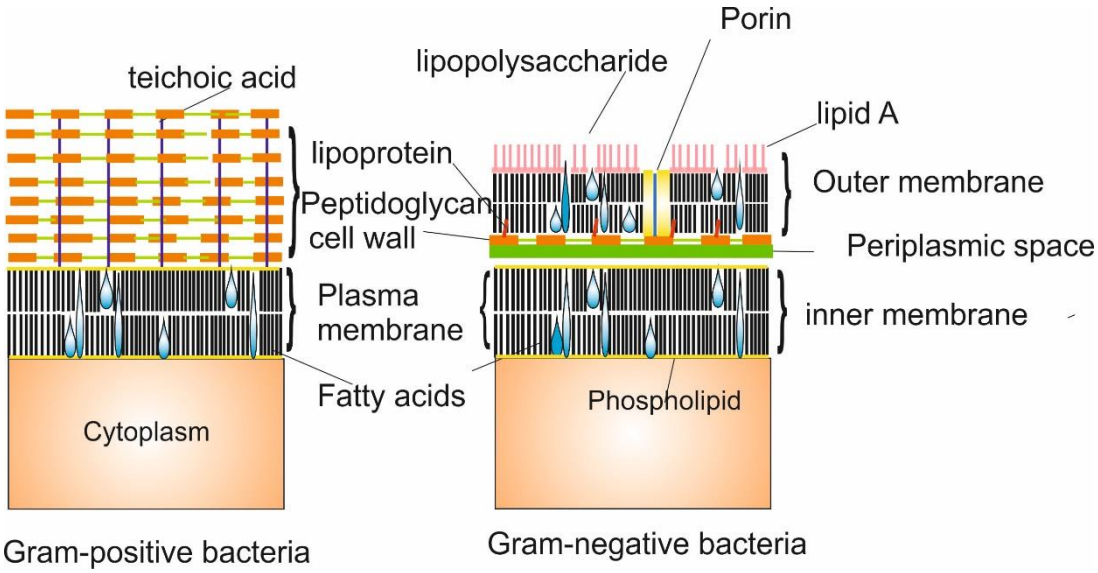

Figure 1.5 Structural difference between Gram-positive and Gram-negative bacterial cell wall.

Cell wall of Gram-positive bacteria contains porous layer of teichoic acid. In Gram-negative bacteria cell wall is densely compact of Lipid A containing six fatty-acid-acylated chains, hydrophilic polysaccharide components with negatively charged phosphate and carboxyl group and teichoic which act as barrier to prevent Gram-negative bacterial strain to penetrate with antimicrobial molecules.

It has already been demonstrated that a positive charge on the photosensitiser molecule allows it to bind to, and in some cases penetrate, the microbial permeability barrier (Niu *et al.*, 2012). Thus, positively charged photosensitisers show efficiency at lower concentrations than neutral and anionic photosensitiser molecules. Indeed, negatively charged photosensitisers are not able to penetrate the Gram-negative barrier but can be effective at higher concentrations. In this case, singlet oxygen that is generated during the irradiation at the outer surface, or in solution in close proximity to the cell is thought to diffuse into bacteria and produce damage to lipids and proteins in the inner membrane (Niu *et al.*, 2012). However, most photosensitiser systems are based on affinity ligands that exhibit efficient antimicrobial activity against Gram-positive strains rather than Gram-negative organisms. In Gram-negative bacteria the highly organized

outer bacterial membrane structure with a highly negatively charged lipid layer, which blocks the cellular attachment between photosensitiser and bacteria and thus reduces the $^1O_2$ the (Nasreen *et al.*, 2013).

Several affinity ligands based on nanoparticles (Bonnett *et al.*, 1993), water-soluble conjugated polymers (Raetz and Whitfield, 2002; Strassert *et al.*, 2009) and polypeptides (Xing *et al.*, 2009b) have been recently developed to achieve close association of photosensitisers to the Gram-negative bacterial strains. These have shown effective photo inactivation to these strains and so the development of simple and specific affinity ligand molecules that can selectively direct photosensitisers to the surface of Gram-negative bacteria pathogens is of great importance and remains a challenge in antimicrobial PDT (Zhu *et al.*, 2011).

Because of their simplicity and biological compatibility a critical aspect of materials with photosensitiser immobilised onto fibres is the diffusion length of singlet O_2 typically tens to hundreds of nm (Najm and Trussel, 1999), which limits photo-oxidation processes to areas in close proximity to the fibre surface. Higher-photo-oxidation efficiency requires the organization of photosensitiser molecules near the fibre surface. This is not easy to control, and/or post processing of the hydrophobic polymeric surface may damage the nanofibre mats.

Although electrospinning is a methodology with considerable potential in various applications, one of the main disadvantages has been the inability to achieve large scale productivity. However, recently multi-jet (Gad *et al.*, 2004) and needless electrospinning techniques (Liu *et al.*, 2012) have emerged to bridge the gap of large scale manufacturing (Srivastava *et al.*, 2007) and commercial equipment is available for continuous production of 1-2 m wide ENFs.

1.12 Synthesis of photosensitisers

Although photodynamic therapy (PDT) was discovered over a hundred years ago by its ability to destroy microorganisms, it has been developed mainly as a cancer therapy. In recent years, due to the inevitable rise in multi-antibiotic resistant strains of pathogens, PDT is being considered as a versatile antimicrobial approach to which microbial cells will not be able to develop resistance.

In recent years the desirable structural features of effective antimicrobial photosensitisers (PS) have become better understood. In addition to the normal requirements of an efficient photosensitiser such as a high absorption band in the red/NIR region of the spectrum and a good triplet yield that allows production of reactive oxygen species upon illumination, additional molecular features are needed. The most important structural feature is either a constitutive cationic charge provided by quaternary nitrogen groups or a set of basic amino groups provided by a cationic polymer. Additional features may include a correct balance between lipophilicity and hydrophilicity and a certain degree of molecular asymmetry.

In this project initially PDI of bacteria was carried out with PPIX, but as expected PPIX failed to inactivate Gram-negative bacteria. So commercially available tetra cationic TMPyP was chosen for PDI Gram-negative bacteria. PDI by TMPyP successfully kill 100% Gram-negative bacteria. Since TMPyP is lacking suitable functional group for covalent bonding with electrospun nanofibre mats, synthesis of novel cationic photosensitiser was in need. TMPyP was an excellent photosensitiser with antimicrobial characteristics. This is why in this project novel synthesised photosensitisers were designed is such a way so that they mock TMPyP structure. These newly synthesised photosensitisers hold constitutive cationic charge provided by quaternary nitrogen groups with suitable functional groups (allyl and $–NH_2$).

Tetrapyrrolic compounds such as porphyrins are known to be prospective chemotherapeutics and photosensitisers for cancer treatment and diagnosis.

In this work, water-soluble, meso-substituted cationic pyridyl-porphyrins with various functional groups (allyl, hydroxyl, and amine) at the nitrogen atom in the pyridine ring were synthesized and characterized by ^{1}H and ^{13}C NMR and UV-visible spectroscopy (Figure 1.6).

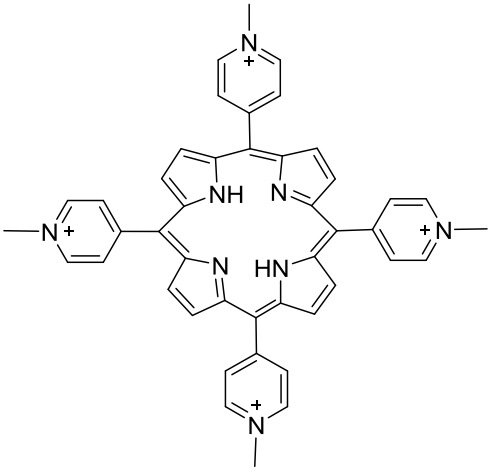

(A) 5,10,15,20- tetrakis (1- methylpyridinium-4-yl) porphyrin **(TMPyP)**

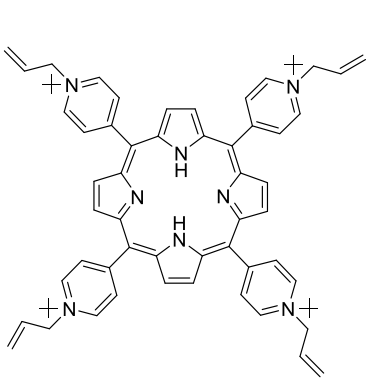

MW 783

(B)

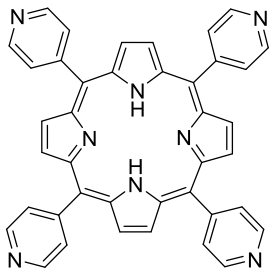

MW 618.69

(C)

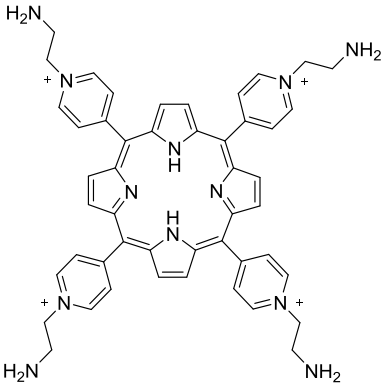

MW: 795.010

(D)

Figure 1.6 Structure of Tetra cationic photosensitisers used in this research.

(A), tetra methyl pyridyl porphyrin (TMPyP); (B) tetra allylic pyridyl porphyrin (TAllylPyP), (C) Starting material, (TPyP) and (D) tetra amine pyridyl porphyrin TMPyP.

Cytotoxic and photodynamic activities of new porphyrins and were investigated in four different strains of bacteria. The porphyrins bearing allyl-functional groups were evidenced to be more phototoxic than those which

included hydroxyl, and amine groups. Special attention was paid to cationic meso-substituted, water-soluble porphyrins which are more stable in biological media than natural porphyrins, chlorines and bacteriochlorines. Moreover, these compounds express monomeric molecular behaviour over a broad concentration range.

1.13 Experimental setup for PDI of water pollutants

The experimental set up for PDI was the first step towards successful development of a photodynamic water sterilisation system. Irrespective of material and methods it was tries to set up such a system where all factors were excluded other than photodynamic effects which can inactivate model pollutants. Usually in different researchers of PDI efforts made to exclude UV light by using cut-off filters or by using light sources that generate visible light. (UV-C-280 nm) is antimicrobial and can degrades range of biomolecules particular those with aromatic character. In this study we avoided using a UV light source and used cold visible light (Section 1.13.1) instead. In addition, all of the PDI experiments were carried out at room temperature 22-21˚C. However, a range of temperature were used also find out the effect of temperature in PDI to mimic the environment of wastewater treatment plant and tropical countries. As the amount of availability of molecular oxygen is a vital factor in the PDI process. In this project to make sure even distribution of oxygen shaker was used to shake the experimental sample in low speed. Whereas such PDI reactor should be built with facility of easy diffusion of molecular oxygen and desired aerobic environment. This present research was carried out in stationary system that doesn't mimic actual wastewater treatment plants or reactor. Thus, further research and application of this developed system in proper prototypes of wastewater treatment process will be needed to validate the applicability and practicability of the present work.

1.13.1 Light source

The studies were carried out with normal halogen flood light (400W), A cold light KL 2500 LCD, (250 W) has been bought to carry out the further studies with controlled continuous intensity and without heating effects. Homogeneous output and illumination intensity can be controlled, and the beam focused.

1.13.2 Model pollutants

In most studies aimed at PDI of Gram-negative bacteria NCTC 10418, Gram-positive bacteria *S*. *Epidermis* and antibiotic resistant bacteria *E. coli* BL21 (DE3). Since faecal coliform testing is one of the nine tests of water quality that form the overall water-quality rating in a process used by the EPA, as faecal coliform bacteria indicate the presence of sewage contamination of a waterway and the possible presence of other pathogenic organisms. The most common faecal coliform is *Escherichia coli*. This is why Gram-negative bacteria *E. coli* were chosen as one of the model microorganisms. In addition

To deal with antibiotic resistance in the water environment and validate the use of the water sterilisation system, antibiotic resistant bacteria *E. coli* BL21 (DE3) was used as model organism.

1.14 Research aims

In broad view the overall objective of this study was construct low energy consuming affordable water sterilisation system that use low energy of visible light, to achieve a high sterilization reduction efficacy for microorganisms in wastewater. The study was based on PDI of microorganisms. These features would allow using this water treatment system in developing countries those are not facilitating with good infrastructures of water treatment plants. Reusability and low energy consumption is also advantageous and lucrative to water companies in developed nations. Disinfection of grey water will allow this to be excluded

from whole water processing and returned to environment which offers reduction of overall energy consumption.

In this study we planned two strategies to achieve the main goal.

The first strategy is the immobilisation of cationic photosensitiser onto the electrospun nanofibre mats through electrostatic attraction. This system will be applicable to treat surface water which is not loaded with high ionic contaminants.

The second strategy is covalent modification of cationic photosensitiser onto the electrospun nanofibre mats. This will be applicable to treat contaminated water even with high ionic contamination.

To accomplish the maximum efficiency of water sterilizer, both strategies were carried out.

Thus, the objectives of the study were as follows:

(i) Production and development of water stable electrospun nanofibre via
   a. electrospinning of nanofibre mats; and
   b. pre or post modification of nanofibre mats to attain water stability, followed by characterisation of electrospun nanofibre mats.

(ii) Synthesis and characterisation of tetra cationic photosensitises;

(iii) Adopt or modification of efficient photosensitiser-electrospun nanofibre mat conjugation procedure; and

(iv) Study of photodynamic inactivation (PDI) of *E. coli* and other bacteria with novel photosensitisers in solution and on photosensitiser immobilised nanofibre mats.

Chapter 2

Materials and Methods

2.1 Materials

All general laboratory reagents used during the experiments were purchased from Sigma Aldrich (Dorset, UK) unless otherwise mentioned and were of best analytical grade available. Key reagents included Protoporphyrin IX (PPIX), tetra phenyl porphyrin (TPP) tetra pyridylporphyrin (TPyP) and tetra methyl pyridyl porphyrin (TMPyP) allyl bromide, 4-bromo phenol, propargyl bromide, palladium acetate, 99% (w/v) 2-bromoethylamine hydrobromide, which were from this supplier.

Bacterial strains: *E. coli* NCTC 10418 and *Staphylococcus epidermis* was kindly provided by Mr. John Wright, School of Molecular and Cellular Biology, University of Leeds. *E. coli* BL21 DE3 competent cells were bought from Agilent Technologies.

Growth media for bacteria: Carbenicillin, disodium salt was obtained from Alfa Aesar in powder form and stock solutions were prepared in sterile deionised water at 50 mg/ml. Tryptic soy broth, tryptone and agar were obtained from Sigma Aldrich, UK. Yeast was purchased from Oxoid.

Buffer solutions: Potassium phosphate buffer 10 mM, and sodium phosphate buffer 10 mM (pH 7.4), MES buffer 0.1 M (pH 5-6), was used unless otherwise mentioned. The solution was dispensed into aliquots and sterilized by autoclaving at 121°C for 20 min.

2.1.1 Light source and conditions for PDI

The light source for PDI experiments was a Schott KL 2500 LCD (Schott Ltd., UK) which provides a cool visible light (Figure 2.1 and Figure 2.2). Fluence rate of illumination during photoinactivation experiments were

measured using a light meter (Clas Ohlson, UK). Stationary and flow models were used for PDI using photosensitiser functionalised polyacrylic acid crosslinked with polyvinyl alcohol (PAA-PVA) or crosslinked with ethylene glycol PAA-EG electrospun nanofibres. Visible light was used and fluence rates (radiant exposure) were 30 mW/cm^2 unless otherwise stated. Illumination was at 20 - 22°C and under aerobic condition.

Figure 2.1 Light source of PDI experiments.

The Schott cold light KL 2500 LCD (250 W), with focusing light guide is shown in (A), front view; (B) side view.

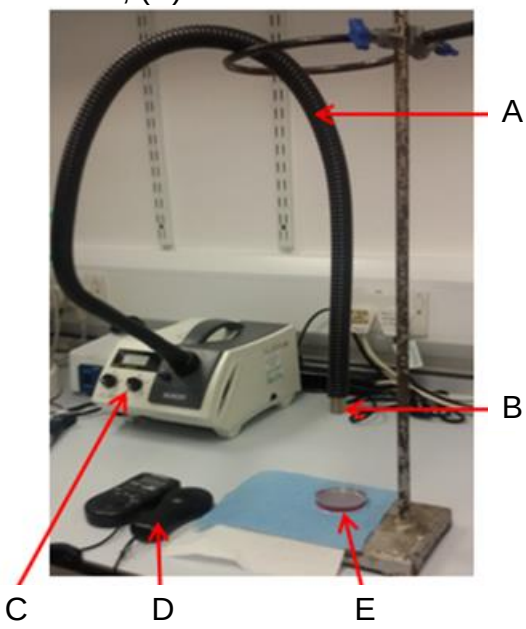

Figure 2.2 Experimental setup for PDI in solution.

(A), flexible light guide; (B) light; (C), clod light source KL2500 LCD; (D), light meter; (E), petri dish containing experimental sample.

Polymers, cross-linkers and solvents used for electrospinning of nanofibres:

Polymers and cross linkers used in this project were bought from Sigma Aldrich, UK unless otherwise mentioned. The polymers, cross linkers and solvent used are summarised in Table 2.1.

Polymer	**Molecular weight**	**Cross linker**	**Solvent**
Polyacrylic acid (PAA)	450,000	Ethylene Glycol and PVA	deionized water/ Ethanol (70:30)
Poly(vinyl alcohol) (PVA) 88% hydrolysed	145,000-180,000	Glutaraldehyde	deionized water
Poly (ethyleneimine) (PEI)	750,000	PVA	deionized water
Polyacrilonitrile (PAN)	150,000	No cross linker	N, N-dimethyl formamide (DMF)

Table 2.1 Polymers, cross-linkers and solvents used for electrospinning of nanofibres.

Schematic diagram of key steps of project. Showing overview of all steps involved in developing system for photo treatments of microbial contaminants, which are described in this subsequent chapter.

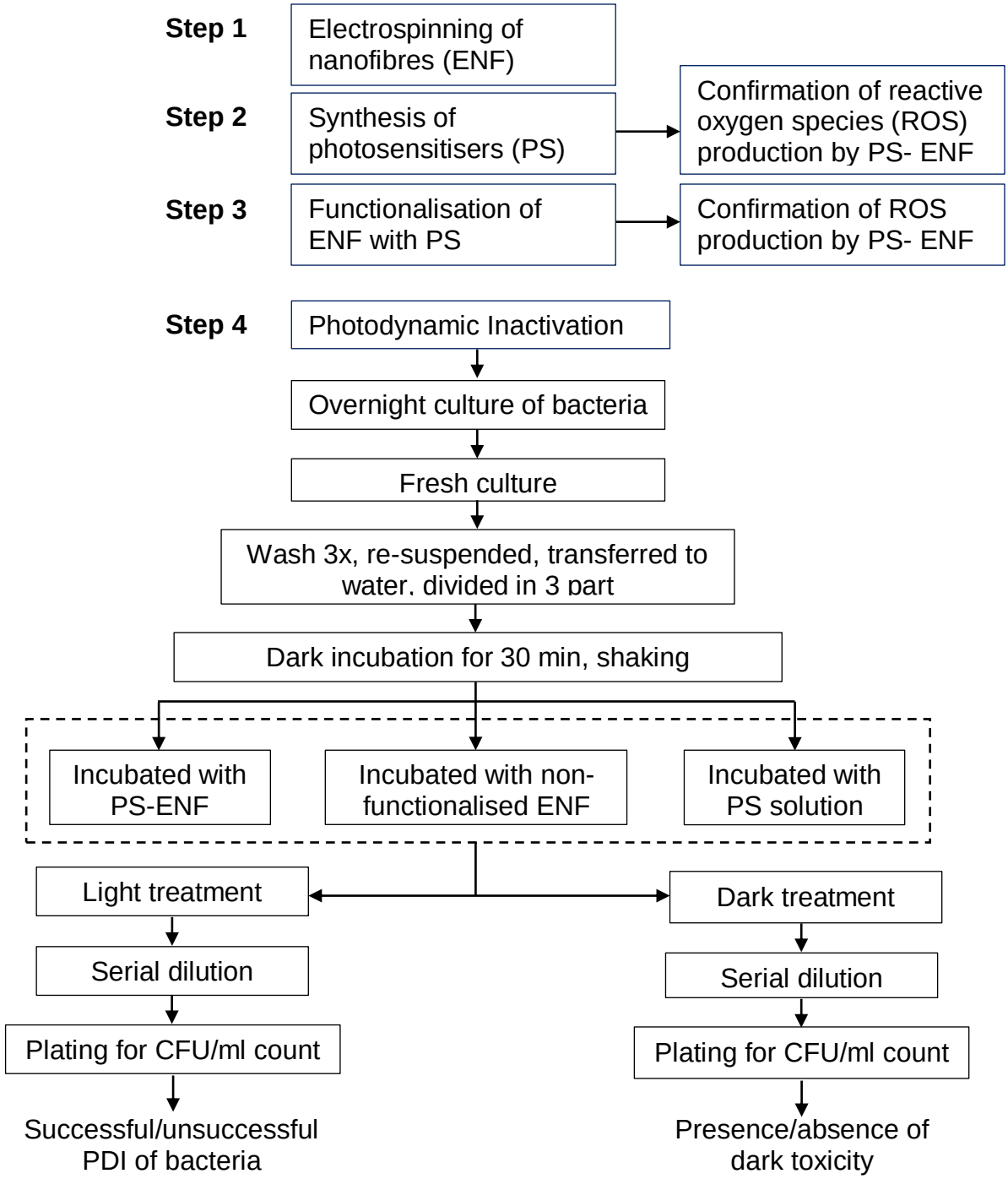

Figure 2.3 Schematic diagram of key steps of this project.

2.2 Electrospinning

For production of nanofibre fabric, needleless electrospinning technology was used. An Elmarco NS lab 200 Nanospider electrospinner was used for nanofibre production unless otherwise mentioned (Figure 2.4). A cylindrical electrode was used for electrospinning all the nanofibres used in this study and the low volume spinning tub (Figure 2.4A) was able to use polymer solution volumes of 20 ml.

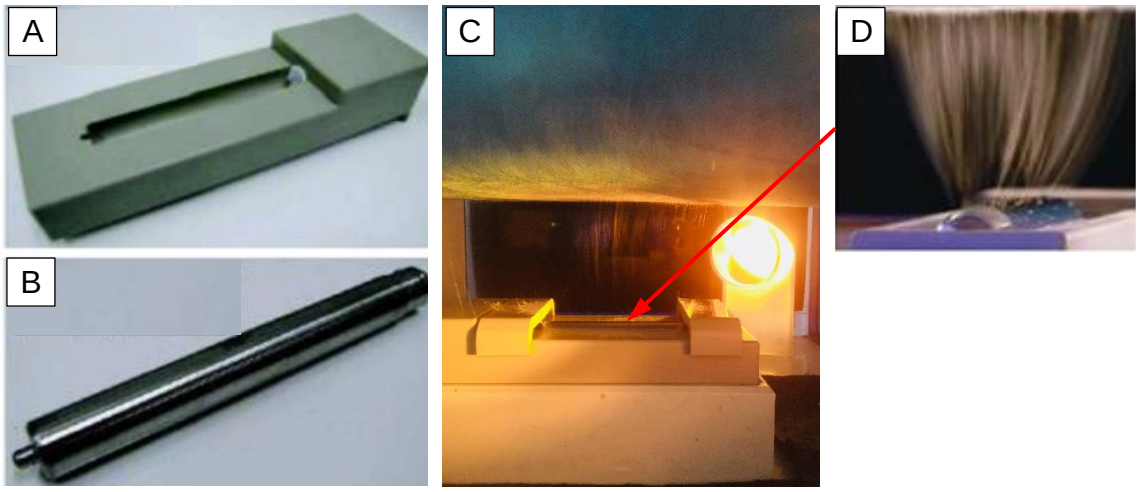

Figure 2.4 Electrospinning of nanofibre mats: apparatus and process.

(A) low volume spinning tub; (B), small cylindrical electrode; (C); polypropylene collector; (D); electrospinning process showing nanofibres.

Preparation of polymer solution for electrospinning:

Six different types of nanofibre were produced in this this study. To construct nanofibre mats, polyacrylic acid polymer was chosen. The aim was to make -COOH functional nanofibres to bind covalently amine or allyl functional photosensitisers. Preparations of polymer solution for nanofibre spinning are stated below.

2.2.1 PAA-PVA nanofibres: preparation of polyacrylic acid nanofibre crosslinked with polyvinyl alcohol

PVA was dissolved in deionised water and gently stirred for 2 h at 60°C to prepare a 24% (w/w) solution. PAA was dissolved in deionised water and stirred for 4 h at room temperature to give 20% (w/w) concentration. Aqueous solutions of PVA (10 g) and PAA (20 g) were mixed 10:6 % (w/w) under stirring at room temperature. The PAA-PVA blend was loaded into a bath of volumes of 20 ml. A small rotating cylindrical electrode was used under following conditions: voltage: 60-67 kV, electrode to substrate distance: 12-13 cm. A spun bond polypropylene cloth was used as the collector and dry PAA-PVA nanofibres were collected onto it.

2.2.1.1 Post electrospinning crosslinking of PAA-PVA nanofibre

Two different methods including heat treatment and exposing the nanofibres to a glutaraldehyde (GA) solution were employed to crosslink the PAA-PVA nanofibres (Fang *et al.*, 2011), rendering the fibrous mats water insoluble. Details of the crosslinking process are as follows:

Thermal crosslinking; PAA-PVA nanofibres were heat treated in a Gallenkamp vacuum oven attached to an Edwards high vacuum pump model E2M5, at 140°C for 30 min to 1 h. After heat treatment the nanofibres were mechanically strong enough to detach from the polypropylene substrate and could be used without support.

GA-crosslinking; to prevent leaching of uncrosslinked poly (vinyl alcohol) (PVA) into water, glutaraldehyde was used to crosslink the PVA. GA treatment was performed by immersing the electrospun PAA-PVA nanofibres mat into an aqueous solution composed of isopropanol (30 mL), water (3.3 mL), concentrated HCl (0.3 mL), and the GA solution (5% w/v, 3.7 mL) for 1 h.

The nanofibres mats treated using on GA solution were rinsed with water 3 times to remove excess GA. All of the treated nanofibre mats were immersed in water. The wash water was subject to MS analyse to confirm that PVA was water.

2.2.2 PAA-EG nanofibre: preparation of ethylene glycol crosslinked polyacrylic acid

PAA solutions were prepared by dissolving the appropriate amount of polymer in water: ethanol (70:30) mixture with concentrations ranging from 9-12 % (w/w). Ethylene glycol (EG) was added to each sample as a crosslinking agent with a concentration 12 % (w/w) relative to the PAA. Complete dissolution was observed after 2.5 h of mixing with a magnetic stirred bar at ambient temperature. Then 25 ml PAA-EG blend was loaded into a spinning bath mixed with sulphuric acid at 50 µL mL^{-1} of 1 M H_2SO_4 was added to the PAA-EG solution just before starting electrospinning. A small rotating cylindrical electrode was used under the following conditions: voltage: 25-39 kV, electrode to substrate distance: 10-12 cm. A spun bond polypropylene cloth was used as collector and dry PAA-EG nanofibres were collected onto it.

2.2.3 PAA-EG-PEI: Covalent modification of PAA-EG nanofibre by Poly (ethyleneimine)

PAA-EG nanofibre mats were prepared and then the coupling of polyethylene imine (PEI) with carboxylic group on the PAA-EG nanofibres was carried out using EDC and sulfo-NHS, adapted from a procedure described by Grabarek and Gergely (Grabarek and Gergely, 1990). The activation reaction with EDC and sulfo-NHS is most efficient at pH 4.5-7.2. However, the reaction of sulfo-NHS-activated molecules with primary amines is most efficient at pH 7-8. For best results, the first reaction with EDC was performed in MES buffer at pH 5-6, then the pH to 7.2-7.5 was raised using phosphate buffer immediately reaction to allow of the amine-containing PEI molecule at. EDC and sulfo-NHS were brought to room temperature before opening the bottles. In 15 ml 0.1 M MES buffer (pH 5.5) EDC (0.4 mg/ml) and sulfo-NHS (1.1 mg/ml) were dissolved. Then, 100 mg PAA-EG nanofibre mats (2 cm^2) were immersed and shake gently for 30 min. Nanofibres were then removed from the EDC, sulfo-NHS mixture and washed with deionised water to quench the reaction. Polyethylene imine (PEI 30 mg) in 5 ml PBS buffer was then added to the activated nanofibres and the reaction mixture

allowed to react overnight at room temperature. To remove the unreacted reagents, nanofibres were washed with 3x 50 ml deionised water with shaking. Then the nanofibres was stored in deionised water.

2.2.4 PAA-EG-TPP: 10% (w/w) PAA-EG nanofibre doped with TPP

10 % (w/w) PAA-EG solutions was prepared as in Section 2.2.2. Then, tetra phenyl porphyrine (TPP) at 1 mg/ml was added to the PAA-EG solution and stirred for two hours. Sulphuric acid (1 mol/ L) was added to the PAA-EG solution immediately before electrospinning processing at a concentration of 50 µL mL^{-1} of spinning PAA-EG.

2.2.4.1 PAA-EG / PVA-PEI bilayer nanofibres

The first layer of 10 % (w/w) PAA-EG nanofibres were prepared a previously described in Section 2.2.2. For the second layer, 15 g of 10% (w/w) PVA in water was stirred for 3 h with 15 g of 10% (w/w) PEI.

2.2.5 Polyacrylonitrile nanofibre blended with Jeffamine (PAN-JEF)

Fine electrospun nanofibre mats with an aminated surface were provided by Professor Bob Stevens, (Nottingham Trent University UK). These were manufactured from a blend of 10% (w/w) polyacrilonitrile (PAN) and 5% (w/w) Jeffamine ED-2003; polyetheramine was used as the source of amine. Electrospinning was carried out with 18.5 KV potential across the nozzle, at 60% humidity and a feed rate of 4 ml/ hr. The polypropylene backing to support the electrospun nanofibres mesh was provided by West Yorkshire Printing. The nanofibre mats were sandwiched in between two punched polypropylene sheets (Figure ***2.5***) and attached by ultra-sonic welding.

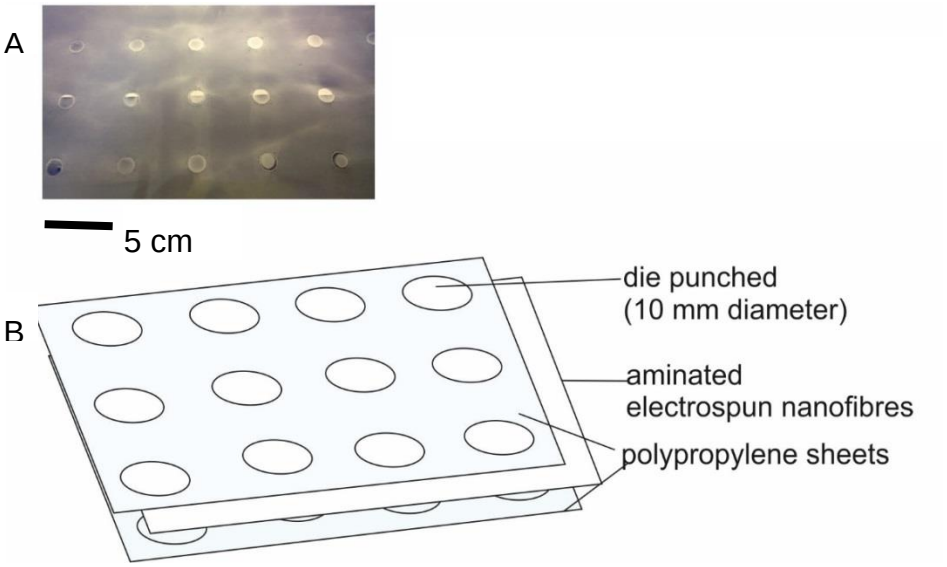

Figure 2.5 Sandwiched electrospun nanofibre (ENF) in between two polypropylene sheets.

(A), ENF supported with two polypropylene sheets joined together by ultrasonic weld; (B), schematic of ENF sandwiched in between two die punched polypropylene sheets.

2.2.5.1 Flow channel made of PAN-JEF nanofibres mat:

In this research PAN-JEF nanofibres mat was also used to construct a flow system for water treatment. These were kindly provided by Professor Bob Stevens, (Nottingham Trent University UK). The architectural design is showing below Figure 2.6.

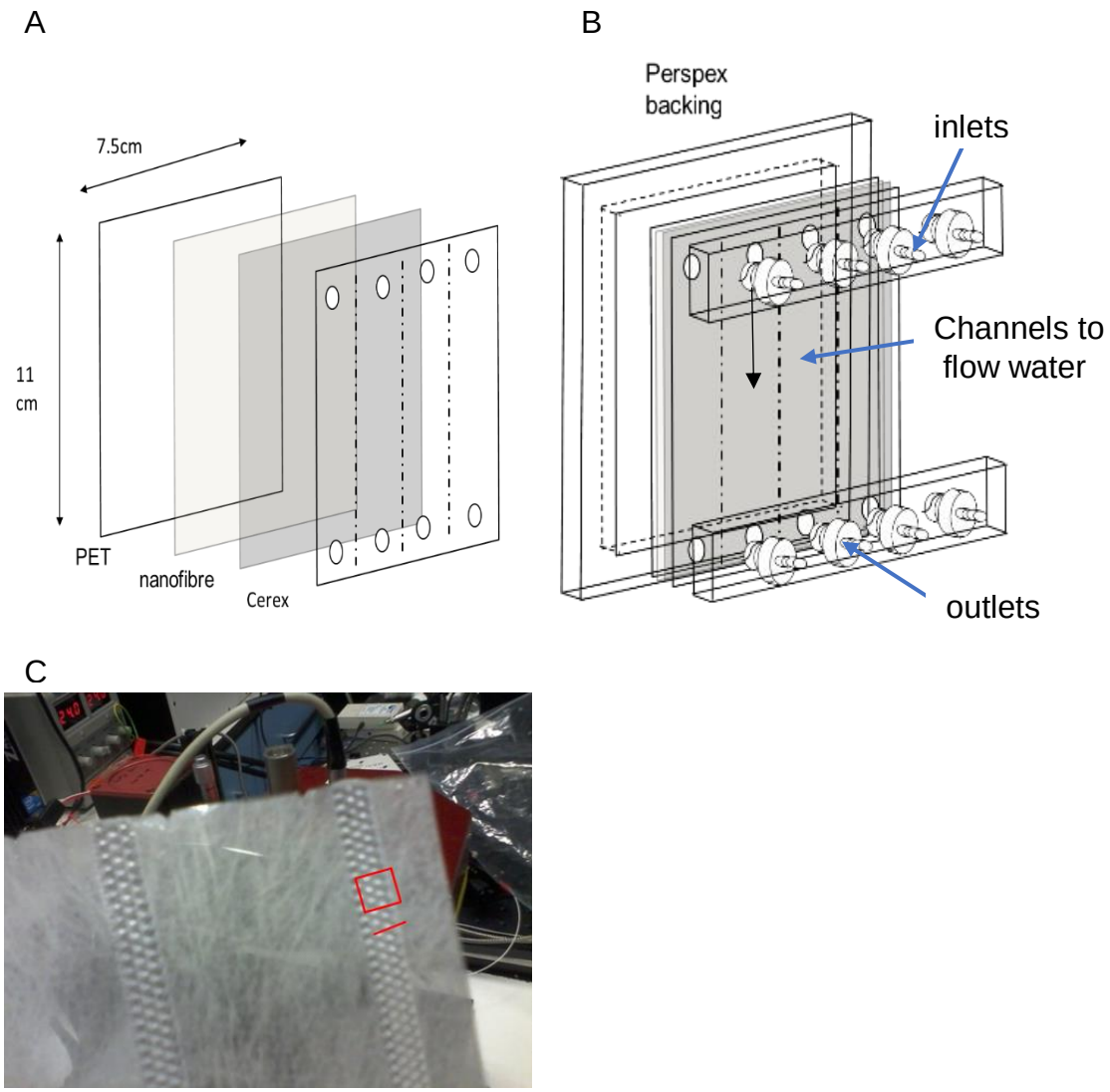

Figure 2.6 Structural design of flow cell for water treatment.

(A) (PAN-JEF) ENF supported with two polyethylene terephthalate sheets joined together by ultrasonic weld

(B) Complete flow cell

(C) Ultrasound welded channel.

The nanofibre is attached to the bottom PET sheet. Then a cerex non-woven matt is put on top and then covered with a top PET sheet with the orifice for the inlet and outlet. Inlets and outlets are connected with luer locks.

Electrospinning condition and parameters for nanofibre production are summarised in Table 2.2.

Nanofibres	Final % of polymers in mixture (w/w)	Distance electrode to collector (cm)	Volt (kV)	Electrode spin speed (rpm/min)	Collector speed
PAA-EG	PAA: 10%, EG:12% of PAA weight	10-12	24-39	3-5	0.1
PAA-PVA-GA	PAA:PVA (9:5)% Post GA treatment 5% (w/v)	10-13	60-67	1	0.1
PAA-EG-PEI		-	-	-	-
PAA-EG-TPP	10% PAA, EG:12% of PAA weight doped with TPP (1 mg/ml)	10-12	24-39	3-5	0.1
PAA-EG / PVA-PEI bilayer	(18:6)% PVA:PEI was electrospun on 10% PAA-EG nanofibre	10-12	24-39	5-7	0.1
PAN-JEF blended nanofibre	5% Jeffamine in 10% of PAN/DMF (w/w)	Kindly provided by Nottingham Trent University			

Table 2.2 Electrospinning condition and parameters for nanofibre production

2.3 Water stability of nanofibre mats

2.3.1 Mass spectroscopic analysis

To confirm the water stability of the nanofibre mats, washings from the nanofibres were analysed by mass spectroscopy. Nanofibres were incubated in water for different periods from 1 d to 60 d. Water washings were diluted to 50% (v/v) in acetonitrile and analysed by Z-spray nanoelectrospray ionisation mass spectrometry (IMS) using a quadrupole-IMS-orthogonal time-of-flight (TOF) MS (Synapt HDMS, Waters UK Ltd.) using in-house fabricated gold/palladium coated nanospray capillaries. The MS was operated in negative TOF mode using a capillary voltage of 1.2 kV, cone voltage of 20 V, nano electrospray nitrogen gas pressure of 0.1 bar,

backing pressure of 2.47 mbar and a trap bias of 4 V. The source and desolvation temperatures were set at 80°C and 150°C, respectively. During time of flight (TOF-MS) acquisition, argon was used as the buffer gas, at a pressure of $4.0x10^{-3}$ mbar in the trap and transfer regions. Mass calibration was performed by a separate injection of sodium iodide at a concentration of 2 µg/µl. Data processing was performed using the Mass Lynx v4.1 suite of software supplied with the mass spectrometer.

2.4 Detection of PAA leaching from heat treated PAA-PVA electrospun nanofibre

Leaching was detected and measured using optical absorption spectrophotometry. Just after heat treatment PAA-PVA electrospun nanofibres were incubated in 20 ml of water at 20°C without pre-wash, and were gently shaken at 4.5 rpm for 2 h to 24 h, then from 3 d to 60 d. A standard calibration curve of absorbance versus PAA concentration was determined by measuring absorbance at 405 nm. The concentration of excess PAA that leached into the water was measured from the calibration curve by determining the absorbance of the nanofibre washed at 405 nm.

2.5 Synthesis of photosensitisers

It is already established that cationic charged photosensitisers are most successful at killing the Gram-negative bacteria (Spagnul *et al.*, 2015). Cationic porphyrins that were not commercially available were synthesised by variations on established methods. The cationic photosensitisers used for photodynamic treatment of contaminants in water are described in Table 2.3.

Photosensitiser	Source	Charge
Protoporphyrin IX (PPIX)	Commercially available	-
Tetramethyl pyridyl porphyrin (TMPyP)	Commercially available	+
Tetra pyridyl porphyrin (TPyP)	Commercially available	Neutral
Tetra allyl pyridyl porphyrin (TAllylPyP)	Synthesised	+
Tetra amine pyridyl porphyrin (TAminePyP)	Synthesised	+

Table 2.3 Description of photosensitisers used for PDI of contaminants in water

Two tetra cationic photosensitisers were synthesised. The materials and procedure of synthesis are described below.

2.5.1 Synthesis and structure of TAllylPyP

Figure 2.7 and Figure 2.8 show the structure of synthesised photosensitisers and reaction scheme of synthesis for both TAllylPyP respectively.

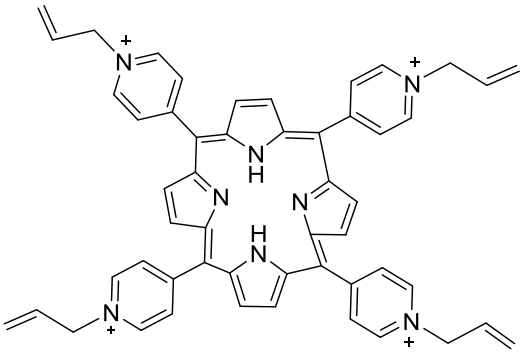

Figure 2.7 Structure of TAllylPyP - (5,10,15,20-Tetrakis(4-N-allylpyridyl)-porphyrin (Tall4PyP).

Materials: 5,10,15,20-tetrakis(4-pyridyl) porphyrin (H_2T_4PyP), N,N-dimethyl formamide (DMF), methanol, 3-bromopropene.

Method: Synthesis of TAllylPyP was carried out by refluxing a mixture of 5, 10, 15, 20-tetrakis (4-pyridyl) porphyrin (500 mg, 0.15 mmol) and excess

amount of 3-bromopropene (10 ml, 92 mmol) for 72 h in N, N-dimethyl formamide (40 ml) and methanol (10 ml) in dry condition under nitrogen. After completion of the reaction, assessed by thin layer chromatography an alumina TLC plates, the solvent was removed under reduced pressure. The residue was washed three times with acetone, chloroform and ethanol respectively and dried. The yield was 113 mg (90%), and TAllylPyP was then characterised by FTIR, NMR and mass spectroscopy.

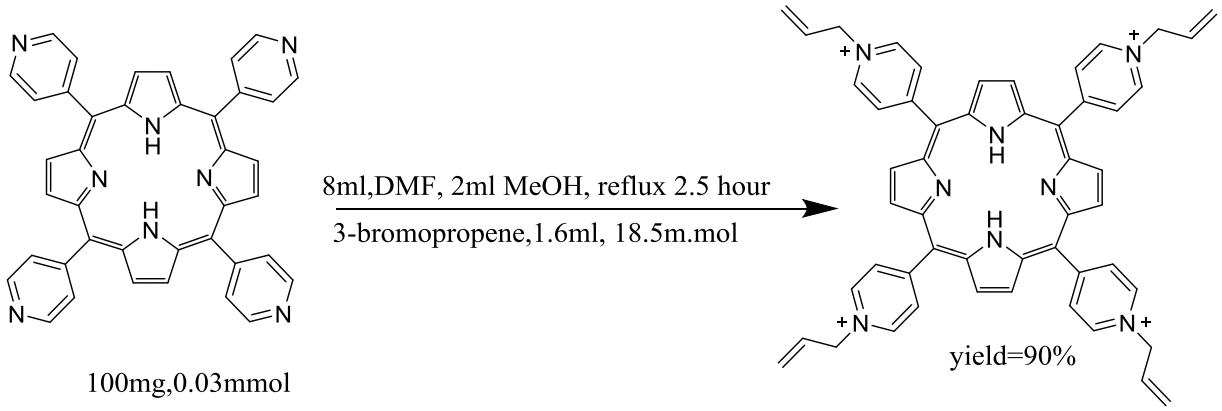

Figure 2.8 Synthesis of TAllylPyP - (5,10,15,20-Tetrakis(4-N-allylpyridyl)-porphyrin (Tall4PyP).

2.5.2 Synthesis and structure of TAminePyP

Figure 2.9 and Figure 2.10 show the structure of synthesised photosensitisers and reaction scheme of synthesis for both TAminePyP respectively.

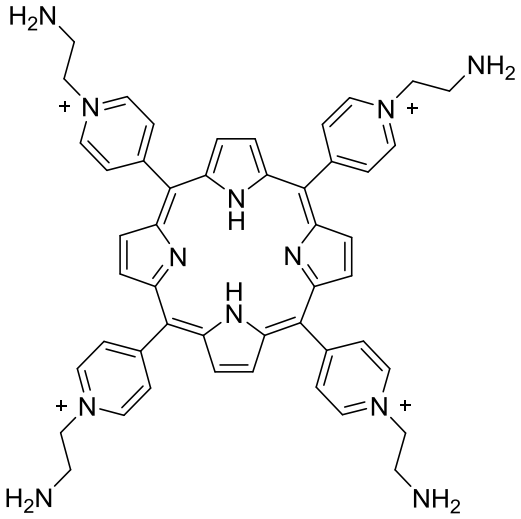

Figure 2.9 Structure of TAminePyP (5,10,15,20-Tetrakis(1-ethylamine-4-pyridyl)-21H,23H-porphyrin).

Materials: 5,10,15,20-tetrakis(4-pyridyl) porphyrin (Py4P), Dimethyl formaldehyde (DMF), ethanol, 3-bromoethylamine.

Method: Synthesis of 5,10,15,20-tetrakis(1-ethylamine-4-pyridyl)-21H,23H-porphyrin was carried out by refluxing a mixture of 5,10,15,20-tetrakis (4-pyridyl) porphyrin (100 mg, 0.016 mmol) and 3-bromoethylamine (0.238.4, 7.25 mmol for 72 h in N,N-dimethyl formamide (8 ml) and ethanol (2 ml) in dry condition. After completion of the reaction that was assessed by thin layer chromatography on alumina plates, the solvent was removed under reduced pressure. The crude product was purified by recrystallization with acetone and the yield was 150 mg (60%).

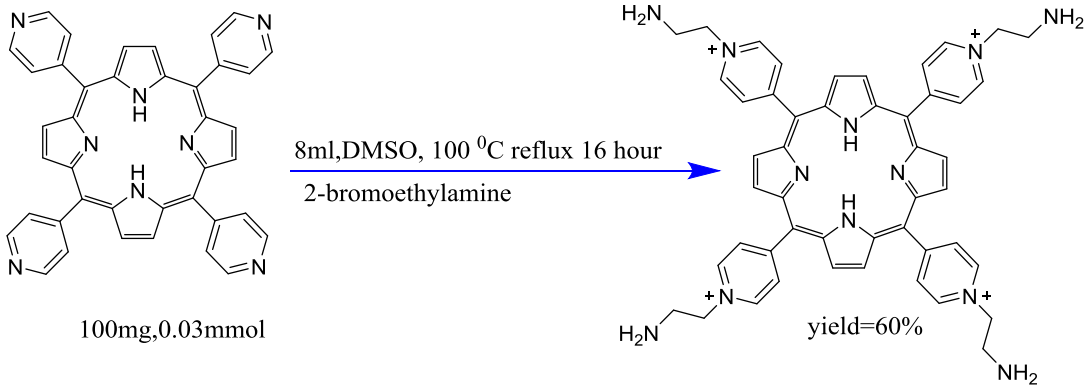

Figure 2.10 Synthesis of TAminePyP (5,10,15,20-Tetrakis(1-ethylamine-4-pyridyl)-21H,23H-porphyrin).

2.6 Determination of *E. coli* NCTC 10418 growth curve

The growth rate and viability of *E. coli* strain NCTC 10418 used for the PDT experiments were inspected by means of plated serial dilutions and growth curves. Freshly prepared LB broth (100 ml) was inoculated with 1 ml of overnight *E. coli* culture. This was placed in a shaking incubator Innova^{TM} 4000 incubator (New Brunswick Scientific Co, Edison, USA) at 120 rpm and 37°C. The growth curve was measured determining OD nm every 30 min until the optical density was between 0.4 and 0.6. At each time point, 8 folds serial dilutions were carried out from 10^{-2} to 10^{-8} using sterile distilled water. 100 µl aliquot of each dilution was spread onto an LB agar plate and incubated overnight at 37°C. After recording the number of colonies, the original bacterial concentration was calculated. On incubation, plates containing of colonies numbering from 30 to 250 were counted (Sutton, 2011; Adams and Moss, 2008).

2.6.1 Determination of *E. coli* BL21 (DE3) growth curve

The growth rate and viability of the carbenicillin resistant *E. coli* BL21 (DE3) used for the PDT experiments were inspected by means of plated serial dilution and growth curves. Carbenicillin disodium salt and kanamycin were obtained from Alfa Aesar in powder form and the stock solutions were prepared in sterile deionised water at 50 mg/ml. Tryptone and agar were obtained from Sigma-Aldrich, whilst glucose and yeast extract were purchased from BDH laboratories and Oxoid respectively. Freshly prepared LB broth (100 ml) was inoculated with carbenicillin antibiotic 1 ml of overnight *E. coli* BL21 (DE3) culture. This was placed in a shaking incubator Innova^{TM} 4000 incubator (New Brunswick Scientific Co, Edison, USA) at 120 rpm and 37°C. The growth curve was measured by determining OD nm every 30 min until the optical density was between 0.4 and 0.6. At each time point, serial dilutions were done from 10^{-2} to 10^{-8} using sterile distilled water. An aliquot of 100 µl each dilution was spread onto an LB agar plates and incubated overnight at 37°C. After recording the number of colonies, the original bacterial concentration was calculated by adjusting for dilution. On

incubation, plates comprising of colonies ranging from 30 to 280 (Sutton, 2011; Adams and Moss, 2008) were counted.

2.7 Determination of dark toxicity of photosensitisers in solution

Before doing the light treatment with the photosensitisers, dark toxicity of all photosensitisers was tested over range of concentrations. Five ml of bacterial suspension was incubated without photosensitiser in the dark. In different petri dishes each 5 ml of bacterial suspension was mixed with photosensitiser so that its final concentrations was from 1 µM to 50 µM. The photosensitisers were covered with aluminium foil and incubated in the dark for 30 min. After this, for each concentration of photosensitiser and stored. Serial dilutions were done from 10^{-2} to 10^{-8} using sterile distilled water. An aliquot of 100 µl of each dilution was spread onto an LB agar plate and incubated overnight at 37°C. After recording the number of colonies, the original bacterial concentration was calculated. Plates with from 30 to 250 colonies were counted (Sutton, 2011; Adams and Moss, 2008).

2.8 Photodynamic inactivation (PDI) of bacteria by photosensitisers in solution

PDI of Gram-positive and Gram-negative bacteria were carried out by both commercially available photosensitisers and newly synthesised photosensitiser in solution. Photosensitiser in solution were used for PDI of bacteria and their antibacterial activity are listed in Table 2.4.

Name of photosensitisers	**Antibacterial activity observed** Gram-negative bacteria
Protoporphyrin IX (PPIX)	✓
Tetramethyl pyridyl porphyrin (TMPyP)	✓
Tetra allyl pyridyl porphyrin (TAllylPyP)	✓
Tetra amine pyridyl porphyrin (TAminePyP)	✓

Table 2.4 Antibacterial activity of photosensitiser in solutions.

2.8.1 PDI of bacteria in solution

Stock solutions of photosensitisers was prepared in water soluble except for PPIX where DMSO was used. The stock solution was covered in foil and kept in the dark until further use. A standard preparation for PDI (Feuerstein *et al.*, 2004; Feuerstein *et al.*, 2005; Bezman *et al.*, 1978) of bacteria was carried out as follows. 30 ml of media was inoculated with bacteria and incubated overnight with shaking at 37°C at 140 rpm for 12 h. Then, 1 ml of overnight culture was inoculated into 50 ml of medium for 4 h (~OD 0.700-800). The suspension 50 ml transferred to Universal tube and centrifuged at 3000 rpm for 10 min. Supernatant was discarded. This step was repeated three times to wash the pellet and the bacteria re-suspended in 50 ml of 0.1 M potassium phosphate buffer (pH 7.4). The optical density of final washed suspension was measured, and the suspension dilute up to a total of 10^8 to 10^9 bacterial CFU/ml. This procedure was followed to prepare samples for all PDI experiments.

In each well of a 24 well plate, 1 ml of 10^8 to 10^9 bacterial CFU/ml were incubated with 25 µM to 100 µM of photosensitiser for 30 min in the dark. At the end of the dark incubation period, the cells were illuminated for 30-90 min under cold white light at 32 mW/cm^2. The light was set 30 cm above from the surface of the bacterial plate. Two sets of controls (Figure 2.11), with and without photosensitiser in the dark, were examined. A further control with illumination without any photosensitiser was included. After illumination, survival of the bacteria was determined by plating onto LB agar plates and counting the numbers of colonies. Serially diluted aliquots (100 µl) of cells from each dilution were plated onto LB agar and incubated at 37°C for 18 h.

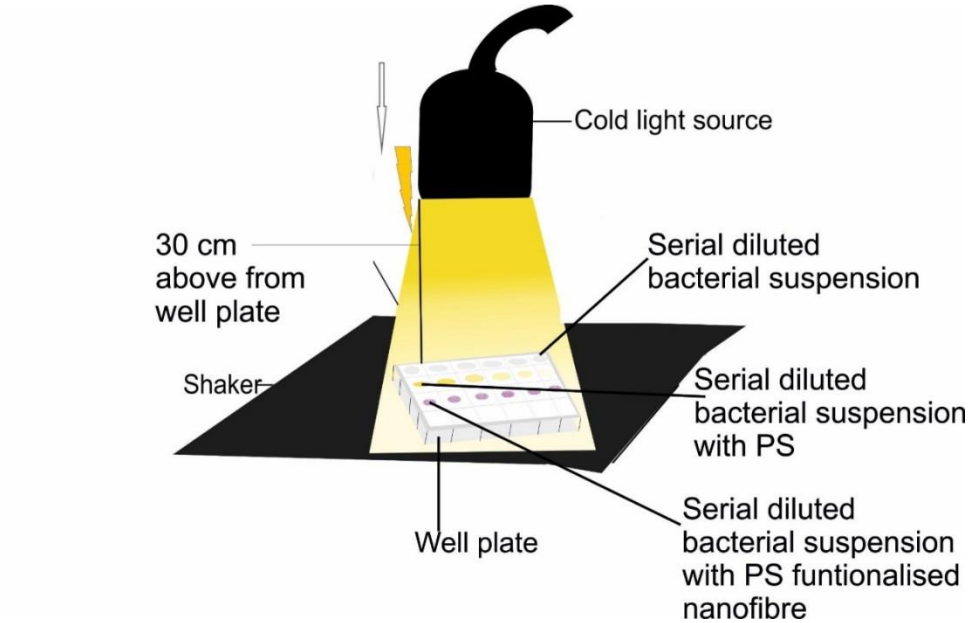

Figure 2.11 Schematic of experimental set up of PDI by photosensitiser in solution and photosensitiser functionalised electrospun nanofibre mats.

2.9 Functionalisation of nanofibres with photosensitisers

For functionalisation of nanofibre with photosensitiser in two different techniques were used. Photosensitisers were either adsorbed or covalently attached.

2.9.1 Adsorption

It has been established that cationic photosensitisers are the most effective of killing Gram-negative bacteria (Gyulkhandanyan *et al.*, 2009; Spagnul *et al.*, 2015). Keeping that in mind majority of photosensitisers were selected or synthesised as cationic, and the nanofibres produced were –COOH functionalised was possible functionalisation of the nanofibre mat, by electrostatic adsorption was possible.

2.9.1.1 TMPyP immobilisation onto PAA-PVA nanofibre mats by adsorption

As TMPyP is a tetracationic photosensitiser and does not contain any suitable functional groups for covalent reaction. Electrostatic interaction was possible with TMPyP to functionalise the PAA-PVA nanofibres.

Neutralisation: electrospun PAA-PVA nanofibre material (60 mg) was treated with 20 mL of 1.5 N NaOH to completely replace of H^+ with Na^+ at rt for 30 minutes. Finally, the material was washed with deionised water until the pH value reached pH 6 to 7 and then stored dry at rt. Ion Exchange with TMPyP: the PAA-PVA nanofibre material (2 cm^2) was immersed in 2 mL of a 3 mM aqueous solution of TMPyP in deionised water (30-120 min) in the dark.

2.9.1.2 TAllylPyP immobilisation onto PAA-EG by adsorption

PAA-EG nanofibre was also functionalised with tetra allyl pyridyl porphyrin by adsorption followed by neutralisation of PAA-EG nanofibre (same as 2.9.1.1).

2.9.2 Covalent immobilisation of photosensitisers

Initially PPIX was covalently immobilised onto polyacrylonitrile-Jeffamine blended (PAN-Jef) by coupling of –COOH on the PAN and $–NH_2$ on the Jeffamine. EDC and sulfo-NHS were used as amine conjugation agents. The same procedure was used for coupling of TAminePyP with PAA-EG nanofibre mats. Conjugation of TAllylPyP with PAA-EG nanofibre was carried out C-H coupling reaction. All functionalisation methods are described in the following sections.

2.9.3 Immobilisation of PPIX onto (PAN-JEF) electrospun nanofibre mats

The immobilisation of PPIX onto electrospun nanofibre mats was carried out by amine coupling with -COOH group chemistry, where the carboxylic group in PPIX couples covalently to the amines present on the surface of the nanofibre mats. A slight modification to the procedure by (Hermanson, 2013) was made. A 2.5 ml aliquot of a 0.01 M stock solution of PPIX, 2.5 ml of 1 mg/ml N-hydroxy sulfosuccinimide (sulfo-NHS) in DMSO and 2.0 ml aliquot of 1 mg/ml 1-ethyl-3-(3-dimethylaminopropyl) carbodiimide (EDC) in MES buffer were added to 22.5 ml of 0.1 M sodium phosphate buffer (pH 6.5) solution to prepare 29 ml of reaction solution for the process of conjugation. The aminated electro-spun nanofibre discs were added to the reaction solution and were incubated at room temperature for 2 h. The EDC and sulfo-NHS coupling reaction is efficient and increases the yield of conjugation and the reaction scheme is shown in Figure 2.12. After 2 h the fibre mats were washed 3 times with deionized water to get rid of excess reactants and by-products.

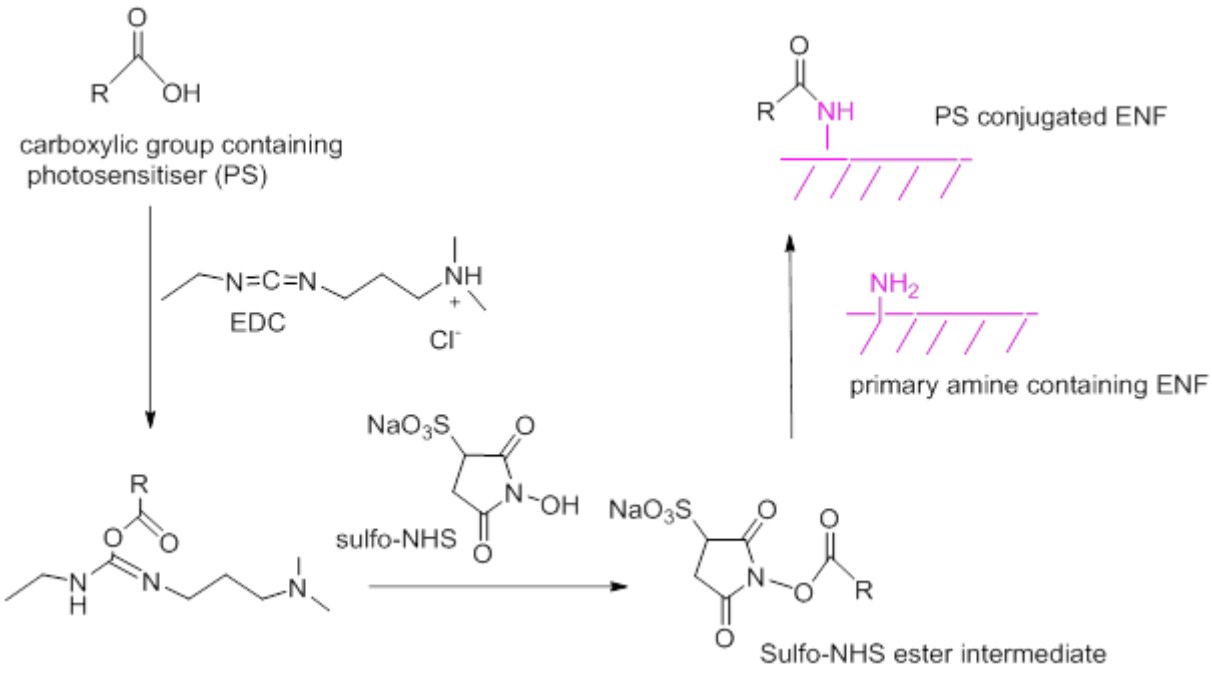

Figure 2.12 Reaction scheme of photosensitiser immobilisation onto the electrospun nanofibre surface.

The reaction scheme shows the covalent modification of aminated ENF with photosensitiser containing carboxylic group. EDC and sulfo-NHS are the coupling reagents.

2.9.3.1 Amidation of carboxylic groups

As the PDI of NCTC 10418 by PPIX was inconsistent, it was assumed that there might be some free carboxylic group left w after PPIX immobilisation onto the nanofibre discs, which acted to repel the bacteria. Thus, steps were taken to block the remaining carboxylic group of PPIX after immobilisation (Figure 2.13)**.** Propylamine and water-soluble coupling carbodiimide reagent EDC were used to amidate any remaining carboxylic groups. Five ml of 50 mM of propyl amine was added to six PPIX immobilised nanofibres discs. Then 5 ml of EDC, pH 5.5 to a final concentration of 5 mM was added and the nanofibre discs incubated for 4 h. Then the nanofibres discs were washed three times with distilled water.

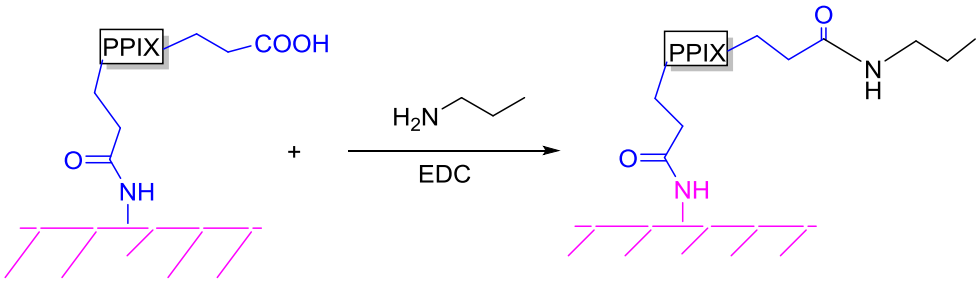

Conjugated ENF-PS with free carboxylic group

amidation with free carboxylic group

Figure 2.13 Amidation to block the free carboxylic group of PPIX by Propylamine was coupled to free –COOH using EDC.

2.9.4 Determination of amine availability and confirmation of PPIX conjugation onto (PAN-Jeff)

Midland blotting: attempts to quantify amines on the surface of (PAN-Jeff) were carried out by “Midland blotting” (Rushworth *et al.*, 2013). Briefly, aminated nanofibre mat surfaces were incubated for 30 min with NHS biotin. Then after washing with phosphate buffer incubated with streptavidin-HRP prior to further washing in in PFS. To detect free amine (NH_2) groups, functionalised nanofibre mats were incubated in the presence of NHS-biotin (1mg/ml in PBS containing 10% (v/v) DMSO) for 30 min in order to attach biotin to the free amine groups (Figure 2.14). After five washes with dH_2O, the nanofibres were incubated with HRP-streptavidin (50 fold diluted in PBS) for 30 min.

ECL reagent was then added and the image recorded. To avoid evaporation of small volumes of reagents pipetted onto the nanofibres, all incubations were conducted in a moist chamber comprising a closed petri dish containing a moist tissue box.

The nanofibre mats were very soft and fragile and this technique contained many washing steps. To strengthen the (PAN-Jeff) nanofibres it was cut into 1 cm^2 pieces. The top polypropylene sheet of each square piece was punched (0.5 cm diameter). Then with black tape each square piece was placed on a microscopic slide the punched open end left uncovered. The reagents were added to this open 0.5 cm disc.

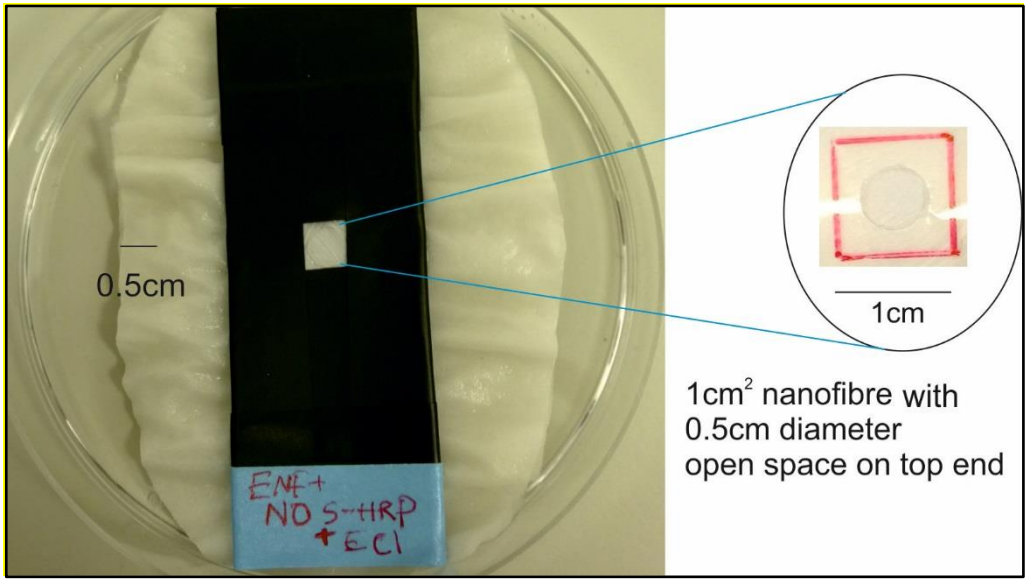

Figure 2.14 Amine determination onto nanofibre surface (midland blotting).

Left panel of picture is showing the 0.5 cm diameter open circular space is a subject of midland blotting. Rest of the part of nanofibre was covered with black tape to obtain clean optical signal. Right panel shows the 1 cm^2 nanofibre sample in between two polypropylene sheets. The top polypropylene sheet was punched so that reagents can be added. This 0.5 cm diameter open space was subject to Midland blotting. The diagram is not up to scale.

Image quantitation; chemiluminescence and bright field images obtained on a G: BOX imager were saved as .tif files and analysed using Image J software (NIH; Bethesda, Maryland, USA). Following background subtraction, the integrated signal intensity of each nanofibre disc was measured by marking out an appropriate area around the nanofibre using

the bright field image as a guide. Images presented are either chemiluminescence (white light on a black background), bright field images (pictures of nanofibre material), or a superimposition of both, where chemiluminescence has been false coloured green to aid viewing.

2.9.5 Hydoxylation of PAN to polyacrilic acid (PAA) and conjugation of PPIX with PAA

The flow cell was built using polyacrilonitrile (PAN) and Cerex fabric. PAN-Jeff nanofibre and Cerex was lined into nanofibre flow cells. The design allows connection to the inlet and outlet aperture using Luer lock fittings (Figure 2.6).

(i) De-ionised water was pumped through the flow cell, using a peristaltic pump with silicone tubing and luer fittings. Flow cell was placed in a water bath at 80˚C

(ii) 3N concentration of sodium hydroxide aqueous solution was pumped through the cell.

(iii) Rinsed with de-ionised water to remove the unreacted NaOH.

(iv) A low molar concentration of hydrochloric acid was pumped through the cell, to create COOH groups on the surface of the PAN and the PAN regions of the PAN-Jeff fibre.

(v) Cell was rinsed with de-ionised water.

(vi) Low molar concentration of hexamethylenediamine dissolved in water was pumped a through the cell for amine and COOH groupsconjugation to form stable amide bonds.

(vii) Flow cell was again rinsed with de-ionised water to remove unreacted hexamethylenediamine.

(viii) PPIX was dissolved in methanol and pumped through the cell at 90˚C, to react the COOH of the PPIX with the free amine on the hexamethylenediamine molecule.

(ix) Flow cell was finally rinsed with DI water to remove unreacted chemicals and dry.

2.9.6 Covalent immobilisation of TAllylPyP onto PAA-EG nanofibre mats

To functionalise the PAA-EG nanofibre mats with TAllylPyP, palladium catalysed allylic acyloxylation of the terminal alkene was conducted in the presence of a base. The methodology was adopted and modified from a literature reported by Thiery *et al.* (2010). As the application for these nanofibres is water treatment, throughout the project use of hazardous chemicals were avoided where possible or minimised. The solvent system used by Thiery *et al.* (2010) was modified so that after covalent immobilisation followed by water treatment, the TAllylPyP$_{cov}$-(PAA-EG) did not cause secondary contamination or toxicity. Water was used as the main solvent system in this reaction, but a minimal amount of chloroform was necessary to solubilise the palladium acetate. Figure 2.15 shows the schematic of palladium catalysed allylic acyloxylation to immobilise TAllylPyP onto PAA-EG nanofbre mats.

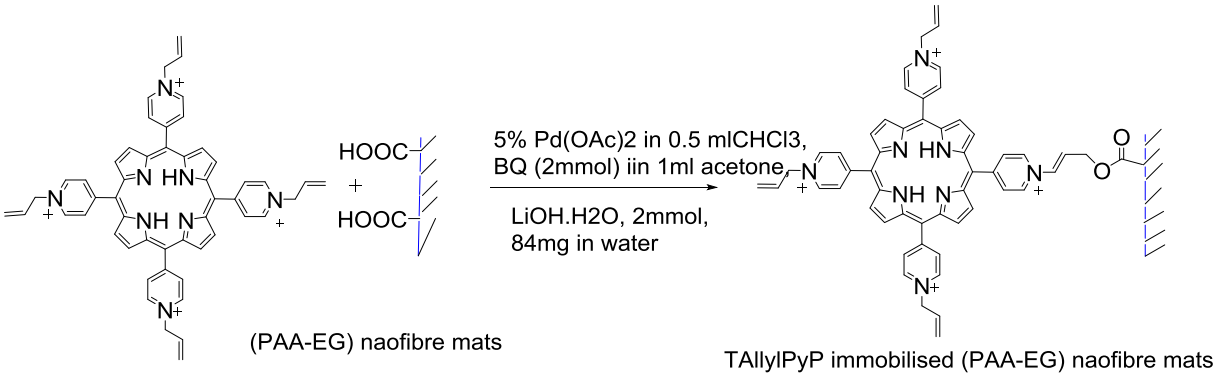

Figure 2.15 Schematic of palladium catalysed allylic acyloxylation to immobilise TAllylPyP onto PAA-EG nanofbre. ( ), nanofibre mats.

To perform the TAllylPyP immobilisation, a round-bottomed flask was charged with LiOH.H_2O (2.0 mmol, 84 mg) in 5 ml of deionised water. Then, 120 mg of PAA-EG nanofibre mat was immersed and the mixture was heated (oil bath, 40°C) for 10 min. benjoquinone (2.0 mmol, 216 mg) was dissolved in 1 ml of acetone. $Pd(OAc)_2$ (0.1 mmol, 22.4 mg) was dissolved in 0.5 ml of $CHCl_3$, and then an extra 5 ml acetone was added to mix with

nanofibre. The mixture was stirred at rt for 15 min, and then heated (oil bath, 40°C) for 24 h. After cooling to rt, the mixture was filtered through a sintered funnel, which was washed with Et_2O (50 mL). NaOH (3N, 25 mL) was then added, and the mixture was stirred for 15 min. Then thus nanofibre mats were washed with deionised water (3x25 mL), three times, organic phase was washed with the aqueous combined phases were extracted with di ethyl ether (25 mL). Finally to remove the extra unreacted adsorbed chemicals from the PAA-EG nanofibre mat, 3 N NaOH was used to wash it until the washings became colourless. The modified reddish brown PAA-EG nanofibre mats were washed with deionised water several times until the pH reached 7.

2.9.7 Covalent immobilisation of TAminePyP onto PAA-EG nanofibre mats

TAminePyP immobilisation onto PAA-EG mats was conducted using two-step coupling of –COOH and $–NH_2$ Using EDC and sulfo-NHS. The following procedure was adapted from a procedure described by Grabarek and Gergely (1990) and is shown in Figure 2.16.

Materials; 0.1 M MES, 0.5 M NaCl, pH 6.0, phosphate-buffered saline (PBS), containing 100 mM sodium phosphate, 150 mM NaCl; pH 7.2 (Product No. 28372), PAA-EG nanofibre 12 mg, TAminePyP was dissolved in phosphate-buffered saline, sulfo-NHS.

Procedure; 0.4 mg EDC (~2 mM) and 1.1mg of sulfo-NHS (~5mM) were added to the reaction mixture containing PAA-EG in 5 mL MES. The nanofibre mat and reactants were incubated for 15 min at rt with slow shaking. To quench the reaction nanofibre were removed from reaction mixture and washed. Then, TAminePyP was added to the activated PAA-EG and the reaction mixture kept in shaker with slow shaking for 24 h at rt. To remove unreacted chemicals the PAA-EG mat was washed three times with 2N NaOH.

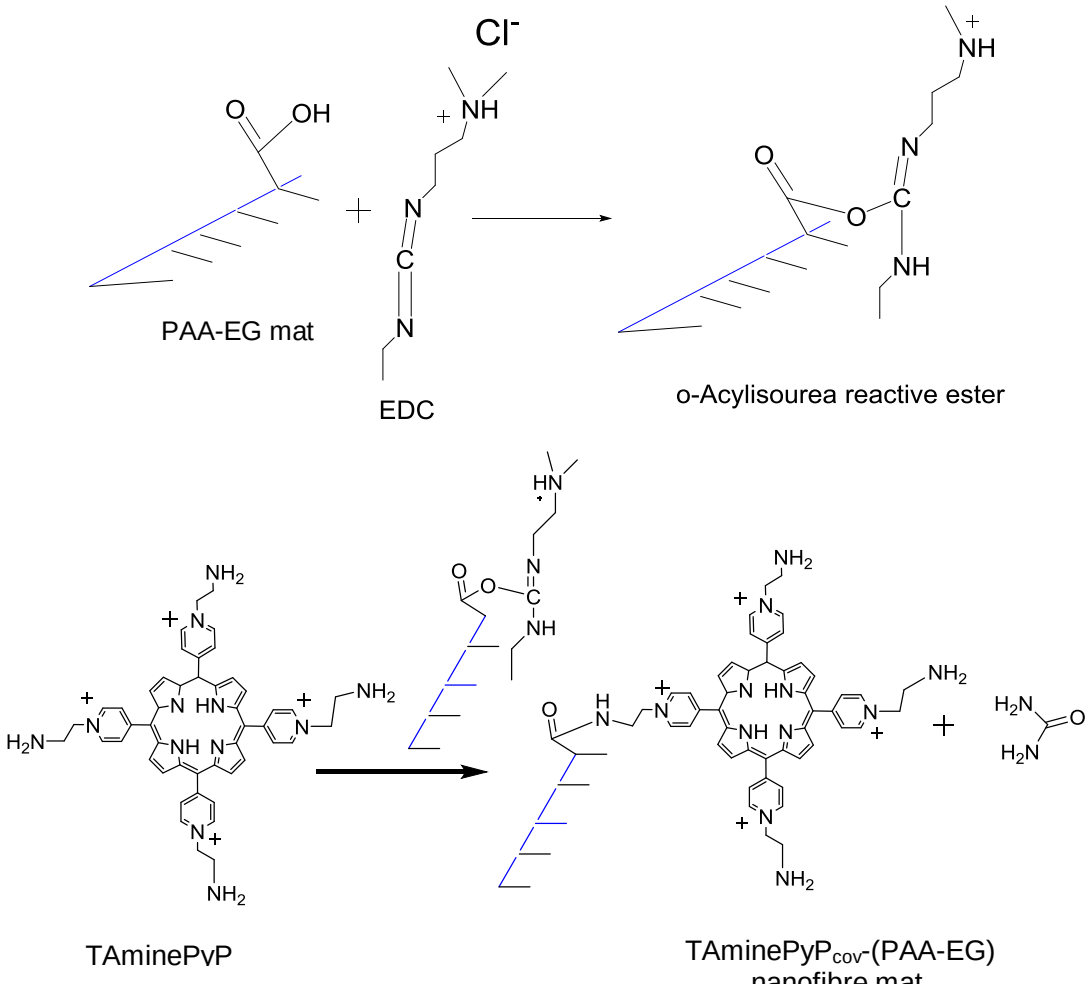

Figure 2.16 Schematic of TAminePyP immobilisation on to PAA-EG nanofibre mats.

The reaction scheme shows the covalent modification of carboxylic group functionalised PAA-EG nanofibre mats with amin functionalised TAminePyP photosensitiser. EDC and sulfo-NHS were used as coupling reagents.

2.10 Characterisation of functionalised nanofibre

For characterisation of nanofibres mats FTIR, SEM and XPS were carried out. To estimate the carboxylic groups of polyacrylic acid, potentiometric acid-base titration was carried out. Due to non-homogeneous morphology of nanofibres mats this measurement was considered as semi quantitative at best. Adsorbed photosensitisers were estimated by measuring absorbance before and after their adsorption.

2.10.1 Scanning electron microscopy (SEM)

Nanofibre morphology was studied via SEM on aFEI Quanta 200F FEG-Scanning Electron Microscopes with an operating voltage of 15 kV. Prior to measurements, the nanofibrous mats were sputter coated with a 4 nm-thick Pt film.

2.10.2 FTIR

For characterisation of functional groups on the nanofibres, FTIR spectra were recorded using a Nicolet 5700 FTIR spectrometer (Thermo Nicolet Corporation) at ambient conditions.

2.10.3 Estimation of TMPyP bound to PAA-PVA nanofibre mats

To estimate the bound photosensitiser loading, the difference on the initial concentration and unbound photosensitiser concentration was monitored at A_{420}.

2.10.4 Estimation of functional groups

To estimate the amount of –COOH groups on PAA-PVA nanofibre a potentiometric acid-base titration was carried out. First, carboxylic groups of nanofibre were completely protonated by washing the nanofibre mats for several times with 10 mM HCl. After this, from calibration curve the H+

concentration in liquid was obtained and then all H+ bound and in solution was determined by titration with NaOH solution.

2.11 Assay of singlet oxygen generation by photosensitiser functionalised nanofibre mats

Singlet oxygen generation by photosensitiser functionalised nanofibre mats was analysed by observing the decrease in A_{318} of 2-amino-3-hydroxypyridine when it reacted with singlet oxygen (Amat-Guerri *et al.*, 1999; Komagoe *et al.*, 2011). The following assay conditions were tested: (a) 1 µM TMPyP as positive control; (b) TAllylPyp, TAminePyP at 1µM concentration was dissolved in 200mM of 2-amino-3-hydroxypyridine (c) 1 cm^2 photosensitiser immobilised nanofibre mat was immersed in 3.5 ml of 200 mM 2-amino-3-hydroxypyridine UV-Vis measuring cell. The samples were then illuminated in white light for 1 min at a distance of 30 cm and fluence rate of 32 mW cm^{-2}. Every alternate 2 minutes the reading changes in the absorbance before and after irradiation were measured at 318 nm.

Chapter 3

PDI of bacteria in water by photosensitiser in solution

3.1 Overview

With the aim of inactivation of microorganisms in water, two model bacteria were selected: Gram-negative bacteria *E. coli* NCTC 10418 and carbenicillin resistant *E. coli* BL21 (DE3).

During the photodynamic inactivation (PDI) process, the photosensitiser (PS) is the critical element. So it was crucial to select an efficient photosensitiser, with the illumination of appropriate wavelengths of light that can cause efficient PDI of microorganisms in water. It has been reported previously that almost all photosensitisers can inactivate the Gram-positive bacteria (Surdel *et al.*, 2017; George *et al.*, 2009), whereas inactivation of Gram-negative bacteria is the challenge because of their complicated cell wall and membrane structure. Gram-negative bacteria are of prime interest of this research because they are an indicator of sewage pollution. Thus, it was essential to choose photosensitiser which can effectively kill Gram-negative bacteria. Initially protoporphyrin IX (PPIX) was used for complete PDI of Gram-negative bacteria, but photo-killing by PPIX was not successful as overall negative charge of PPIX was repelled (George *et al.*, 2009). Commercially available tetra cationic TMPyP was successfully used for PDI of Gram-negative bacteria. PDI of carbenicillin resistant Gram-negative bacteria BL21 (DE3) by TMPyP in solution was also carried out successfully. In this research, optimisation of photosensitiser concentration for PDI was carried out. The effect of light intensity and illumination time were also studied for PDI. PDI bacterial strains used in this research was also studied using newly synthesised water-soluble tetra-cationic photosensitiser, tetra allyl pyridyl porphyrin (TAllylPyP), and tetra amino pyridyl porphyrin (TAminePyP). Concentration, illumination time and intensity were optimised for these photosensitisers. Dark toxicity were also studied for all

photosensitisers. In this Chapter, all PDI experiments using photosensitiser in solution were documented.

3.2 Determination of growth kinetics of model bacteria

Growth curves were determined to confirm the activity of *E. coli* NCTC 10418 and carbenicillin resistant *E. coli* BL21 (DE3).

3.2.1 Growth kinetics of *E. coli* NCTC 10418

NCTC 10418 was the *E. coli* strain generally used for PDI studies. To confirm that the *E. coli* strain used in the experiment was viable and behaved normally, a growth curve of *E. coli* NCTC 10418 was obtained by measuring OD every 30 min for 4 h. From each point, cells were plated at multiple dilutions to enable CFU to be determined. As expected, three characteristic phases of the growth cycle curve were documented (Figure 3.1). Initially the cells were in the lag phase, where they take time to start cell division. During the log phase, continuous cell division takes place and a sharp increase in the absorbance was observed. Finally, the cell division slowed down as their growth became limited by nutrient supply and they entered the stationary phase (Figure 3.1). Serial dilutions were carried out from 10^{-2} to 10^{-8} and CFU/ ml was determined. The data showed that *E. coli* NCTC 10418 was viable and capable of yielding a good number of colonies.

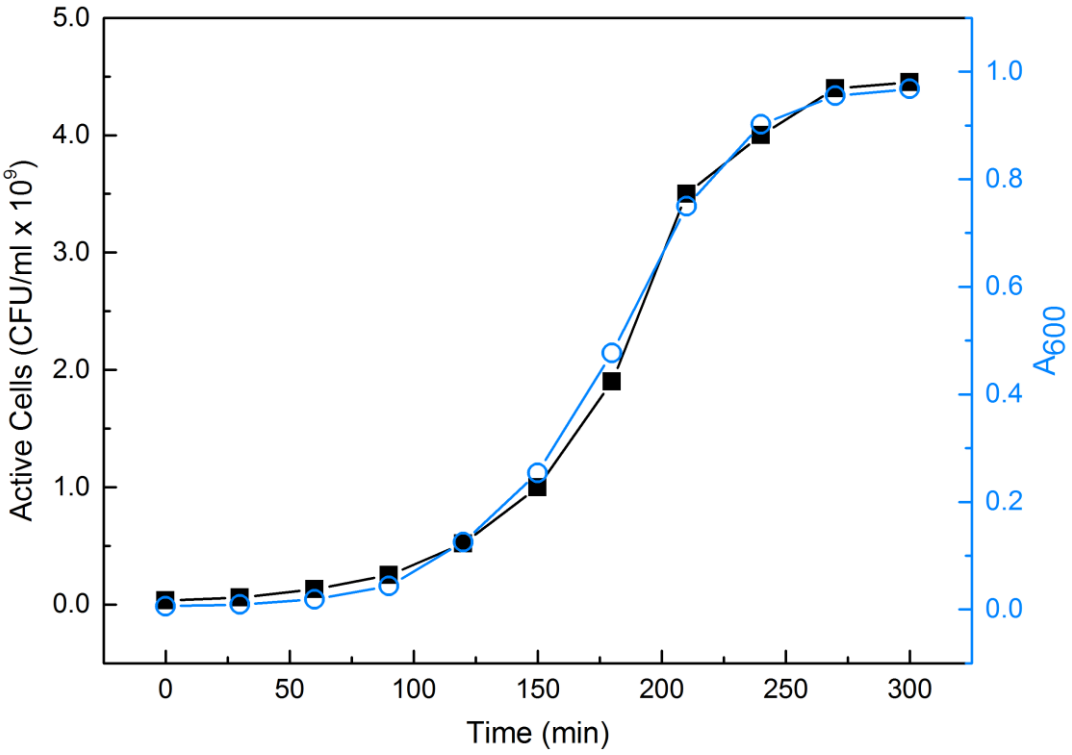

Figure 3.1 Growth curves of *E. coli* NCTC 10418.

(−■−), A_{600} (OD) versus time of incubation; (−○−), CFU/ml. Data are mean ± Standard deviation (n=3). Error bars are smaller than the symbol size.

The rate of growth and the number of colony growth with time is shown in Figure 3.1. The lag phase is observed between 0 and 60 min, just before rapid division commences. In the log phase, there is continuous cell division taking place, which is observed between 60 and 240 min. Finally, the stationary phase was seen, where cell division reduced at 240 (4 hours) min onwards (Figure 3.1).

3.2.2 Growth kinetics of *E. coli* BL21 (DE3)

BL21 (DE3) is a carbenicillin resistant *E. coli* strain used as model strain in this research to investigate the efficiency of PDI for water sterilisation system against antibiotic resistant bacteria. Again, confirmation of the viability of BL21 (DE3) growth kinetics was studied by measuring OD every 30 min for 5 h. As expected three same characteristic phases of the growth were documented (Figure 3.2). Initially the cells were in the lag phase, then they entered in log phase and finally to the stationary phase. BL21 (DE3) behaved essentially the same as NCTC 10418 as shown in Figure 3.2 A

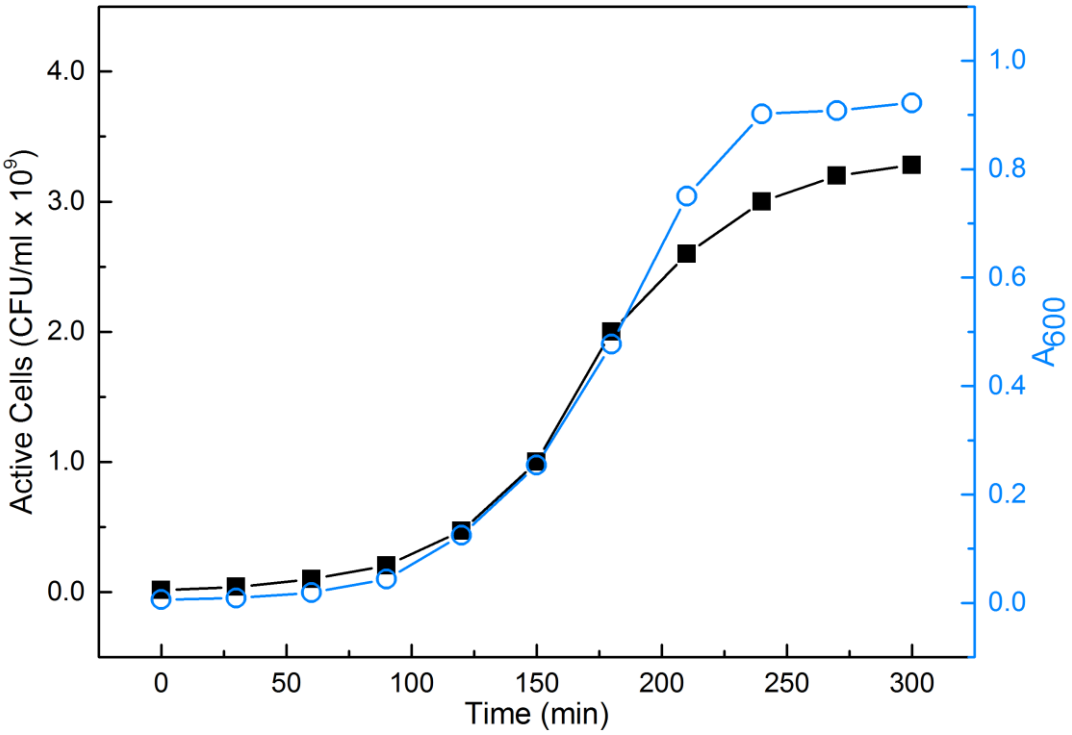

Figure 3.2 Growth curve of *E.coli* BL21 (DE3).

(−■−), A_{600} (OD) versus time of incubation; (−○−), CFU/ml. Data are mean ± Standard deviation (n=3). Error bars are smaller than the symbol size.

3.3 Measurement of light intensity on the sample surface

The intensity of the KL 2500 LCD, (250 W) cold light source light was measured at different distances from the light to the sample surface. Intensity was measured from 10 to 32 cm and the highest intensity of 234 mW/cm^2 was measured at 10 cm from the sample, whilst the minimum intensity of 44.32 mW/cm^2 was at 32 cm. Intensity of used cold light decreases with the increase of light, indicating that this parameter is of no significance for the tested organisms. (Figure 3.3).

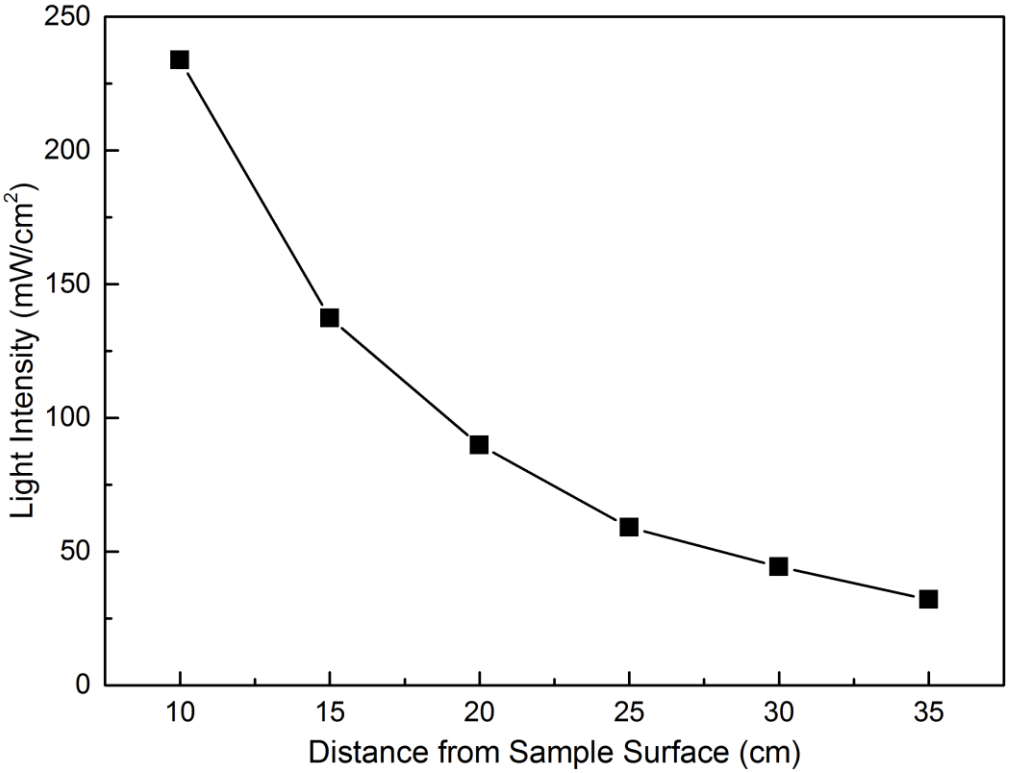

Figure 3.3 Calibration of light intensity at sample surface.

(■) Light intensity was measured using light meter at the sample surface, by pointing the KL 2500 LCD (250 W) light sources 10 to 32 cm distance.

In majority of the experiments in this project the light intensity used was 30 mW/cm^2 unless otherwise indicated. This light intensity is low and equivalent to just 3% of bright midday sunlight under clear sky conditions. PDI experiments were also performed at a higher intensity of light 70 mW/cm^2. But also, showing that efficient PDI occurs at low light intensity mean it could be applied in the UK and other northern European nations where sunlight is not availability is poor. This would be advantageous for reduction of energy consumption in the water treatment sector.

3.4 Selection of photosensitisers

PDI of microbial contaminants in water was studied with different photosensitisers in solution to identify the effectiveness of photosensitiser by optimal concentration. The light intensity and the duration of illumination were also studied using various photosensitiser solutions. Two commercially available photosensitisers used in this study are:

(i) protoporphyrin IX (PPIX); and
(ii) tetra methyl pyridyl porphyrin (TMPyP).

For covalently functionalise the electrospun nanofibre two new photosensitisers were synthesised for this research. These are:

(i) tetra allyl pyridyl porphyrin (TAllylPyP); and
(ii) tetra amine pyridyl porphyrin (TaminePyP).

PDI efficiency against the model microorganisms (Section 3.2) of all of the above four photosensitisers are described in the following sections.

3.4.1 PDI of Gram-negative bacteria with PPIX in solution

At first, PDI was carried out with PPIX in solution as described in Section 2.7.1.The surviving *E. coli* NCTC 10418 cells were measured after exposure to PPIX (25 - 300 µM) in the dark or after irradiation with visible light for 30 min. The change in CFU/ml indicated no substantial cell death due to PDI (Figure 3.4), which was in agreement of similar findings presented by Surdel *et al.* (2017); Malik *et al.* (1992).

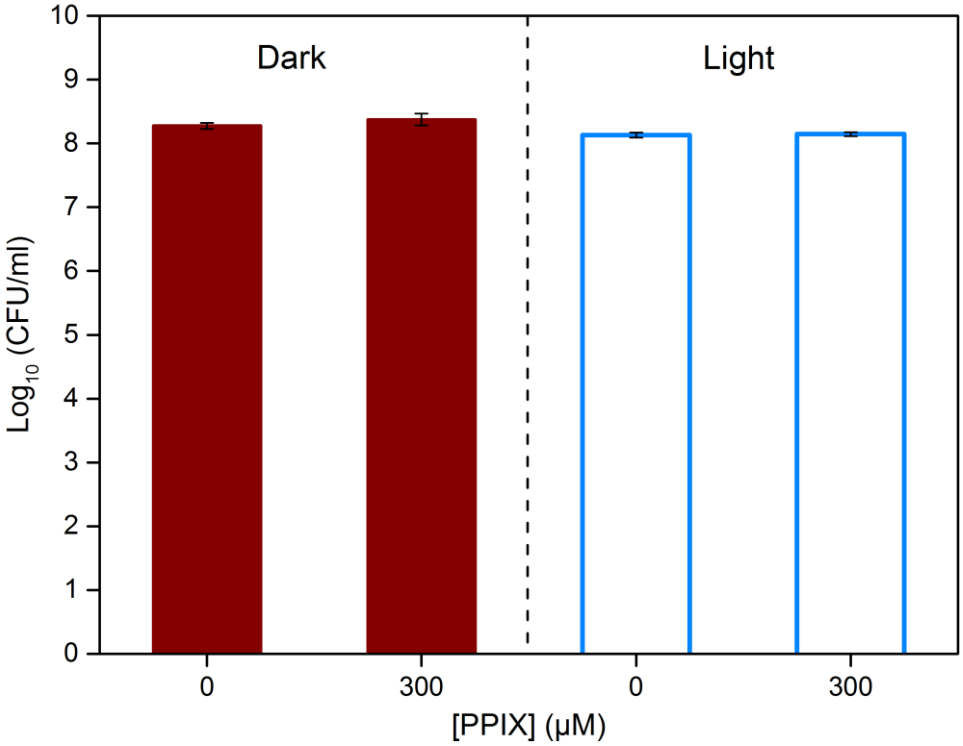

Figure 3.4 PDI of Gram-negative bacteria *E. coli* NCTC 10418 by PPIX in solution.

E. coli NCTC 10418 cells at 8 log CFU/ml in water were exposed to 0 or 300 μM PPIX for 30 min in the dark or under 70 mW/cm^2 illumination. Cell number was then determined by serial dilution followed by plating. (■), dark treated; (□), light treated. Data are mean ± SEM, (n=3).

Previous studies reported that Gram-negative bacteria contains a highly organised outer bacterial membrane structure with a negatively charged phospholipid layer (Malik *et al.*, 1992; Jori *et al.*, 2006; Spagnul *et al.*, 2016; Bartolomeu *et al.*, 2017; Surdel *et al.*, 2017). It is likely that negatively charged phospholipid because of porous prevents the cellular attachment of anionic photosensitiser and also $^1O_2$ cannot penetrate close enough to cause PDI. Thus, PDI was performed for Gram-positive bacteria *Staphaylococcus epidermis* to investigate the PDI activity of PPIX.

3.4.2 PDI of Gram-positive bacteria with PPIX in solution

For comparison, the PDI of the Gram-positive bacteria, *Staphylococcus epidermidis* with PPIX in solution was successful (Figure 3.5). In both cases the numbers of cells surviving with and without PPIX were compared statistically using the Dunnett's multiple comparisons test in ANOVA.

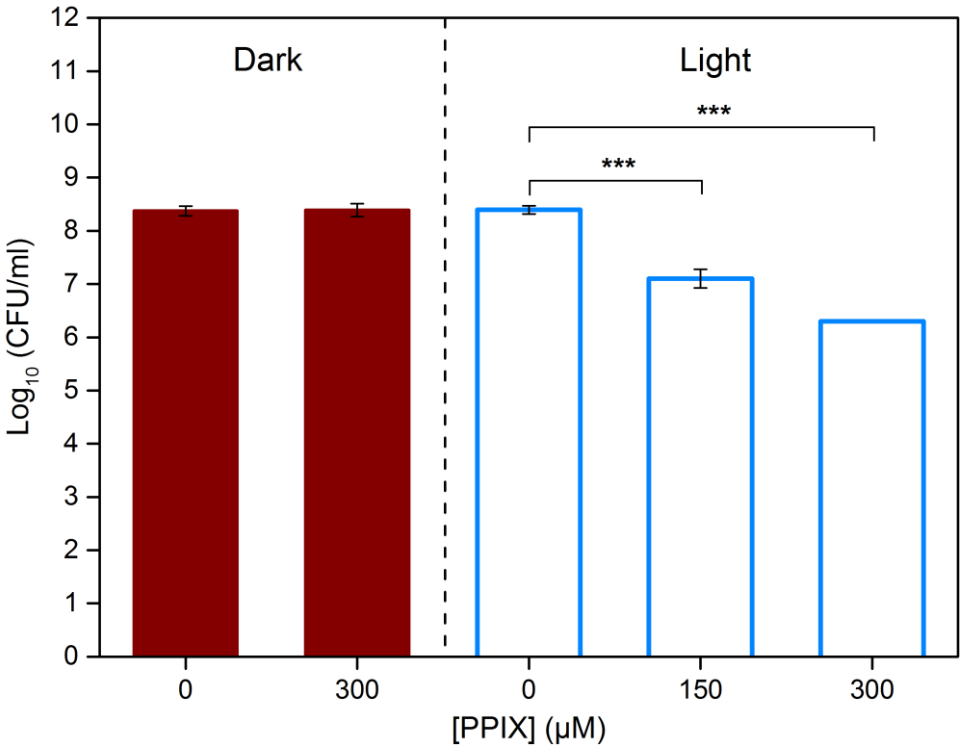

Figure 3.5 PDI of Gram-positive bacteria *Staphylococcus epidermidis* with PPIX in solution.

Staphylococcus epidermidis cells 8.5 log CFU/ml in water were exposed to 0, 150 and 300 µM PPIX for 30 min in the dark or under 70 mW/cm^2 illumination. Cell number was then determined by serial dilution followed by plating. (■), Dark treated; (□), light treated. Data are mean ± SEM, (n=3). The values were compared statistically for with and without PPIX using the Dennett's multiple comparisons.

Hence, it was clear that PPIX was able to cause PDI with Gram-positive bacteria because of porous and permeable structure of Gram-positive cell wall. Whereas quasi compact cell wall of Gram-negative *E. coli* NCTC 10418 prevent the PPIX to be closer to kill the *E.coli*. As an indicator of sewage pollution, which is a major source of human pathogens, Gram-negative bacteria is the prime target in this research.

3.5 PDI with TMPyP in solution

PDI of Gram-negative bacteria by PPIX in solution was not successful (Section 3.4.1), because of overall negative charge on PPIX (George *et al.*, 2009; Malik *et al.*, 1992; Spagnul *et al.*, 2016). The tetra cationic photosensitiser TMPyP was chosen for PDI of Gram-negative bacteria because of mainly two important features (Bartolomeu *et al.*, 2017; Almeida *et al.*, 2011):

- commercial availability; and
- PDI efficiency to both Gram-positive and Gram-negative bacteria and other types of microorganisms.

The presence of positive charges in the macrocycle core is crucial characteristics of efficient photosensitiser to inactivate Gram-negative bacteria.These positive charges increase the interaction with negative lipopolysaccharides sites of external membrane of Gram-negative bacteria. To confirm that the cell killing was due to PDI, dark toxicity must be ruled out.

3.5.1 Study of dark toxicity of TMPyP

Initially *E. coli* was incubated with different concentrations of TMPyP from 1 to 50 µM and incubation times for 60 min under dark conditions. No substantial changes were observed in the survival rates compared to controls without TMPyP (Figure 3.6). At low concentration, there is minimal dark toxicity even at higher concentrations toxicity increased minimal

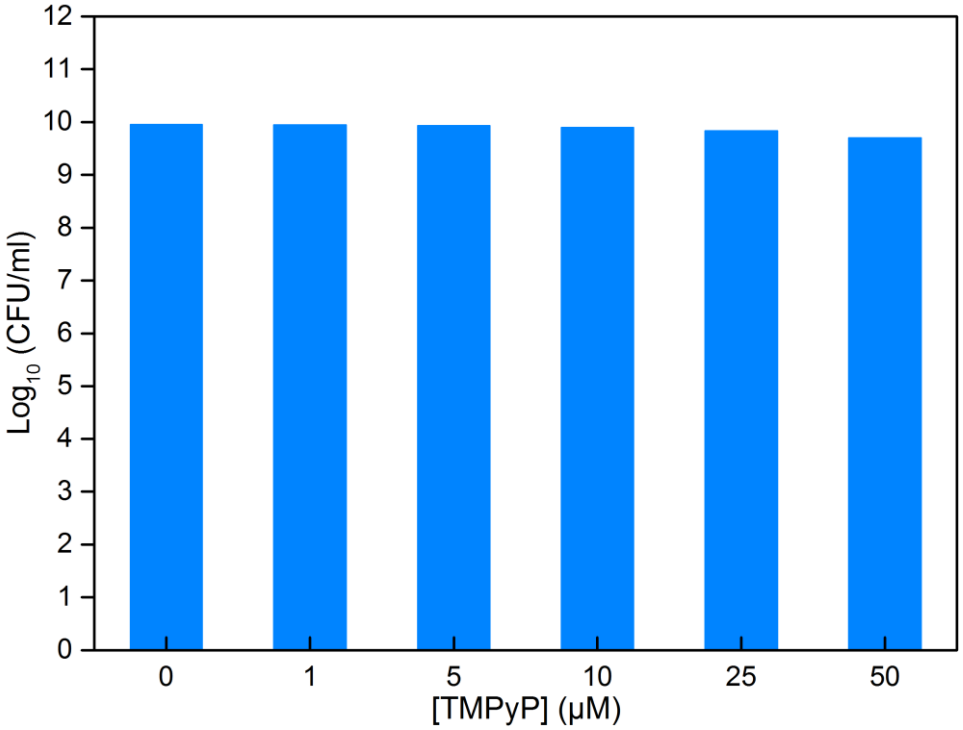

Figure 3.6 Dark toxicity of TMPyP in solution with Gram-negative bacteria *E. coli* NCTC 10418.

10 Log CFU/ml cells were incubated with different [TMPyP] from 1 to 50 µM for 1 h in dark before viable cell determination. Cells were determined by plating following serial dilution. Data are average ± SEM, (n=3).

3.6 Photodynamic inactivation by cationic photosensitiser

3.6.1 PDI of *E. coli* NCTC 10418 TMPyP in solution

TMPyP solution was used for PDI of *E. coli* NCTC 10418 in water. Figure 3.8 shows the survived cells of *E. coli* NCTC 10418 strains after exposure to TMPyP at 50 µM; either in the dark or after irradiation with visible light at 30 mW/cm^2 for 30 and 60 min. After 60 min of light exposure, no cells survived. This showed that in *E. coli* NCTC 10418, the tetra cationic TMPyP was able to generate ROS close enough to the outer membrane of Gram-negative bacteria to cause damage to cells, which is in agreement with the findings of Bartolomeu *et al.* (2017).

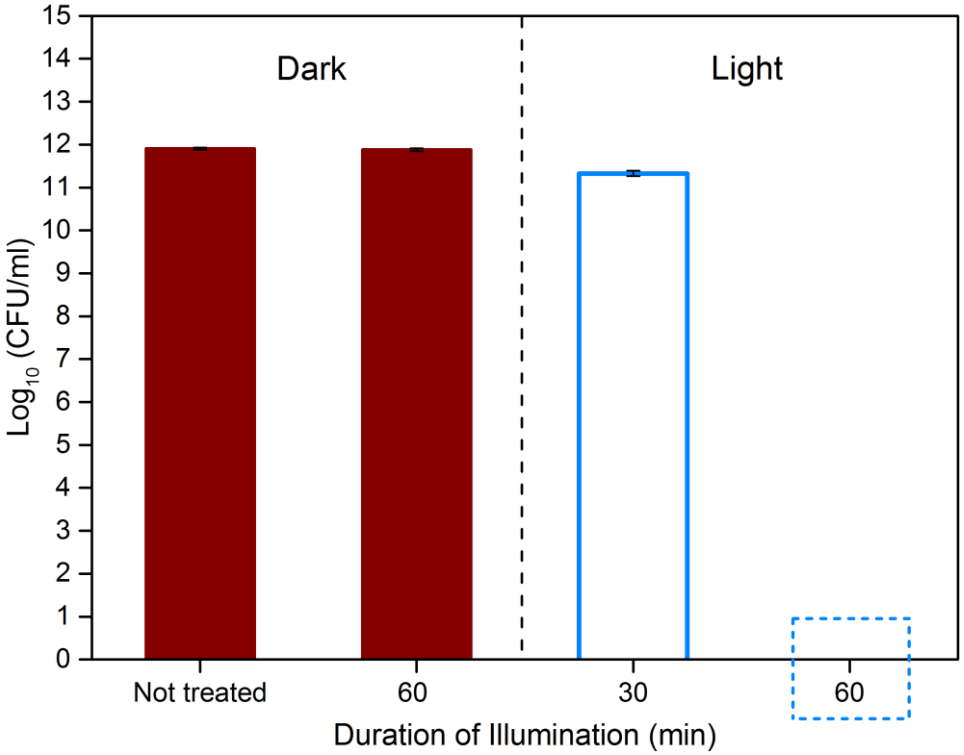

Figure 3.7 PDI of Gram-negative bacteria *E. coli* NCTC 10418 with TMPyP in solution.

E. coli NCTC 10418 12 log CFU/ml cells in water were exposed to 0 and 50 µM TMPyP and for 60 min in dark or for 30 and 60 min under 30 mW/cm^2 illumination. Cell numbers are determined by plating and serial dilution. (▬), dark treated; (▭), light treated; and (▭), complete sterilisation. Data are average ± SEM, (n=3).

3.6.2 The effect of light intensities and duration of light illumination

PDI with TMPyP was also carried out at a higher light intensity approximately twice the previous intensity was used (Figure 3.8). At 72 mW/cm^2 only 30 min illumination was needed for complete sterilisation of the *E. coli* NCTC 10418. This is equivalent to 6% of natural sunlight. Thus, this study indicates the potential scope to use the sunlight for water sterilisation in countries like UK and other European countries where intensity of sunlight is relatively low. In Asian and Africa countries the natural sunlight intensity will make even more worthwhile to use this system for water sterilisation without man made energy.

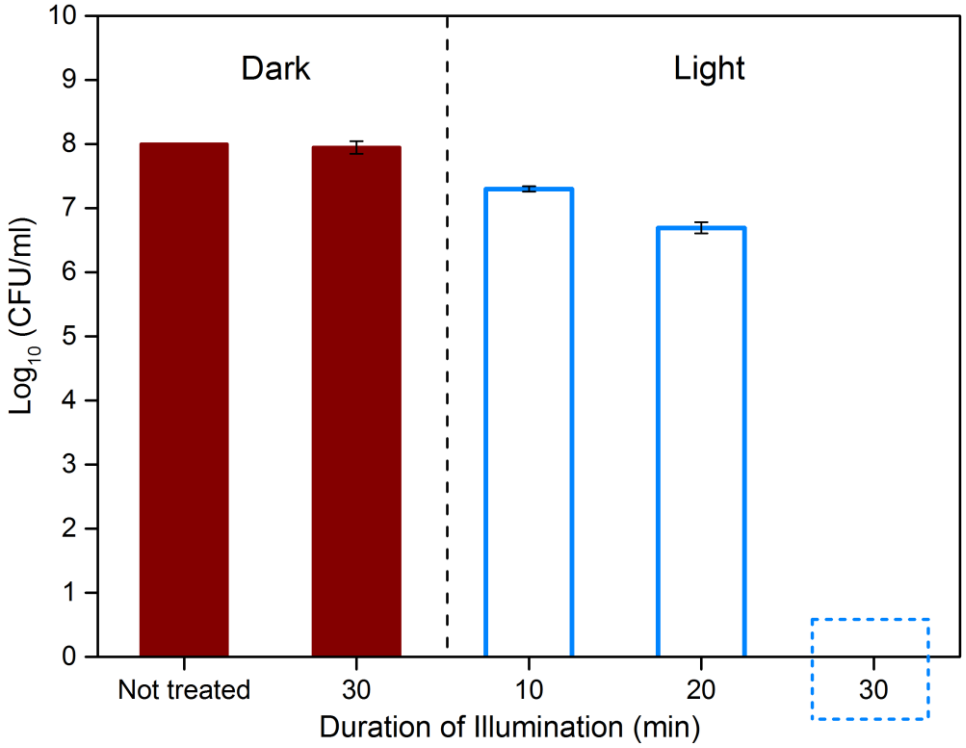

Figure 3.8 PDI of Gram-negative *E. coli* NCTC 10418 at higher intensity light with TMPyP in solution.

E. coli NCTC 10418 8 log CFU/ml was exposed to 50 µM TMPyP for different durations (10, 20 and 30 min) under 72 mW/cm^2 illumination for 60 min in dark. Cell numbers are determined by plating and serial dilution. (▬), dark treated; (▭), light treated; and (▭), complete sterilisation. Data are mean ± SEM, (n=3).

3.7 PDI effects of TAllylPyP in solution

Due to the absence of suitable functional groups for covalent immobilisation in TMPyP, it was necessary to synthesise new tetra cationic photosensitisers with reactive side chain. TMPyP analogue were synthesised to allow the covalent attachment to electrospun nanofibres. Thus, TAllylPyP was synthesised (Section 2.5.1). As an analogue of TMPyP, it posses an allyl group for covalent bonding to –COOH of polyacrylic acid crosslinking with polyacrylic acid/ethylene glycol (PAA-EG) nanofibres mat. Before functionalisation of nanofibres mat with TAllylPyP, it was necessary to confirm the PDI activity of TAllylPyP. Thus, PDI of Gram-negative bacteria *E. coli* strain NCTC 10418 was carried out with TAllylPyP in solution. Concentration optimisation of TAllylPyP and PDI at two different light intensities were studied.

3.7.1 Concentration optimisation of TAllylPyP for PDI

To optimise the effective concentration of TAllylPyP 0 to 50 µM TallylPyP concentration was used. After treatment with the highest concentration 50µM for 60 min at 30 mW/cm2 complete cell death resulted. As expected, it was clear that the PDI of NCTC 10418 with TAllylPyP was not concentration dependent (Figure 3.9). In Figure 3.10 the surviving cell at proportion above 5 to 10 µM of TAllylPyP was low.

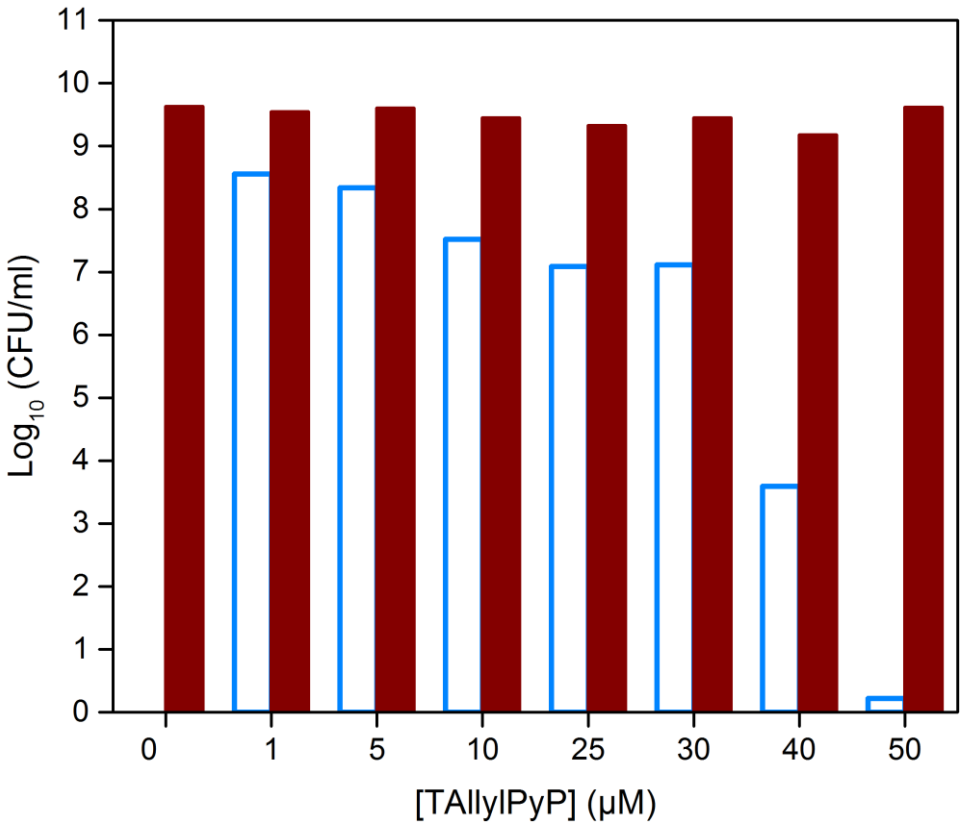

Figure 3.9 PDI of bacteria *E. coli* NCTC 10418 by different concentration of TAllylPyP solution at low intensity of light.

Showing the survived 9.7 log CFU/ml of *E. coli* NCTC 10418 cells after exposure to TAllylPyP in the dark or irradiated with visible light with 1 - 50 µM concentration of TAllylPyP for 60 min. (■), dark treated; (□), light treated.

At the same time dark toxicity was studied for the concentration range of TAllylPyP (Figure 3.9). At higher concentrations dark toxicity was observed but did not show any trend as the results were highly variable.

3.7.2 Optimisation of light intensity

PDI of *E. coli* NCTC 10418 was studied with newly synthesised photosensitiser TAllylPyP at two different light intensities. For complete cell death of *at* low intensity (30.8 mW/cm^2), it required 60 min illumination (Figure 3.10). At higher intensity (70 mW/cm^2), it took only 30 min for complete cell death (Figure 3.11).

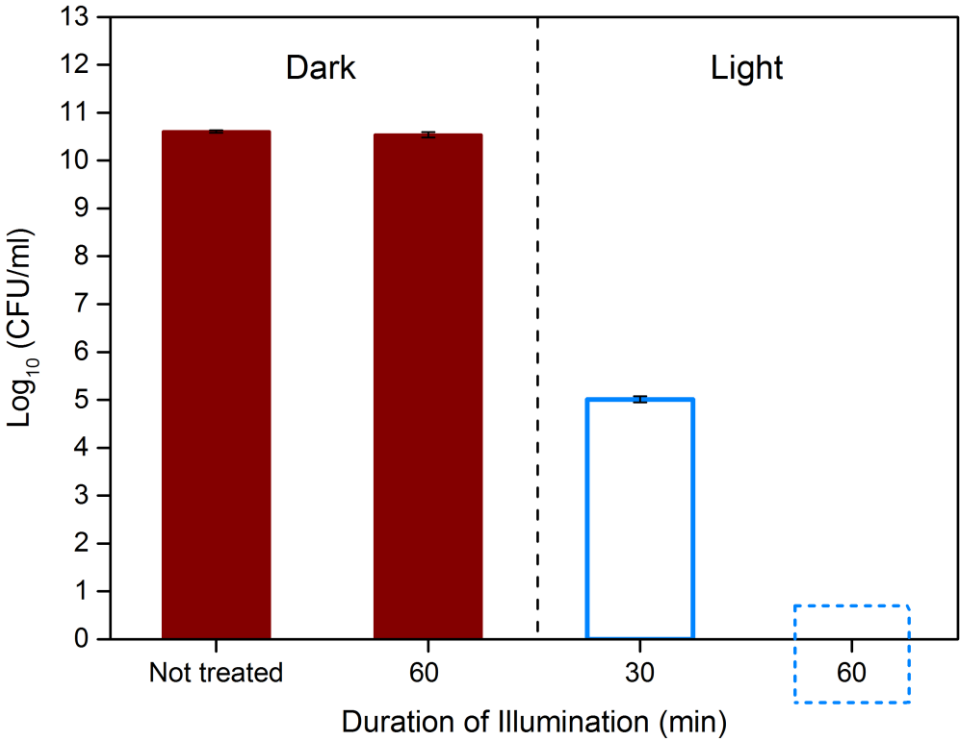

Figure 3.10 PDI of bacteria *E. coli* NCTC 10418 by low intensities of cold light with 50 µM TAllylPyP in solution.

Showing the survived 10.5 log CFU/ml of *E. coli* NCTC 10418 cells after exposure to 50 µM TAllylPyP in the dark for 60 min and irradiated with visible light at 30.8 mW/cm^2 intensity for 30 min and 60 min. ( ), dark treated; ( ), light treated; and ( ), complete sterilisation. The error bars are average ± SEM, where n=3.

From Figure 3.10 and Figure 3.11, it was clearly observed that by increasing light intensity, duration of light illumination can be reduced. So this implies the potentiality of direct sunlight use for this technology. That can reduce the manmade energy consumption in water treatment.

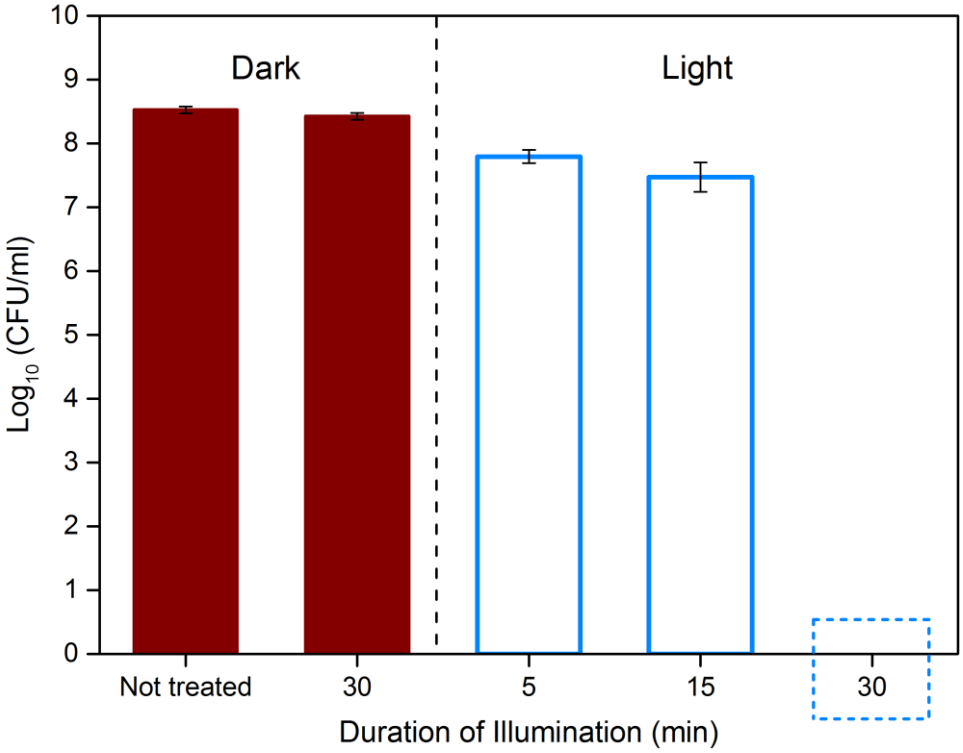

Figure 3.11 PDI of bacteria *E. coli* NCTC 10418 by high intensities of cold light with 50 µM TAminPyP solution.

Showing the survived 8.5 log CFU/ml of *E. coli* NCTC 10418 cells after exposure to 50 µM TAllylPyP in the dark for 30 min and irradiated with visible light at 70mW/cm^2 intensity for 5 to 15 min. (▬), dark treated; (▭), light treated; and (┈), complete sterilisation. The error bars are average ± SEM, where n=3.

3.8 PDI with tetra amine pyridyl porphyrin (TAminePyP)

Another new photosensitiser tetra amine pyridyl porphyrin (TAminePyP) with amine functionality was synthesised and PDI was again studied for *E. coli* NCTC 10418. A 30 µM of TAminePyP was used for PDI (Figure 3.12). Almost 90% inactivation was observed with 30 µM TAminePyP solution after 60 min of illumination at 70 mW/cm^2 and 1 log reduction was observed.

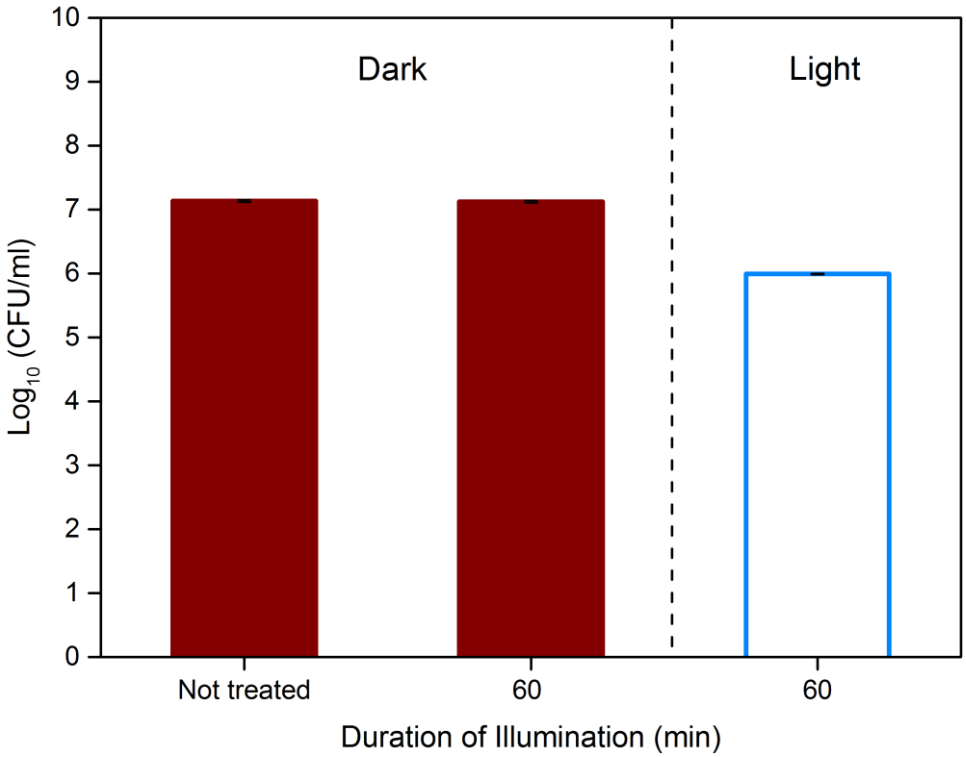

Figure 3.12 PDI of bacteria *E. coli* NCTC 10418 at high intensity of cold light with 30 µM TAminePyP in solution.

Showing the survived 7.2 log CFU/ml of *E. coli* NCTC 10418 cells after exposure to 30 µM TAminePyP in the dark and irradiated with visible light at 70 mW/cm^2 intensity for 60 min. (■), dark treated; (□), light treated. The error bars are average ± SEM, where n=3.

Because of time limitation, optimisation of the concentration of TAminePyP was not carried out. As the main aim of this research work was study of PDI by photosensitiser functionalised electrospun nanofibre. Thus more emphasis was given to functionalise PAA-EG nanofibre with TAminePyP (Section 2.9.7.)

3.9 PDI of antibiotic resistant bacteria

3.9.1 PDI of carbenicillin resistant bacteria BL21 (DE3) with TMPyP in solution

One of the emergent issues in water quality is antibiotic resistance in bacteria. Thus, one of the objectives was to study of PDI against antibiotic resistant *E. coli*. For this experiment, the carbenicillin resistant *E. coli*. BL21 (DE3) was used and PDI by TMPyP in solution was carried out. The surviving fraction of cells was measured after treatment with 50 µM TMPyP in solution, either in the dark or after irradiation with visible light for 60 min at as 30 mW/cm^2 (Figure 3.13). After 30 min illumination by 50 µM upto 3 log reduction was observed.

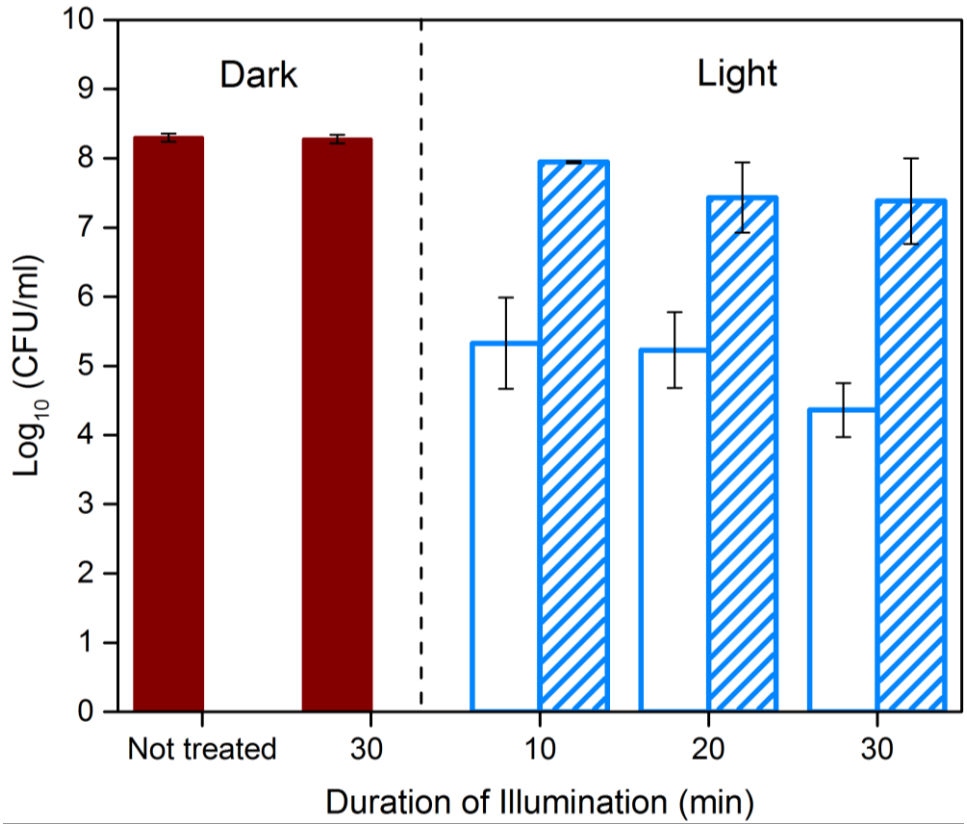

Figure 3.13 PDI of carbenicillin resistant bacteria BL21 (DE3) by TMPyP in solution at low intensity of light.

Showing the survived 8.5 log CFU/ml of *E. coli* NCTC 10418 cells after exposure to 50 µM TMPyP in the dark and to 25-50 µM TMPyP irradiated with visible light at 30 mW/cm^2 intensity for 10-30 min. (▮), dark treated; (▭), 50 µM TMPyP light treated; (▨), 25 µM TMPyP light treated. The error bars are average ± SEM, where n=3.

PDI of BL21 (DE3) was highly effective, after 60 min exposure to light no BL21 (DE3) survived. Whereas treatment with a lower concentration of TMPyP (25 µM) solution only 2 log reduction was observed after 60 min treatment. This is also indicates that successful PDI of carbenicillin resistant BL21 (DE3) was concentration dependant (Figure 3.13)

3.9.2 PDI of carbenicillin resistant bacteria BL21 (DE3) by TAllylPyP in solution

After successful inactivation of *E. coli* by tetra allyl pyridyl porphyrin PDI was studied against the antibiotic carbenicillin resistant *E.coli* BL21 (DE3). The surviving fraction of BL21 (DE3) was counted before and after exposure to TAllylPyP (50 µM) in the dark or after irradiation with visible light at 25-60 min at 70 mW/cm^2 light. PDI of BL21 (DE3) was successful.

After 60 min exposure to light, complete inactivation of BL21 (DE3) was observed (Figure 3.14). Although after 60 min treatment with 25 min of TMPyP in solution, 2 log CFU/ml reduction of BL21 (DE3) bacterial was observed. That indicates successful PDI of carbenicillin resistant BL21 (DE3) was not only concentration, dependant but also illumination time dependent

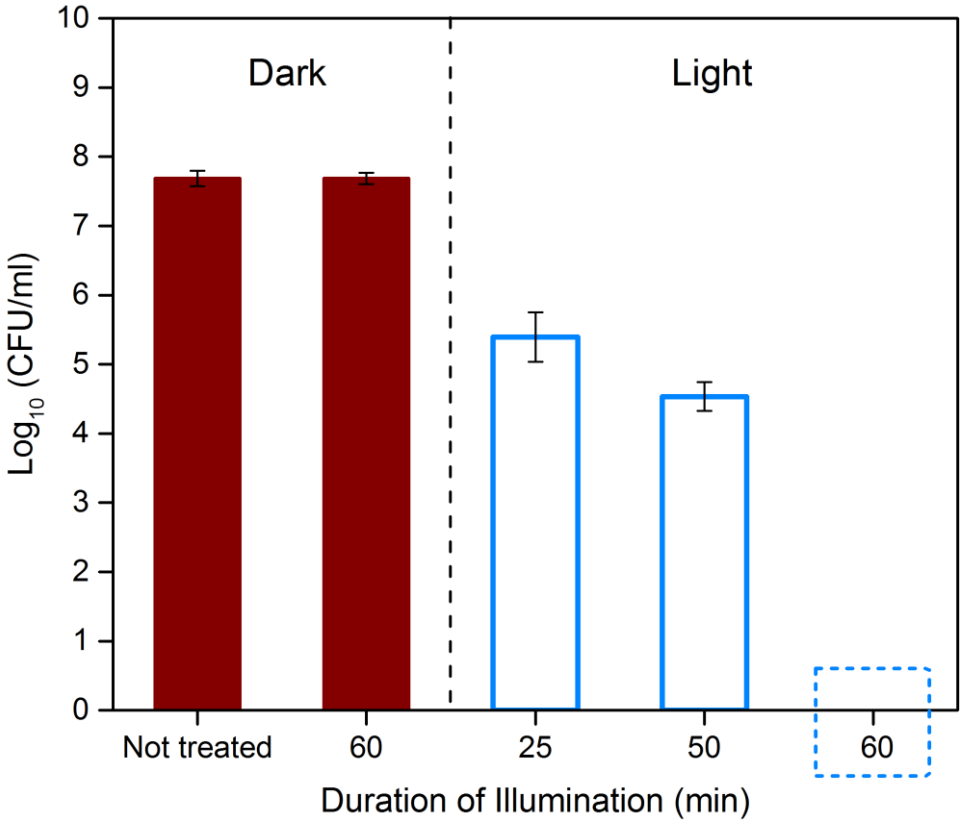

Figure 3.14 PDI of carbenicillin resistant bacteria BL21 (DE3) by TAllylPyP in solution at 70 mW/cm^2.

Showing the survived 7.8 log CFU/ml of *E. coli* BL21 (DE3) strains after exposure to 50 µM TAllylPyP in the dark and irradiated with visible light at 70 mW/cm^2 intensity for 25-60 min. (▬), dark treated; (▭), light treated; and (▭), complete sterilisation. The error bars are average ± SEM, where n=3.

3.10 Conclusion

Data in this chapter shows that the concentration of photosensitisers; (TMPyP, TAllylPyP and TAminePyP), duration of illumination and light intensity were all crucial for successful PDI of *E. coli* NCTC 10418 and carbenicillin resistant BL21 (DE3). Commercially available tetra cationic TMPyP successfully and efficiently inactivate model (Section 3.6). Newly synthesised TAllylPyP (Section 3.7) and TAminePyP (Section 3.8) were also successful in causing PDI of model strains of bacteria. However, TAllylPyP was the most successful and efficient in causing PDI.

High efficiency and the PDI ability of TMPyP at 40-50 µM, in solution made it a photosensitiser of interest for immobilisation onto electrospun nanofibres, polyacrylic acid crosslinked with polyvinyl alcohol PAA-PVA and PAA-EG However, due to lack of reactive group in TMPyP for covalent immobilisation of onto (PAA-PVA) and (PAA-EG) nanofibres was done only by adsorption (Chapter 5). This limitation of the TMPyP structure created the need to synthesis new tetra cationic photosensitisers TAllylPyP and TAminePyP bearing allyl and primary amine reactive group respectively (Chapter 4) Reasonably low concentration of TMPyP were needed for complete inactivation of *E. coli* NCTC 10418 and carbenicillin resistant bacteria BL21 (DE3) at low light intensity. In this chapter visible cold white light was used 30mW/cm^2 fluence rate (radiant exposure) used for most PDI experiments was. This light intensity is only about 3% of bright mid-day time sunlight under clear sky conditions in Sub-Saharan Africa and about 10% of mid-day time sunlight during summer in Northern Europe. In this chapter it was also shown that by increasing the intensity of light we can reduce the duration of illumination (Figure 3.11). This is an indication that ultimately sunlight could be used as source of light for water disinfection. Advantage of using low light intensity will allow this system to be used in countries likes UK and Europe where sunlight availability is poor. So option of using low intensity light will allow to reduce energy consumption in waste water treatment.

Chapter 4

Characterisation of photosensitiser and photosensitiser functionalised electrospun nanofibre

4.1 Overview

Selection of the correct photosensitiser is crucial task for efficient PDI performance, particularly in the case of inactivating Gram-negative bacteria or antibiotic resistant bacteria (Abrahamse and Hamblin, 2016; Castano *et al.*, 2004; Maisch *et al.*, 2007). It is unfortunate that the origins of PDT over 100 years ago were for killing micro-organisms, but throughout the period from the 1970s to 2010, cancer treatment received the most attention in PDT research. With the rise of antibiotic resistance PDI has attracted renewed interest. There are noticeable differences between anti-cancer photosensitiser (PS) and antimicrobial ones; anti-cancer PS needs to be lipophilic where charge, either positive or negative (Abrahamse and Hamblin, 2016). In comparison, antimicrobial photosensitisers should be cationic with more charge bringing better efficiency for inactivating Gram-negative bacteria. The principal reason for this is that virtually all microorganisms are polyanionic. In addition, anticancer photosensitisers should preferably have long wavelength (far red/near-infrared) absorption bands for good tissue penetration of the exciting light. For antimicrobial photosensitisers, this property is not important since broad spectrum white light is often used. After synthesis, purification and characterisation of water soluble, cationic antibacterial photosensitisers is quite challenging. Because of the cationic charges these photosensitisers are susceptible to make complex with another unreacted reactant in the reaction mixture. Even in mass analysis the signals are visible as dimers.

As the research in this thesis was aimed to deal with microorganisms in environmental water and Gram-negative bacteria and antibiotic resistant bacteria are the main targets cationic photosensitisers were the main focus. Despites success in causing bacterial PDI, TMPyP (Figure 4.1) has the

disadvantage of lacking suitable functional group for covalent bonding to the nanofibre fabric.

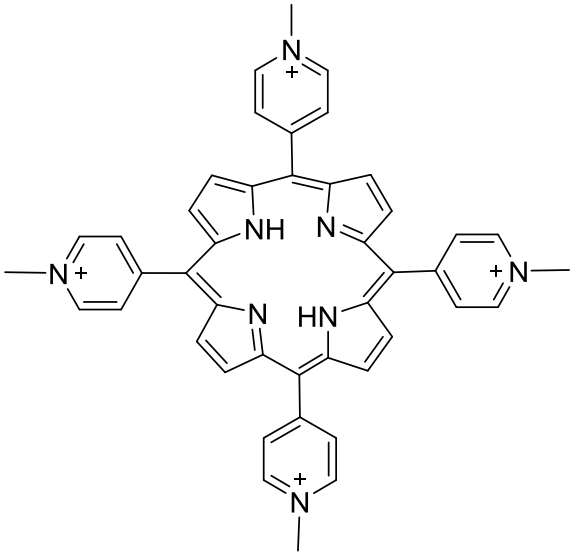

Figure 4.1 Structure of 5, 10, 15, 20- tetrakis (1- methylpyridinium-4-yl) porphyrin (TMPyP).

Thus two new tetra cationic photosensitisers were synthesised (see Chapter 2) and characterised in this chapter. Tetra-allyl-pyridyl-porphyrin (TAllylPyP) possesses four pendant allyl groups whereas its analogue tetra amine pyridyl porphyrin (TAminePyP) has four pendant amine groups. In both cases the functional groups are attached to the pyridinium nitrogens. The structures of these two newly synthesised porphyrins, Tetra allyl pyridyl porphyrin (TAllylPyP) and Tetra amine pyridyl porphyrin (TAminePyP) are shown in Figure 4.2 and Figure 4.3 respectively.

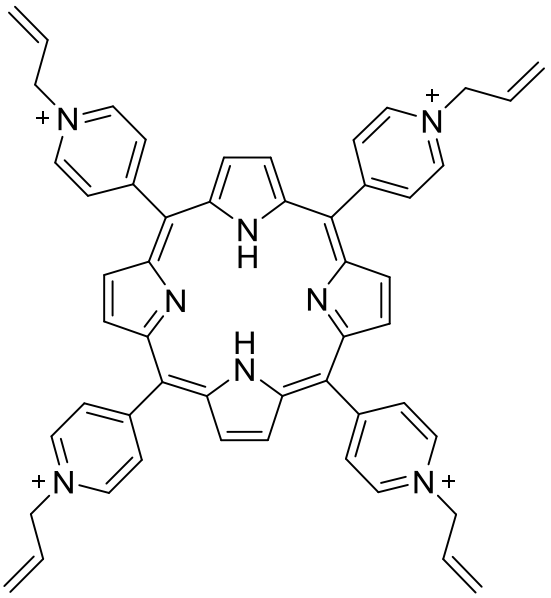

MW: 783

Figure 4.2 Structure of Tetra allyl pyridyl porphyrin (TAllylPyP).

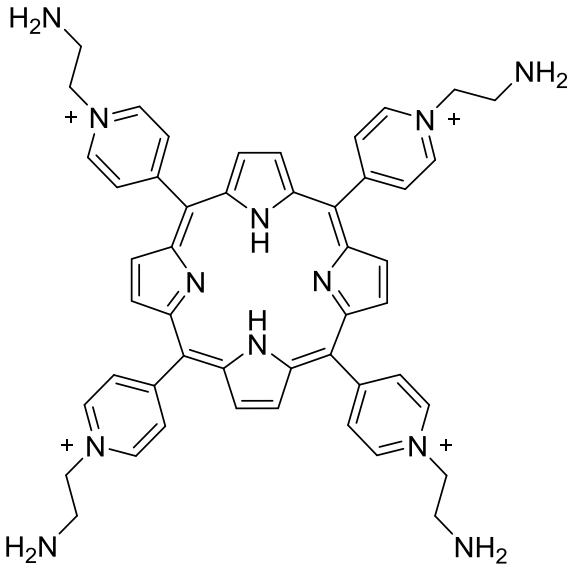

MW: 759

Figure 4.3 Structure of Tetra amine pyridyl porphyrin (TAminelPyP).

FTIR, NMR and mass spectrometry analyses were carried out to characterise these two photosensitisers and are described in this chapter. Electrospun nanofibres PAA-PVA and PAA-EG were also produced and characterised by FTIR, SEM. To make sure the nanofibre fabric was water resistant two types of crosslinking were carried out (Section 2.2.1.1). The

crosslinking process and investigation of water resistance of these nanofibres are also described in Chapter 2. Then, the PAA-PVA and PAA-EG nanofibre mats were functionalised with the tetracationic photosensitisers TMPyP, TAllylPyP and TAminePyP. In addition, PPIX also used to functionalise Jeffamine doped polyacrilonitrile PAN-Jeff nanofibres. For TMPyP and PPIX immobilised onto the nanofibres was via adsorption whilst for TAllylPyP and TAminePyP covalent modification was carried out. This chapter contains data on the characterisation of photosensitiser-functionalised electrospun nanofibres by FTIR, SEM analysis (Table 4.1). Subsequently, singlet oxygen generation by the photosensitisers functionalised nanofibres was also assessed.

This chapter contains study of characterisation of photosensitisers functionalised electrospun nanofibres (listed below) by FTIR, SEM analysis.

(i) $TMPyP_{ads}$-(PAA-PVA);
(ii) $TMPyP_{ads}$-(PAA-EG);
(iii) $TAllylPyP_{ads}$-(PAA-EG);
(iv) $PPIX_{cov}$-(PAN-Jeff);
(v) $TAllylPyP_{cov}$-(PAA-EG); and
(vi) $TAminePyP_{cov}$-(PAA-EG).

Above lists of photosensitiser-functionalised nanofibre fabrics studied. PAA-PVA or PAA-EG nanofirbre mats, spun as described in Section 2.2, were functionalised by the photosensitisers indicate by adsorption (ads) or covalent coupling (cov). Functionalisation processes are described in Section 2.9.

4.2 Characterisation of photosensitisers

4.2.1 Tetra allyl pyridyl porphyrin (TAllylPyP)

^{1}H NMR and mass analysis and UV- Vis spectrometry were done to characterise the TAllylPyP. That was complete in agreement of characterisation by Dancil group (Dancil *et al.*, 1997; Gyulkhandanyan *et al.*, 2009).

^{1}H nmr (DMSO-d_6): δ_H ppm 9.54 (d, 8H, py, J = 6.7 Hz), 9.24 (s, 8H, β-pyrrole-H), 9.05 (d, 8H, py, J = 6.7 Hz, C_5H_4N), , 6.51 (ddt, 8H, H_1, J_1 = 17.1, J_2 = 10.3, J_3 = 6.2 Hz, =CH-), 5.84 (d, 4H, H_1, J = 17.1 Hz, -=CH_2),,5.75 (d, 4H, H_1, J = 10.3 Hz, =CH_2),, 5.68 (m, 8H, H_1, J = 6.2 Hz, -NCH_2), -3.08 (s, 2H, internal pyrrole -NH); UV/Vis (water, nm): λ_{max} 421,520, 556, 587;

MS m/z, 260.43^{+}, 350^{2+}, 383.9 (M+H). 3a_AccMass_Loop_Positive. m maXis impact, ESI, Positive Ion Polarity. NMR and mass spectra are enclosed in appendices A and B respectively.

4.2.2 FTIR

FTIR spectra of photosensitisers were recorded using a Nicolet 5700 FTIR spectrometer (Thermo Nicolet Corporation) at ambient conditions a broad-range scan to show general spectral features of TAllylPyP is shown in Figure 4.4

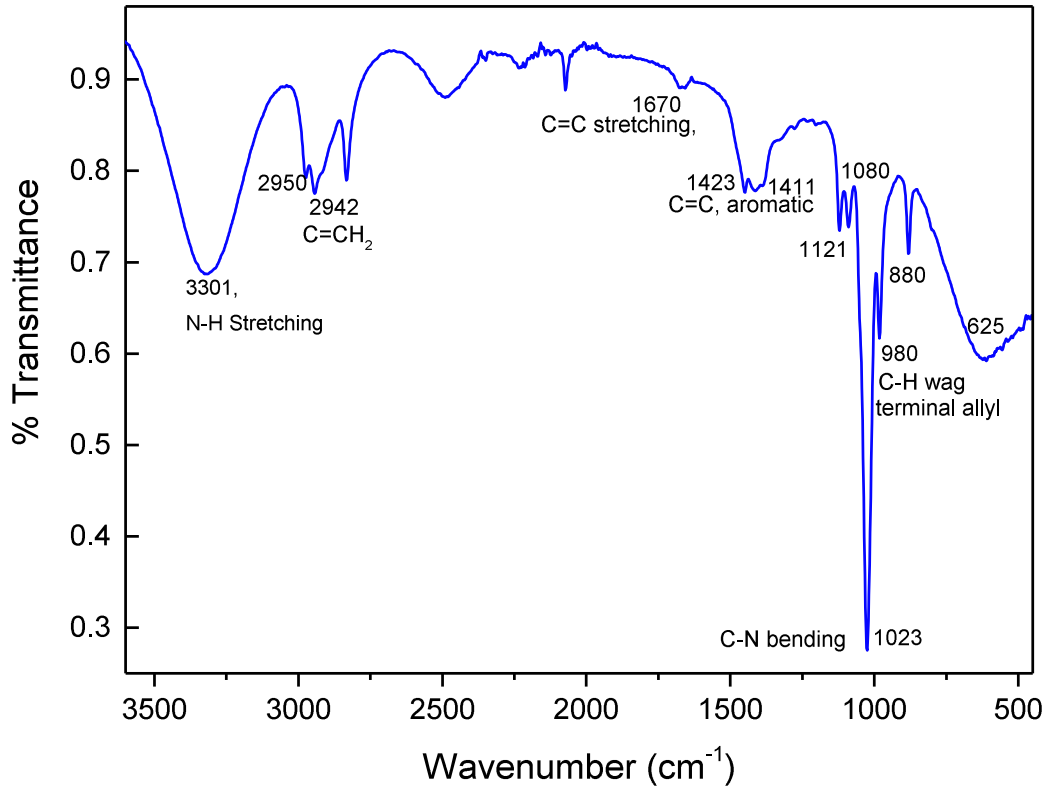

Figure 4.4 FTIR spectra of tetra allyl pyridyl porphyrin (TAllylPyP). Nicolet 5700 FTIR spectrometer (Thermo Nicolet Corporation)

The FT- IR data of TAllyPyP is was compared with the starting material tetra pyridyl porphyrin (TPyP) from literature data (Fagadar-Cosmaa *et al.*, 2007; Dancil *et al.*, 1997).The spectrum of TAllylPyP shows the following signals: Signal 3301 cm^{-1} (stretching vibrations of N-H), 1121, 1088 and 1023 cm^{-1} are attributed to bending vibration of C-N, are the characteristic for porphyrin free base (Dancil *et al.*, 1997; Barreiro *et al.*, 2015). The bands at 1423, 1411 cm^{-1} (C=C on aromatic ring) and weak band at 1670 cm^{-1} are due to stretching vibrations of C=C (Slota *et al.*, 2011) (Dong *et al.*, 2014). The intense bands at 980 and 880 cm-1 are attributed to the vibration of C-H (terminal allyl group) (Fagadar-Cosmaa *et al.*, 2007; Barreiro *et al.*, 2015; Dancil *et al.*, 1997; Li *et al.*, 1993; Slota *et al.*, 2011).

4.2.3 Tetra amine pyridyl porphyrin (TAminePyP)

^{1}H NMR and mass analysis and UV- Vis spectrometry were done to characterise the TAminePyP. But due to solubility issue NMR spectra was not clear. Several NMR was carried out changing solvent system. In D_2O the spectra was clearly showing the peaks in

^{1}H nmr (D_2O): δ_H ppm 2.01 (d), 2.35 (s) and 2.68 (D) but in δ_H ppm 6-8 there were no peak visible. On the other hand NMR in the 10% TFA and D_2O contained three clear peaks at ppm 7.9, 8.2, 8.5. Thus due to time limitation this problem was not solved yet. NMR and Mass will be carried out again. λ_{max} 425, 525, 554, 582; MS m/z, 793(M+H). maXis impact , ESI, Positive Ion Polarity. Mass and NMR spectra are provided in appendices.

4.2.4 FTIR of TAminePyP

The FTIR spectrum of photosensitiser TAminePyP was recorded using a Nicolet 5700 FTIR spectrometer (Thermo Nicolet Corporation) at ambient conditions. Again, a broad-range scan to show general spectral features of TAllylPyP was recorded and is shown in Figure 4.5.

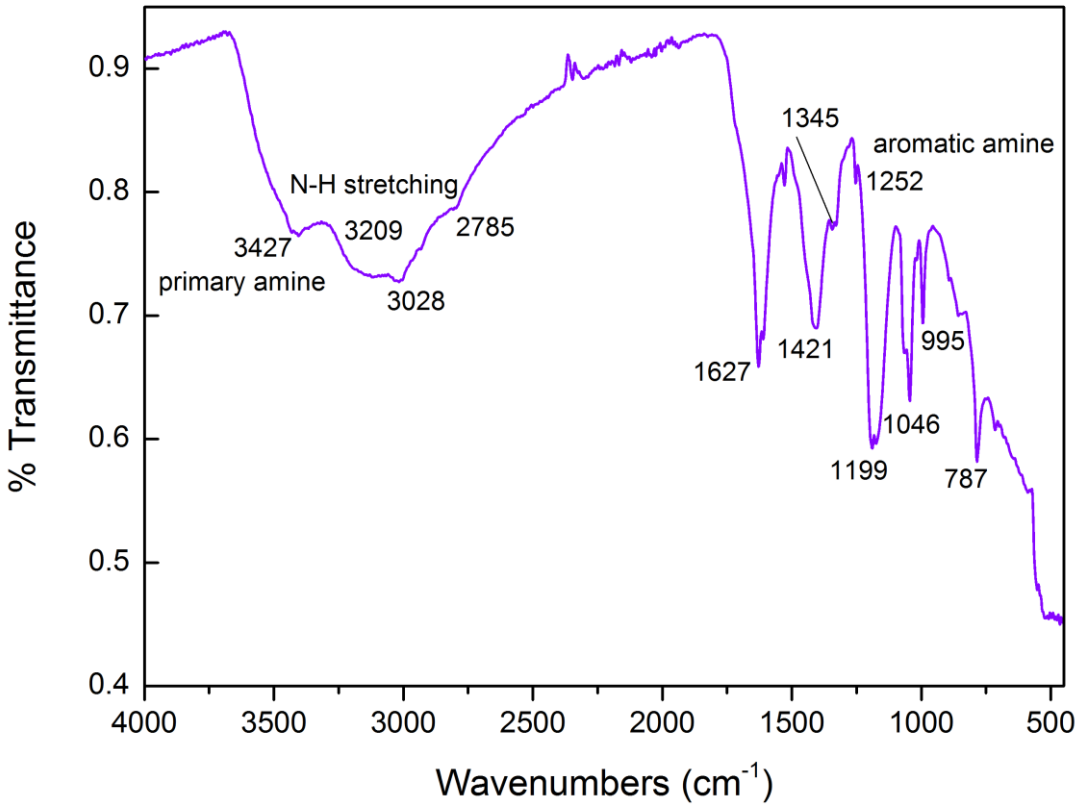

Figure 4.5 FTIR spectra of tetra amine pyridyl porphyrin (TAminePyP). Nicolet 5700 FTIR spectrometer (Thermo Nicolet Corporation)

The FT-IR data of tetra amine pyridyl porphyrin (TAminePyP) is was compared with the starting material tetra pyridyl porphyrin (TPyP) and NH_2-TPP (Belali *et al.*, 2018) from literature data (Fagadar-Cosmaa *et al.*, 2007; Dancil *et al.*, 1997; Belali *et al.*, 2018).The spectrum of TAminePyP shows the following signals: The signal at 3209 cm^{-1} (stretching vibrations of N-H) (Belali *et al.*, 2018) and 995 and 1199 (bending and stretching vibration of C-N, respectively), which are the characteristic of porphyrin free base (Dancil *et al.*, 1997; Barreiro *et al.*, 2015; Belali *et al.*, 2018). The bands in the range 1400 - 1600 cm^{-1} (stretching vibration of C=C on aromatic ring). The intense absorption band at 787 cm^{-1} is attributed to the vibration of C-H bond from pyrrole (Fagadar-Cosmaa *et al.*, 2007). The absorptions at 1345 and 1252 cm^{-1} are attributed to C-N stretching of aromatic amine. Whereas, medium band at 3427 cm^{-1} (N-H stretch primary amine) (Belali *et al.*, 2018) characterised for primary amine. NMR and mass spectra are enclosed in appendices C and D respectively.

4.3 Characterisation of electrospun nanofibres

4.3.1 PAA-PVA

PAA-PVA nanofibre was characterising by conducting SEM, FTIR. Water resistance of PAA-PVA nanofibre was tested by conducting mass analysis of PAA-PVA nanofibres mats washing.

Preparation and morphology of the nanofibre fabric

The structure of the original electrospun PAA-PVA nanofibre materials was visualised by SEM (Figure 4.6). Neutralisation of the original electrospun nanofibre materials using NaOH led to the formation of cation exchange functionality of–COOH groups on the nanofibre surfaces. The nanofibrous character of the materials was not changed by this treatments and functionalisation (Figure 4.6, B-D) or by long-term storage in water. Morphologies of the electrospun PAA/PVA nanofibre was observed using SEM (FEI Quanta 200F FEG-Scanning Electron Microscope) with an operating voltage of 15 kV. Prior to measurements, the nanofibrous mats were sputter coated with a 4 nm-thick Pt film.

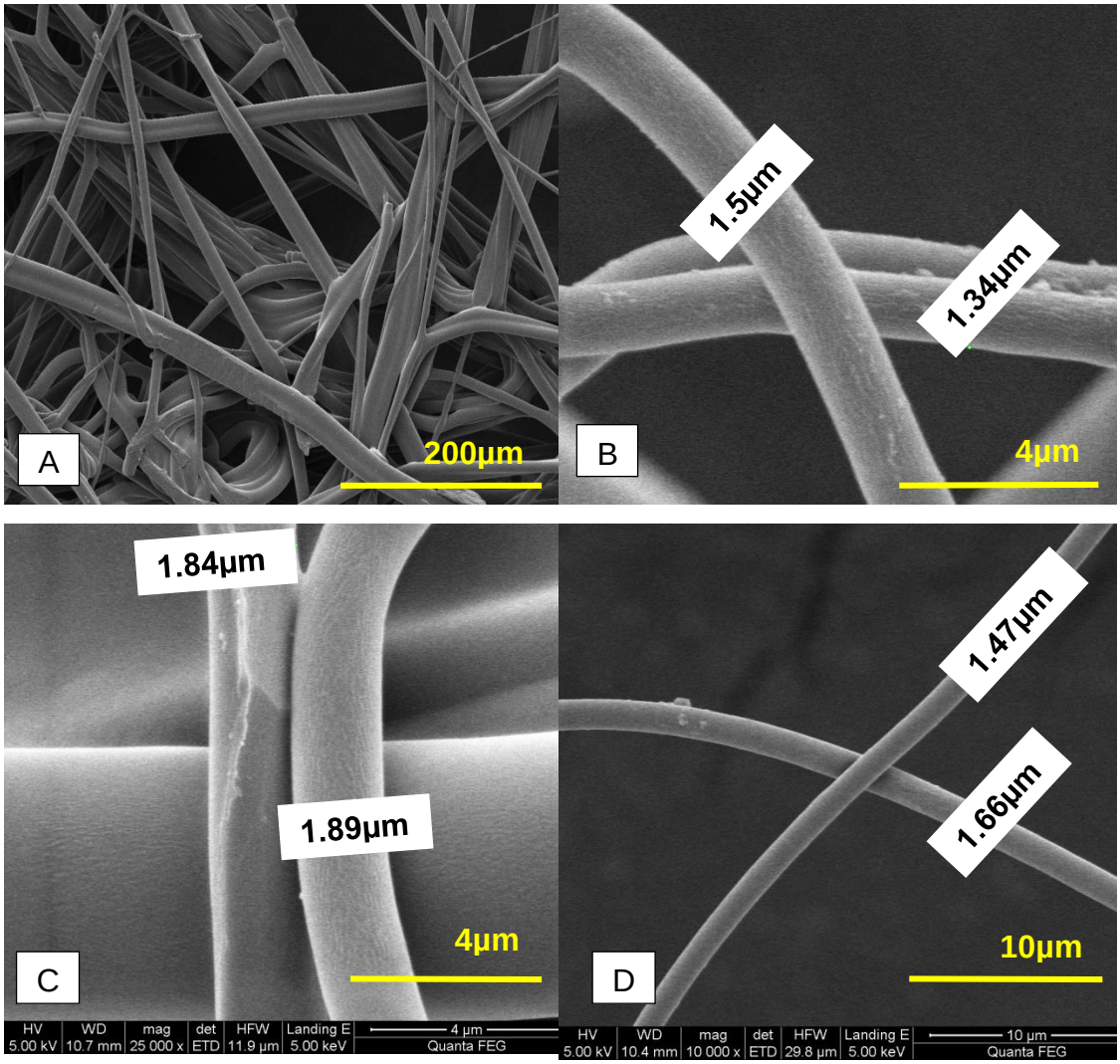

Figure 4.6 SEM images of different stages of functionalisation of PAA-PVA nanofibre mats.

(A), Before thermal crosslinking; (B), after thermal crosslinking; (C), after 2nd crosslinking with GA; (D), TMPyP functionalised PAA-PVA-GA nanofibre.

From SEM it was observed that majority of fibres were nano scale but there were some fibres with diameter of few microns (Figure 4.6). After 10 times reusing the $TMPyP_{ads}$-(PAA-PVA) nanofibre SEM images (Figure 4.6 A&B). were taken. The images reveal the cracks in the fibres (Figure 4.67B), which was not visible in bare eyes. Potential reason of cracking can be dehydration (as was not stored in water) or reuse. It needs further research to investigate the potential degree of reuse.

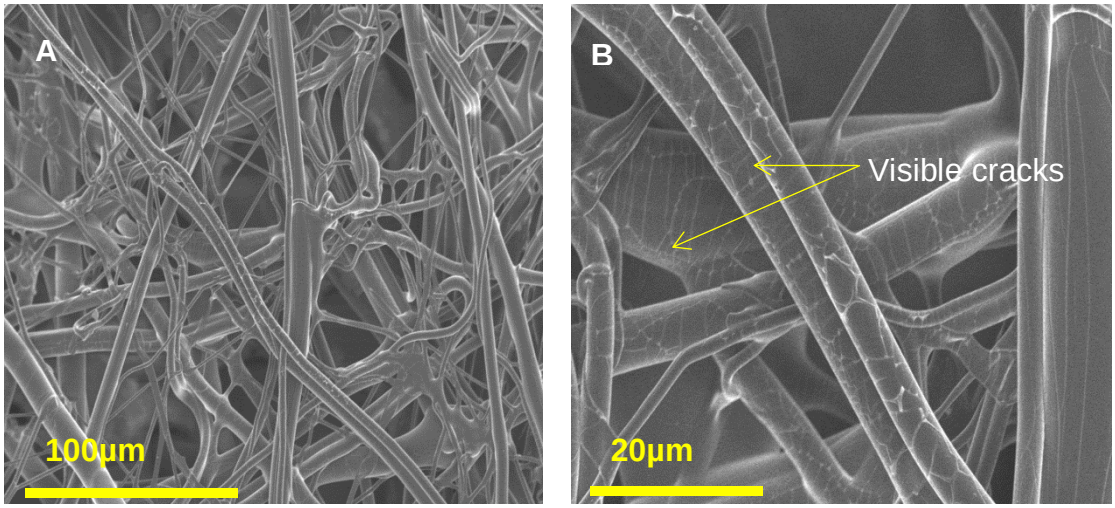

Figure 4.7 SEM images of $TMPyP_{ads}$-(PAA-PVA) after reuse several times of nanofibres.

(A), low magnify image where dehydration is not visible; (B), at higher magnification, visible cracks in fibres of $TMPyP_{ads}$-(PAA-PVA).

4.3.2 FTIR: PAA-PVA nanofibre mat before and after thermal crosslinking.

As both PAA and PVA are water-soluble, the electrospun PAA-PVA nanofibres could be dissolved in water easily. To make their fibre structure more water resistant, the PAA-PVA nanofibrous mats were treated at 140°C for 30 minutes to 1 h to form intermolecular crosslinking between the carboxyl groups of the PAA and the hydroxyl groups of the PVA (Figure 4.8 and 4.9). The nanofibrous mats thus obtained became water-insoluble and retained their porous fibre structure even after immersion in water for two months. In contrast, without heat treatment to crosslink PAA and PVA, nanofibre was almost completely dissolved into water only after 10 min.

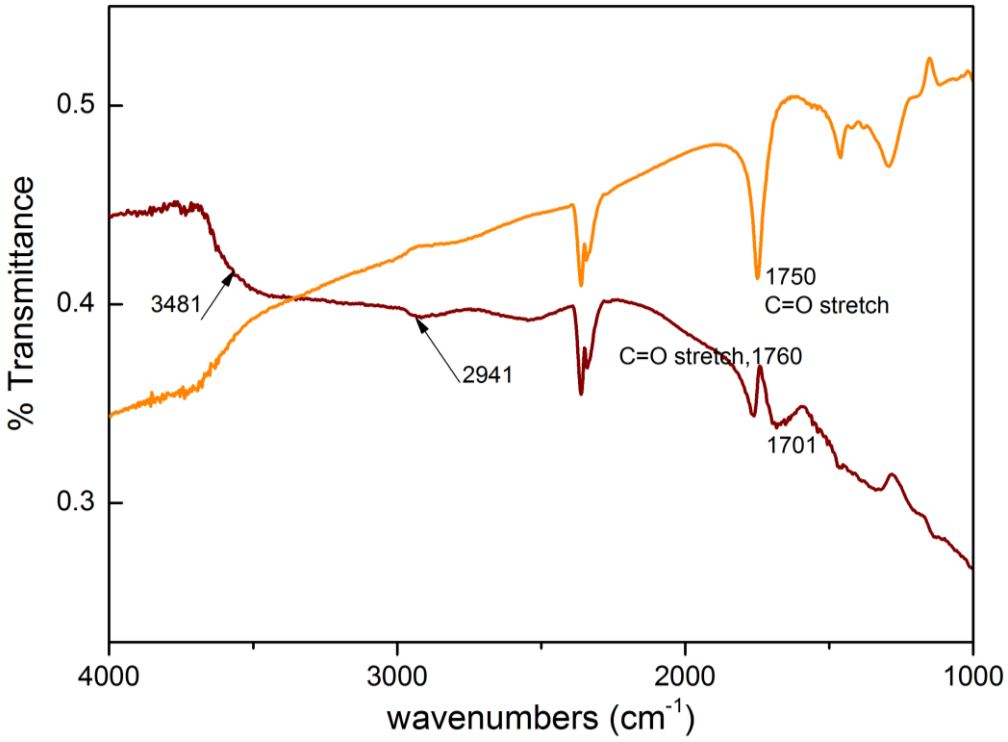

Figure 4.8 FTIR spectra of PAA-PVA electrospun nanofibre mat before and after thermal crosslinking.

(—), before thermal crosslinking; (—), after thermal crosslinking. Nicolet 5700 FTIR spectrometer (Thermo Nicolet Corporation)

FTIR spectra were recorded using a Nicolet 5700 FTIR spectrometer (Thermo Nicolet Corporation) at ambient conditions. Chemical crosslinking between PVA and PAA occurred through ester formation between the –OH groups in PVA and –COOH groups in PAA during heat treatment at 140°C for 1 h. This was confirmed by the FTIR analysis representing the FTIR spectra before (A), after (B) heat treated (Figure 4.8).

The intensity of C=O stretching band at 1701 cm^{-1} agrees well with the relative amount of PAA in blends (A). The band at 3481 cm^{-1} corresponds to O-H stretching and decreased with after heat treatment (B), eventually overlapping with the broad -COOH band at 2400–3400 cm^{-1}, which corresponds to PAA. After thermal treatment, the OH and C-O stretching bands decreased due to the formation of anhydride, ketone and ester groups (Jin and Hsieh, 2005; Arndt *et al.*, 1999; Thomas *et al.*, 2001)

Even though FTIR spectrum shows a considerable amount of –OH groups left in the nanofibre (3300-3600 cm^{-1} region), it can be clearly seen that the –C=O stretching vibration of ester at 1749 cm^{-1} becomes stronger after heat treatment (Figure 4.8). The peak around 1759 cm^{-1} in spectrum (B) clearly shows that a carbonyl group such as a ketone produced by the degradation of PVA and carbonyl of the ester linkage is forming the crosslinking (Santiago-Morales *et al.*, 2016). Modification shifts the peak to left at 1750 cm^{-1} (Figure 4.8).

4.3.3 Crosslinking of PAA-PVA and PVA-GA

As both PAA and PVA are water-soluble, the electrospun PAA-PVA nanofibres could be dissolved in water immediately. To retain their unique fibre structure in water, the PAA-PVA nanofibrous mats were treated at 140°C for 30 minutes to 1 h to form intermolecular (Figure 4.9) crosslinking between the carboxyl groups of the PAA and the hydroxyl groups of the PVA. The nanofibrous mats thus obtained became water-insoluble and kept excellent porous fibre structure even after immersion in water for two months. In contrast, without heat treatment to crosslink PAA and PVA, nanofibre was almost completely dissolved into water only after 10 minutes.

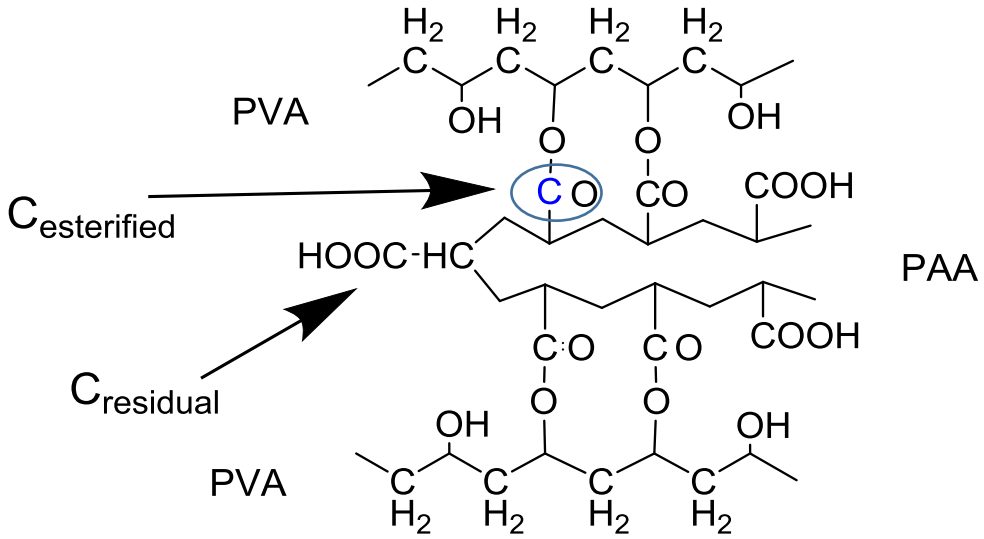

Figure 4.9 Expected crosslinking between PAA and PVA because of heat treatment.

The esterified carboxy group is shown in circle.

From mass spectrometry of heat treated PAA-PVA, it was found that there was still some unreacted PVA. So to prevent leaching of the remaining PVA the nanofibres were treated with glutaraldehyde (GA) solution (5% w/v, 3.7 mL). Crosslinking process is described in (Section 2.2.1.1). If a crosslinking agent is added to the polymer there is the possibility of intermolecular and intramolecular crosslinking (Figure 4.10).

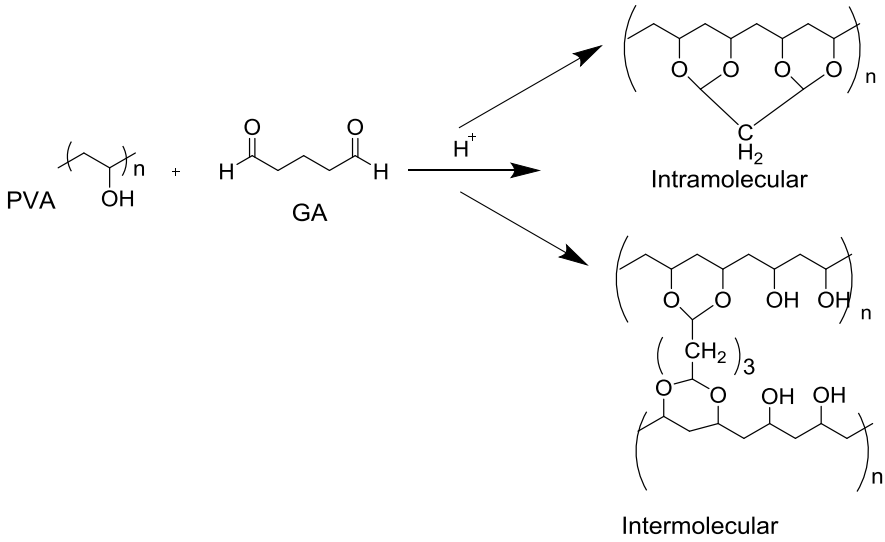

Figure 4.10 Schematic illustration of expected intramolecular and intermolecular crosslinking between PVA and GA.

After treatment with GA solution, mass spectral analysis revealed no peak of PVA (FTIR spectrum in appendices) suggesting that crosslinking of PVA with GA was successful to prevent PVA leaching into water.

4.3.3.1 Water resistance of PAA in PAA-PVA crosslinked nanofibres

Incubation of heat treated but not pre-washed PAA/PVA nanofibre was carried out for 60 d. Optical density of PAA at 405 nm was measured over the time period. At 2 h a sharp increase in A_{405} (OD) from wash solution was observed. All over the period OD were stable (

Figure 4.11). This suggests that after 2 h of incubation with shaking PAA did not release in to water. After 4 h of incubation no change in A_{405} was observed for up to 60 days of incubation. After 7 days of incubation a piece

of nanofibre was washed and re-incubated for 3 days and A_{405} change was observed as 0.0007.

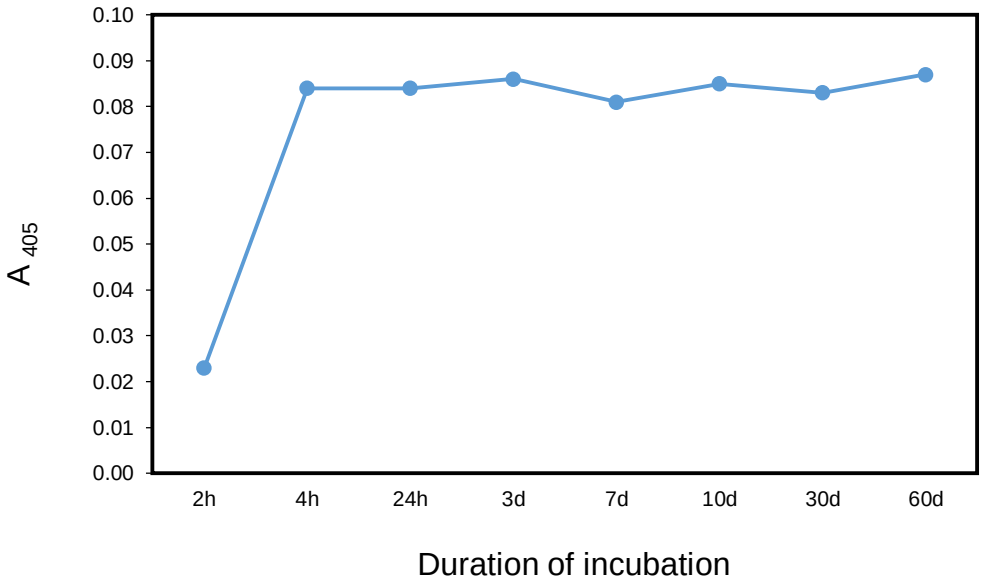

Figure 4.11 Absorbance (405 nm) of polyacrylic acid during incubation of PAA/PVA nanofibre into water over 60 days.

( ) represents incubation of PAA-PVA nanofibre mat without prewash.

4.3.4 Water resistance of nanofibre: mass spectrometry

Mass spectrometry nanofibre washings were performed to confirm the insolubility of poly (acrylic acid)/ poly (vinyl alcohol) crosslinked nanofibre in water. Z-spray nano electrospray ionisation mass spectrometry (IMS) using a quadrupole- IMS-orthogonal time-of-flight (TOF) MS (Synapt HDMS, Waters UK Ltd.) was used. After heat treatment, MS was carried out of nanofibres washings solutions for several conditions. From MS analysis of the first and second washes (Figure 4.12 C & D) there appears to be polymer related peaks from both PAA and PVA species. MS indicates the presence PVA (44 DA mass unit) peaks in third wash of nanofibre.

Specifically, two pieces of nanofibre were taken, the first (Figure 4.12C) was incubated for 24 h at room temperature in water without pre wash. Whereas, the second piece (Figure 4.12D) was incubated for 30 minutes at room temperature with gentle shaking in water, before being washed 3 times in water and then incubated for 24 h at r.t. This clearly showed that nanofibre without pre-washing (Figure 4.12D) contained traces of PAA and PVA (72 and 44 D mass respectively). However, after a three pre-washes (Figure 4.11 D) unused PAA was almost all removed interestingly there is another entity with unit mass 82 (denoted with * in Figure 4.12D), which came from PVA as a common by product of PVA hydrolysis. All original spectra are presented in Appendix A.

Then the nanofibres were treated with glutaraldehyde (GA) (5% w/v, 3.7 mL) solution to crosslink the remaining PVA with GA .There was a high signal to noise ratio throughout but the sample showed evidence of the presence of polyacrylic acid), as expected because this incubation was carried out without any pre-washing.

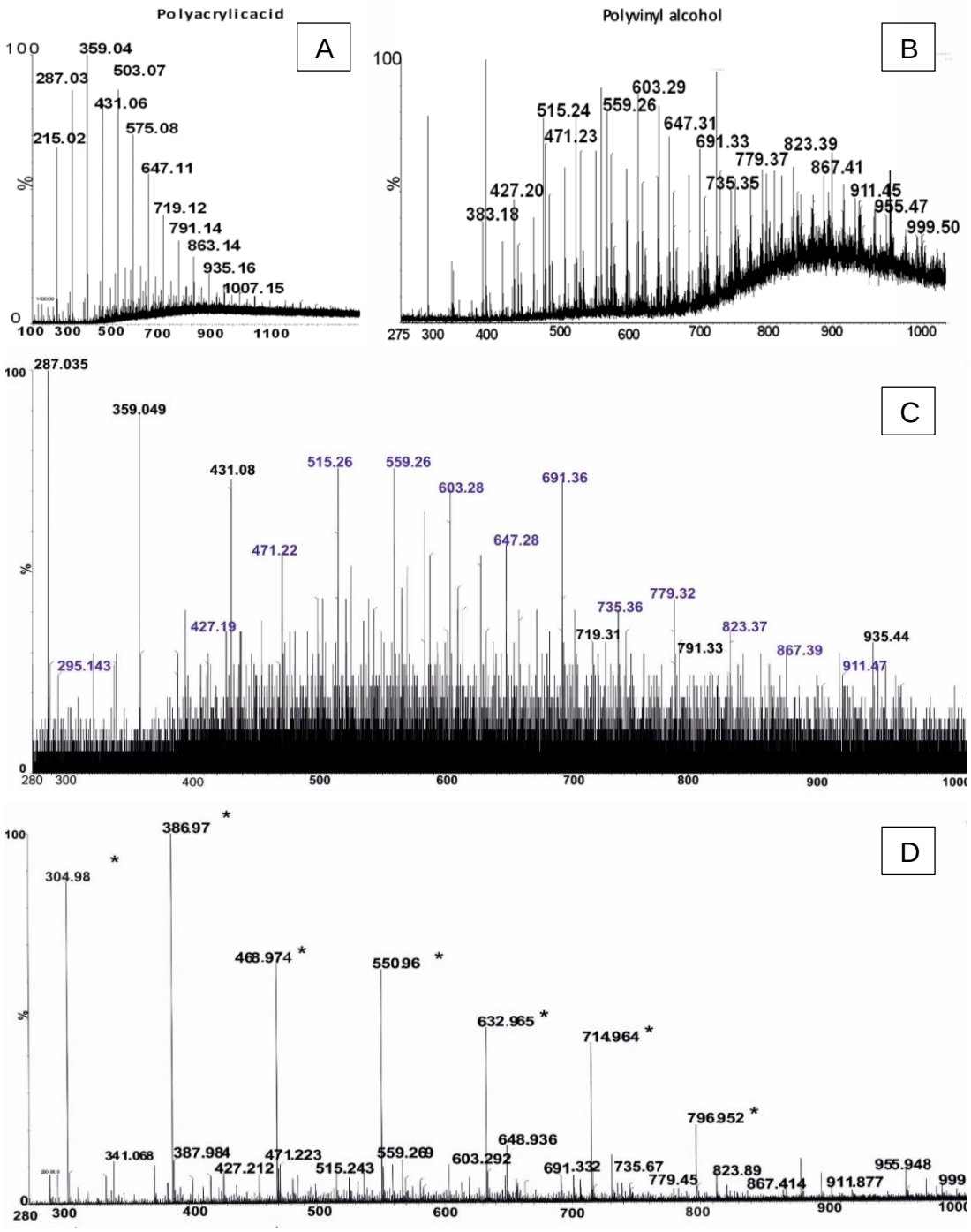

Figure 4.12 Ionisation Mass spectra of pure PAA-PVA washing.

Mass spectra of pure PAA-PVA at m/z 359.04 (A) and PVA (B), mass spectrum of PAA/PVA nanofibre washing (C) without pre wash, mass fragments denoted in blue are from PAA. Black are from PVA. (D) Mass spectra of nanofibre washes which had a good pre wash in water. (*) noted values are from sodium acetate –common by-product of PVA. Z-spray nano electrospray ionisation mass spectrometry (IMS), quadrupole- IMS-orthogonal time-of-flight (TOF) MS (Synapt HDMS, Waters UK Ltd.)

4.3.5 Ethylene glycol crosslinked polyacrylicacid (PAA-EG) nanofibre mats

Preparation and morphology of the PAA-EG nanofibre materials

The structure of the original electrospun PAA-EG nanofibre materials was visualised by SEM (Figure 4.13). After preparation of n PAA-EG nanofibres were heat treated. The nanofibrous character of the materials was not changed by this heat treatments (Figure 4.13). Morphologies of this electrospun PAA-PVA nanofibre was observed using Hitachi SU8230 FESEM with an operating voltage of 20 kV. Prior to measurements, the nanofibrous mats were sputter coated with a 7.7 nm-thick carbon film using Quorum Q150TE.

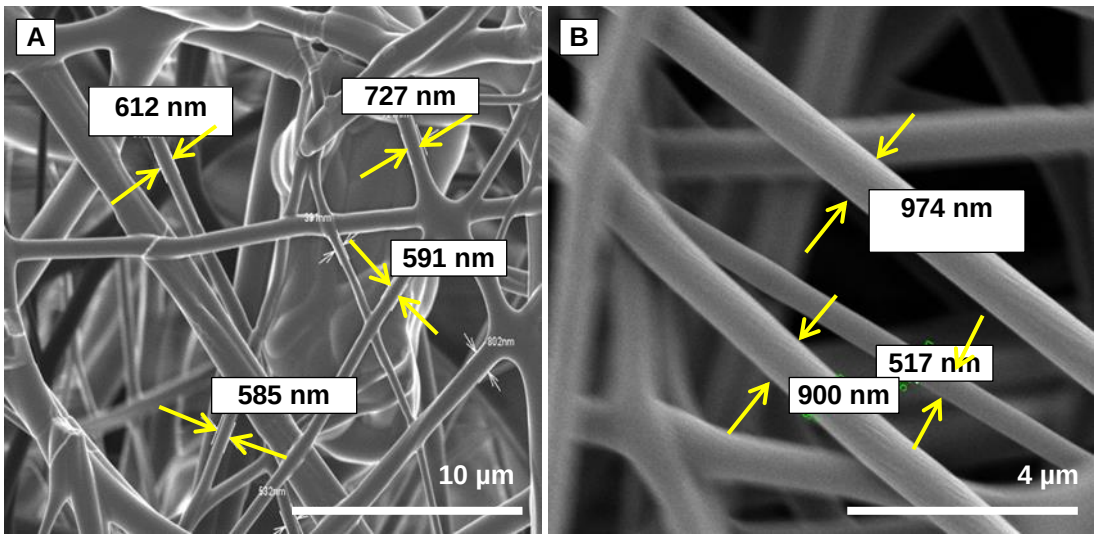

Figure 4.13 SEM images of PAA-EG before and after heat treatment of nanofibre.

(A), at low magnification image before heat treatment; (B), at higher magnification, after heat treatment. Figures in nm.

4.3.6 FTIR: PAA-EG crosslinked nanofibre mats

Figure 4.14 shows that the FTIR spectrum of PAA-EG before heat treatment (red line) was carbonyl peak of its –COOH functional groups at 1640 cm^{-1} and broad –OH peak at (3200-350) cm^{-1} region overlapping with $–CH_2$ peak 2960 cm^{-1}. The completion of crosslinking of PAA and its cross linker EG is evident from the complete absence of –OH peak. And presence of $–CH_2$ peak in the spectrum of heat treated PAA-EG (black line) (Meng *et al.*, 2015; Shavini *et al.*, 2015; Khampieng *et al.*, 2014).

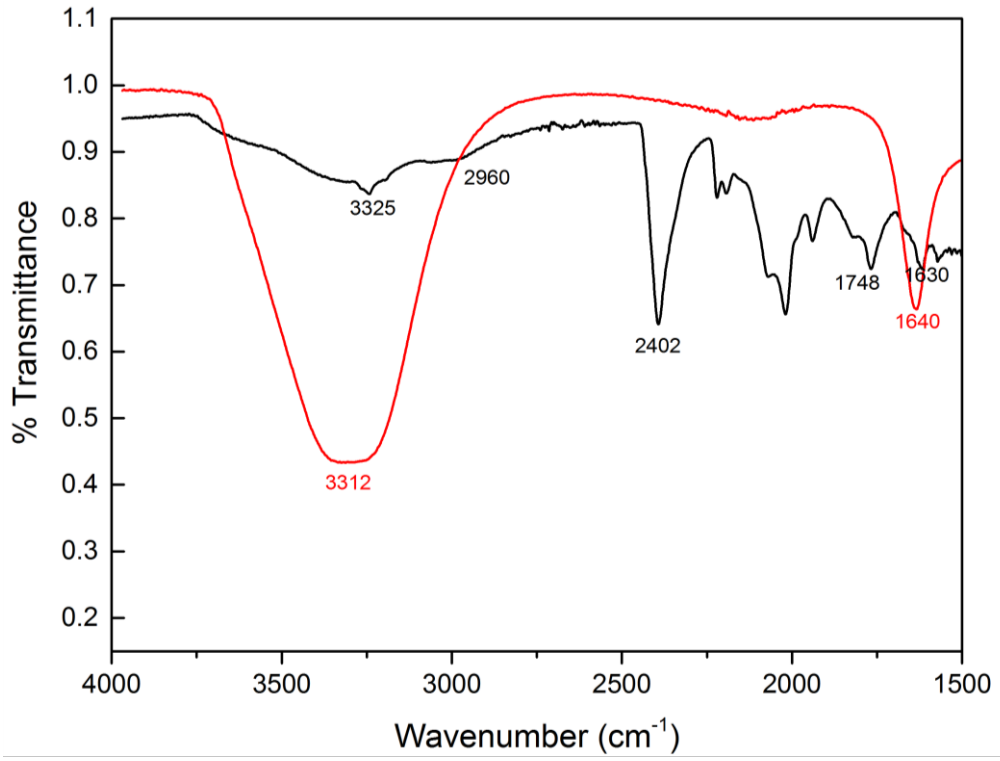

Figure 4.14 FTIR spectrum of PAA-EG before and after thermal crosslinking. (——), before heat treatment; (——), after heat treatment. Nicolet 5700 FTIR spectrometer (Thermo Nicolet Corporation,)

4.3.7 TAllylPyP$_{ads}$-(PAA-EG)

FTIR

FTIR spectra of TAllylPyP$_{ads}$-(PAA-EG) shows clear difference in non modified PAA-EG and modified PAA-EG at 980 by presence of terminal allyl (Figure 4.14).

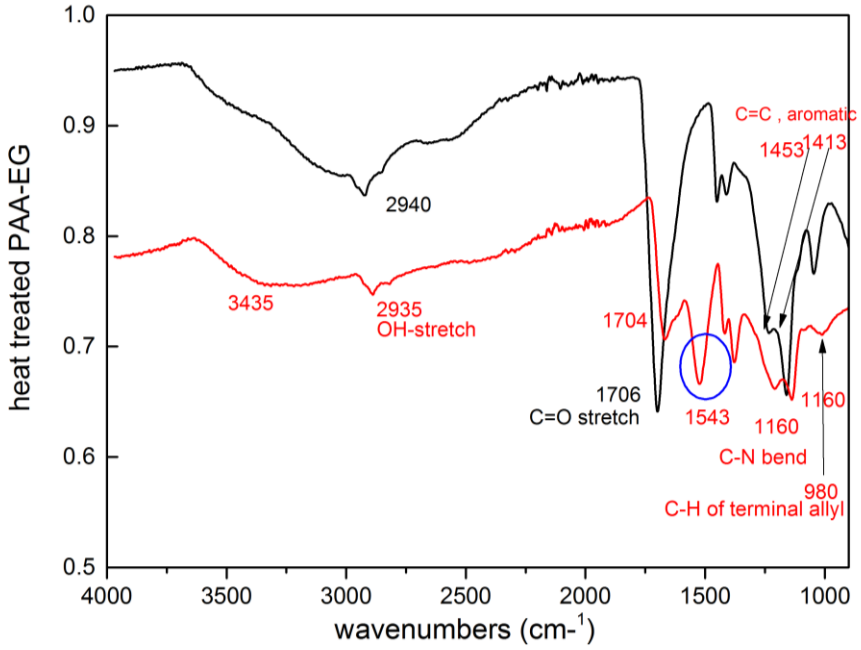

Figure 4.15 FTIR spectrum of PAA-EG before and after TAllyl adsorbed nanofibres.

(——), before and after; (——) PAA-EG nanofibres mat. Nicolet 5700 FTIR spectrometer (Thermo Nicolet Corporation)

4.4 Characterisation of covalently functionalised electrospun nanofibres (ENF) with photosensitisers

Two different electrospun nanofibres used in this study for covalent modification;

a. Jeffamine doped polyacrylonitrile (PAN-Jeff) nanofibre mat and
b. polyacrylic acid crosslinked with ethylene glycol PAA-EG nanofibre mats. Thus in this study three types of covalently modified photosensitisers functionalised nanofibres were used for PDI of Gram-negative bacteria.

The modified nanofibres were;

i. PPIX covalently immobilised onto PAN-Jeff nanofibres mat (termed as PPIXcov-(PAN-Jeff)
ii. TAllylPyP covalently immobilised onto PAA-EG nanofibres mat [termed as TAllylPyPcov-(PAA-EG)]
iii. TAmine covalently immobilised onto PAA-EG nanofibres mat [termed as TAminePyPcov-(PAA-EG)]

Characterisation of covalently modified nanofibres (i-iii) are described below:

4.4.1 Morphology of PAN-Jeff nanofibres mats

The structure and morphology of the original aminated electrospun nanofibres (ENF) material was characterized by optical microscopy. The sample of ENF was cut from the same ENF sheet. The thread arrangement of the ENF was observed carefully measuring exactly same scale (100 µm). Surprisingly, different areas showed different thicknesses (Figure 4.16) and the inconsistency in thickness was confirmed by taking the weight of ten 1 cm^2 nanofibres pieces.

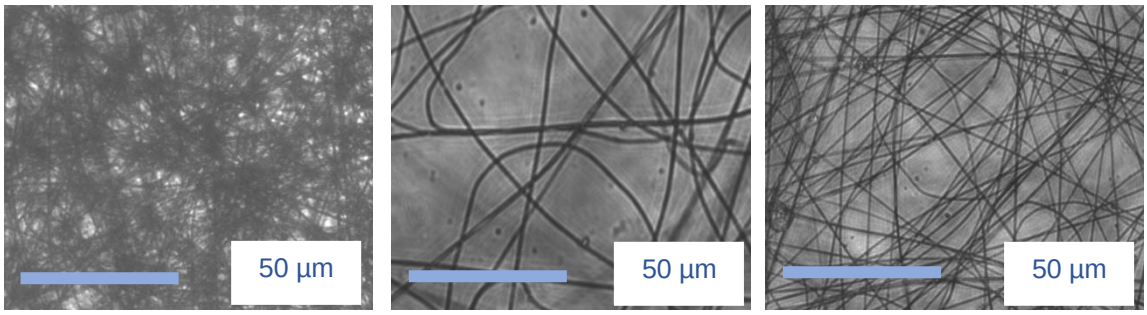

Figure 4.16 Microscopic pictures of nanofibres with three different thickness of same mother ENF sheet.

The microscopic pictures of ENF demonstrate the thickness inconsistency of three different pieces of ENF (1 cm^2) from a same ENF source. Adjusting for the weight of the two supporting polypropylene sheet (0.0106 g/cm^2) the weight of ENF varies from 0.0006 g to 0.1134 g, with a mean± SE of A±B (n=10).

4.4.2 Immobilisation of PPIX onto PAN-Jeff nanofibres

The majority of the PDI experiments involved in the treatment of water have been conducted with photosensitisers in solution. This method of water treatment is not viable commercially due to the presence of residual traces of photosensitisers in the water. Here, immobilisation of the photosensitisers onto a support having high surface area and small diameter of pore was proposed. In this study the aminated electrospun nanofibres were used as the surface for immobilisation. The carboxyl groups of PPIX and amines present on the surface of the electrospun nanofibres bind covalently as

shown in (Section 2.9.3). The electrospun nanofibres were cut in to circular disc (22 mm) to fit into the 6 well plates during the PDI process.

On addition of the reaction solution containing PPIX onto PAN-Jeff fibres mat at room temperature conjugation takes place. The quantification of the total amount of photosensitisers immobilised on the electrospun nanofibres PAN-Jeff is an important factor to determine the percentage of cells killed on completion of the PDI study by that concentration of PPIX. As the actual concentration of amine/cm^2 of PAN-Jeff were unknown, a semi quantitative method was developed to measure the amount of photosensitisers bound to the PAN-Jeff by measuring A_{410} of different concentration of PPIX solution before and after immobilisation . From this calibration curve it was observed that PPIX coupling was approximately proportional to the applied PPIX concentration. The total concentration of photosensitisers immobilised onto ENF was determined by taking the difference between original solutions before immobilisation and photosensitisers in the reaction solution as well as the wash solutions after immobilisation.

The difference of A_{410} of PPIX before and after was almost same at 100 µM and 50 µM PPIX. That indicated that the nanofibres discs became almost saturated at beyond 50 µM of PPIX, whereas the difference was very low at 5 and 10 µM of PPIX. Figure 4.17 show that at 100 µM and 50 µM PPIX each 22 mm diameter circular disc of nanofibre could couple almost same amount of PPIX. Difference of uptake is not significant. Figure 4.17 was plotted with the amount of PPIX immobilised against the time of incubation and shows the percentage of amount of PPIX taken up by PAN-Jeff with varying concentration of PPIX.

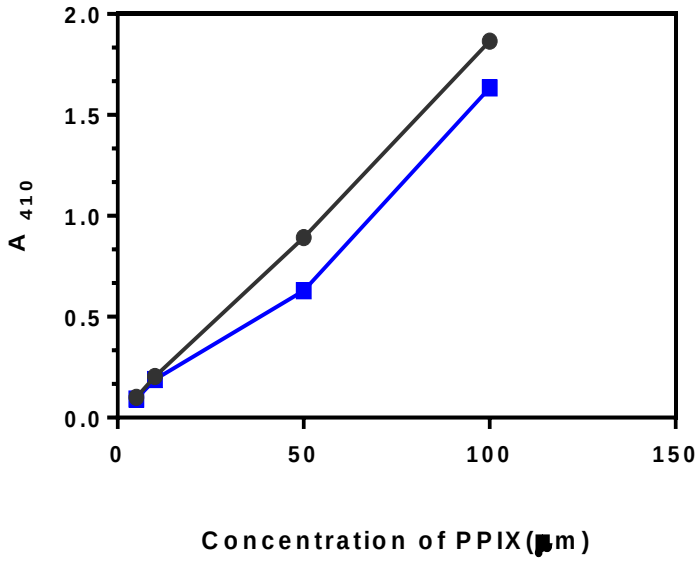

Figure 4.17 Calibration of PPIX immobilisation onto ENF with OD_{410}.

(), represents the absorbance of different concentration of PPIX before immobilisation onto electrospun nanofibres; (), represents the absorbance of different concentration of PPIX after immobilisation onto electrospun nanofibres.

Concentration of PPIX in Reaction Mixture (µM)	A410 of RM before Immobilisation	A410 after Immobilisation	Taken up PPIX % onto PAN-Jeff	Uptake nmole/cm^2
100	1.86	1.635	12.09	6.36
50	0.89	0.63	29.37	7.68
10	0.20	0.189	7.352	0.289
5	0.10	0.093	7.920	0.184

Table 4.1 Percentage of amount of PPIX uptake by PAN-Jeff with varying concentration of PPIX.

Table 4.2 shows the percentage of immobilised PPIX onto PAN-Jeff.

A_{410} before immobilisation PPIX (100 µM)	Incubation time (h)	A_{410} after immobilisation	Difference	Uptake %	PPIX uptake nmole/cm^2
1.075	1	1.014	0.061	5.6	1.49
	2	0.924	0.151	14	3.69
	6	0.894	0.181	16.8	4.43
	24	0.831	0.244	22.69	5.97

Table 4.2 Determination of amount of PPIX (100µm) immobilised onto PAN-Jeff with varying incubation time.

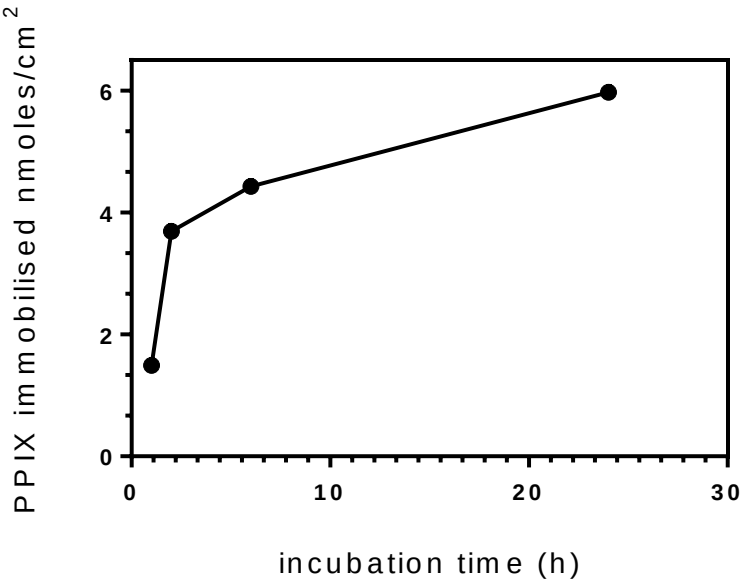

Figure 4.18 Percentage of PPIX immobilisation with time.

Immobilisation of PPIX onto PAN-Jeff, The A410 was measured after 1, 2, 6 and 24 h incubation with PPIX reaction mixture.

4.4.3 Determination of amine availability on functionalised ENF

The ENF was made of polyacrilonitrile (PAN) and it was doped with the diamine compound Jeffamine. The Jeffamine provides a source of free pendant amine groups. The polymer-aminated nanofibres were then incubated in the presence of NHS-biotin in order to label the free amine groups with biotin. Finally, HRP-conjugated streptavidin was added, which forms a very strong interaction with biotin. Upon addition of ECL reagent, a chemiluminescent signal was generated. As routine work to confirm the amine availability onto the ENF, Midland blotting (Figure 4.19) was performed several times (Figure 4.18 and Figure 4.19). However due to the fibrous character of PAN a small amount of non-specific signal (Figure 4.19) was observed on those slides which were treated without NHS-Biotin, but with S-HRP thus it was difficult be confirmed about the conjugation.

In this case as PAN-Jeff are non-woven fibre, the thread distribution is not uniform. However from this technique it was possible to confirm presence of low availability of amine functional group on the PAN-Jeff (Figure 4.19).

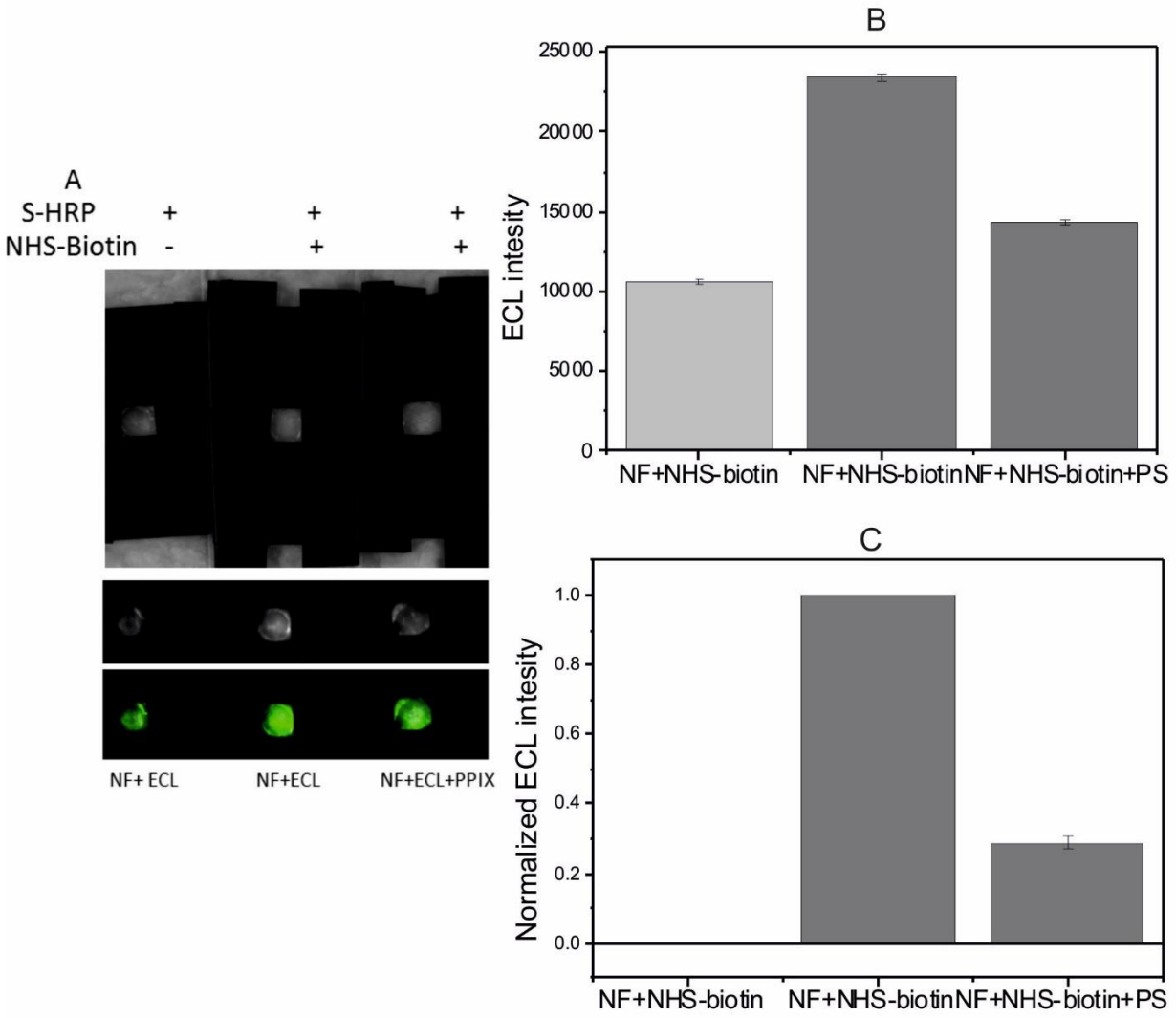

Figure 4.19 Characterization of photosensitiser functionalized electrospun nanofibre surface by midland blotting.

(A), Upper panel: Light micrograph of blot set up. Middle panel: ECL signal obtained and lower panel: superimposed image of top two panels with ECL false green colour; (B), ECL intensity of three experimental conditions; (C) normalized ECL intensity from (B). Data are average ± SD (n=3).

The data also show evidence of PPIX- amine coupling (Figure 4.19C) right column. Although the nanofibre without NHS-biotin showed some chemi-luminescence (Figure 4.19A). The reason for this is nonspecific absorption of S-HRP onto ENF. Thus the graph was normalized in Origin-Pro to subtract the intensity results from nonspecific binding. Then plots were prepared from raw data (middle panel A) not from the false colour image.

To obtain evidence of non- specific binding is not binding to free amines; acetic anhydride was used as a control to form a neutral conjugate with amine. Acetylation of amine on nanofibres surface can be made (Figure 4.20).The aim was to study the difference in chemiluminescent signal as acetic anhydride blocked the surface amines. That should result low or no ECL signal intensity. The column 2 and 3 showed very low intensity as expected where acetic anhydride was incubated and no NHS-biotin was added.

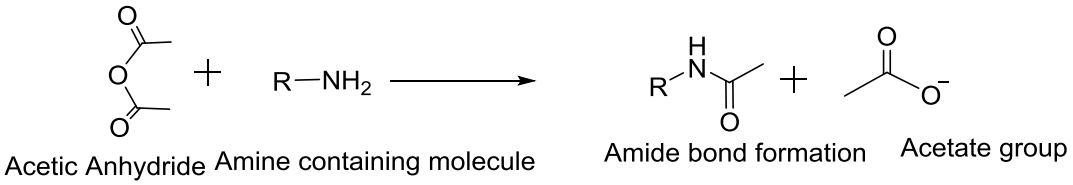

Figure 4.20 Acetic anhydride reacts with amines to form amide bond derivatives.

(A)

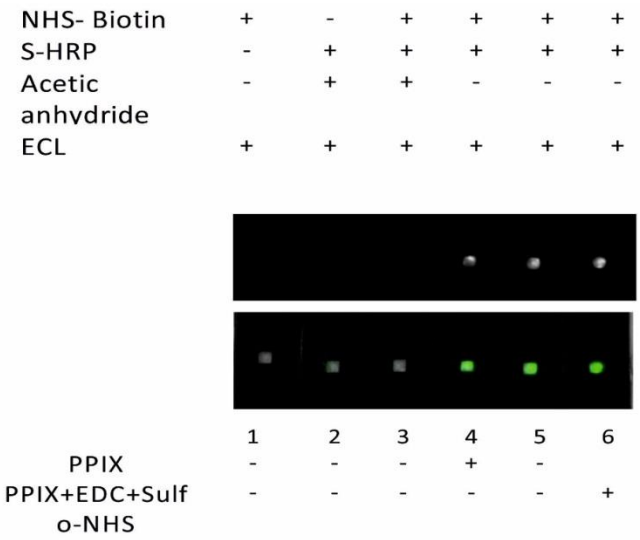

(B)

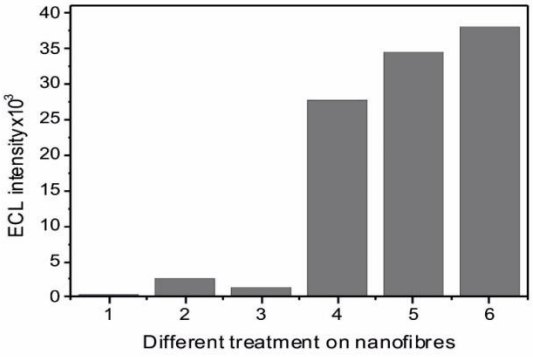

Figure 4.21 Characterization of photosensitiser functionalized electrospun nanofibre surface by Midland blotting.

(A) Upper panel: Light micrograph of experimental set up. Middle Panel: ECL signal obtained by the imager and lower Panel: Superimposed image of top two panels with ECL false green colour.

(B) ECL intensity of six experimental conditions, Column 1 shows nonspecific binding (no added S-HRP), and Column 2 nonspecific binding as all amine was blocked by acetic anhydride (no added NHS-biotin).Column 3 shows nonspecific binding (NHS-biotin added after addition of acetic anhydride). Column 4 is a positive control as shows the ECL signal of due to binding of NHS-biotin with surface amine. ECL signal intensity at position 6 is demonstrating that after PPIX conjugation with surface amine there still free amine left to conjugate with NHS biotin.

The observed signal in column 1, 2, 3 and shows that the non-specific binding was very low (Figure 4.20). Addition of acetic anhydride successfully blocked the amines though there was still some nonspecific binding (Figure 4.21). The positive control, column 4 also showed that NHS- biotin could successfully bind to the amine. Interestingly, data in column 6 showed that after PPIX immobilisation onto surface amine there were still free amines that bind with NHS- biotin and gave higher ECL signal intensity.

4.4.4 TAllylPyP$_{cov}$-(PAA-EG)

The newly synthesised tetra allyl pyridyl porphyrin was covalently immobilised onto PAA-EG nanofibre. Physical and chemical characterisation was done by SEM, FTIR analysis.

4.4.5 Functionalisation of PAA-EG with TAllylPyP

To functionalise the PAA-EG with TAllylPyP palladium catalysed allylic acyloxylation of terminal alkene was conducted in presence of base. The methodology was adopted and modified from a literature reported by Thiery *et al.* (2010). As the application field of nanofibre is water treatment, so all through the project consciously hazardous chemicals were avoided or minimized in all steps. Solvent system used by Thiery group was modified so that after covalent immobilisation followed by water treatment this TAllylPyP$_{cov}$-(PAA-EG) doesn't cause any secondary contamination or toxicity. Water was used as main solvent system in this reaction. Minimal amount of chloroform was used to solubilise palladium acetate. Reaction procedure is described in Section 2.9.6.

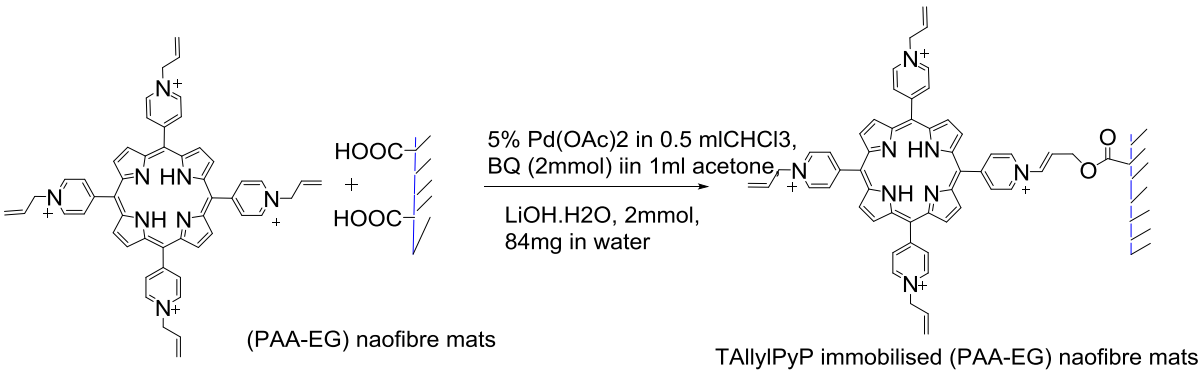

Figure 4.22 Reaction scheme of TAllylPyP immobilisation onto PAA-EG electrospun nanofibres mate surface.

The reaction scheme is showing the covalent modification of carboxylic functionalised PAA-EG by palladium catalysed allylic acyloxylation of terminal alkene of TAllylPyP.

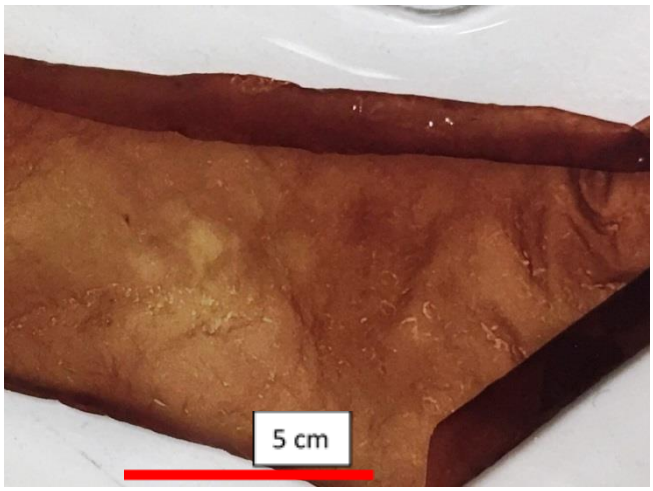

Figure 4.23 Tetra allyl pyridyl porphyrin functionalised PAA-EG: TAllylPyPcov-(PAA-EG).

4.4.6 FTIR TAllylPyP$_{cov}$-(PAA-EG)

FTIR spectrum of TAllylPyP$_{cov}$-(PAA-EG) was in complete agreement with Thiery *et al.* (2010) showing the presence of -C-O- of bond in the fingerprint region at 1543 cm^{-1}, which was clearly absent in the spectrum of TAllylPyP and PAA-EG. At 1708 cm^{-1} decrease of intensity of –COOH indicates the modification of –COOH. 1465 cm$^{-1,}$ 1245 cm^{-1}, and peak in 1170 also shows the agreement of modification of PAA-EG by covalent bonding with TAllylPyP.

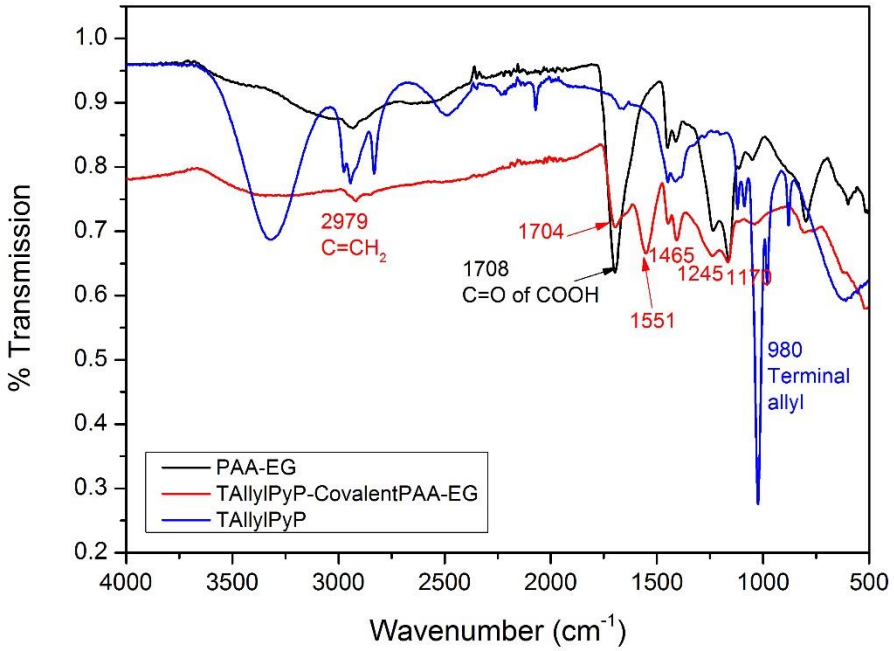

Figure 4.24 FTIR spectra of tetra allyl pyridyl porphyrin (TAllylPyP) immobilised onto PAA-EG nanofibre mat TAllylPyP$_{cov}$-(PAA-EG).

This FTIR spectra is showing the changes before and after covalent immobilisation of TAllylPyP onto PAA-EG nanofibre mats. (——), PAA-EG; (——) TAllylPyP; and (——) TAllylPyP$_{cov}$-(PAA-EG) nanofibres mat. Green circle represents presence of amide bon.

4.4.7 SEM of TAllylPyP$_{cov}$-(PAA-EG)

Morphological changes were investigated by SEM image of covalently immobilised TAllylPyP$_{cov}$-(PAA-EG). No major changes in morphology of PAA-EG nanofibres before (Figure 4.25A) and after (Figure 4.25B) immobilisation was not observed.

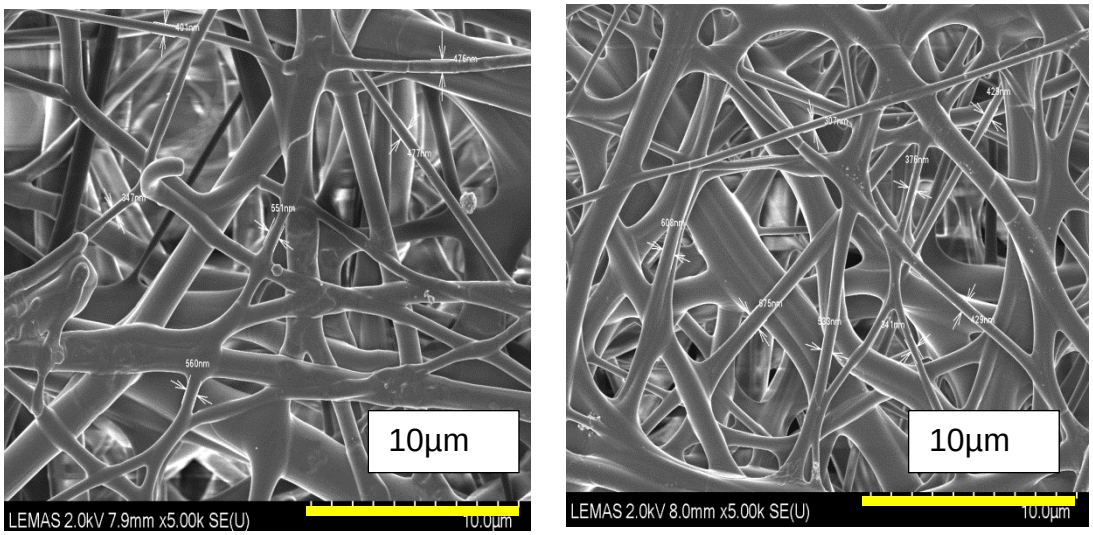

A B

Figure 4.25 SEM of tetra allyl pyridyl porphyrin (TAllylPyP) immobilised onto PAA-EG nanofibre mat TAllylPyP$_{cov}$-(PAA-EG).

(A), before; (B) after modification.

4.4.8 TAminelPyP$_{cov}$-(PAA-EG)

The newly synthesised tetra amine pyridyl porphyrin was covalently immobilised onto PAA-EG nanofibre. Physical and chemical characterisation was done by SEM, FTIR analysis.

4.4.9 Functionalisation of PAA-EG with TAminePyP

TAminePyP immobilisation on to PAA-EG was conducted using Two-step Coupling of –COOH and –NH_2 Using EDC and Sulfo-NHS. The following procedure was, adapted from a procedure described by Grabarek and Gergely (1990). The functionalisation method is described in (Section 2.9.7).

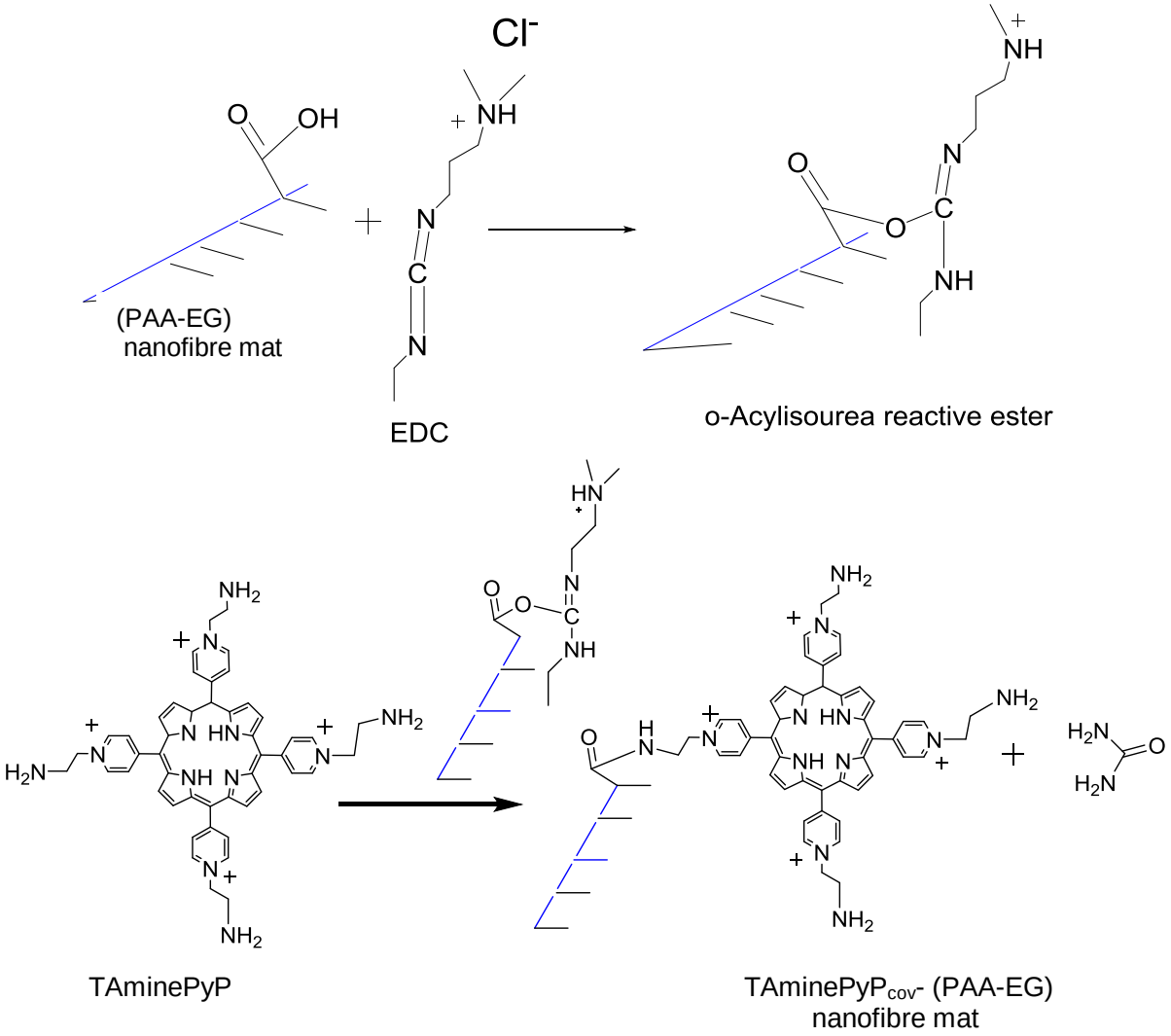

Figure 4.26 Reaction scheme of TAminePyP immobilisation onto PAA-EG electrospun nanofibres mate surface.

The reaction scheme is showing the covalent modification of carboxylic functionalised PAA-EG with amine containing TAminePyP. EDC and sulfo-NHS are coupling reagents.

Figure 4.27 Tetra amine pyridyl porphyrin functionalised PAA-EG: TAminePyP$_{cov}$-(PAA-EG)

FTIR

After covalent immobilisation of TAminePyP onto PAA-EG, the TAminePyP$_{cov}$-(PAA-EG) nanofibre mat was characterised by FTIR. It was compared with FTIR of PAA-EG and TAminePyP photosensitiser before immobilisation (Figure 4.23). FTIR of TAminePyP photosensitiser clearly showing the presence of primary amine signal at 3427cm^{-1} clear absence of signal in the region of C=O stretching of –COOH group. Where as for PAA-EG at 1700 cm^{-1} presents intense peak of C=O stretching of –COOH group, FTIR of TAminePyP$_{cov}$-(PAA-EG) also contain the peak of low intensity at same region which indicates incomplete conversion of amide from carboxylic group. On the other hand TAminePyP$_{cov}$-(PAA-EG) (red spectrum) contain a new peak of c+O of amide at 1545 cm^{-1}. Where as other two spectrums of (PAA_EG) and TAminePyP (black and Blue respectively) are missing signals at this region. Red and black lines are showing the signal of OH-stretching at 2948 cm^{-1} whereas blue line of TAminePyP photosensitiser does not showing any signal at this region.

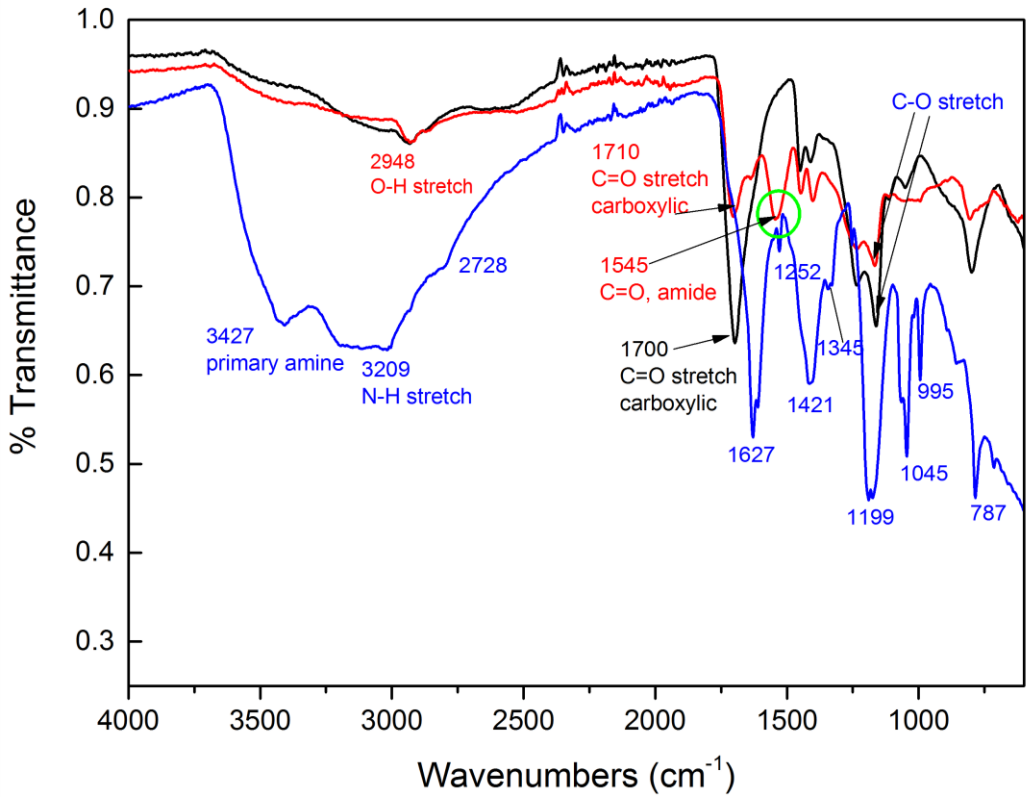

Figure 4.28 FTIR spectra of tetra amine pyridyl porphyrin (TAminePyP) immobilised onto PAA-EG nanofibre mat TAminePyP$_{cov}$-(PAA-EG).

Three spectrums are presenting as (—), PAA-EG; (—)TAminePyP; and (—)TAminePyP$_{cov}$-(PAA-EG) nanofibre mats.

4.4.10 SEM of TAminePyP$_{cov}$-(PAA-EG).

Morphological changes were investigated by SEM image of covalently immobilised TAminePyP$_{cov}$-(PAA-EG). No major changes in morphology of PAA-EG nanofibres before (Figure 4.29A) and after (Figure 4.29B) immobilisation was not observed.

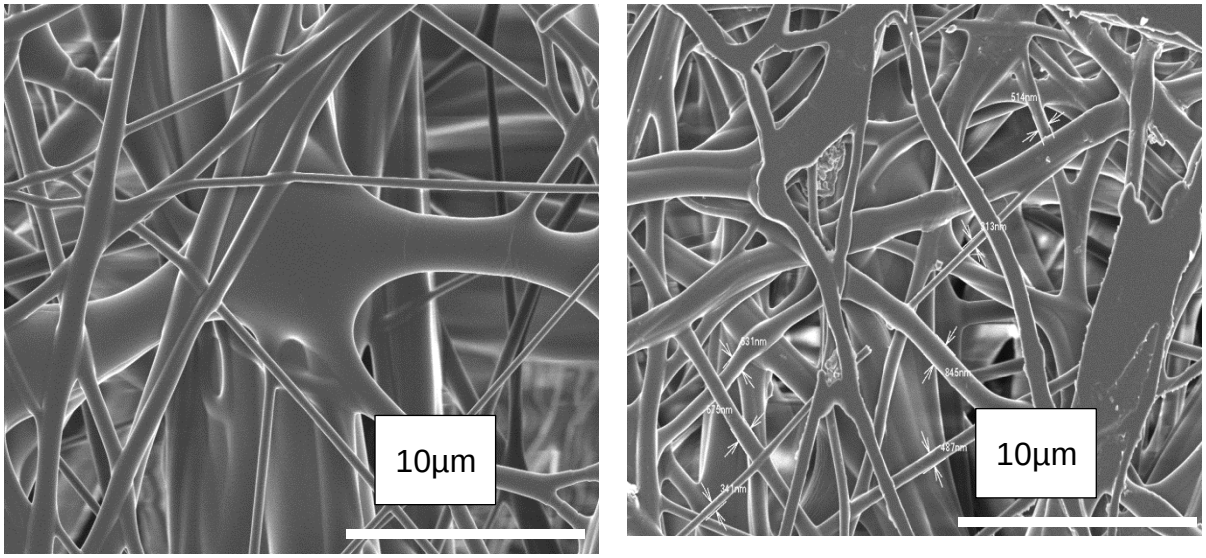

Figure 4.29 SEM image of PAA-EG nanofibre before and after covalent modification with TAminePyP photosensitiser.

(A), PAA-EG; and (B) TAminePyP$_{cov}$-(PAA-EG) nanofibre mats.

4.5 Confirmation of covalent immobilisation of TAllylPyP and TaminePyP onto PAA-EG nanofibre

As nanofibre mats are super adsorptive , that is why it was also confirmed that the bonding was covalent not adsorption of TAllylPyP and TAminePyP onto PAA-EG was tested incubating of TAllylpyP$_{cov}$-(PAA-EG) and TAminePyP$_{cov}$-(PAA-EG) nanofibres mat in 2M NaOH solution for 1h. And after 1h no release of TAllylPyP and TAminePyP was observed (Figure 4.30). Whereas in NaOH, TMPyP adsorbed PAA-EG nanofibre showed complete release of TMPyP (Figure 4.31) within a minutes.

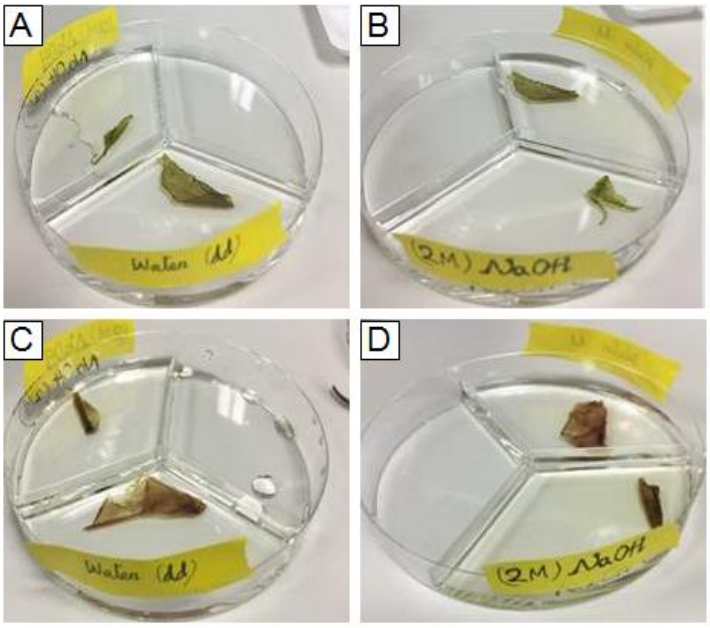

Figure 4.30 Confirmation of strong binding of TAllyLPyP and TAminePyP onto PAA-EG nanofibres instead of adsorption.

(A), TAminePyPcov-(PAA-EG) in deionised water; (B) TAminePyPcov-(PAA-EG) in 2 M NaOH; (C) TAllylPyPcov-(PAA-EG) in deionised water; (D) TAllylPyPcov-(PAA-EG) in 2 M NaOH.

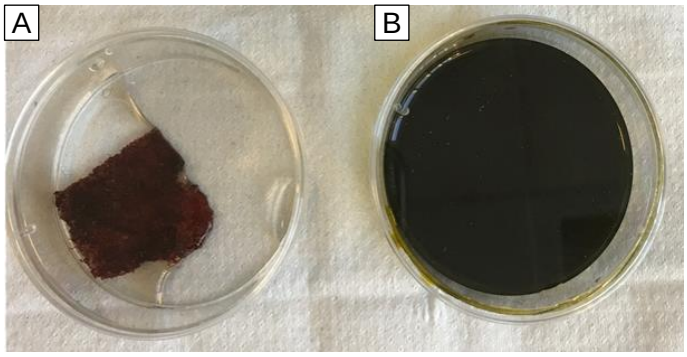

Figure 4.31 TMPyP release in water due to weak electrostatic bonding with PAA-EG nanofibre mat in NaOH.

(A), $TMPyP_{ads}$-(PAA-EG) in deionised water; (B), $TMPyP_{ads}$-(PAA-EG) in 2 M NaOH.

4.6 Confirmation of singlet oxygen generation by photosensitiser immobilised nanofibre mat.

Singlet oxygen generation was studied (Section 2.11) for two newly developed nanofibres: $TMPyP_{ads}$-(PAA-PVA) and TAllylPyPcov-(PAA-EG). Here in this assay 2-amino-3-hydroxy pyridine (AHP) used as singlet oxygen quencher. The absorbance of 200 mM 2-amino-3-hydroxy pyridine (AHP) decreased to zero within 5 minutes when AHP was illuminated with free TMPyP solution in assay. Whereas a slower decrease of absorbance was observed in case of $TMPyP_{ads}$-(PAA-PVA) nanofibre mat illuminated with AHP (Figure 4.32). This shows that singlet oxygen generation by $TMPyP_{ads}$-(PAA-PVA) nanofibre mat was slower than free TMPyP. On the other hand TAllylPyPcov-(PAA-EG) showed singlet oxygen generation by TAllylPyPcov-(PAA nanofibre mat was faster than $TMPyP_{ads}$-(PAA-PVA).

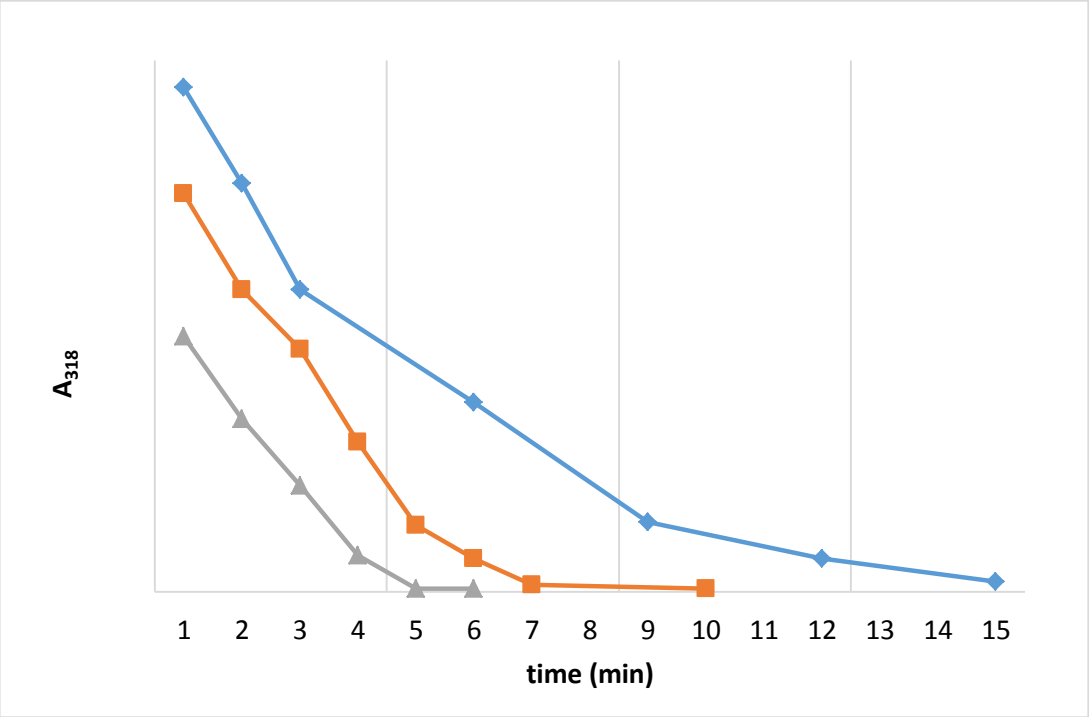

Figure 4.32 Singlet oxygen production by TMPyP and TAllylPyP immobilised nanofibre mats.

(—▲—), TMPyP; (—◆—) $TMPyP_{ads}$-(PAA-PVA) and (—■—), $TAminePyP_{cov}$-(PAA-EG) nanofibre mats.

Chapter 5

Photodynamic inactivation by functionalised electrospun nanofibres

5.1 Overview

For disinfectant free water it is necessary to find the way of cost effective and efficient technology for complete removal of disinfectant after treatment. Photodynamic inactivation (PDI) of bacteria in water by using soluble photosensitiser (PS) is well studied (Abrahamse and Hamblin, 2016; Almeida *et al.*, 2014; Bartolomeu *et al.*, 2017). This chapter presents immobilisation of photosensitisers with water-stable electrospun nanofibre so that photosensitisers remain attached to the nanofibre mat. After treatment and removal of the photosensitiser functionalised nanofibre, the sterile water should be completely photosensitiser free. Three different types of electrospun nanofibre mats were used in this study. Jeffamine-doped polyacrylonitrile (PAN-Jeff) nanofibre mat was kindly provided by Prof Bob Stevens (Nottingham Trent University, UK). Two other types of water stable nanofibre mats were produced by electrospinning and modified by crosslinking to introduce water stability as part of this research. Water resistance of these nanofibre mats was confirmed by mass analysis of nanofibres washings (Section 4.3.4). Then the nanofibre mats were functionalised (Bartolomeu *et al.*, 2017) with four photosensitisers, which were all porphyrins. Amongst them two of the photosensitisers were commercially available, prototoporphyrin IX (PPIX) and tetra methyl pyridyl porphyrin (TMPyP), whereas the other two tetra-allyl-pyridyl-porphyrin (TAllylPyP) and tetra-amine-pyridyl-porphyrin (TAminePyP) were synthesised as described in Chapter 3. With PPIX, it was not possible to inactivate Gram-negative bacteria because of the overall negative charge on PPIX (Bernigaud *et al.*, 2008) and so tetra cationic TMPyP was tested and proved more effective for inactivation of Gram-negative organisms. TMPyP was also successful for inactivation of carbenicillin resistant BL21 (DE3) *E. coli*. However, it was not possible to functionalise electrospun nanofibre

covalently with this photosensitiser due to its lack of a reactive group. Adsorption by electrostatic interaction of TMPyP with carboxy group on the support was carried out to functionalise nanofibre with TMPyP.

Due to these limitation two new photosensitisers, analogues of porphyrin were synthesised with suitable reactive pendant groups (amine and allyl).

5.1.1 Adsorption of photosensitiser to nanofibre mats

Using adsorption, polyacrylic acid crosslinked with polyvinyl alcohol (PAA-PVA) electrospun nanofibre mat and polyacrylic acid crosslinked with ethylene glycol (PAA-EG) were functionalised with TMPyP and TAllylPyP. These will be referred as follows.

i. Tetra $TMPyP_{ads}$-(PAA-PVA),
ii. $TMPyP_{ads}$-(PAA-EG), and
iii. $TAllylPyP_{ads}$-(PAA-EG).
Where ‘ads’ denotes the photosensitiser is adsorbed.

These nanofibre mats were successfully functionalised and characterised using FTIR, SEM and XPS (Section 4.5). PDI was successfully carried out for *E. coli* NCTC10418 and carbenicillin resistant bacteria BL21 (DE3) by these two types of nanofibre mats. In both cases, complete PDI of bacteria was observed. PDI was also tested for reuse of functionalised nanofibre mat.

5.1.2 Covalent modification of nanofibre mats with photosensitisers

PPIX was covalently immobilised onto Jeffamine doped polyacrylonitrile nanofibre mats, referred as PPIX-(PAN-Jeff) (Section 2.9.3). Newly synthesised photosensitisers TAllylPyP and TAminePyP were covalently immobilised onto with PAA-EG nanofibre mats. These are referred as follows.

i. TAllylPyPcov-(PAA-EG), and
ii. TAminePyPcov-(PAA-EG) respectively.
Where ‘cov’ indicates covalent attachment of the photosensitiser.

5.2 PDI by Jeffamine doped polyacrilonitrile (PAN-Jeff) nanofibre mats

Though the PPIX molecule is itself neutral, it has two pendant carboxylic groups that make the overall compound negatively charged. It was hypothesised that if PPIX was successfully immobilised by its carboxylic groups onto aminated PAN-Jeff, this could cancel the negative charge. This experiment was carried out for several times with triple replicates. In few cases, a small percentage of PDI was observed, but these data were not reproducible, so this approach was abandoned.

5.2.1 PDI of *E.coli* by PPIX-(PAN-Jeff) nanofibre mats

As the PDI of *E. coli* by PPIX-(PAN-Jeff) was not successful, it was proposed that after immobilisation there might be free carboxylic groups left, i.e. the amide bond was formed at only one carboxylic group of PPIX. So to block the remaining carboxylic group after PPIX conjugation with PAN-Jeff nanofibre, amidation (Section 2.9.3) was carried out with propyl amine using carbodiimide mediated peptide bond formation (Grabarek and Gergely, 1990). However, PDI after amidation was tested and showed no significant difference in the percentage of *E. coli* photoinactivation either before or after blocking the carboxylic groups.

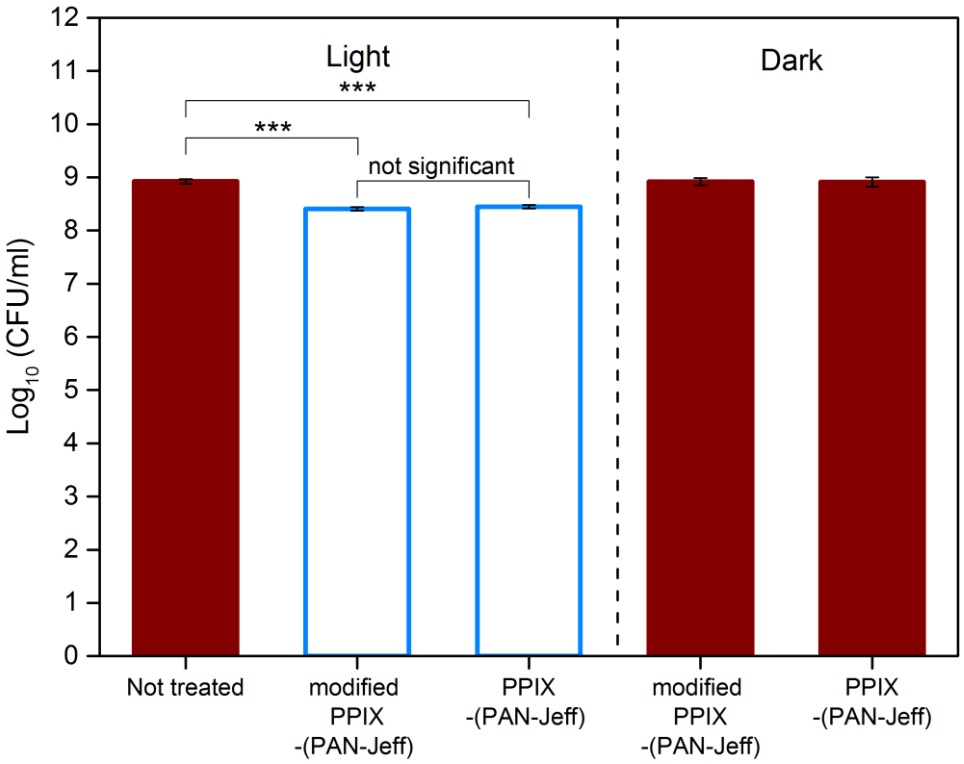

Figure 5.1 PDI with PPIX-(PAN-Jeff) (with and without blocking the remaining carboxylic group of PPIX).

E. coli (9 log CFU/ml) in water were exposed with and without PPIX, PPIX propylamine-(PAN-Jeff) nanofibre mat in the dark or light for 30 min. (▬), controls and dark treated; (▭), light treated. Cell number was determined by plating. Data are mean ± SEM, (n=3). The values was compared statistically for with and without PPIX using the Dunnett's multiple comparisons test in ANOVA; ***, $p<0.001$.

Figure 5.1 shows that PDI with PPIX immobilised onto PAN-Jeff nanofibre mat caused cell killing although the difference between cell killing by propylamine blocked PPIX-Jeffamine (modified PPIX-PAN-Jeff) and unblocked PPIX-Jeffamine (PPIX-PAN-Jeff) was not significant.

It is worth mentioning that PAN was only doped with amine functionalised Jeffamine and Jeffamine is partially water soluble. Also, there was no chemical bonding between the PAN and Jeffamine. During the functionalisation of PAN-Jeff it was noticed that after amine coupling the nanofibres turned brown but when the nanofibre mats were washed to remove excess PPIX, the nanofibre mats became almost white again (Figure 5.2). This showed that PPIX bond to Jeffamine part was mostly washed away (characterisation of this aminated nanofibre mat is described

(Section 4.6.3). Later, using mass spectrometry analysis of nanofibre washings it was confirmed that Jeffamine was not water stable enough to retain PPIX on the PAN nanofibre. This is likely to explain the unsuccessful PDI of *E. coli* NCTC 10418 using PPIX functionalised PAN-Jeff nanofibre discs.

(A) (B) (C)

Figure 5.2 PPIX immobilised onto PAN-Jeff (before and after).
(A), before functionalisation of PAN-Jeff with PPIX; (B), after functionalisation of PAN-Jeff with PPIX, before wash with water; (C) after wash of PPIX, functionalised PAN-Jeff nanofibre disc.

5.2.2 PDI of *E.coli* by PPIX-(PAN-Jeff) nanofibre mats

As the PDI of *E. coli* by PPIX-(PAN-Jeff) was not successful, PAN nanofibre mat were used to construct a flow cell system for water treatment. These flow cells were kindly provided by Professor Bob Stevens, (Nottingham Trent University UK) [Section 2.2.5.1; Figure 2.6]. In this study, ployacrylonitrile (PAN) nanofibre were hydrolysed with sodium hydroxide to convert PAN to polyacrylic acid (PAA). Then PAA was modified with hexamethylenediamine so that -COOH of PPIX can conjugate with amine of hexamethylenediamine. The PAA was covalently conjugated with PPIX to functionalise PAA nanofibre mat (Section 2.9.5). Since PAA is water soluble and only 5% (w/w) of PAN was used to electrospin the nanofibres mats. Then after hydroxylation of PAN to PAA followed by washing steps to remove unused NaOH and PPIX, it was found that PAA was washed away (Figure 5.3). Functionalisation (Section 2.9.5) was carried out using the same flow system, because of too low concentration of PAA or the absence of PAA no change was observed after PDI (Figure 5.4). In the IR spectra no amide

bond was found to be present. Thus, this approach and the nanofibres made of PAN was abandoned. Later water stable PAA nanofibre mats were developed which are described (Section 2.2).

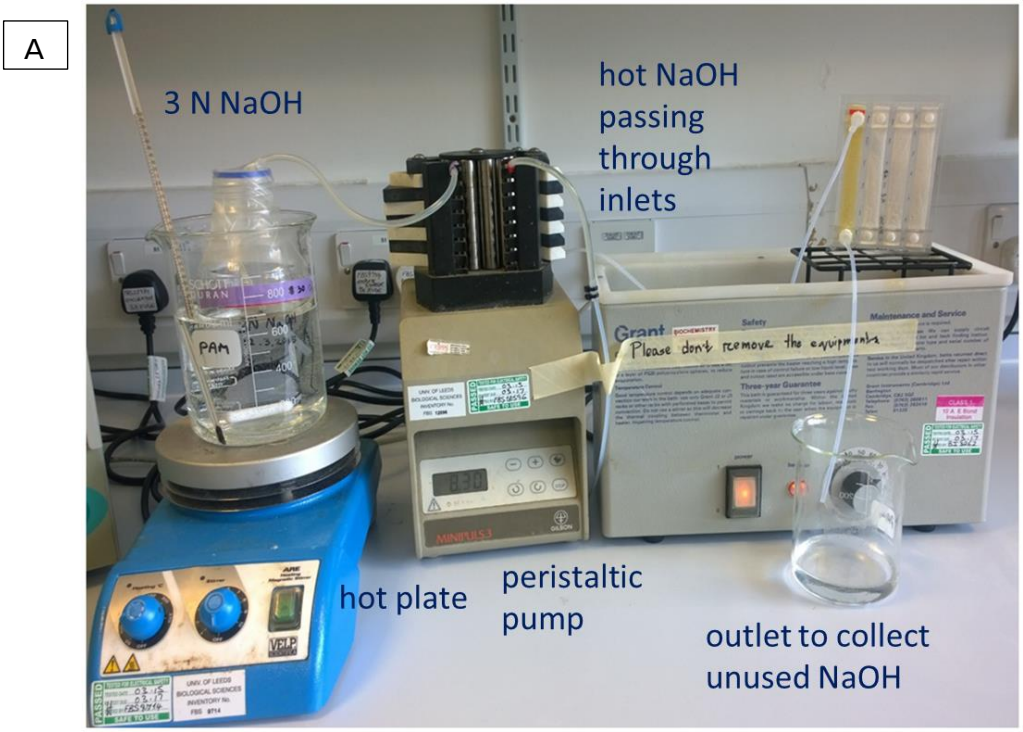

before washing of PPIX functionalised PAA nanofibre

After washing of PPIX functionalised PAA nanofibre

Figure 5.3 Flow system to convert of PAN to PAA and PPIX immobilisation onto PAA.

(A) Complete set up; (B) Before washing of PPIX functionalised PAA; (C) After functionalisation and washing with water.

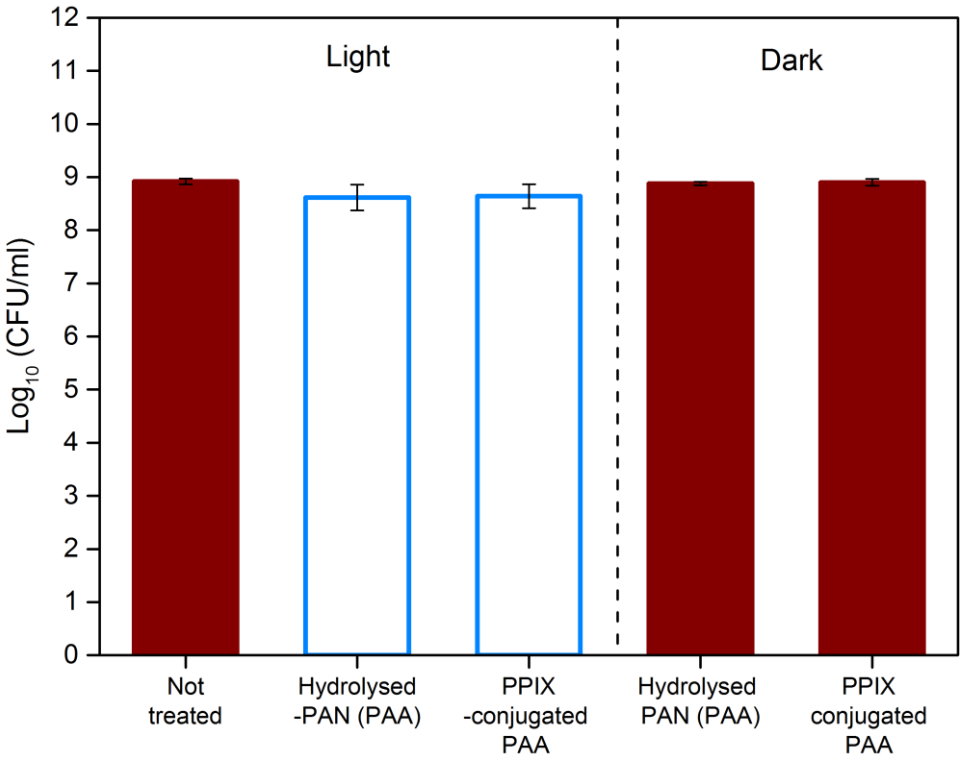

Figure 5.4 Photo treatment of *E. coli* NCTC 10418 in flow cell made of PPIX conjugated PAA nanofibre.

E. coli (9 log CFU/ml) in water was flow through flow cell. Then *E. coli* were exposed with and without PPIX conjugated PAA nanofibre, nanofibre mat in the dark or light for 60 min. (■), controls and dark treated; (□), light treated. Cell number was determined by plating. Data are mean ± SEM, (n=3).

5.3 PDI of carbenicillin resistant *E. coli* BL21 (DE3) by TMPyP immobilised (adsorbed) onto PAA-PVA nanofibre mats

Water resistant Polyacrylic acid crosslinked with polyvinyl alcohol (PAA-PVA), nanofibre mat, were functionalised with TMPyP, using adsorption (Section 2.9.1.1). Electrostatic interaction was the main force to hold TMPyP to the PAA-PVA nanofibres since TMPyP is tetra-cationic and PAA-PVA is polyanionic.

PDI of carbenicillin resistant *E. coli strain* BL21 (DE3) was carried out with $TMPyP_{ads}$-(PAA-PVA). TMPyP solution at 50 µM was used for PDI as positive and negative controls, either light treated for 90 min at 30 mW/cm^2

or kept dark for same duration. In light treated cells at 90 min, complete sterilisation of BL21 (DE3) was observed. The reduction in colony count of BL21 (DE3) after the PDI by $TMPyP_{ads}$-(PAA-PVA) was observed clearly when bacterial agar plates were compared (Figure 5.5).

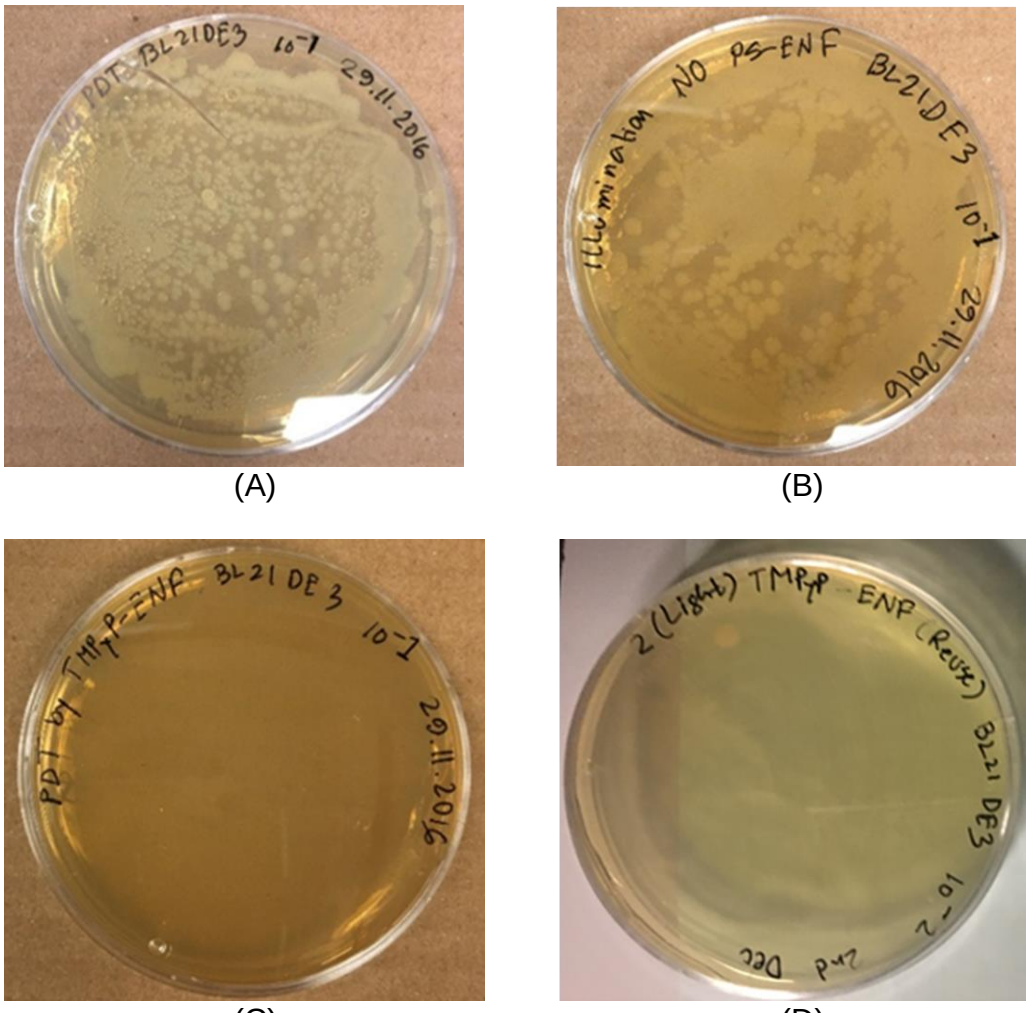

(A) (B)

(C) (D)

Figure 5.5 Effect of PDI of BL21 (DE3) by $TMPyP_{ads}$-(PAA-PVA) in bacteria agar plates.

(A), No TMPyP, no photo treatment BL21(DE3); (B), No $TMPyP_{ads}$-(PAA-PVA), BL21(DE3) (photo-treated); (C), Photo-treated BL21(DE3) by $TMPyP_{ads}$-(PAA-PVA); (D), Photo-treated BL21(DE3) by $TMPyP_{ads}$-(PAA-PVA).

All experiments were triplicated using same set of $TMPyP_{ads}$-(PAA-PVA) mats and TMPyP solution. After serial dilution, plating was used to determine cell survival and the extent of PDI in *E. coli* BL21 (DE3), which is shown in Figure 5.6.

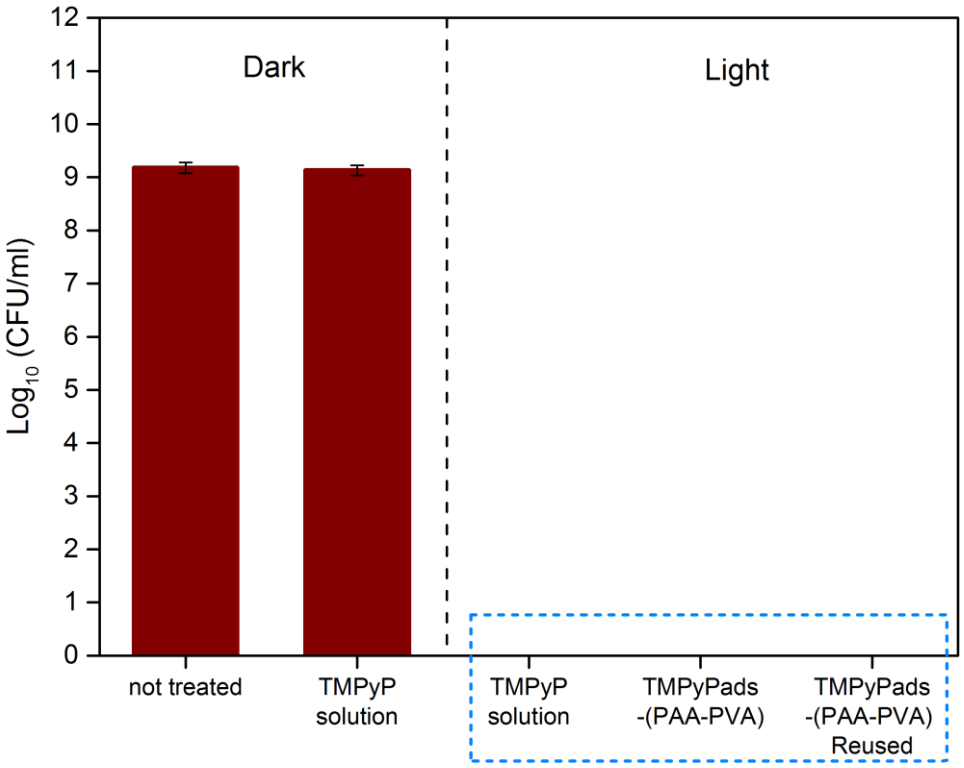

Figure 5.6 PDI of carbenicillin resistant *E. coli* strain BL21 (DE3) with $TMPyP_{ads}$-(PAA-PVA) nanofibre.

Cells (9 log CFU/ml) were incubated for 90 min in the absence or presence of TMPyP at 50 µM or $TMPyP_{ads}$-(PAA-PVA) nanofibre. Cells were incubated in the dark or light at 30 mW/cm^2. (▬), dark treated; (▭), complete sterilisation. Cell number was determined by plating. Data are mean ± SEM, (n=3). PAA-PVA was reused 3 times.

To confirm the reusability of $TMPyP_{ads}$-(PAA-PVA), the nanofibre was reused three times. Complete sterilisation (9 log reduction) was observed even after three times use. Clearly multiple reuse cycle will be needed to completely confirm the stability of the $TMPyP_{ads}$-(PAA-PVA) mat, but this was beyond the scope of this study.

5.4 PDI of *E. coli* NCTC 10418 by TMPyP immobilised (adsorbed) onto PAA-EG nanofibre mats

Water resistant polyacrylic acid crosslinked with ethylene glycol, PAA-EG nanofibre mats, were newly developed in this research and functionalised with TMPyP, again by using adsorption (Section 2.9.1.1). As with the PAA-EG composite, electrostatic interaction was the main force to hold TMPyP onto the PAA-EG nanofibre mat. PDI of *E. coli* NCTC 10418 was carried out with $TMPyP_{ads}$-(PAA-EG) nanofibre mat (Figure 5.7). Non-treated NCTC 10418 and $TMPyP_{ads}$-(PAA-EG) nanofibre exposed NCTC 10418 out in the dark as a negative control showed little offset. PDI was observed for 10-30 min. After 10 and at 20 min illumination 2 and 3 log reduction was observed respectively. Finally at illumination 30 min, complete sterilisation of NCTC10418 was observed.

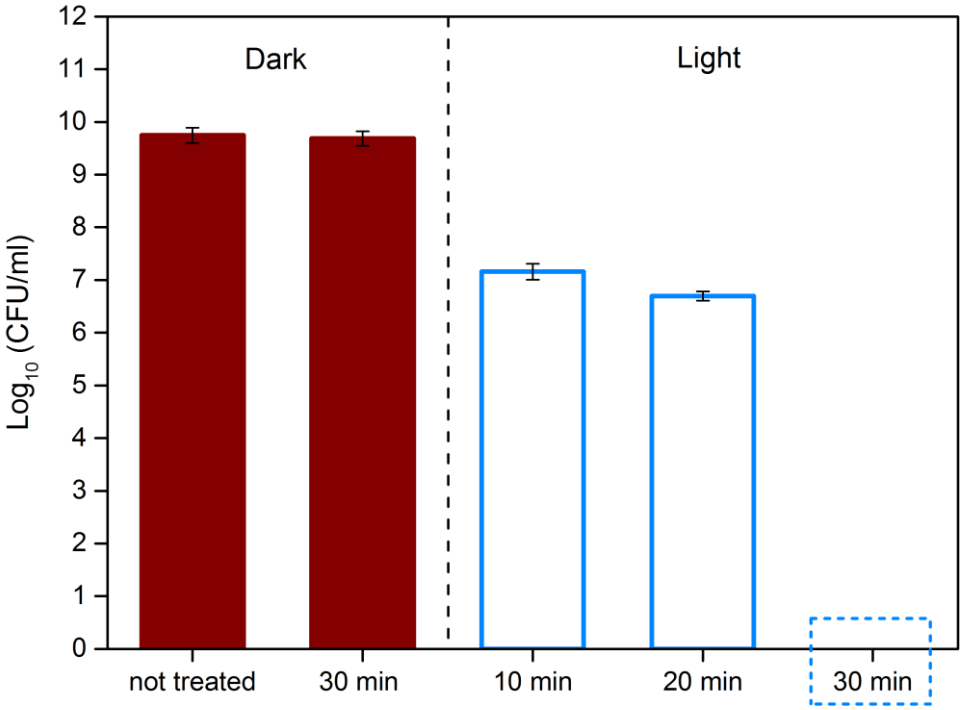

Figure 5.7 PDI of *E. coli* NCTC 10418 with $TMPyP_{ads}$-(PAA-EG) nanofibre mat.

Cells 9.8 log CFU/ml of *E. coli* strain NCTC 10418 were incubated for 30 min in absence or presence of $TMPyP_{ads}$-(PAA-EG) nanofibre mats in the dark or at 70 mW/cm^2 illumination for 10 - 30 min. (▬), dark treated; (▭), light treated and (▭), complete sterilisation. Cell number was determined by plating. Data are mean ± SEM, (n=3).

As described for the PDI with TMPyP in solution (Section 3.6), with an increase of light intensity it was possible to decrease the duration of light treatment. At 70 mW/cm^2, the intensity is still only about 7% of full sunlight at low latitudes. This is an indication that with the use of sunlight with the higher intensity, this water sterilisation system can be a great solution for water treatment in Asian and sub-Shaharan Africa countries.

5.5 PDI of *E. coli* NCTC 10418 by TAllylPyP immobilised (adsorbed) onto PAA-EG nanofibre mat

According to previous PDI studies on Gram-negative bacteria, tetra cationic photosensitiser is the most efficient PDI agent (Malatesti *et al.*, 2017). The ultimate goal of the work in this thesis was covalent immobilisation of photosensitiser onto the surface of electrospun nanofibre mats. This could permit sterilisation of water without releasing disinfectant (the photosensitiser) in the treated water. TMPyP was proved to be a very efficient PDI agent. However, it lacks suitable functional groups for covalent bonding leading to the need to synthesis TMPyP analogue with useful functional group (Gyulkhandanyan *et al.*, 2009). An allyl functionalised pyridyl porphyrin analogue, tetra allyl pyridyl porphyrin (TAllylPyP) was synthesised following method already reported by Gyulkhandanyan *et al.* (2009). Initially, PAA-EG nanofibre mats were functionalised with TAllylPyP using adsorption so as to compare directly with adsorbed TMPyP and PDI efficiency was investigated. Figure 5.8 shows the efficiency of the TAllylPyP$_{ads}$-(PAA-EG) nanofibre mat. As with the other photosensitisers nanofibre composite, photo killing of NCTC 10418 was monitored after 5 to 30 min of light treatment. After 5 min of light treatment more than 50% cells were killed and complete sterilisation was observed after 30 min of light treatment.

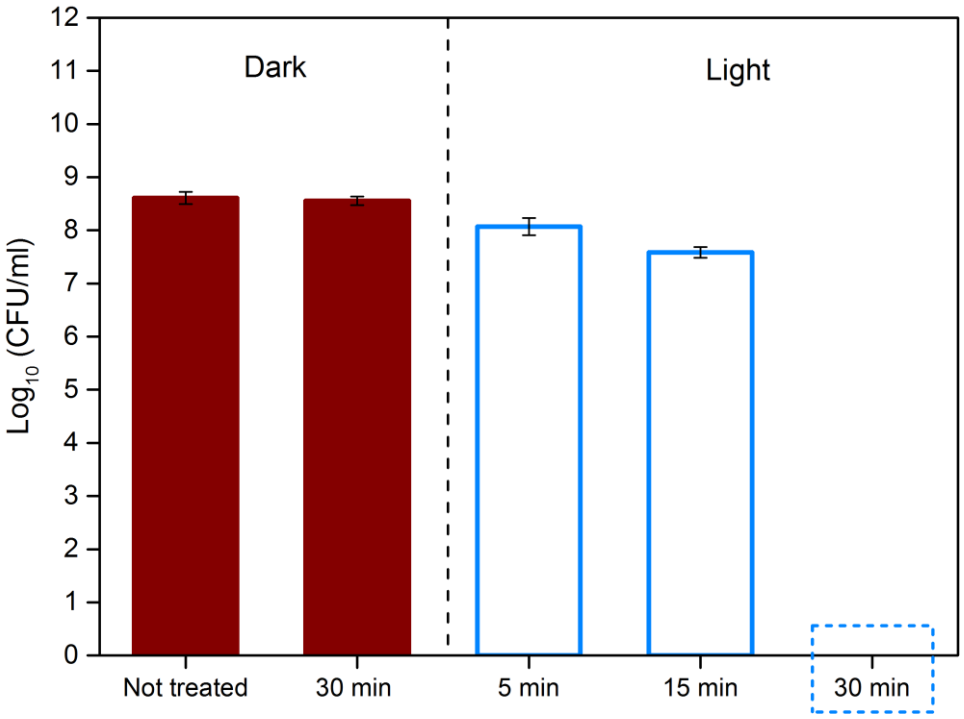

Figure 5.8 PDI Study of *E. coli* NCTC 10418 with TAllylPyP$_{ads}$-(PAA-EG) nanofibre mat.

Cells 8.5 log CFU/ml of *E. coli* strain NCTC 10418 were incubated for 30 min in absence or presence of TAllylP$_{ads}$-(PAA-EG) nanofibre mats in the dark or at 70 mW/cm^2 illumination for 5-30 min. ( ), dark treated; ( ), light treated; ( ), complete sterilisation. Cell number was determined by plating. Data are mean ± SEM, (n=3).

In this study, non-treated NCTC 10418 and TAllylPyP$_{ads}$-(PAA-EG) treated *E. coli* NCTC 10418 as negative controls, were just kept in the dark for 30 min. Slight dark toxicity of TAllylPyP was observed but this was not substantial.

5.6 PDI of *E. coli* NCTC 10418 by TAllylPyP covalently immobilised onto PAA-EG nanofibre mats

After complete inactivation of *E. coli* strain NCTC 10418 by TAllylPyP adsorbed onto PAA-EG nanofibre mats, the material was covalently functionalised with TAllylPyP [termed TAllylPyP$_{cov}$-(PAA-EG)].To functionalise the PAA-EG with TAllylPyP, palladium catalysed allylic acyloxylation of terminal alkene was conducted in presence of base. The methodology was adopted and modified from a methogology reported by the Thiery group (Thiery *et al.*, 2010)

PDI of *E. coli* strain NCTC 10418 was performed by TAllylPyP$_{cov}$-(PAA-EG) nanofibre mats at 70 mW/cm^2. The reduction in colony count of *E. coli* NCTC 10418 after the PDI by TAllylPyP$_{cov}$-(PAA-EG) was observed clearly when bacteria agar plates were compared (Figure 5.9).

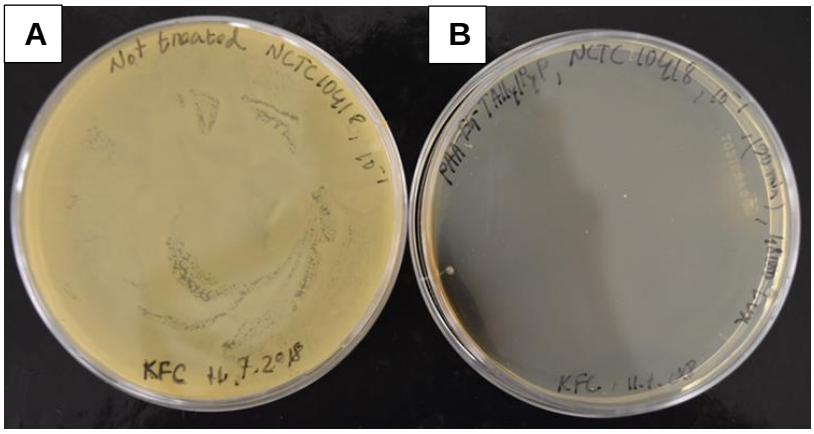

Figure 5.9 Effect of PDI of *E. coli* NCTC 10418 by TAllylPyP$_{cov}$-(PAA-EG) in bacteria agar plates.

(A), survived cells before treatment; (B), after treatment.

Figure 5.10 shows the efficiency of the TAllylPyP$_{cov}$-(PAA-EG) nanofibre mat. Untreated *E. coli* NCTC 10418 and TAllylPyP$_{cov}$-(PAA-EG) treated cells incubated in the dark were used as negative controls. In addition, exposure to PAA-EG nanofibre mat alone confirmed that there was no toxicity from the PAA-EG nanofibres. Almost complete sterilisation was observed as only one colony of *E. coli* NCTC 10418 survived in one of three plates. 70 mW/cm^2 intensity light was used for 60 min, during PDI by TAllylPyP$_{cov}$-(PAA-EG) nanofibre mats. Although illumination time dependency was not investigated,

with the TAllylPyP$_{ads}$ mat (Section 5.5) , it is likely that much less than 60 min would be needed for complete cell killing.

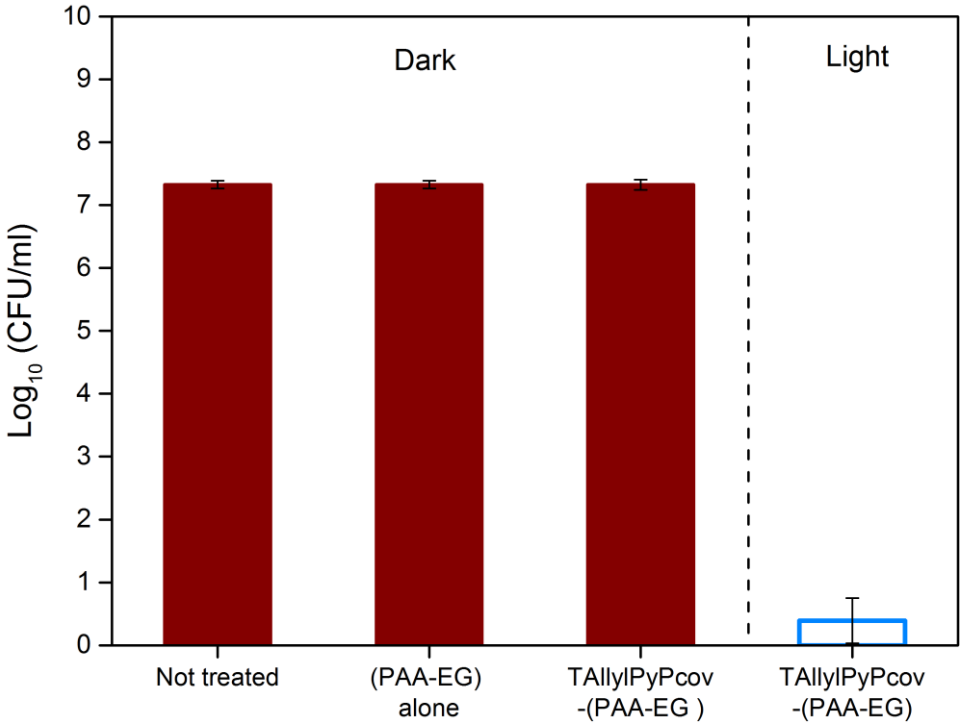

Figure 5.10 PDI study of *E. coli* NCTC 10418 with covalently immobilised TAllylPyP with PAA-EG nanofibre mat.

Cells at 7.4 log CFU/ml *E. coli* NCTC 10418 were incubated in the absence or presence of TAllylPyP onto PAA-EG nanofibre mat and TAllylPyP$_{cov}$-(PAA-EG) nanofibre mat for 60 min in the dark and under 70 mW/cm^2 illumination. (■), dark treated; (□), light treated and complete sterilisation. Data are mean ± SEM, (n=3).

5.7 PDI of *E. coli* NCTC 10418 by TAminePyP covalently immobilised onto PAA-EG nanofibre mats

In addition to TAllylPyP, an amine functionalised photosensitiser, tetra-amine-pyridyl porphyrin (TAminePyP) was also synthesised (Section 2.5.1). Covalent immobilisation of TAminePyP onto PAA-EG nanofibre was carried out. TAminePyP immobilisation onto PAA-EG was conducted using a two-step coupling between –COOH and –NH2 using EDC and sulfo-NHS. The following procedure was adapted from a procedure described by Grabarek and Gergely. The reduction in colony count of *E. coli* NCTC 10418 after the PDI by TAminePyP$_{cov}$-(PAA-EG) was observed clearly when bacteria agar plates were compared (Figure 5.11).

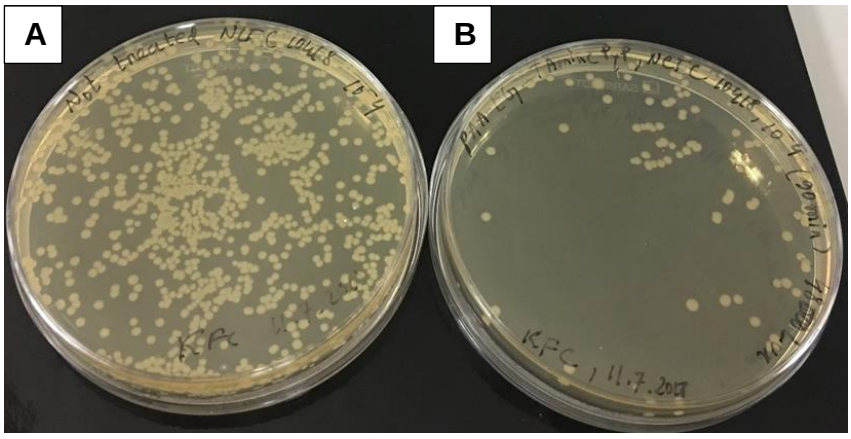

Figure 5.11 Effect of PDI of *E. coli* NCTC 10418 by TAminePyP$_{cov}$-(PAA-EG) in bacteria agar plates.

(A), survived cells before treatment; (B), after treatment.

Figure 5.12 shows that the PDI by TAminePyP$_{cov}$-(PAA-EG) and TAminePyP in solution (25 µM). In both cases, 60 min light treatment was carried out and reduction of 1 log CFU/ml by developed TAminePyP$_{cov}$-(PAA-EG) functionalised nanofibre mats was observed. With a 25 µM solution of TAminePyP, around 0.5 log CFU/ml of cells were inactivated. In this experiment, *E. coli* NCTC 10418 with 25 µM solution of TAminePyP and TAminePyP$_{cov}$-(PAA-EG) nanofibres were treated in the dark. There appeared to be some dark toxicity of TAminePyP, but PAA-EG nanofibre mat alone showed no toxicity (Figure 5.12).

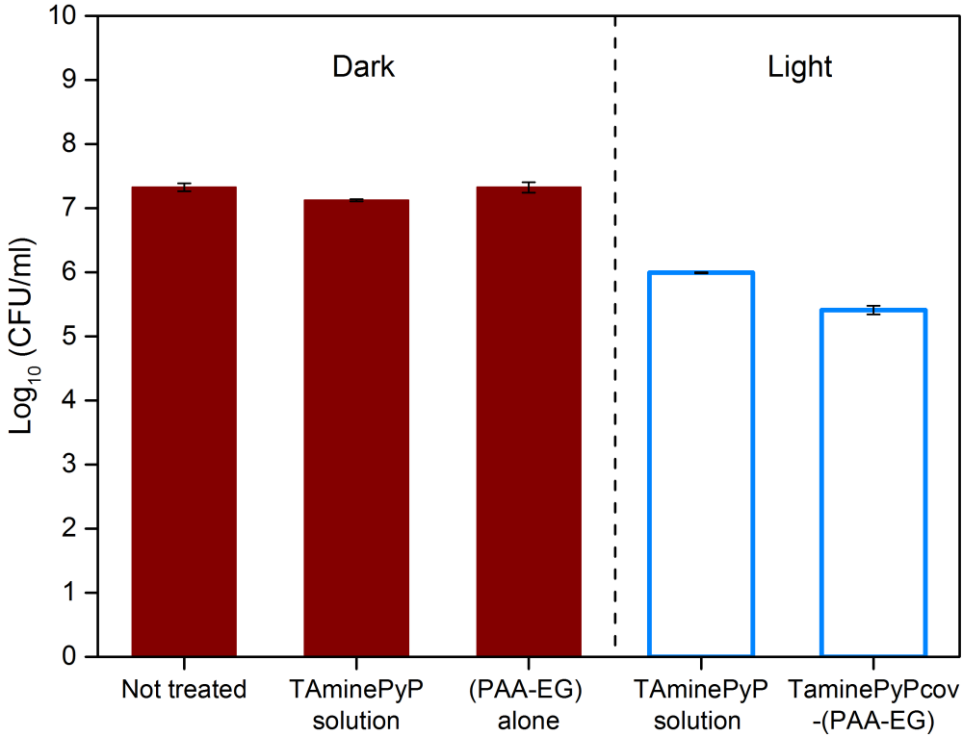

Figure 5.12 PDI Study of *E. coli* NCTC 10418 with covalently functionalised TAminePyP with PAA-EG nanofibre mats.

Cells at 7.2 log CFU/ml *E. coli* NCTC 10418 were incubated in the absence or presence of TAminePyP onto PAA-EG nanofibre mat and TAminePyP$_{cov}$-(PAA-EG) nanofibre mat for 60 min in the dark and under 70 mW/cm^2 illumination. (■), dark treated; (□), light treated. Data are mean ± SEM, (n=3).

During PDI by TAminePyP$_{cov}$-(PAA-EG) complete inactivation of *E. coli* of NCTC 10418 was not observed, although only 10% of cells remained viable. This may be due to the variable morphology of the nanofibres so that the concentration of TAminePyP could vary over the TAminePyP$_{cov}$-(PAA-EG) material. This can be a potential reason of not killing all of bacteria. During this project, it was noticed that thinner pieces of photosensitiser functionalised nanofibre needed longer illumination time for complete inactivation of bacteria, whereas thick nanofibre or bigger pieces of nanofibre mats could inactivate cells completely in shorter times than expected. Further investigation might be carried out to optimise the time of illumination and thickness or size of nanofibre mats. Since the primary aim was to investigate of photo killing of bacteria by photosensitiser functionalised electrospun nanofibre mats, it was beyond the scope to optimise all other variable affecting the PDI of bacteria.

5.8 Conclusions

Data presented in this chapter have shown that commercially available tetra cationic photosensitiser TMPyP adsorbed onto nanofibre mat were able to inactivate Gram-negative bacteria. With the increasing light intensity it was possible to reduce the duration of illumination. As of lack of suitable reactive group in TMPyP it was not possible to covalently immobilise onto nanofibre mat although preliminary findings showed inactivation of bacteria by photosensitiser adsorbed onto the nanofibre mats. Thus, suitable reactive group ($–NH_2$ and allyl) containing photosensitisers TAllylPyP and TAminePyP were synthesised successfully immobilised onto PAA-EG nanofibre mat. TAllylPyP was immobilised onto PAA-EG nanofibre mat using both adsorption and covalent bonding. For covalent bonding of TAllylPyP with PAA-EG), palladium catalysed allylic acyloxylation of the terminal alkene conducted with nanofibre was conducted in the presence of base. Both of these photosensitiser functionalised nanofibre mats caused almost complete inactivation of Gram-negative bacteria. Again covalent immobilisation of TAminePyP onto PAA-EG nanofibre mat was conducted using two-step coupling of –COOH and $–NH_2$ using EDC and sulfo-NHS. The TAminePyP$_{cov}$-(PAA-EG) nanofibre mat showed 95% success in killing the *E. coli*. This indicates that TAminePyP$_{cov}$-(PAA-EG) and TAllylPyP$_{cov}$-(PAA-EG) nanofibres mats could both be used as an energy efficient, simple, affordable, eco-friendly system for water sterilisation. The nanofibres mats used in this project were developed to be water resistant so that no polymer leaches into water. Covalent immobilisation of photosensitisers confirmed on enduring attachment to the nanofibre mats that would ensure disinfectants free water sterilisation. The fact that TAminePyP$_{cov}$-(PAA-EG) and TAllylPyP$_{cov}$-(PAA-EG) were able to kill two strains of *E. coli*, one antibiotic resistant at low intensity of 30 mW/cm^2 is an indication that a sunlight driven water sterilisation system would be viable.

Chapter 6

General Discussion

6.1 Introduction

Photodynamic inactivation by using immobilised photosensitisers for water disinfection was first proposed in 1994 (Bonnett *et al.*, 1994). It would be particularly applicable in developing tropical countries, where contaminated surface water is a common problem and there is intense sunlight. After almost two decades there has been no significant progress in this field. Some common issues have been slow progress in developing immobilised photosensitisers. High energy consumption in the water treatment sector has motivated research to develop affordable and low energy water sterilisation techniques which minimise use of hazardous chemicals and promote eco-friendly solutions. These issues motivated the work in this thesis to develop a low energy consuming water sterilisation system where sunlight could be the source for photo-sterilisation using photosensitisers attached to electrospun nanofibre mats. Covalent attachment of the photosensitiser to the nanofibres prevents release of photosensitisers into treated water. Moreover, use of low cost electrospinning technology and use of energy from sunlight would make the system affordable globally.

6.2 Specific outcomes : covalent immobilisation of tetra cationic photosensitisers with ENF

The concept of using photosensitisers immobilised onto a solid phase surface such as a fabric or nanofibre mat for water sterilisation is intended to address a range of economic, ecological and public health issues. So far a number of studies have been carried out with photosensitising molecules that have been immobilised onto solid supports for different PDI applications. Different supports such as cotton, nanoparticles and even PS adsobtion with nanofibres etc. have been used (Spagnul *et al.*, 2015; El-Khordagui *et al.*, 2017; Faust *et al.*, 1999; Henke *et al.*, 2013), as well as a range of target

microorganisms and the effectiveness of particular combinations of support and photosensitiser has been studied with TMPyP which is a well-researched photosensitiser (Spagnul *et al*., 2015). Initially, in this thesis PPIX was chosen as a readily available, cheap and non-toxic photosensitiser that is often used medically. However, due to the membrane structure of Gram-negative bacteria and their anionic character (Kömerik and Wilson, 2002) negatively charged PPIX was unsuccessful in inactivating *E. coli*. Different strategy such as , adding propyl amine with PPIX as a pendant functional groups to increase the overall positive charge in PPIX was also studied to make PPIX effective against Gram-negative bacteria, though that were not successful. As a well-studied photosensitiser in PDI (Almeida *et al.*, 2014; Henke *et al.*, 2014; Henke *et al.*, 2013), TMPyP was chosen for PDI in this research. But due to the absence of a suitable reactive group in TMPyP for covalent immobilisation onto the nanofibres, initially TMPyP was immobilised by adsorption. They reported about the evidence of PDI but that leaves risk of TMPyP leaching in presence of any larger ion. This present work also present the evidence of killing bacteria with PS adsorbed nanofibres. TMPyP immobilised using adsorption onto PAA-PVA and PAA-EG nanofibre mats successfully caused complete inactivation of *E. coli* NCTC 10418 as well as a carbenicillin resistant *E. coli*. At the same time it was also confirmed that adsorbed PS is unstable in presence of basic solution But covalently modified PS functionalised nanofibre didn't show any leaching of PS (Section 4.5). In parallel work in the Millner Group, TMPyP was also used to functionalise chitosan membrane for PDI of viruses and proved highly effective for this purpose and for inactivation of *E. coli* strain BL21 (DE3) (Majiya *et al*., 2017). However, only a 3 log reduction of bacterial number was possible after 90 min light treatment with TMPyP adsorbed onto chitosan membrane in that study (Majiya *et al*., 2017), whilst the work within this thesis shows that $TMPyP_{ads}$-(PAA-PVA) electrospun nanofibre caused complete inactivation of carbenicillin resistant BL21 (DE3) under the same conditions (Section 5.3). The small diameter of the nanofibres are advantageous for efficient diffusion of $^1O_2$ outside the nanofibres to kill *E. coli* compared to TMPyP adsorbed onto chitosan membranes (Mosinger *et al*., 2007; Henke *et al*., 2014; Managa *et al*., 2014).

TMPyP adsorbed onto a range of solid supports has been used for antibacterial applications. A study on antibacterial activity of TMPyP adsorbed onto polystyrene nanofibres reported an antibacterial response on agar plates but the efficiency and extent of antibacterial ability was not mentioned (Henke *et al.*, 2013).

Our aim of developing a disinfectant free water sterilisation system indicated the need for synthesis of new cationic photosensitisers with suitable reactive groups for covalent immobilisation. In my work, two tetra cationic photosensitisers were synthesised; tetra allyl pyridyl porphyrin (TAllylPyP) and tetra amine pyridyl porphyrin (TAminePyP) were successfully immobilised covalently onto PAA-EG nanofibre mats (Section 2.9.6 and Section 2.9.7 respectively). Among them TAminePyP was newly synthesised (Section 2.5.2). Those nanofibres are referred to as TAllylpyP_{cov}-PAA-EG and TAminePyP_{cov}-PAA-EG. Both of these nanofibre composites were able to successfully inactivate *E.coli* NCTC 10418. TAllylpyP_{cov}-PAA-EG was able to cause complete inactivation (Section 5.6), whereas TAminePyPcov-PAA-EG only caused 90% inactivation of the *E. coli* (Section 5.7).

Gyulkhandanyan *et al*. (2009) reported on PDI of Gram-positive and Gram-negative bacteria by TAllylPyP solution and Mn-TAllylPyP solution. However, there is no report on TAllylPy adsorbed functionalised solid phase material. On the other hand, synthesis and antibacterial property of TAminePyP is reported for the first time in this thesis. The sterilisation of the water by TAminePyP immobilised PAA-EG nanofibres mat is also a novel work and reported for the first time (Section 2.9.7). Thus, successful immobilisation of TAllylPyP and TAminePyP photosensitisers into polyacrylic acid nanofibres and the evidence of stability of TAllylPyP and TAminePyP in presence of larger ions are distinctive from previously reported work. This implies that water sterilisation is possible without using free-floating photosensitisers. This technology only need a low intensity of light to photo treat the bacteria, so that it will eventually create a great impact in the sector of water treatment to reduce energy consumption. This is the first time photosensitiser functionalised electrospun nanofibre was modified covalently and was

confirmed the photosensitiser stability in large ionic presence. It was also successfully demonstrated the PDI of *E.coli* by these developed nanofibres using low intensity light.

6.2.1 Porphyrin conjugation with polymer for water sterilisation

There are several reports of PS immobilisation with polymer supports. Gao group reported on Porphyrins immobilisation on polymeric cellulose diacetate films (Gao *et al.*, 2012) or incorporated into translucent reinforced nylon chitosan membranes by adsorption process using 5,10,15,20-tetra(4-hydroxyphenyl)porphyrin, (p-THPP) or by dissolution and casting with 5,10,15,20-tetra(4-aminophenyl)porphyrin,(p-TAPP) and used in a circulating water photoreactor system as a model for a large-scale water-flow system system (Ribeiro *et al.*, 2010). When tested on *E. coli*, both p-THPP/chitosan and p-TAPP/chitosan membranes displayed a photo-killing ability after 40 mins of white light irradiation. These reported the efficiency of photokilling of bacteria, but no evidence of stability of photosensitisers in presence of larger ions of waste water was documented.

Another study of 5-(2,3,4,5,6-pentafluorophenyl)-10,15,20-triipyridylporphyrin and the corresponding cationic 5,10,15-tri(4-N-methylpyridyl)-20-(2,3,4,5,6-pentafluorophenyl)porphyrins as tri-iodide salt were grafted to cationised silica-coated magnetic nanoparticles of Fe_3O_4 in PACT against the Gram-negative bacteria (Alves et al., 2014).

Xing group reported anionic polythiophene with tetracationic 5,10,15,20-tetra[4-(6-N,N,N-trimethylammoniumhexyloxy)phenyl] porphyrin bromide (TPPN). This electrostatic complex adsorption technique was used to conjugate PS to kill Gram-negative and Gram-positive bacteria. In this case, the photo killing ability of the system was tested against *E. coli* observed after only 5 min of irradiation with white light at a fluence rate of 90 mW/cm^2 (Xing *et al.*, 2009a). All these conjugation were carried out by adsorption, grafting, doping or dissolution technique with polymer. This is where this present research is advantageous over previously reported research work.

Because of the water sterilisation free floating or leaching of PS is not acceptable, adsorption or electrostatic attraction, grafting, doping leave the risk of leaching of PS into water. Only covalent bonding can overcome this problem. In this research, it was also demonstrated that covalent bonding was successful enough to prevent the leaching PS in 3N sodium hydroxide solution.

Ribeiro *et al.* (2010) reported on covalently linked of porphyrins to aminoalkylated silica particles by initial activation of the porphyrin nucleus using chlorosulphonation. But nanoparticles would be difficult to remove after water treatment in their study, whereas it would be very easy to remove nanofabric mats from water after sterilisation to get chemical free water.

6.3 Nanofibre electrospinning

For immobilisation of photosensitiser, the solid support is a crucial component. The solid phase needs to be robust and cost effective for industrial production. Polymer nanofibres are an important class of nanomaterials because of their high surface-to-volume ratio (Feng *et al*., 2013). In particular electrospun nanofibres mats have high porosity and the diameter of fibres is alterable. For water sterilisation, water resistance of nanofibres is a necessary characteristic and to confer this feature both pre- and post- crosslinking were used. Water resistance was confirmed by mass spectrometry analysis of nanofibre washing. Research on using electrospun nanofibre material for water treatment is not new. There are some reports of desalination (Zhang *et al*., 2010), heavy metal-contaminated groundwater treatment (Sang *et al*., 2008) and pre-coagulation filtration of sewage (Xu *et al*., 2008). All these reports are based on the adsorption characteristics or filtration capability of electrospun nanofibres. Work reported in this thesis is the first time, where electrospun nanofibres have used as a solid support for covalent immobilisation of photosensitisers to sterilise water.

In this research, a polyacrylic acid polymer was chosen because of the availability of carboxy groups which offer easy coupling to amine containing

compounds. The polyanionic characteristic of this material was also attractive for TMPyP immobilisation by adsorption.

In this research, new polymer-solvent compositions were developed for PAA-PVA and PAA-EG nanofibre production in an industrial prototype needleless machine. There are a few previous reports on preparing polyacrylic acid nanofibres (Meng *et al.*, 2015; Shavini *et al.*, 2015; Tang *et al.*, 2010). All were reported of using laboratory scale needle-electrospinning (Santiago-Morales *et al.*, 2016; Xiao *et al.*, 2018). However, using this needle technology large scale production is not possible. So, needleless NS LAB 200 Nanospider Electrospinner was used for nanofibre mat production in this study.

6.4 Photosensitiser synthesis

Initially, synthesis of photosensitisers was not the part of the objectives of this research. The lack of commercially available cationic photosensitisers with pendant reactive groups introduced a new objective; synthesis of reactive cationic photosensitisers (Section 2.5.1). Overall, synthesis of 4 different photosensitisers was attempted to add allyl, $–NH_2$, -OH and propene functionalised. However, it was only possible to purify and characterise two of them (allyl,$–NH_2$) (Section 4.7). They are tetra allyl pyridyl porphyrin (TAllylPyP) and tetra amine pyridyl porphyrin (TAminePyP). The yield of other two (-OH and propene) were so poor that purification were not possible and so -OH and propene functionalised porphyrin synthesis was abandoned. Because of cationic and amphiphilic character (-OH and propene porphyrin) analogues, purification of these photosensitisers was challenging as they are susceptible to making dimer and larger complexes. Essentially, synthesis of TAllylPyP and TAminePyP was performed by alkylation of tetra pyridyl porphyrin, the products were then purified by solvent extraction and several washing steps. The new materials were then characterised by FTIR, NMR and mass analysis (Section 4.2.1 and 4.2.2).

6.5 Covalent immobilisation of photosensitisers onto electrospun nanofibres

The PAA-PVA and PAA-EG electrospun nanofibres are –COOH functionalised whereas the photosensitisers used are cationic, allowing electrostatic adsorption. Thus, during covalent immobilisation the adsorption step was rapid and preceded the coupling reaction and initially resulted in poor covalent immobilisation of photosensitiser. For effective covalent immobilisation, photosensitiser was added slowly at the last step and as a dilute solution. As adsorption capacity usually increases with the increase in initial concentration of the sorbate (Nsami and Mbadcam, 2013), slow and dilute addition of photosensitisers prevented the rapid adsorption that enabled successful covalent immobilisation of photosensitisers onto nanofibres mats.

6.6 Solar energy and water disinfection capacity by photosensitiser functionalised nanofibre mats

The light source used in the work was visible light (400 nm - 786 nm) and the light intensity used throughout the project was either 32 mW/cm^2 or 70 mW/cm^2. The lower intensity is equivalent to 3-7% of bright summer sunlight or tropical areas Sub sharan Africa. Such a low intensity was intentionally used so that the details of PDI effects could be studied. Otherwise high intensities would give an “all or none” killing effect. In some experiments a slightly higher intensity (70 mW/cm^2) was to demonstrate greater inactivation of bacteria in a shorter period of illumination (Section 3.7.1.1, Section 5.4 and Section 5.5). However in practice, solar radiation varies from place to place, according to the position of the sun, altitude and latitude. Solar light also has a wide spectrum including UV (<400nm) (Jemli *et al.*, 2002)., visible and near infra-red. The solar disinfection (SODIS) system for water is already used in remote or infrastructure-deficient areas but takes at least 6 h for complete sterilisation and needs water pre-filtration. In the research presented here we propose the use of ours PDI system under direct sun. At real world solar intensities, sterilisation should be completed in a short time, most likely seconds to minutes, and would be a viable system.

6.7 Unique contribution and scopes of future research

One of the unique contributions of this research was synthesis of tetracationic porphyrin analogues containing suitable functional groups for covalent bonding. Current commercially available tetracationic photosensitisers are still missing suitable functional groups. In this thesis, for the first time it has been successfully demonstrated that photosensitisers can be covalently immobilised onto electrospun nanofibre mats and these nanocomposites can cause complete inactivation of Gram-negative and Gram-positive bacteria. In parallel, another Millner group member has showed that TMPyP adsorbed on nanofibre mats can inactivate viruses (Majiya *et al*., 2017), including mammalian pathogens (mouse Norovirus and bovine Enterovirus). This research also demonstrated the use of low intensity visible white light to sterilise the water. This indicates the potential of sunlight driven water sterilisation system.

In this research, a prototype flow system was developed for water treatment, but due to time limitation it was beyond the scope of my work to use the final state of photosensitiser covalently immobilised nanofibre in a flow system based water purifier. However, this should clearly be a next step and will require mechanical engineering expertise to finalise the design a viable flow reactor that should be tested using both artificial, e.g. LED generated and solar light.

It is also worth to mention that in this work a photobleaching study of the developed nanofibre composites was not done, although photosensitiser functionalised mats could be reused several times without loss of activity. Photobleaching of nanofibre composites will need to be carried out over extended time periods and under a range of light intensities. Extensive toxicity test of developed nanofibres should also be performed. Biosensor based water contaminant detection technology is a prime area of research (Barhoum A. *et al.*, 2018; Ding *et al.*, 2010). Development of an integrated contaminant detection and water sterilisation system would also be desirable. This would allow the rapid detection and testing of water quality

before and after treatment of water. Where large infrastructures for water treatment plant are expensive e.g., for developing and under developed countries, the integrated nanofibre based water contaminant detection and sterilisation system could be a potential solution to their challenges to access clean water.

List of Abbreviations

A_{600}	Absorbance at 600nm
bis-Zn-DPA	Zinc-coordinated bis(dipicolylamine)
CFU	Colony Forming Unit
ClO_2	Chlorine dioxide
DCC	*N,N'*-Dicyclohexylcarbodiimide
DIC	N, N'-Diisopropylcarbodiimide
DMF	N, N-Dimethyl formamide
DMSO	Dimethyl Sulfoxide,
DPA	Dipicolylamine
E. coli	*Escherichia coli*
ECL	Enhanced chemiluminescence
EDC	1-ethyl-3-(3-dimethylaminopropyl) carbodiimide
ENF	Electro-spun Nanofibres
ENMs	Electro-spun nanofibrous membranes
EU	European Union
FTIR	Fourier transform infrared spectroscopy
G:BOX	Gel Imaging System (Syngene Ltd.; Cambridge, UK).
HOBt	Hydroxybenzotriazole
HOCl	Hypochloric acid
HOMO	Highest occupied molecular orbital
HRP	Horseradish peroxidase
Hz	Hertz
Jeffamine ED-2003	Polyetheramine
KV	Kilo Volt
LB	Luri bertani
LPS	Lipopolysaccharide
LUMO	Lowest unoccupied molecular orbital
MES	2-(*N*-morpholino) ethanesulfonic acid
mW	Milliwatt
NCTC	National Collection of Type Cultures
NH_3Cl	Chloramines
NHS biotin	*N*-Hydroxysuccinimide biotin
NHS	*N*-Hydroxysuccinimide
NOM	Natural organic material
$^1O_2$	Singlet oxygen

OD	Optical Density
PAN	Polyacrilonitrile
PAN-Jeff	Jeffamine doped polyacrilonitrile nanofibre
PBS	Phosphate buffer solution
PDI	Photodynamic inactivation
PDT	Photodynamic therapy
PEG	Polyethylene glycol
PEGn-amine	polyethylene glycol (PEG)-containing reagents with terminal primary amines
PPIX	Protoporphyrin IX
PPIX-PAN-Jeff	PPIX immobilised PAN-Jeff nanofibre
PS	Photosensitizer
ROS	Reactive oxygen species
S. epidermidis	*Staphylococcus epidermidis*
SEM	Scanning electronic microscopy
S-HRP	Horseradish peroxidase-streptavidin
sulfo-NHS	N-hydroxysulfo succinimide
TiO_2	Titanium dioxide
TMPyP	Tetra methyl pyridyl porphyrin
TAllylPyP	Tetra allyl pyridyl porphyrin
TAminelPyP	Tetra amine pyridyl porphyrin
$TAllylPyP_{ads}$-(PAA-PVA)	TAllylPyP adsorbed PAA-PVA nanofibre
$TAllylPyP_{ads}$-(PAA-EG)	TAllylPyP adsorbed PAA-EG nanofibre
$TMPyP_{ads}$-PAA-PVA)	TMPyP adsorbed PAA-PVA nanofibre
TAllylPyPcov-(PAA-EG)	TAllylPyP covalently immobilised PAA-EG nanofibre
TAminePyPcov-(PAA-EG)	TAminelPyP covalently immobilised PAA-EG nanofibre
UNICEF	United Nations International Children's Emergency Fund
UV/VIS	Ultraviolet–visible
VOCs	Volatile organic compounds
w/w	Mass fraction
WHO	World Health Organisation
XPS	X-ray photoelectron spectroscopy PEGylate

List of References

Abrahamse, H. and Hamblin, Michael R. 2016. New photosensitizers for photodynamic therapy. *Biochemical Journal.* **473**(4), pp.347-364.

Adams, M.R. and Moss, M.O. 2008. *Food microbiology.* 3rd ed. Royal society of chemistry Cambridge.

Almeida, A., Cunha, Â., Faustino, M.A.F., Tomé, A.C. and Neves, M.G.P.M.S. 2011. Porphyrins as antimibrobial photosensitizing agents. In Photodynamic Inactivation of Microbial Pathogens: Medical and Environmental Applications. *Royal Society of Chemistry: Cambridge, UK, 2011.* pp.83–160.

Almeida, J., Tomé, J.P.C., Neves, M.G.P.M.S., Tomé, A.C., Cavaleiro, J.A.S., Cunha, Â., Costa, L., Faustino, M.A.F. and Almeida, A. 2014. Photodynamic inactivation of multidrug-resistant bacteria in hospital wastewaters: influence of residual antibiotics. *Photochemical & Photobiological Sciences.* **13**(4), pp.626-633.

Alves, E., Rodrigues, J.M.M., Faustino, M.A.F., Neves, M.G.P.M.S., Cavaleiro, J.A.S., Lin, Z., Cunha, Â., Nadais, M.H., Tomé, J.P.C. and Almeida, A. 2014. A new insight on nanomagnet-porphyrin hybrids for photodynamic inactivation of microorganisms. *Dyes and Pigments.* **110**, pp.80-88.

Amat-Guerri, F., Pajares, A., Gianotti, J., Haggi, E., Stettler, G., Bertolotti, S., Miskoski, S. and García, N.A. 1999. Singlet molecular oxygen-mediated photooxidation of 2-substituted 3-hydroxypyridines. *Journal of Photochemistry and Photobiology A: Chemistry.* **126**(1–3), pp.59-64.

Amin, M., Hashemi, H., Mohammadi, A. and Tse Hung, Y. 2013. *A review on wastewater disinfection.*

Arndt, K.-F., Richter, A., Ludwig, S., Zimmermann, J., Kressler, J., Kuckling, D. and Adler, H.-J. 1999. Poly(vinyl alcohol)/poly(acrylic acid) hydrogels: FT-IR spectroscopic characterization of crosslinking reaction and work at transition point. *Acta Polymerica.* **50**(11-12), pp.383-390.

Artarsky, S., Dimitrova, S., Bonnett, R. and Krysteva, M. 2006. Immobilization of zinc phthalocyanines in silicate matrices and investigation of their photobactericidal effect on E-coli. *TheScientificWorldJOURNAL.* **6**, pp.374-382.

Aussawasathien, D., Teerawattananon, C. and Vongachariya, A. 2008. Separation of micron to sub-micron particles from water: Electrospun nylon-6 nanofibrous membranes as pre-filters. *Journal of Membrane Science.* **315**(1–2), pp.11-19.

Avetta, P., Bella, F., Bianco Prevot, A., Laurenti, E., Montoneri, E., Arques, A. and Carlos, L. 2013. Waste Cleaning Waste: Photodegradation of Monochlorophenols in the Presence of Waste-Derived Photosensitizer. *ACS Sustainable Chemistry & Engineering.* **1**(12), pp.1545-1550.

Baker, K.H., Hegarty, J., Redmond, B., Reed, N.A. and Herson, D.S. 2002. Effect of Oxidizing Disinfectants (Chlorine, Monochloramine, and Ozone) on Helicobacter pylor. *Applied and Environmental Microbiology* **68** (2), pp.981–984.

Baldursson, S. and Karanis, P. 2011. Waterborne transmission of protozoan parasites: Review of worldwide outbreaks - An update 2004-2010. *Water Research.* **45**(20), pp.6603-6614.

Barhoum A., Bechelany M., Makhlouf A. and S., S. 2018. Nanofiber Electrodes for Biosensors.

Barreiro, E.V., Ramos, A.J., López, F.F., Tato, J.V. and Seijas, J. 2015. Study of the crosslinking reaction between Bisphenol A diglycidyl ether (BADGE) and a Zinc Porphyrin by Fourier transform infrared spectroscopy. *The 19th International Electronic Conference on Synthetic Organic Chemistry.*

Barrett, S.E., Krasner, S.W. and Amy, G.L. 2000. *Natural Organic Matter and Disinfection By-Products.* American Chemical Society.

Bartolomeu, M., Reis, S., Fontes, M., Neves, M., Faustino, M. and Almeida, A. 2017. Photodynamic Action against Wastewater Microorganisms and Chemical Pollutants: An Effective Approach with Low Environmental Impact. *Water.* **9**(9), p630.

Belali, S., Karimi, A.R. and Hadizadeh, M. 2018. Cell-specific and pH-sensitive nanostructure hydrogel based on chitosan as a photosensitizer carrier for selective photodynamic therapy. *International Journal of Biological Macromolecules.* **110**, pp.437-448.

Benabbou, A.K., Guillard, C., Pigeot-Rémy, S., Cantau, C., Pigot, T., Lejeune, P., Derriche, Z. and Lacombe, S. 2011. Water disinfection using photosensitizers supported on silica. *Journal of Photochemistry and Photobiology A: Chemistry.* **219**(1), pp.101-108.

Benga, G. 1985. *Structure and Properties of Cell Membrane Structure and Properties of Cell Membranes.* 18 January 2018 ed.

Bernigaud, V., Drenck, K., Huber, B.A., Hvelplund, P., Jabot, T., Kadhane, U., Kirketerp, M.-B.S., Liu, B., Lykkegaard, M.K., Manil, B. and Nielsen, S.B. 2008. Electron-Capture–Induced Dissociation of Protoporphyrin IX Ions. *Journal of the American Society for Mass Spectrometry.* **19**(6), pp.809-813.

Bezman, S.A., Burtis, P.A., Izod, T.P.J. and Thayer, M.A. 1978. Photodynamic inactivation of E. Coli by rose bengal immobilized on polystyrene beads. *Photochemistry and Photobiology.* **28**(3), pp.325-329.

Bonnett, R., Buckley, D.G., Burrow, T., Galia, A.B.B., Saville, B. and Songca, S.P. 1993. Photobactericidal materials based on porphyrins and phthalocyanines. *J. Mater. Chem.* **3**, p323.

Bonnett, R., Buckley, D.G., Galia, A.B., Burrow, T. and Saville, B. 1994. PDT sensitisers: a new approach to clinical applications. *Biologic Effects of Light.* pp. 303-311.

Bonnett, R., Evans, R.L. and Galia, A.B.B. 1997. Immobilized photosensitizers: photosensitizer films with microbicidal effects. In, pp.79-88.

Bonnett, R., Krysteva, M.A., Lalov, I.G. and Artarsky, S.V. 2006. Water disinfection using photosensitizers immobilized on chitosan. *Water Research.* **40**(6), pp.1269-1275.

Cabiscol, E., Tamarit, J. and Ros, J. 2000. *Oxidative stress in bacteria and protein damage by reactive oxygen species.*

Cabral, J.P.S. 2010. Water Microbiology. Bacterial Pathogens and Water. *International Journal of Environmental Research and Public Health.* **7**(10), pp.3657-3703.

Castano, A.P., Demidova, T.N. and Hamblin, M.R. 2004. Mechanisms in photodynamic therapy: part one—photosensitizers, photochemistry and cellular localization. *Photodiagnosis and Photodynamic Therapy.* **1**(4), pp.279-293.

Corfield, W.H. 1897. Typhoid Epidemic at Maidstone. *Journal of the Sanitary Institute* **17**, p388.

Costa, D.C.S., Gomes, M.C., Faustino, M.A.F., Neves, M.G.P.M.S., Cunha, A., Cavaleiro, J.A.S., Almeida, A. and Tome, J.P.C. 2012. Comparative photodynamic inactivation of antibiotic resistant bacteria by first and second generation cationic photosensitizers. *Photochemical & Photobiological Sciences.* **11**(12), pp.1905-1913.

Dancil, K.-P.S., Hilario, L.F., Khoury, R.G., Mai, K.U., Nguyen, C.K., Weddle, K.S. and Shachter, A.M. 1997. Synthesis and aggregation of cationic porphyrins. *Journal of Heterocyclic Chemistry.* **34**(3), pp.749-755.

Dargel, R. 1992. Lipid peroxidation - a common pathogenetic mechanism? *Experimental and Toxicologic Pathology.* **44**(4), pp.169-181.

De Rosa, M.C. and Crutchley, R.J. 2002. Photosensitized singlet oxygen and its applications. *Coordination Chemistry Review.* **233**, pp. 351-371.

Ding, B., Wang, M., Wang, X., Yu, J. and Sun, G. 2010. Electrospun nanomaterials for ultrasensitive sensors. *Materials Today.* **13**(11), pp.16-27.

Dong, R., Bo, Y., Tong, G., Zhou, Y., Zhu, X. and Lu, Y. 2014. Self-assembly and optical properties of a porphyrin-based amphiphile. *Nanoscale.* **6**(9), pp.4544-4550.

Doyle, J., Choudhari, S., Ramakrishna, S., Seeram, B. and Ramesh, P. 2013. Electrospun Nanomaterials: Biotechnology, Food, Water, Environment, and Energy. In: *Conference Papers in Materials Science*. pp.1-14.

El-Khordagui, L., El-Sayed, N., Galal, S., El-Gowelli, H., Omar, H. and Mohamed, M. 2017. Photosensitizer-eluting nanofibers for enhanced photodynamic therapy of wounds: A preclinical study in immunocompromized rats. *International Journal of Pharmaceutics.* **520**(1), pp.139-148.

Escalada, J.P., Pajares, A., Gianotti, J., Biasutti, A., Criado, S., Molina, P., Massad, W., Amat-Guerri, F. and Garcia, N.A. 2011. Photosensitized degradation in water of the phenolic pesticides bromoxynil and dichlorophen in the presence of riboflavin, as a model of their natural photodecomposition in the environment. *Journal of Hazardous Materials.* **186**(1), pp.466-472.

Fagadar-Cosmaa, E., Enachea, C., Armeanua, I. and Fagadar-Cosmab, G. 2007. Comparative investigations of the absorption and fluorescence spectra of tetrapyridylporphyrine and zn (ii) tetrapyridylporphyrine. *Journal of Nanomaterials and Biostructures.* **2**(1), pp.175-183.

Fang, X., Xiao, S., Shen, M., Guo, R., Wang, S. and Shi, X. 2011. Fabrication and characterization of water-stable electrospun polyethyleneimine/polyvinyl alcohol nanofibers with super dye sorption capability. *New Journal of Chemistry.* **35**(2), pp.360-368.

Farhaoui, M. and Derraz, M. 2016. Review on Optimization of Drinking Water Treatment Process. *Journal of Water Resource and Protection.* **8, 777-786**.

Farr, S.B. and Kogoma, T. 1991. Oxidative stress responses in Escherichia coli and Salmonella typhimurium. *Microbiological reviews.* **55**(4), pp.561-585.

Farr, S.B., Touati, D. and Kogoma, T. 1988. Effects of oxygen stress on membrane functions in Escherichia coli: role of HPI catalase. *Journal of bacteriology.* **170**(4), pp.1837-1842.

Faust, D., Funken, K.H., Horneck, G., Milow, B., Ortner, J., Sattlegger, M., Schäfer, M. and Schmitz, C. 1999. IMMOBILIZED PHOTOSENSITIZERS FOR SOLAR PHOTOCHEMICAL APPLICATIONS. *Solar Energy.* **65**(1), pp.71-74.

Feng, C., Khulbe, K.C., Matsuura, T., Tabe, S. and Ismail, A.F. 2013. Preparation and characterization of electro-spun nanofiber membranes and their possible applications in water treatment. *Separation and Purification Technology.* **102**, pp.118-135.

Feng, C.Y. 2009. *Development of Novel Nanofiber Membranes for Seawater Desalination by Air-gap Membrane Distillation*. Ph.D. thesis, University of Ottawa.

Feuerstein, O., Ginsburg, I., Dayan, E., Veler, D. and Weiss, E.I. 2005. Mechanism of Visible Light Phototoxicity on Porphyromonas gingivalis and Fusobacterium nucleatum. *Photochemistry and Photobiology.* **81**(5), pp.1186-1189.

Feuerstein, O., Persman, N. and Weiss, E.I. 2004. Phototoxic Effect of Visible Light on Porphyromonas gingivalis and Fusobacterium nucleatum: An In Vitro Study. *Photochemistry and Photobiology.* **80**(3), pp.412-415.

Foote, C.S. and Peters, J.W. 1971. Chemistry of singlet oxygen. XIV. Reactive intermediate in sulfide photooxidation. *J. Am. Chem. Soc.* **93**(15), pp.3795-96.

Frederiksen, P.K., McIlroy, S.P., Nielsen, C.B., Nikolajsen, L., Skovsen, E., Jørgensen, M., Mikkelsen, K.V. and Ogilby, P.R. 2005. Two-Photon Photosensitized Production of Singlet Oxygen in Water. *Journal of the American Chemical Society.* **127**(1), pp.255-269.

Gad, F., Zahra, T., Francis, K.P., Hasan, T. and Hamblin, M.R. 2004. Targeted photodynamic therapy of established soft-tissue infections in mice. *Photochemical & Photobiological Sciences.* **3**(5), pp.451-458.

Gao, B., Chen, Y. and Lei, Q. 2012. Realizing porphyrin-functionalization of crosslinked polystyrene microspheres via two special polymer reactions. *Polymers for Advanced Technologies.* **23**(3), pp.491-499.

George, S., Hamblin, M.R. and Kishen, A. 2009. Uptake pathways of anionic and cationic photosensitizers into bacteria. *Photochemical & Photobiological Sciences.* **8**(6), pp.788-795.

Grabarek, Z. and Gergely, J. 1990. Zero-length crosslinking procedure with the use of active esters. *Analytical Biochemistry.* **185**(1), pp.131-135.

Greiner, A. and Wendorff, J.H. 2007. Electrospinning: a fascinating method for the preparation of ultrathin fibers. *Angew. Chem., Int. Ed.* **46**, p5670.

Gryglik, D., Miller, J.S. and Ledakowicz, S. 2007. Singlet molecular oxygen application for 2-chlorophenol removal. *Journal of Hazardous Materials.* **146**(3), pp.502-507.

Gyulkhandanyan, G.V., Paronyan, M.H., Hovsepyan, A.S., Ghazaryan, R.K., Tovmasyan, A.G., Gyulkhandanyan, A.G., Gyulkhandanyan, A.G. and Amelyan, G.V. 2009. Photodynamic inactivation of Gram (-) and Gram (+) microorganisms by cationic porphyrins and metalloporphyrins. In: *12th World Congress of the International Photodynamic Association*: SPIE, p.7.

Han, S.K., Sik, R.H., Motten, A.G., Chignell, C.F. and Bilski, P.J. 2009. Photosensitized oxidation of tetrabromobisphenol a by humic acid in aqueous solution. *Photochem. Photobiol.* **85**(6), p1299.

Henke, P., Kozak, H., Artemenko, A., Kubát, P., Forstová, J. and Mosinger, J. 2014. Superhydrophilic Polystyrene Nanofiber Materials Generating O2(1Δg): Postprocessing Surface Modifications toward Efficient Antibacterial Effect. *ACS Applied Materials & Interfaces.* **6**(15), pp.13007-13014.

Henke, P., Lang, K., Kubát, P., Sýkora, J., Šlouf, M. and Mosinger, J. 2013. Polystyrene Nanofiber Materials Modified with an Externally Bound Porphyrin Photosensitizer. *Acs Applied Materials & Interfaces.* **5**(9), pp.3776-3783.

Hermanson, G. 2013. Bioconjugate Techniques. *Book.* [Online]. 3rd ed. Academic Press.

Jackson, P.J., Andrews, K.O., Chambers, V.K., Connor, K.J., Egerton, A., Hall, T., Irving, T.E., Stanfield, G. and Fawell, J.K. 1999a. *Alternatives to chemical disinfection of drinking water.*

Jackson, Z., Meghji, S., MacRobert, A., Henderson, B. and Wilson, M. 1999b. Killing of the yeast and hyphal forms of Candida albicans using a light-activated antimicrobial agent. *Lasers in Medical Science.* **14**(2), pp.150-157.

Jemli, M., Alouini, Z., Sabbahi, S. and Gueddari, M. 2002. Destruction of fecal bacteria in wastewater by three photosensitizers. *Journal of Environmental Monitoring.* **4**(4), pp.511-516.

Jensen, A.W. and Daniels, C. 2003. Fullerene-Coated Beads as Reusable Catalysts. *J. Org. Chem.* **68**(2), p207.

Jin, X. and Hsieh, Y.-L. 2005. pH-responsive swelling behavior of poly(vinyl alcohol)/poly(acrylic acid) bi-component fibrous hydrogel membranes. *Polymer.* **46**(14), pp.5149-5160.

John, F. and Mark, J.N. 2003. Contaminants in drinking water. *British Medical Bulletin.* [Online]. **68**, pp.199-208.

Jori, G., Camerin, M., Soncin, M., Guidolin, L. and Coppellotti, O. 2011. Chapter 1 Antimicrobial Photodynamic Therapy: Basic Principles. *Photodynamic Inactivation of Microbial Pathogens: Medical and Environmental Applications.* The Royal Society of Chemistry, pp.1-18.

Jori, G., Fabris, C., Soncin, M., Ferro, S., Coppellotti, O., Dei, D., Fantetti, L., Chiti, G. and Roncucci, G. 2006. Photodynamic therapy in the treatment of microbial infections: Basic principles and perspective applications. *Lasers in Surgery and Medicine.* **38**(5), pp.468-481.

Kashket, E.R. 1985. The proton motive force in bacteria: a critical assessment of methods. *Annu. Rev. Microbiol.* **39:**, pp.219-242.

Khampieng, T., Wnek, G.E. and Supaphol, P. 2014. Electrospun DOXY-h loaded-poly(acrylic acid) nanofiber mats: in vitro drug release and antibacterial properties investigation. *Journal of Biomaterials Science, Polymer Edition.* **25**(12), pp.1292-1305.

Kim, H., Kim, W., Mackeyev, Y., Lee, G.-S., Kim, H.-J., Tachikawa, T., Hong, S., Lee, S., Kim, J., Wilson, L.J., Majima, T., Alvarez, P.J.J., Choi, W. and Lee, J. 2012. Selective Oxidative Degradation of Organic Pollutants by Singlet Oxygen-Mediated Photosensitization: Tin Porphyrin versus C60 Aminofullerene Systems. *Environmental Science & Technology.* **46**(17), pp.9606-9613.

Kohn, T., Grandbois, M., McNeill, K. and Nelson, K.L. 2007. Association with natural organic matter enhances the sunlight-mediated inactivation of MS2 coliphage by singlet oxygen. *Environmental Science & Technology.* **41**(13), pp.4626-4632.

Kohn, T. and Nelson, K.L. 2007. Sunlight-mediated inactivation of MS2 coliphage via exogenous singlet oxygen produced by sensitizers in natural waters. *Environmental Science & Technology.* **41**(1), pp.192-197.

Komagoe, K., Kato, H., Inoue, T. and Katsu, T. 2011. Continuous real-time monitoring of cationic porphyrin-induced photodynamic inactivation of bacterial membrane functions using electrochemical sensors. *Photochemical & Photobiological Sciences.* **10**(7), pp.1181-1188.

Kömerik, N. and Wilson, M. 2002. Factors influencing the susceptibility of Gram-negative bacteria to toluidine blue O-mediated lethal photosensitization. *Journal of Applied Microbiology.* **92**(4), pp.618-623.

Kong, L. and Ferry, J.L. 2004. Photochemical oxidation of chrysene at the silica gel-water interface. *Journal of Photochemistry and Photobiology a-Chemistry.* **162**(2-3), pp.415-421.

Kumar, U. 2006. Agricultural products and by-products as a low cost adsorbent for heavy metal removal from water and wastewater: A review *Scientific Research and Essay.* **1**(2), pp.33-37.

Kwon, B.M. and Foote, C.S. 1988. Chemistry of singlet oxygen. 50. Hydroperoxide intermediates in the photooxygenation of ascorbic acid. *Journal of the American Chemical Society.* **110**(19), pp.6582-6583.

Larsen, S.H., J. Adler, J. J. Gargus, and R. W. Hogg. 1. 1974. Chemomechanical coupling without ATP: the sourse of energy for motility and chemotaxis in bacteria. . *Proc. Natl. Acad. Sci.* **71**, pp.1239-1243.

Leive, L. 1974. THE BARRIER FUNCTION OF THE GRAM-NEGATIVE ENVELOPE. *Annals of the New York Academy of Sciences.* **235**(1), pp.109-129.

Lewis, C., Suffet, I.H. and Ritz, B. 2006. Estimated Effects of Disinfection By-products on Birth Weight in a Population Served by a Single Water Utility. *American Journal of Epidemiology.* **163**(1), pp.38-47.

Li, D., Swanson, B.I., Robinson, J.M. and Hoffbauer, M.A. 1993. Porphyrin based self-assembled monolayer thin films: synthesis and characterization. *Journal of the American Chemical Society.* **115**(15), pp.6975-6980.

Liu, F., Soh Yan Ni, A., Lim, Y., Mohanram, H., Bhattacharjya, S. and Xing, B. 2012. Lipopolysaccharide Neutralizing Peptide–Porphyrin Conjugates for Effective Photoinactivation and Intracellular Imaging of Gram-Negative Bacteria Strains. *Bioconjugate Chemistry.* **23**(8), pp.1639-1647.

Maisch, T., Baier, J., Franz, B., Maier, M., Landthaler, M., Szeimies, R.-M. and Bäumler, W. 2007. The role of singlet oxygen and oxygen concentration in photodynamic inactivation of bacteria. *Proceedings of the National Academy of Sciences.* **104**(17), pp.7223-7228.

Majiya, H., Chowdhury, K.F., Stonehouse, N.J. and Millner, P. 2017. TMPyP functionalised chitosan membrane for efficient sunlight driven water disinfection. *Journal of Water Process Engineering.*

Malatesti, N., Munitic, I. and Jurak, I. 2017. Porphyrin-based cationic amphiphilic photosensitisers as potential anticancer, antimicrobial and immunosuppressive agents. *Biophysical reviews.* **9**(2), pp.149-168.

Malato, S., Fernández-Ibáñez, P., Maldonado, M.I., Blanco, J. and Gernjak, W. 2009. Decontamination and disinfection of water by solar photocatalysis: Recent overview and trends. *Catalysis Today.* **147**(1), pp.1-59.

Malik, Z., Ladan, H. and Nitzan, Y. 1992. Photodynamic inactivation of Gram-negative bacteria: Problems and possible solutions. *Journal of Photochemistry and Photobiology B: Biology.* **14**(3), pp.262-266.

Managa, M., Antunes, E. and Nyokong, T. 2014. Conjugates of platinum nanoparticles with gallium tetra – (4-Carboxyphenyl) porphyrin and their use in photodynamic antimicrobial chemotherapy when in solution or embedded in electrospun fiber. *Polyhedron.* **76**, pp.94-101.

McCord, J.M., Keele, B.B., Jr. and Fridovich, I. 1971. An enzyme-based theory of obligate anaerobiosis: the physiological function of superoxide dismutase. *Proceedings of the National Academy of Sciences of the United States of America.* **68**(5), pp.1024-1027.

Meng, L., Klinkajon, W., K-hasuwan, P.-r., Harkin, S., Supaphol, P. and Wnek, G.E. 2015. Electrospun crosslinked poly(acrylic acid) fiber constructs: towards a synthetic model of the cortical layer of nerve. *Polymer International.* **64**(1), pp.42-48.

Mosinger, J., Jirsak, O., Kubat, P., Lang, K. and Mosinger, B. 2007. Bactericidal nanofabrics based on photoproduction of singlet oxygen. *Journal of Materials Chemistry.* **17**(2), pp.164-166.

Muruganandham, M., Suri, R.P.S., Jafari, S., Sillanpää, M., Lee, G.J., Wu, J.J. and Swaminathan, M. 2014. Recent developments in homogeneous advanced oxidation processes for water and wastewater treatment. *International Journal of Photoenergy.* **2014**.

Najm, I. and Trussel, R.R. 1999. New and Emerging Drinking Water Treatment Technologies in Identifying Future Drinking Water Contaminants. *National Academy Press, Washington, DC* pp. 220–243.

Nakonechny, F., Pinkus, A., Hai, S., Yehosha, O., Nitzan, Y. and Nisnevitch, M. 2013. Eradication of Gram-Positive and Gram-Negative Bacteria by Photosensitizers Immobilized in Polystyrene. *Photochemistry and Photobiology.* **89**(3), pp.671-678.

Nasreen, S., Sundarrajan, S., Nizar, S., Balamurugan, R. and Ramakrishna, S. 2013. Advancement in Electrospun Nanofibrous Membranes Modification and Their Application in Water Treatment. *Membranes.* **3**(4), pp.266-284.

Neumann, H. 1981. Bacteriological safety of hot tapwater in developing countries. *Public Health Rep.* **84**, pp.812-814.

Nikaido, H. 1994. Prevention of drug access to bacterial targets: permeability barriers and active efflux. *Science.* **264**(5157), p382.

Niki, E., Yoshida, Y., Saito, Y. and Noguchi, N. 2005. Lipid peroxidation: Mechanisms, inhibition, and biological effects. *Biochemical and Biophysical Research Communications.* **338**(1), pp.668-676.

Niu, H., Wang, X. and Lin, T. 2012. Upward Needleless Electrospinning of Nanofibers. *Journal of Engineered Fibers and Fabrics.* **7**, pp.17-22.

Nsami, N.J. and Mbadcam, K.J. 2013. The Adsorption Efficiency of Chemically Prepared Activated Carbon from Cola Nut Shells by on Methylene Blue. *Journal of Chemistry.* **2013**, p7.

Pooi, C.K. and Ng, H.Y. 2018. Review of low-cost point-of-use water treatment systems for developing communities. *npj Clean Water.* **1**(1), p11.

Raetz, C.R. and Whitfield, C. 2002. Lipopolysaccharide endotoxins. *Annu. Rev. Biochem.* **71**, pp.635-700.

Rashed, M.N. 2013. Adsorption Technique for the Removal of Organic Pollutants from Water and Wastewater. pp.167-194.

Razavi, B.B.A., S. Song, W. H. O'Shea, K. E. Cooper, W. J. 2011. Photochemical fate of atorvastatin (lipitor) in simulated natural waters. *Wat. Res.* **45**(2), pp.625-631.

Reneker, D.H. and Chun, I. 1996. Nanometre diameter fibres of polymer, produced by electrospinning. *Nanotechnology.* **7**(3), pp.216-223.

Ribeiro, S.M., Serra, A.C. and Rocha Gonsalves, A.M.d. 2010. Covalently immobilized porphyrins on silica modified structures as photooxidation catalysts. *Journal of Molecular Catalysis A: Chemical.* **326**(1-2), pp.121-127.

Romero, O.C., Straub, A.P., Kohn, T. and Nguyen, T.H. 2011. Role of temperature and Suwannee River natural organic matter on inactivation kinetics of rotavirus and bacteriophage MS2 by solar irradiation. *Environ. Sci. Technol.* **45**(24), pp.10385-10393.

Rushworth, J.V., Ahmed, A. and Millner, P.A. 2013. Midland Blotting: A Rapid, Semi-Quantitative Method for Biosensor Surface Characterization. *J Biosens Bioelectron.* **4**(5).

Sang, Y., Li, F., Gu, Q., Liang, C. and Chen, J. 2008. Heavy metal-contaminated groundwater treatment by a novel nanofiber membrane. *Desalination.* **223**(1-3), pp.349-360.

Santiago-Morales, J., Amariei, G., Letón, P. and Rosal, R. 2016. Antimicrobial activity of poly(vinyl alcohol)-poly(acrylic acid) electrospun nanofibers. *Colloids and Surfaces B: Biointerfaces.* **146**, pp.144-151.

Shannon, M.A., Bohn, P.W., Elimelech, M., Georgiadis, J.G., Marinas, B.J. and Mayes, A.M. 2008. Science and technology for water purification in the coming decades. *Nature.* **452**(7185), pp.301-310.

Shavini, W., Krishna, B., Ruth, M. and Wamadeva, B. 2015. Insoluble electrospun membranes for analyte pre-concentration in saliva. *ESA Annual Meeting on Electrostatics 2015*

Skovsen, E., Snyder, J.W., Lambert, J.D.C. and Ogilby, P.R. 2005. Lifetime and Diffusion of Singlet Oxygen in a Cell. *The Journal of Physical Chemistry B.* **109**(18), pp.8570-8573.

Slota, R., Broda, M.A., Dyrda, G., Ejsmont, K. and Mele, G. 2011. Structural and Molecular Characterization of meso-Substituted Zinc Porphyrins: A DFT Supported Study. *Molecules.* **16**(12), pp.9957-9971.

Somani, S.B. and Ingole, N.W. 2011. Alternative approach to chlorination for disinfection of drinking water- an overview. *International Journal of Advanced Engineering Research and Studies.* [Online]. pp.47-50. [Accessed October-December, 2011].

Spagnul, C., Greenman, J., Wainwright, M., Kamil, Z. and Boyle, R.W. 2016. Synthesis, characterization and biological evaluation of a new photoactive hydrogel against Gram-positive and Gram-negative bacteria. *Journal of Materials Chemistry B.* **4**(8), pp.1499-1509.

Spagnul, C., Turner, L.C. and Boyle, R.W. 2015. Immobilized photosensitizers for antimicrobial applications. *Journal of Photochemistry and Photobiology B: Biology.* **150**, pp.11-30.

Srivastava, Y., Marquez, M. and Thorsen, T. 2007. Multijet electrospinning of conducting nanofibers from microfluidic manifolds. *Journal of Applied Polymer Science.* **106**(5), pp.3171-3178.

Strassert, C.A., Otter, M., Albuquerque, R.Q., Hoene, A., Vida, Y., Maier, B. and De Cola, L. 2009. Photoactive Hybrid Nanomaterial for Targeting, Labeling, and Killing Antibiotic-Resistant Bacteria. *Angewandte Chemie-International Edition.* **48**(42), pp.7928-7931.

Surdel, M.C., Horvath, D.J., Lojek, L.J., Fullen, A.R., Simpson, J., Dutter, B.F., Salleng, K.J., Ford, J.B., Jenkins, J.L., Nagarajan, R., Teixeira, P.L., Albertolle, M., Georgiev, I.S., Jansen, E.D., Sulikowski, G.A., Lacy, D.B., Dailey, H.A. and Skaar, E.P. 2017. Antibacterial photosensitization through activation of coproporphyrinogen oxidase. *Proceedings of the National Academy of Sciences.* **114**(32), pE6652.

Sutton, S. 2011. Accuracy of plate counts. *Journal of validation technology.* **17**(3), pp.42-46.

Tang, C., Saquing, C.D., Harding, J.R. and Khan, S.A. 2010. In Situ Cross-Linking of Electrospun Poly(vinyl alcohol) Nanofibers. *Macromolecules.* **43**(2), pp.630-637.

Thiery, E., Aouf, C., Belloy, J., Harakat, D., Le Bras, J. and Muzart, J. 2010. Palladium-Catalyzed Allylic Acyloxylation of Terminal Alkenes in the Presence of a Base. *The Journal of Organic Chemistry.* **75**(5), pp.1771-1774.

Thomas, P.S., Guerbois, J.-P., Russell, G.F. and Briscoe, B.J. 2001. FTIR Study of the Thermal Degradation of Poly(vinyl Alcohol). *Journal of Thermal Analysis and Calorimetry.* **64**(2), pp.501-508.

Triantaphylidès, C., Krischke, M., Hoeberichts, F.A., Ksas, B., Gresser, G., Havaux, M., Van Breusegem, F. and Mueller, M.J. 2008. Singlet Oxygen Is the Major Reactive Oxygen Species Involved in Photooxidative Damage to Plants. *Plant Physiology.* **148**(2), pp.960-968.

Turneaure, F.E. and Russell, H.L. 1916. Public Water-Supplies: Requirements, Resources, and the Construction of Works 1st ed. New York, J. Wiley and Sons, Inc. London, p.493.

Vatansever, F., de Melo, W.C.M.A., Avci, P., Vecchio, D., Sadasivam, M., Gupta, A., Chandran, R., Karimi, M., Parizotto, N.A., Yin, R., Tegos, G.P. and Hamblin, M.R. 2013. Antimicrobial strategies centered around reactive oxygen species – bactericidal antibiotics, photodynamic therapy, and beyond. *FEMS Microbiology Reviews.* **37**(6), pp.955-989.

Villanueva, C.M., Cantor, K.P., Cordier, S., Jaakkola, J.J.K., King, W.D., Lynch, C.F., Porru, S. and Kogevinas, M. 2004. Disinfection Byproducts and Bladder Cancer: A Pooled Analysis. *Epidemiology.* **15**(3), pp.357-367.

Villanueva, C.M., Cordier, S., Font-Ribera, L., Salas, L.A. and Levallois, P. 2015. Overview of Disinfection By-products and Associated Health Effects. *Current Environmental Health Reports.* **2**(1), pp.107-115.

Villén, L., Manjón, F., García-Fresnadillo, D. and Orellana, G. 2006. Solar water disinfection by photocatalytic singlet oxygen production in heterogeneous medium. *Applied Catalysis B: Environmental.* **69**(1-2), pp.1-9.

Weinberg, H.S. 2009. Modern approaches to the analysis of disinfection by-products in drinking water. **367**(1904), pp.4097-118.

WHO and UNICEF. 2017. Progress on Drinking Water, Sanitation and Hygiene: 2017 Update and SDG Baselines. Geneva.

WHO and UNISEF. 2008. *Safer water, better health: costs, benefits and sustainability of interventions to protect and promote health.* World Health Organization, Geneva.

Wright, J.M., Schwartz, J. and Dockery, D.W. 2003. Effect of trihalomethane exposure on fetal development. *Occupational and Environmental Medicine.* **60**(3), pp.173-180.

Xiao, M., Chery, J. and Frey, M.W. 2018. Functionalization of Electrospun Poly(vinyl alcohol) (PVA) Nanofiber Membranes for Selective Chemical Capture. *ACS Applied Nano Materials.* **1**(2), pp.722-729.

Xing, C., Xu, Q., Tang, H., Liu, L. and Wang, S. 2009a. Conjugated Polymer/Porphyrin Complexes for Efficient Energy Transfer and Improving Light-Activated Antibacterial Activity. *Journal of the American Chemical Society.* **131**(36), pp.13117-13124.

Xing, C.F., Xu, Q.L., Tang, H.W., Liu, L.B. and Wang, S. 2009b. Conjugated Polymer/Porphyrin Complexes for Efficient Energy Transfer and Improving Light-Activated Antibacterial Activity. *Journal of the American Chemical Society.* **131**, p13117.

Xu, Z., Gu, Q., Hu, H. and Li, F. 2008. A novel electrospun polysulfone fiber membrane: Application to advanced treatment of secondary bio-treatment sewage. *Environmental Technology.* **29**(1), pp.13-21.

Zhang, J., Dow, N., Duke, M., Ostarcevic, E., Li, J.D. and Gray, S. 2010. Identification of material and physical features of membrane distillation membranes for high performance desalination. *Journal of Membrane Science.* **349**(1-2), pp.295-303.

Zhu, C., Yang, Q., Liu, L., Lv, F., Li, S., Yang, G. and Wang, S. 2011. Multifunctional Cationic Poly(p-phenylene vinylene) Polyelectrolytes for Selective Recognition, Imaging, and Killing of Bacteria Over Mammalian Cells. *Advanced materials.* **23**, p4805.

Zhu, J. and Sun, G. 2012. Preparation and photo-oxidative functions of poly(ethylene-co-methacrylic acid) (PE-co-MAA) nanofibrous membrane supported porphyrins. *Journal of Materials Chemistry.* **22**(21), pp.10581-10588.

Appendix A. Proton NMR of TAllylPyP

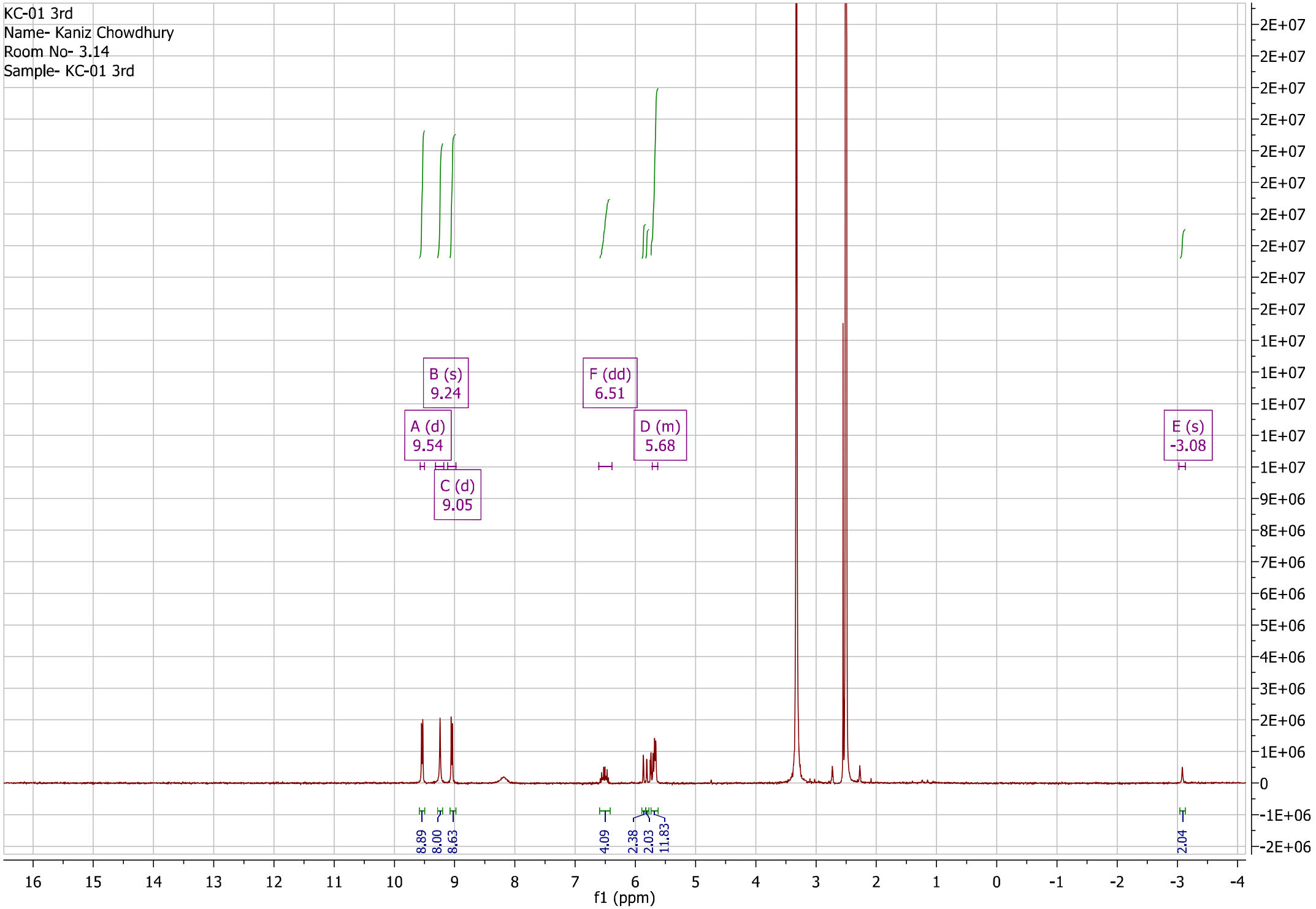
KC-01 3rd
Name- Kaniz Chowdhury
Room No- 3.14
Sample- KC-01 3rd
B (s)
9.24
A (d)
9.54
C (d)
9.05
F (dd)
6.51
D (m)
5.68
E (s)
-3.08
8.89
8.00
8.63
4.09
2.38
2.03
11.83
2.04
f1 (ppm)

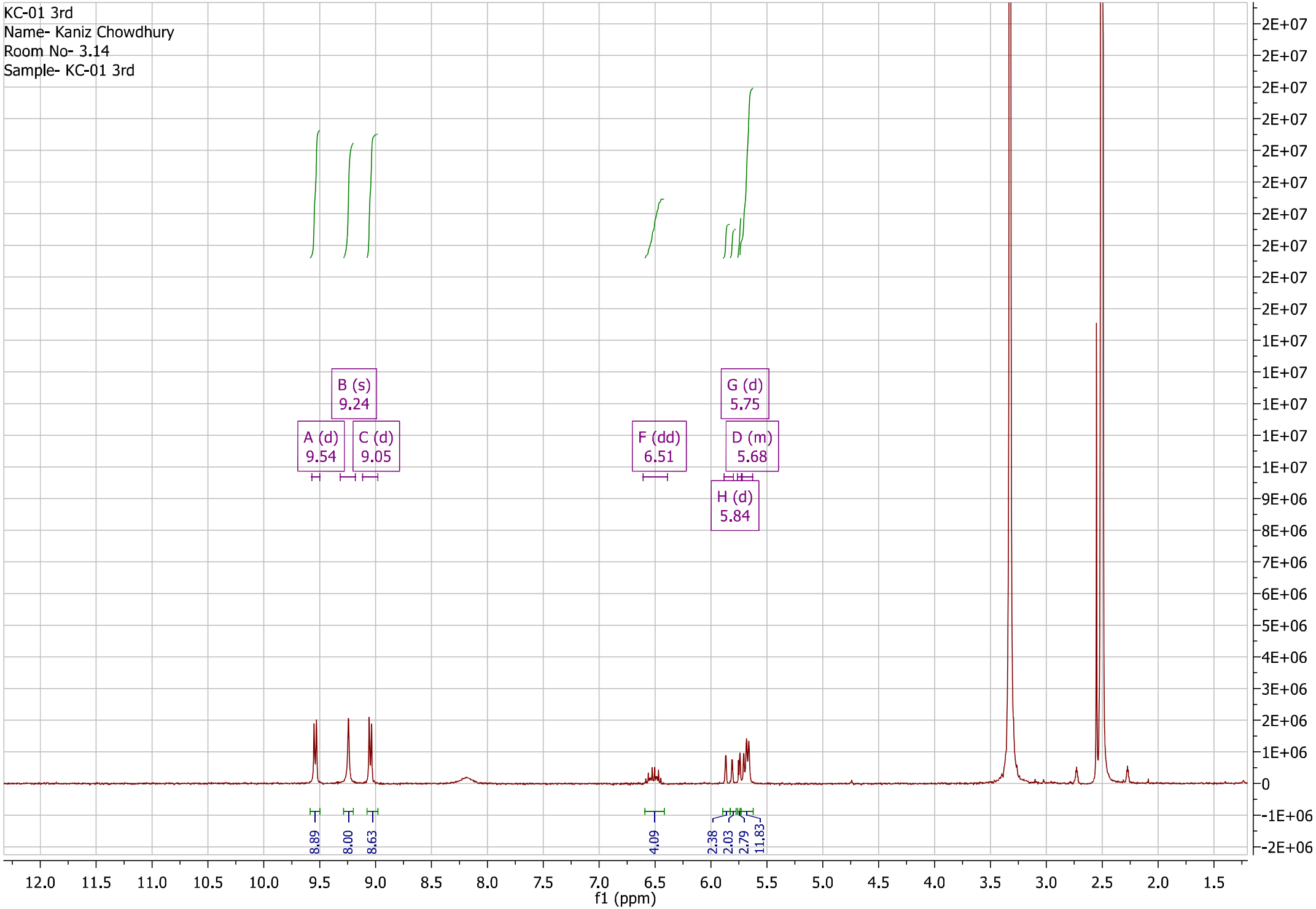
KC-01 3rd
Name- Kaniz Chowdhury
Room No- 3.14
Sample- KC-01 3rd
B (s)
9.24
A (d)
9.54
C (d)
9.05
F (dd)
6.51
G (d)
5.75
D (m)
5.68
H (d)
5.84
8.89
8.00
8.63
4.09
2.38
2.03
2.79
11.83
f1 (ppm)

Appendix B. Mass Spectra of TAllylPyP

School of Chemistry Mass Spectrometry Service

SampleID	KC01_MeOH 2nd 27th mar			**Submitter**	Kaniz Chowdhury
Sample Description					
Analysis Name	KC01_MeOH 2nd 27th mar_232996_GD1_01_44257.d			**Supervisor**	Robin Bon
Method	3a_AccMass_Loop_Positive.m			**Acquisition Date**	27/03/2018 18:21:44
Instrument	maXis impact	**Source Type**	ESI	**Ion Polarity**	Positive
Scan Begin	50 m/z	**Scan End**	1500 m/z		

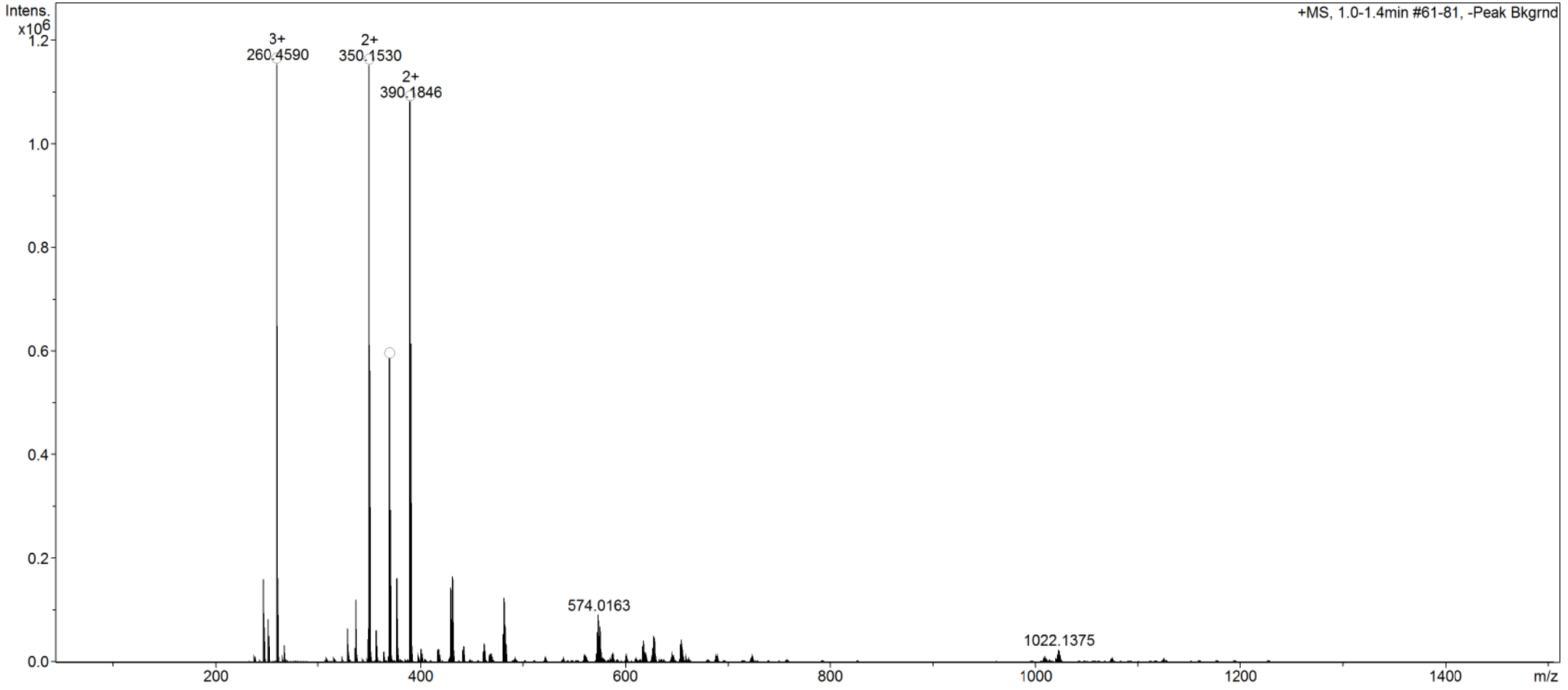

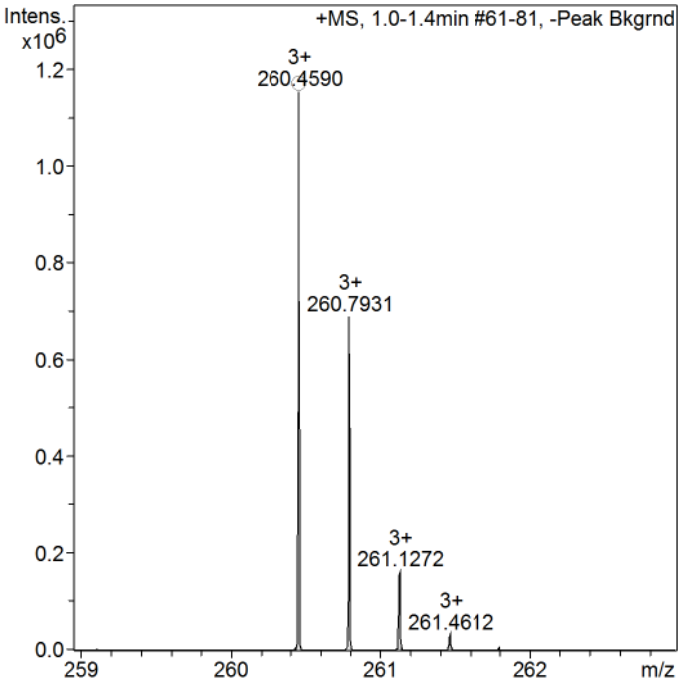

Smart Formula Parameter	Value
Expected Formula	
Adducts Considered	
Smart Formula Search Parameters	
CHNO and adducts considered implicitly	
Formula Search Minimum	
Formula Search Maximum	
Algorithm Parameters	
Tolerance	4 ppm
Match to Isotope Pattern(mSigma)	40
Electron Configuration	even
Estimate No of Carbons	yes
Filter by H/C Ratio	0< H/C < 3
Number of Double Bonds & Rings	0< rings&DB < 80

Confirm/Find Formula Results

The section below shows the results of formula calculation. If an expected formula was provided and found these are the results that are listed. If no formula was provided or no matches were found the system has attempted to determine the formula constrained by the parameters listed to the left

Meas. m/z	Ion Formula	z	m/z	err [mDa]	err [ppm]	mSigma	Score	Sum Formula	Adduct
260.459023	C52H45N8	3+	260.458358	-0.7	-2.6	17.5	100.00	C52H42N8	M+H
	C56H49N2O2	3+	260.459253	0.2	0.9	29.2	94.72	C56H46N2O2	M+H
	C52H45N8	3+	260.458358	-0.7	-2.6	17.5	100.00	C52H33N5	M+NH4
	C52H45N8	3+	260.458358	-0.7	-2.6	17.5	100.00	C26H21N4	2M+H
	C56H49N2O2	3+	260.459253	0.2	0.9	29.2	94.72	C28H23NO	2M+H
350.153010	C45H40N4O4	2+	350.151929	-1.1	-3.1	17.8	86.18	C45H38N4O4	M+H
	C46H36N8	2+	350.152598	-0.4	-1.2	27.0	100.00	C46H34N8	M+H
	C35H36N14O3	2+	350.154192	1.2	3.4	27.2	65.90	C35H34N14O3	M+H
	C34H40N10O7	2+	350.153523	0.5	1.5	38.9	70.50	C34H38N10O7	M+H
	C37H48O13	2+	350.154197	1.2	3.4	39.3	48.40	C37H46O13	M+H
	C31H32N20O	2+	350.152849	-0.2	-0.5	39.6	81.20	C31H30N20O	M+H
	C45H40N4O4	2+	350.151929	-1.1	-3.1	17.8	86.18	C45H32N2O4	M+NH4
	C46H36N8	2+	350.152598	-0.4	-1.2	27.0	100.00	C46H28N6	M+NH4
	C35H36N14O3	2+	350.154192	1.2	3.4	27.2	65.90	C35H28N12O3	M+NH4
	C34H40N10O7	2+	350.153523	0.5	1.5	38.9	70.50	C34H32N8O7	M+NH4
	C31H32N20O	2+	350.152849	-0.2	-0.5	39.6	81.20	C31H24N18O	M+NH4
	C40H48Na4O5	2+	350.154077	1.1	3.0	24.5	89.29	C40H48Na2O5	M+Na
	C36H44N6Na4O3	2+	350.152735	-0.3	-0.8	36.5	100.00	C36H44N6Na2O3	M+Na
	C46H36N8	2+	350.152598	-0.4	-1.2	27.0	100.00	C23H17N4	2M+H
370.168642	C38H40N14O3	2+	370.169842	1.2	3.2	18.2	78.92	C38H38N14O3	M+H
	C48H44N4O4	2+	370.167579	-1.1	-2.9	23.2	76.88	C48H42N4O4	M+H
	C40H52O13	2+	370.169847	1.2	3.3	29.0	61.72	C40H50O13	M+H
	C37H44N10O7	2+	370.169173	0.5	1.4	29.6	87.95	C37H42N10O7	M+H
	C34H36N20O	2+	370.168499	-0.1	-0.4	31.6	100.00	C34H34N20O	M+H
	C49H40N8	2+	370.168248	-0.4	-1.1	34.5	83.11	C49H38N8	M+H
	C38H40N14O3	2+	370.169842	1.2	3.2	18.2	78.92	C38H32N12O3	M+NH4
	C48H44N4O4	2+	370.167579	-1.1	-2.9	23.2	76.88	C48H36N2O4	M+NH4
	C37H44N10O7	2+	370.169173	0.5	1.4	29.6	87.95	C37H36N8O7	M+NH4
	C34H36N20O	2+	370.168499	-0.1	-0.4	31.6	100.00	C34H28N18O	M+NH4
	C49H40N8	2+	370.168248	-0.4	-1.1	34.5	83.11	C49H32N6	M+NH4
	C43H52Na4O5	2+	370.169727	1.1	2.9	14.7	87.16	C43H52Na2O5	M+Na
	C39H48N6Na4O3	2+	370.168385	-0.3	-0.7	27.9	100.00	C39H48N6Na2O3	M+Na
	C38H52N2Na4O7	2+	370.167716	-0.9	-2.5	39.1	53.86	C38H52N2Na2O7	M+Na
	C48H44N4O4	2+	370.167579	-1.1	-2.9	23.2	76.88	C24H21N2O2	2M+H

Meas. m/z	Ion Formula	z	m/z	err [mDa]	err [ppm]	mSigma	Score	Sum Formula	Adduct
390.184559	C51H48N4O4	2+	390.183229	-1.3	-3.4	8.5	81.62	C51H46N4O4	M+H
	C52H44N8	2+	390.183898	-0.7	-1.7	17.6	100.00	C52H42N8	M+H
	C56H48N2O2	2+	390.185241	0.7	1.7	32.3	70.83	C56H46N2O2	M+H
	C41H44N14O3	2+	390.185492	0.9	2.4	36.3	55.93	C41H42N14O3	M+H
	C51H48N4O4	2+	390.183229	-1.3	-3.4	8.5	81.62	C51H40N2O4	M+NH4
	C52H44N8	2+	390.183898	-0.7	-1.7	17.6	100.00	C52H36N6	M+NH4
	C56H48N2O2	2+	390.185241	0.7	1.7	32.3	70.83	C56H40O2	M+NH4
	C41H44N14O3	2+	390.185492	0.9	2.4	36.3	55.93	C41H36N12O3	M+NH4
	C47H52N4Na4O	2+	390.186046	1.5	3.8	21.1	87.99	C47H52N4Na2O	M+Na
	C46H56Na4O5	2+	390.185377	0.8	2.1	32.7	100.00	C46H56Na2O5	M+Na
	C52H44N8	2+	390.183898	-0.7	-1.7	17.6	100.00	C26H21N4	2M+H
	C56H48N2O2	2+	390.185241	0.7	1.7	32.3	70.83	C28H23NO	2M+H

Appendix C. Proton NMR of TAminePyP

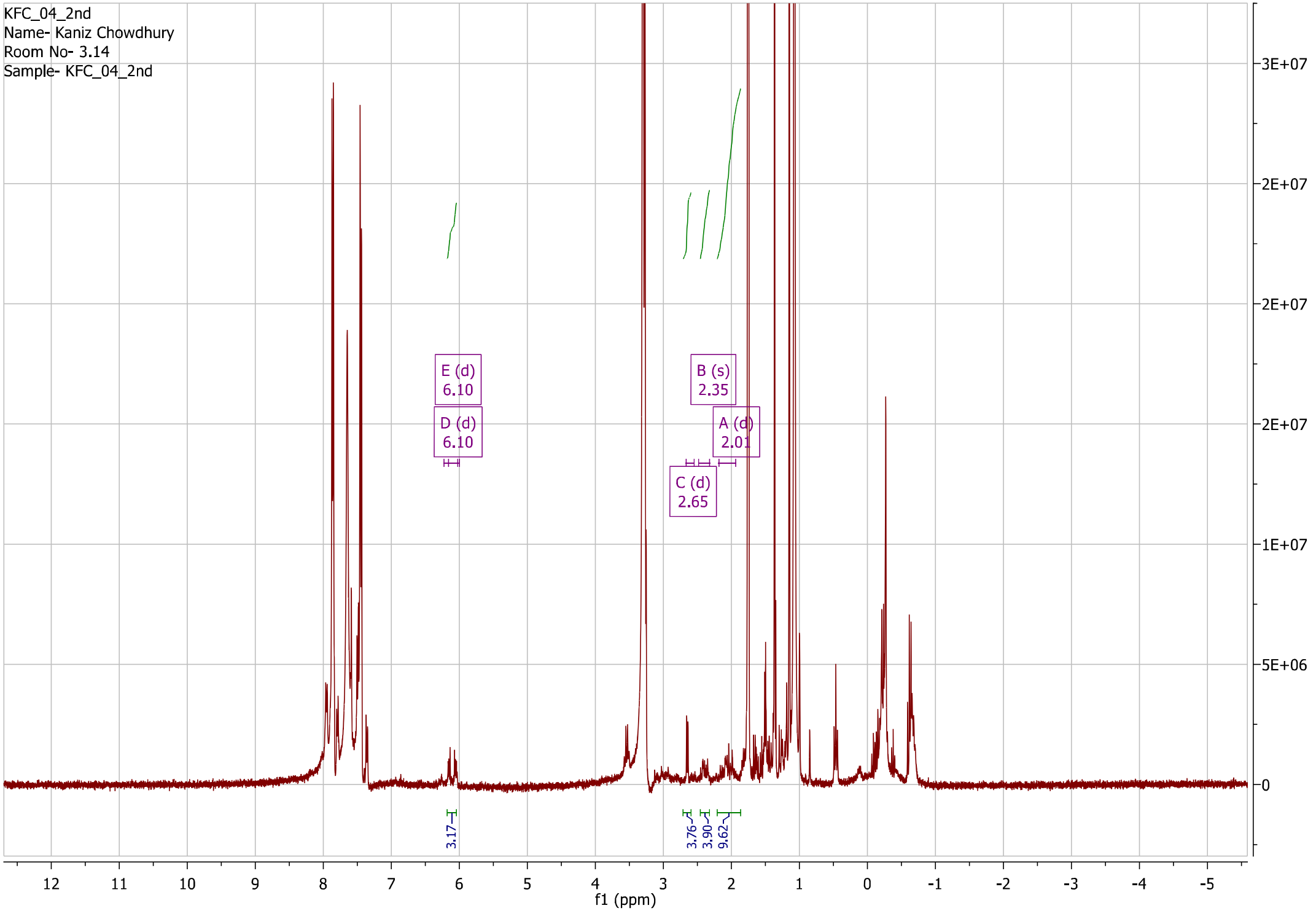
KFC_04_2nd
Name- Kaniz Chowdhury
Room No- 3.14
Sample- KFC_04_2nd
E (d)
6.10
D (d)
6.10
B (s)
2.35
A (d)
2.01
C (d)
2.65
3.17
3.76
3.90
9.62
3E+07
2E+07
2E+07
2E+07
1E+07
5E+06
0
12
11
10
9
8
7
6
5
4
3
2
1
0
-1
-2
-3
-4
-5
f1 (ppm)

Appendix D. Mass Spectra of TAminePyP

School of Chemistry Mass Spectrometry Service

SampleID	KC04_EtOH				**Submitter**	Kaniz Chowdhury	
Sample Description							
Analysis Name	D:\Data\robinbon\cm11kfc\KC04_EtOH_233940_GC6_01_45091.d				**Supervisor**	Robin Bon	
Method	3a_AccMass_Loop_Positive.m				**Acquisition Date**	09/04/2018 16:43:26	
Instrument	maXis impact	**Source Type**	ESI	**Ion Polarity**	Positive	**Scan Begin** 50 m/z	**Scan End** 1500 m/z

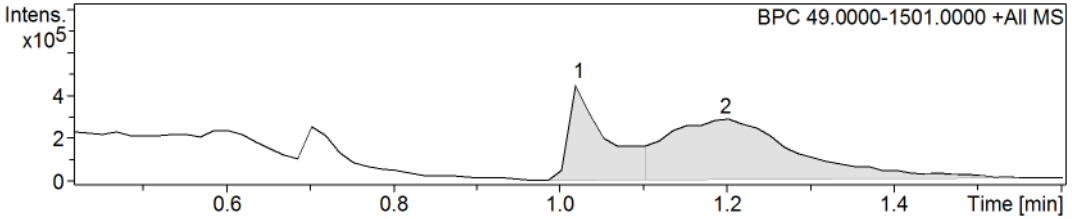

Summary of Results

Name	RT	BPC Area(%)	UV Area(%)	Confirm Formula Results
Cmpd 1, 1.0 min	1.02	30.9	no uv	
Cmpd 2, 1.2 min	1.20	69.1	no uv	

Cmpd 1, 1.0 min

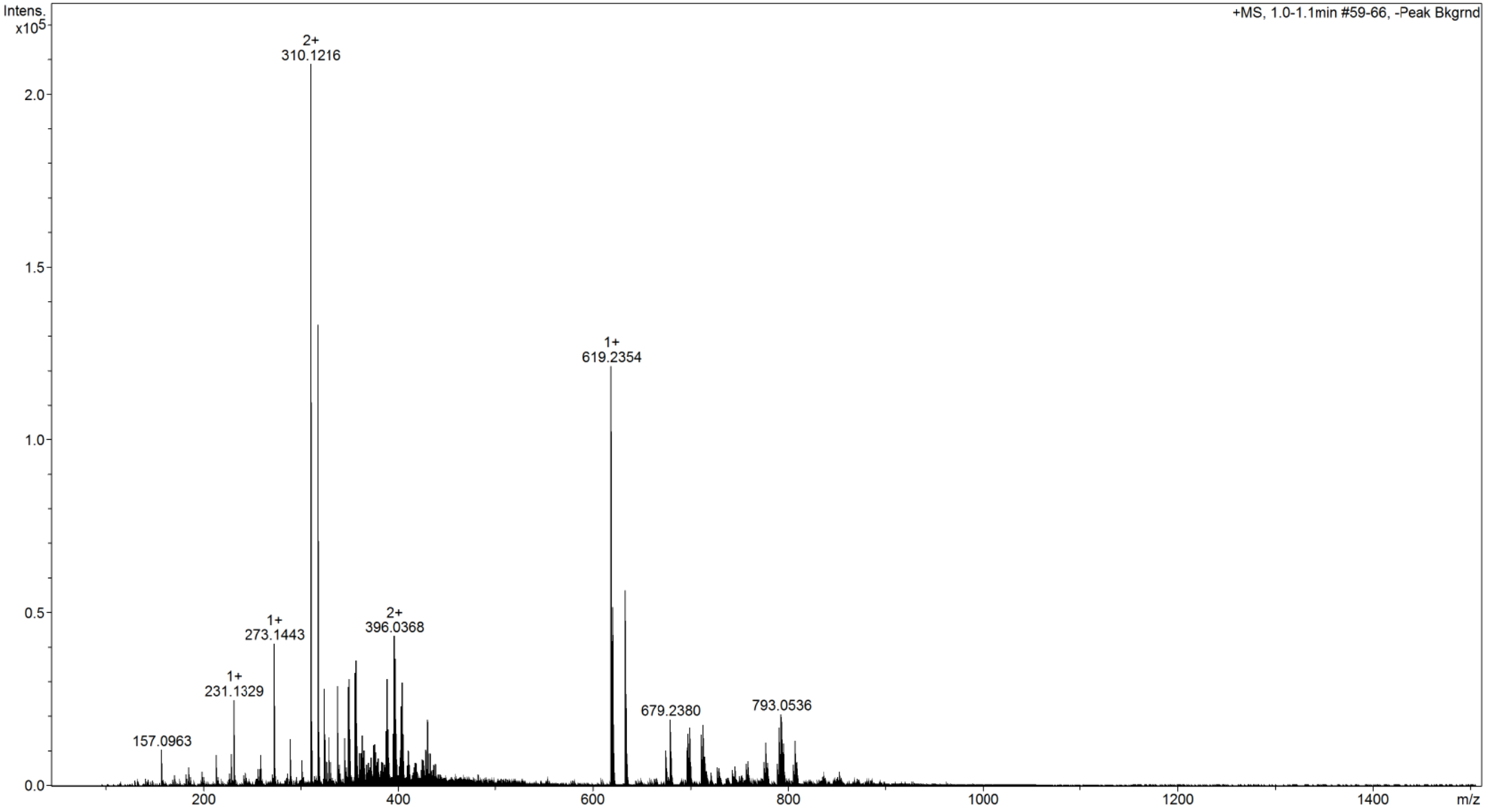
Intens.
x10^5
+MS, 1.0-1.1min #59-66, -Peak Bkgrnd
2+
310.1216
1+
619.2354
1+
273.1443
2+
396.0368
1+
231.1329
679.2380
793.0536
157.0963
2.0
1.5
1.0
0.5
0.0
200
400
600
800
1000
1200
1400
m/z

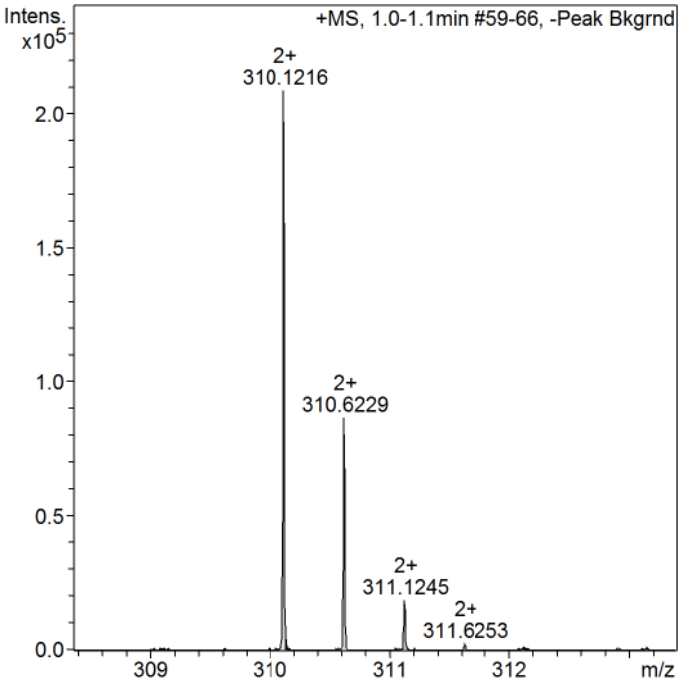

Smart Formula Parameter	Value
Expected Formula	
Adducts Considered	
Smart Formula Search Parameters	
CHNO and adducts considered implicitly	
Formula Search Minimum	
Formula Search Maximum	
Algorithm Parameters	
Tolerance	4 ppm
Match to Isotope Pattern(mSigma)	40
Electron Configuration	even
Estimate No of Carbons	yes
Filter by H/C Ratio	0< H/C < 3
Number of Double Bonds & Rings	0< rings&DB < 80

Confirm/Find Formula Results

The section below shows the results of formula calculation. If an expected formula was provided and found these are the results that are listed. If no formula was provided or no matches were found the system has attempted to determine the formula constrained by the parameters listed to the left

Cmpd 1, 1.0 min

Meas. m/z	Ion Formula	z	m/z	err [mDa]	err [ppm]	mSigma	Score	Sum Formula	Adduct
310.121601	C39H32N4O4	2+	310.120629	-1.0	-3.1	14.5	90.51	C39H30N4O4	M+H
	C40H28N8	2+	310.121298	-0.3	-1.0	25.7	100.00	C40H26N8	M+H
	C28H32N10O7	2+	310.122223	0.6	2.0	36.4	66.08	C28H30N10O7	M+H
	C25H24N20O	2+	310.121549	-0.1	-0.2	37.9	82.21	C25H22N20O	M+H
	C44H32N2O2	2+	310.122641	1.0	3.4	39.0	49.18	C44H30N2O2	M+H
	C39H32N4O4	2+	310.120629	-1.0	-3.1	14.5	90.51	C39H24N2O4	M+NH4
	C40H28N8	2+	310.121298	-0.3	-1.0	25.7	100.00	C40H20N6	M+NH4
	C28H32N10O7	2+	310.122223	0.6	2.0	36.4	66.08	C28H24N8O7	M+NH4
	C25H24N20O	2+	310.121549	-0.1	-0.2	37.9	82.21	C25H16N18O	M+NH4
	C44H32N2O2	2+	310.122641	1.0	3.4	39.0	49.18	C44H24O2	M+NH4
	C34H40Na4O5	2+	310.122777	1.2	3.8	21.8	80.48	C34H40Na2O5	M+Na
	C30H36N6Na4O3	2+	310.121435	-0.2	-0.5	34.5	100.00	C30H36N6Na2O3	M+Na
	C40H28N8	2+	310.121298	-0.3	-1.0	25.7	100.00	C20H13N4	2M+H
	C44H32N2O2	2+	310.122641	1.0	3.4	39.0	49.18	C22H15NO	2M+H
317.129358	C41H30N8	2+	317.129123	-0.2	-0.7	3.0	100.00	C41H28N8	M+H
	C45H34N2O2	2+	317.130466	1.1	3.5	11.6	54.86	C45H32N2O2	M+H
	C40H34N4O4	2+	317.128454	-0.9	-2.8	13.2	59.70	C40H32N4O4	M+H
	C41H30N8	2+	317.129123	-0.2	-0.7	3.0	100.00	C41H22N6	M+NH4
	C45H34N2O2	2+	317.130466	1.1	3.5	11.6	54.86	C45H26O2	M+NH4
	C40H34N4O4	2+	317.128454	-0.9	-2.8	13.2	59.70	C40H26N2O4	M+NH4
	C40H34N4O4	2+	317.128454	-0.9	-2.8	13.2	59.70	C20H16N2O2	2M+H
619.235433	C39H31N4O4	1+	619.233982	-1.5	-2.3	9.5	61.23	C39H30N4O4	M+H
	C40H27N8	1+	619.235319	-0.1	-0.2	20.6	100.00	C40H26N8	M+H
	C39H31N4O4	1+	619.233982	-1.5	-2.3	9.5	61.23	C39H27N3O4	M+NH4
	C40H27N8	1+	619.235319	-0.1	-0.2	20.6	100.00	C40H23N7	M+NH4
	C38H28N8Na	1+	619.232914	-2.5	-4.1	9.0	28.86	C38H28N8	M+Na
	C42H32N2NaO2	1+	619.235599	0.2	0.3	21.9	100.00	C42H32N2O2	M+Na
	C35H32KN8O	1+	619.233066	-2.4	-3.8	35.3	23.17	C35H32N8O	M+K
	C39H36KN2O3	1+	619.235751	0.3	0.5	37.9	100.00	C39H36N2O3	M+K
	C40H33N2Na2O2	1+	619.233193	-2.2	-3.6	10.1	82.90	C40H34N2O2	M+Na2-H
	C30H29N12Na2O	1+	619.237719	2.3	3.7	29.5	52.83	C30H30N12O	M+Na2-H
	C45H33Na2	1+	619.237216	1.8	2.9	34.7	68.29	C45H34	M+Na2-H
	C40H27N8	1+	619.235319	-0.1	-0.2	20.6	100.00	C20H13N4	2M+H
	C38H28N8Na	1+	619.232914	-2.5	-4.1	9.0	28.86	C19H14N4	2M+Na

Meas. m/z	Ion Formula	z	m/z	err [mDa]	err [ppm]	mSigma	Score	Sum Formula	Adduct
	C42H32N2NaO2	1+	619.235599	0.2	0.3	21.9	100.00	C21H16NO	2M+Na

Cmpd 2, 1.2 min

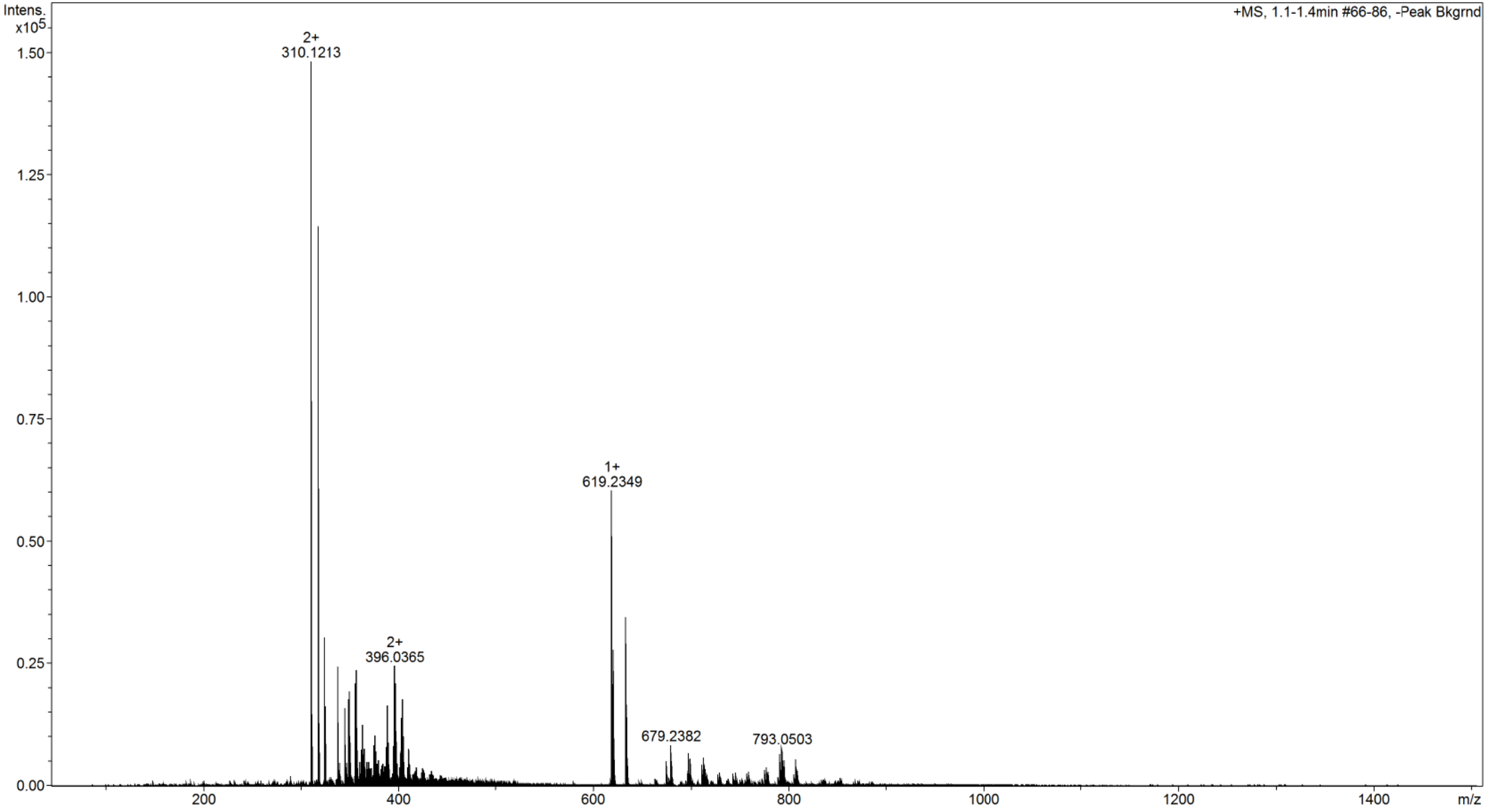
Intens.
x10^5
1.50
1.25
1.00
0.75
0.50
0.25
0.00
+MS, 1.1-1.4min #66-86, -Peak Bkgrnd
2+
310.1213
2+
396.0365
1+
619.2349
679.2382
793.0503
200
400
600
800
1000
1200
1400
m/z

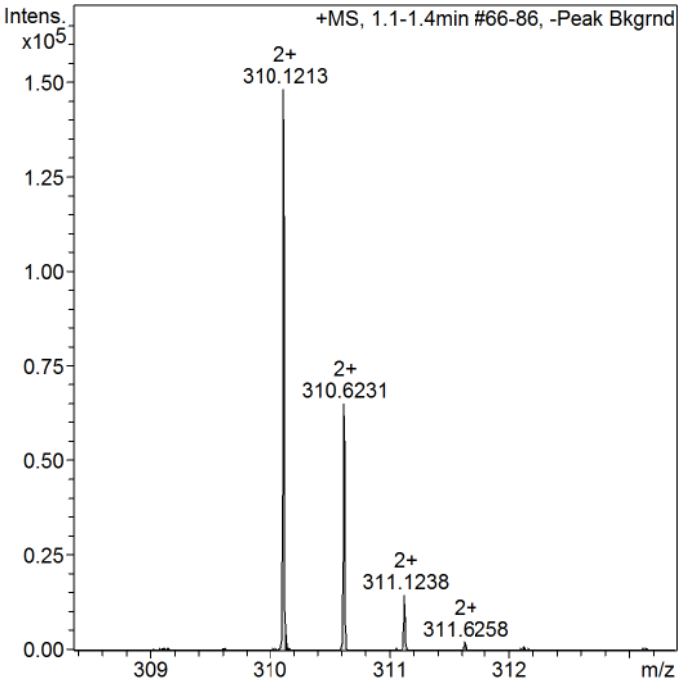

Smart Formula Parameter	Value
Expected Formula	
Adducts Considered	
Smart Formula Search Parameters	
CHNO and adducts considered implicitly	
Formula Search Minimum	
Formula Search Maximum	
Algorithm Parameters	
Tolerance	4 ppm
Match to Isotope Pattern(mSigma)	40
Electron Configuration	even
Estimate No of Carbons	yes
Filter by H/C Ratio	0< H/C < 3
Number of Double Bonds & Rings	0< rings&DB < 80

Confirm/Find Formula Results

The section below shows the results of formula calculation. If an expected formula was provided and found these are the results that are listed. If no formula was provided or no matches were found the system has attempted to determine the formula constrained by the parameters listed to the left

Cmpd 2, 1.2 min

Meas. m/z	Ion Formula	z	m/z	err [mDa]	err [ppm]	mSigma	Score	Sum Formula	Adduct
310.121341	C39H32N4O4	2+	310.120629	-0.7	-2.3	2.5	88.74	C39H30N4O4	M+H
	C40H28N8	2+	310.121298	-0.0	-0.1	13.0	100.00	C40H26N8	M+H
	C39H32N4O4	2+	310.120629	-0.7	-2.3	2.5	88.74	C39H24N2O4	M+NH4
	C40H28N8	2+	310.121298	-0.0	-0.1	13.0	100.00	C40H20N6	M+NH4
	C40H28N8	2+	310.121298	-0.0	-0.1	13.0	100.00	C20H13N4	2M+H
317.129107	C41H30N8	2+	317.129123	0.0	0.1	8.7	100.00	C41H28N8	M+H
	C40H34N4O4	2+	317.128454	-0.7	-2.1	20.4	59.36	C40H32N4O4	M+H
	C41H30N8	2+	317.129123	0.0	0.1	8.7	100.00	C41H22N6	M+NH4
	C40H34N4O4	2+	317.128454	-0.7	-2.1	20.4	59.36	C40H26N2O4	M+NH4
	C40H34N4O4	2+	317.128454	-0.7	-2.1	20.4	59.36	C20H16N2O2	2M+H
619.234933	C40H27N8	1+	619.235319	0.4	0.6	3.8	100.00	C40H26N8	M+H
	C39H31N4O4	1+	619.233982	-1.0	-1.5	9.9	67.21	C39H30N4O4	M+H
	C38H35O8	1+	619.232644	-2.3	-3.7	21.4	21.21	C38H34O8	M+H
	C40H27N8	1+	619.235319	0.4	0.6	3.8	100.00	C40H23N7	M+NH4
	C39H31N4O4	1+	619.233982	-1.0	-1.5	9.9	67.21	C39H27N3O4	M+NH4
	C42H32N2NaO2	1+	619.235599	0.7	1.1	4.1	100.00	C42H32N2O2	M+Na
	C38H28N8Na	1+	619.232914	-2.0	-3.3	10.7	37.56	C38H28N8	M+Na
	C39H36KN2O3	1+	619.235751	0.8	1.3	33.3	100.00	C39H36N2O3	M+K
	C35H32KN8O	1+	619.233066	-1.9	-3.0	36.6	37.75	C35H32N8O	M+K
	C40H33N2Na2O2	1+	619.233193	-1.7	-2.8	9.1	100.00	C40H34N2O2	M+Na2-H
	C45H33Na2	1+	619.237216	2.3	3.7	16.2	57.52	C45H34	M+Na2-H
	C40H27N8	1+	619.235319	0.4	0.6	3.8	100.00	C20H13N4	2M+H
	C38H35O8	1+	619.232644	-2.3	-3.7	21.4	21.21	C19H17O4	2M+H
	C42H32N2NaO2	1+	619.235599	0.7	1.1	4.1	100.00	C21H16NO	2M+Na
	C38H28N8Na	1+	619.232914	-2.0	-3.3	10.7	37.56	C19H14N4	2M+Na

Appendix E. List of Publications

- *"Development of photosensitiser functionalised electrospun nanofiber for microbial disinfection of waste water".* ***K. F. Chowdhury***, P. Millner, N. Sergeeva, S. Russell, *2018 TechConnect world innovation conference proceedings, Los Angles, USA.*

- "Photosensitiser immobilised antimicrobial nanofibers: solution for chemicals free energy efficient waste water treatment". ***K. F. Chowdhury***, P. Millner, N. Sergeeva, S. Russell, 2018 [J. Nanoparticle Research – under review].

- *"Photosynthesiser functionalised electrospun nanofibre for photo killing of antibiotic resistant of bacteria in water".* ***K. F. Chowdhury,*** P. Millner, S. Russell, R. Gharaei, M. Tausif. The 18th UK-Young professionals, IWA (International water association) conference, Bath, UK 2017.

- *"TMPyP functionalised chitosan membrane for efficient sunlight driven water disinfection".* H. Majiya, ***K. F. Chowdhury***, N. J. Stonehouse, P. Millner [*J. Water Process Engineering., 2017, Journal of Water Process Engineering*, 2017 DOI:10.1016/j.jwpe.2017.08.013.

- ***"****Synthesis and Biological Evaluation of Colchicine B-Ring Analogues Tethered with Halogenated Benzyl Moieties".* L. Cosentino, M. Redondo-Horcajo, Y. Zhao, A. R. Santos, ***K. F. Chowdhury***, V. Vinader, Q. M. A. Abdallah, H. Abdel-Rahman, J. F. Dit Chabert, S. D. Shnyder, W. Fang, J. F. Díaz, I. Barasoain, P. A. Burns, K. Pors. [*J. Med. Chem.*, 2012, 55 (24), pp 11062–11066, DOI: 10.1021/jm301151t].